Chromosome Dynamics and Molecular Motor Proteins in the Interphase Nuclei of Proliferating and Non-Proliferating Cells

A Thesis submitted for the degree of

Doctor of Philosophy

By

Kumars Riyahi

College of Health, Medicine and Life Sciences

Department of Life Sciences

Brunel University London

September 2023

Abstract

Interphase chromosome dynamics is an important area of research related to the control of genomic function and gene regulation at the level of the 3D conformation and mobility of chromosomes. This also has relevance to cellular states which can show differences in chromosome organisation at interphase, when proliferating and non-proliferating cells are compared. These comparative studies are important to understanding the regulation of cell proliferation and processes such as ageing. The work in this thesis has taken the aspect of a broad approach to address the exploration of chromosome dynamics. This exploration has involved both extensive laboratory work and in silico analyses to reveal possible candidate proteins involved in chromosome mobility. A main hypothesis in this project is that there are fundamental differences between proliferating and non-proliferating cells with regards to the functions of nuclear myosin motor proteins and this would be reflected in the functions of these proteins, specifically related to chromosome mobility. Further to this, a key aspect of this work is related to the hypothesis that in non-proliferating cells chromosome mobility in response to stimuli is impaired, and this is caused by the relevant nuclear myosins not functioning as they would in proliferating cells. Using the technique of 2D Fluorescence In-Situ Hybridisation (2D FISH), the dynamic mobility of interphase chromosomes was studied in the nuclei of human dermal fibroblast cells, in order to gain further understanding regarding their responses to stress stimuli in the form of serum inhibited conditions and heat shock. Immmunofluorescence studies were performed to determine the patterns and frequency of myosin proteins (MYO5B, MYO16 and MYO18B) in proliferating and non-proliferating cells. Another aspect of the search for possible candidate proteins was an in silico bioinformatics exploration, to find not only other myosins but also actin related proteins and other classes of proteins that may be part of the overall mechanism of interphase chromosome mobility. In this work a heat shock assay in human dermal fibroblast cells has been developed with chromosome 11. In addition to this a novel chromosome 11 relocation has been found in response to heat shock and importantly, it has been found that in non-proliferating cells this relocation of chromosome 11 in response to heat shock does not occur. The results also show that the nuclear staining characteristics and frequency of the various myosin proteins studied show significant differences when compared in proliferating and non-proliferating cells. Using the bioinformatics approach other interesting candidate

proteins were identified with possible potential to be involved with the process of chromosome mobility. A possible role for myosin 5b has been implicated in the mobility of splicing speckles, as shown by co-localisation with splicing speckles for the first time. A suggestion is made by inference, that older cells may possibly also have diminished chromosome relocation potential compared with younger cells.

Declaration

I hereby declare that all the work presented in this thesis has been performed by me unless otherwise stated.

Kumars Riyahi

Acknowledgments

I wish to thank my Principle Supervisor Professor Joanna M. Bridger for all her advice, help and patience over the long and difficult duration of my PhD degree. She has been the perfect Supervisor for me and she understood well my various characteristics and successfully managed to guide me through the difficult trek towards a PhD degree. I would also like to thank my second Supervisor Professor Michael Themis whose kind support and advice throughout my PhD degree helped me to keep going at difficult times. I would also like to thank the examiners of my progress panel, Professor Amanda Harvey and Dr. Predrag Slijepcevic who have helped me to become a better and more capable scientist by guiding me on how to improve.

I wish to say a big thank you to Brunel University London for giving me the opportunity to undertake a PhD degree, a major goal of my life for many years.
I wish to thank my dear parents and two brothers for all their love, patience and support throughout my PhD journey over the many years.
I am most grateful to have reached this stage of achieving a PhD degree after a long and difficult journey and thankful that I was not forsaken.

Table of Contents

List of Abbreviations

ABD   Actin binding domain

APD   Accumulated population doublings

ARP   Actin related protein

ATP   Adenosine triphosphate

BLAST   Basic local alignment search tool

BSA   Bovine serum albumen

CBs   Cajal bodies

CDD   Conserved domains database

CR   Cytoplasmic ring

Cy3   Cyanine 3

DAPI   4', 6-Diamidino-2-phenylindole

DMEM   Dulbecco's modified eagles medium

DNA   Deoxyribonucleic acid

DOP-PCR   Degenerate oligonucleatide primed polymerase chain reaction

EDC   Epidermal differentiation complex

ELC   Essential light chain

ER   Endoplasmic reticulum

FCS   Fetal calf serum

FITC   Fluorescein Isothiocyanate

FISH   Fluorescence in situ hybridisation

IC   Interchromatin compartment

ICD   Interchromosomal domain

IFN-γ   Interferon-gamma

INM   Inner nuclear membrane

IR   Inner ring

kDa   Kilodalton

LADs   Lamina-associated domains

LAP   Lamin associated polypeptides

LECA   Last eukaryotic common ancestor

LIC   Light intermediate chain

LINC   Linker of nucleoskeleton and cytoskeleton

MDa   Megadalton

MHC   Major histocompatibility complex

MMPs	Matrix metalloproteinases
mRNA	Messenger RNA
miRNA	MicroRNA
mRNPs	Messenger ribonucleoproteins
rRNA	Ribosomal RNA
NCBI	National centre for biotechnology information
NES	Nuclear export signal
NLS	Nuclear localisation signal
Nm	Nanometer
NOR	Nucleolar organiser region
NPC	Nuclear pore complex
NR	Nucleoplasmic ring
NTRs	Nuclear transport receptors
Nups	Nucleoporins
ONM	Outer nuclear membrane
PBS	Phosphate buffered saline
PCR	Polymerase chain reaction

PML   Promyelocytic leukemia

PNS   Perinuclear space

rDNA   Ribosomal DNA

RNA   Ribonucleic acid

ROS   Reactive oxygen species

rpm   Revolutions per minute

SA-β-gal   Senescence-associated-beta-galactosidase

SEM   Standard error of the mean

SFC   Splicing factor compartments

snRNPs   Small nuclear ribonucleoproteins

SSC   Saline sodium citrate

STRING   Search tool for the retrieval of interacting genes/proteins

TAD   Topologically associating domain

TPR   Tetratricopeptide repeat domain

TRITC   Tetramethylrhodamine

Chapter 1: General Introduction

1.1 The nucleus.

1.2 Chromosome organisation and dynamics.

1.3 Molecular motors; myosins.

1.4 Cellular quiescence and senescence.

1.5 Aims of project.

1.1 The Nucleus

The cell nucleus is among the most complex and important structures in living systems and is an organelle found exclusively in eukaryotic cells. Research on the cell nucleus is increasingly essential and despite many years of extensive research on the structure and functions of the cell nucleus, deeper layers of complexity regarding its fine structure and functions continue to be revealed (Figure 1.1). The nucleus contains genetic information within the chromosomes it encapsulates and therefore it plays a central role in the control of gene expression and so is involved in all life processes such as development, growth and physiological function. This key role played by the nucleus compels ever more thorough investigations regarding the detailed mechanisms involved in its functions. In the early studies in cell and molecular biology, the complexity of the nucleus was somewhat underestimated and was thought to be composed of an unstructured mixture of components such as various proteins, freely interacting with an immobile DNA. However, this view in the light of progressive insights into the structures and mechanisms found in the nucleus has changed dramatically to reveal a highly ordered and organised dynamic nucleus which has structural and functional integrity and stability, as well as dynamics and changeability (Newport and Forbes 1987; Lamond and Earnshaw 1998; Lelievre et al. 2000; Dundr and Mistelli 2001; Belmont 2003; Rippe 2007; Bridger 2011; Mercer and Mattick 2013; Zidovska 2020).
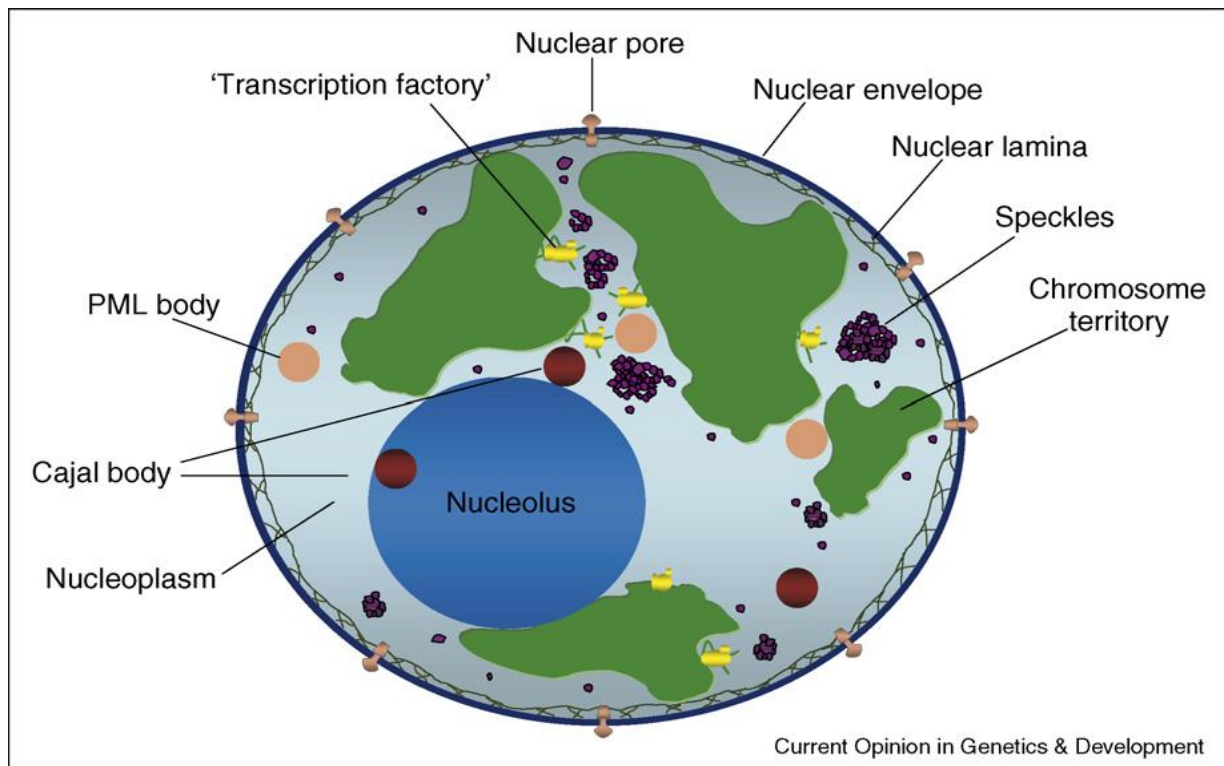
Figure 1.1. A schematic illustration of the detailed structure of an interphase nucleus. The main nuclear substructures are shown together with representative chromosome territories. At the edge of the nucleus, the nuclear envelope is the barrier separating the nuclear interior from the cytoplasm, and is where transport takes place through the nuclear pore complex. The position of the nuclear lamina is shown in contact with the inner surface of the nuclear envelope. Transcription factories and splicing speckles are shown in proximity to each other and positioned in the regions separating the chromosome territories. PML (promyelocytic leukemia) bodies and Cajal bodies are also shown positioned in regions of the nucleoplasm, and in the case of Cajal bodies, associated with the prominent nucleolus.
(Taken from Pontes and Pikaard 2008).

1.1.1 Nuclear Envelope and Nuclear Pore Complex

The nuclear envelope is a lipid bilayer or double membrane system with an intricate structure composed of many different proteins and is the barrier separating the cytoplasm and the nuclear interior. In between the two membranes on the nuclear envelope is the perinuclear space (PNS) which is a lumen connecting directly with

the endoplasmic reticulum (ER) (Lu et al. 2008). With the nucleus being among the most important structures in the eukaryotes, the nuclear envelope may be described as one of the most defining features of the nucleus.

The nuclear envelope bilayer is composed of the inner nuclear membrane (INM) and the outer nuclear membrane (ONM) (Figure 1.3). Nucleocytoplasmic transport is a crucial process in eukaryotic cells and occurs at nuclear pore complexes (NPCs) which are embedded in the nuclear envelope, and selectively control the movement of molecules across the nuclear envelope (Figures 1.2 and 1.3). NPCs appear as prominent structures over the surface of the nuclear envelope and are very large protein complexes, with molecular mass of approximately 110 MDa (Kosinski et al. 2016), forming aqueous channels for the regulated movement of molecules. This includes transport of large proteins, ribosomal subunits and messenger ribonucleoproteins (mRNPs) across the NPCs. Small molecules less than about 40 kDa or about 5 nm in diameter, ions and metabolites can move across the NPCs freely (Wente and Rout 2010). There is therefore a balance of both active and passive transport across the nuclear envelope via the NPCs, with the transport of larger molecules being actively regulated and controlled in this respect. This may also be of importance in avoiding excessive amounts of larger molecules entering the nucleoplasm when not needed, thus avoiding molecular overcrowding of the compact nuclear environment. The proteins of the NPC are called nucleoporins (Nups) and there are approximately 30 different nucleoporins, and in humans over 1000 nucleoporins form the NPC (Dultz et al. 2022).

The overall architecture of the NPC consists of three main ring shaped structures (Figure 1.3) which are, the centrally positioned inner ring (IR), to which are connected two outer rings, known as the nucleoplasmic ring (NR) associated with a nuclear basket structure extending to the nucleoplasm, and the cytoplasmic ring (CR) associated with cytoplasmic filaments which extend to the cytoplasm (Allen et al. 2000; Beck and Hurt 2017; Schuller et al. 2021). For the import and export of proteins, the selectivity of the nuclear pore complexes involves protein sequence recognition to allow the correct proteins to move across the nuclear pores. This involves specific short amino acid sequences on the proteins being transported through the NPCs by shuttling receptors, known as nuclear transport receptors

(NTRs) which include importins, exportins and transportins, mostly belonging to a large family of NTRs known as karyopherins (Wente and Rout 2010; Paci et al. 2021; Wing et al. 2022). Sequences for proteins entering the nucleus are known as nuclear localisation signals (NLSs) and sequences for proteins leaving the nucleus are known as nuclear export signals (NESs) (Wente and Rout 2010, Dzijak et al. 2012). The process of nucleocytoplasmic protein transport involves the formation of an import or export complex, by the binding of NTRs with the NLS or NES of cargo proteins either directly or via adapter proteins (Paci et al. 2021). NPCs can also be considered as locations where the double membrane system can be structurally stabilised by forming connections at these complexes, where the ONM and INM fuse (Suntharalingam et al. 2003; Zuleger et al. 2011; Kabachinski and Schwartz 2015).

1.1.2 Nuclear Lamina

Covering the inner surface of the nuclear envelope is the nuclear lamina which is a protein meshwork composed of intermediate filaments of the lamin family of proteins (Figure 1.2). The nuclear lamina helps to maintain the structural integrity of the nuclear envelope by providing structural support as well as providing attachment sites for chromatin (Gerace and Huber 2011; Shevelyov and Ulianov 2019). As with most substructures in the nucleus, extensive research has revealed that the nuclear lamina is more complex than initially believed and has more functions. These further functions include regulation of cell signalling and negative regulation of gene activity by gene silencing, as well as providing a mechanical link between the cytoskeleton in the cytoplasm and the nuclear envelope (Lu et al. 2008; Gerace and Huber 2011; Shevelyov and Nurminsky 2012).

At the INM, the nuclear lamina is in contact with many different proteins including emerin, lamin B receptor and lamin associated polypeptides (LAP) and MAN1 (Lin et al. 2000) (reviewed by Foster and Bridger 2005; De Magistris and Antonin 2018). LAP2α interacts with A-type lamins specifically, which are composed of the lamin A and lamin C isoforms and play an important role in chromatin organisation (Dechat et

al. 2008; Gesson et al. 2014). LAP2α is involved with the translocation of A-type lamins from the lamina at the nuclear periphery to the nucleoplasm (Figure 1.2), where they may interact with interphase chromosomes in their role of maintaining chromosome territories (Ranade et al. 2019). Lamina-Associated Domains (LADs) are heterochromatic regions in contact with the nuclear lamina and involved with gene repression, since most genes at LADs are not expressed or show low transcriptional activity (van Steensel and Belmont 2017).
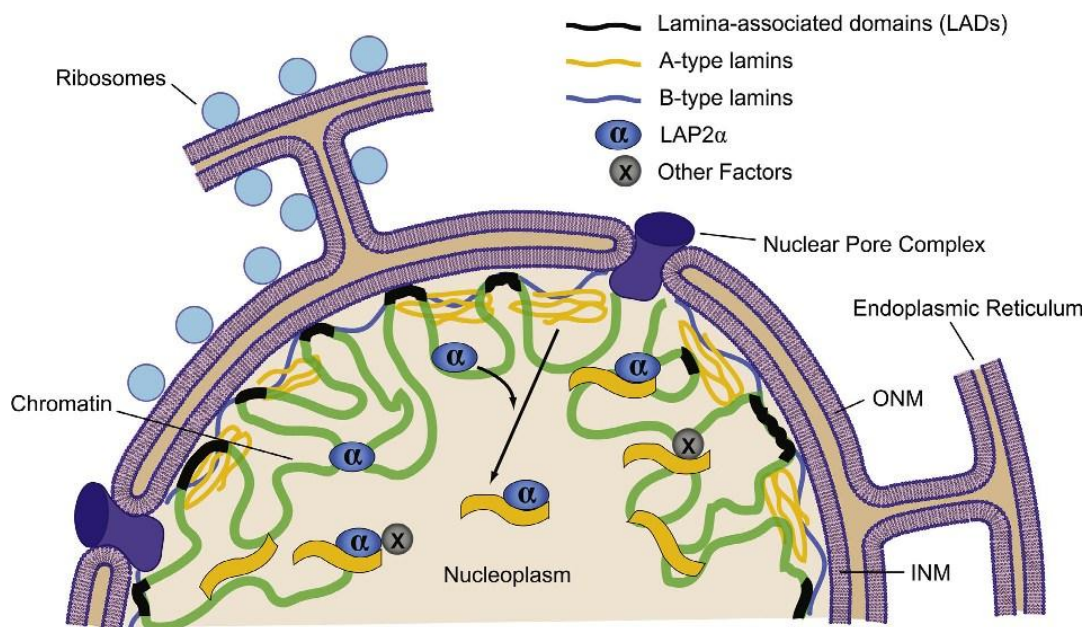
Figure 1.2. Illustration of the nucleus focusing on the nuclear lamina, showing the main components and highlighting the action of LAP2α. LAP2α is important in allowing the transportation of A-type lamins from the lamina to the nucleoplasm, thus facilitating a key role of these lamins in regulating chromatin organisation (Ranade et al. 2019). As shown in this figure, B-type lamins are closely associated with the INM. LADs are shown in close association with the lamina. Also, in this figure it is clearly shown how the lumen of the nuclear envelope is continuous with the endoplasmic reticulum. (Taken from Gesson et al. 2014).

The detailed organisation of the nuclear envelope reveals a highly ordered and interlinked array of proteins which create a structural and functional link from the

nucleoplasmic side of the nuclear envelope via the INM to the cytoplasmic side of the envelope via the ONM (Figure 1.3). Two of the important families of proteins operating in this respect across the nuclear envelope are SUN-domain and KASH-domain proteins. Together these protein families form parts of the LINC complex (Linker of Nucleoskeleton and Cytoskeleton) (Taranum et al. 2012; Lu et al. 2012). The SUN-domain proteins are situated at the INM and the KASH-domain proteins are situated at the ONM and these proteins interact by linking in the region of the perinuclear space (PNS) (Lu et al. 2008). The PNS therefore has an important role in providing a physical space for crucial molecular interactions necessary for structural and functional properties of the nuclear envelope. The KASH domain proteins include the Nesprins which function as linker proteins connecting to the cytoskeleton (Figure 1.3). Nesprin-1 and Nesprin-2 contain an actin binding domain (ABD) at the N-terminal and are therefore able to directly bind F-actin. Nesprin-1 has also been shown to interact with Nesprin-3 (Taranum et al. 2012). Nesprin-3 does not contain an ABD but does contain a binding site for Plectin at the N-terminal (Taranum et al. 2012). Plectin is a cytolinker and can interact with microtubules, intermediate filaments and both F-actin and G-actin (Andrä et al. 1998; Lu et al. 2008; Taranum et al. 2012). Nesprin-4 binds to kif5b which is a subunit of the kinesin-1 motor protein (Roux et al. 2009; Rajgor and Shanahan 2013). It has also been shown that Nesprins may form a filamentous meshwork at the surface of the ONM thus providing mechanical support as well as controlling nuclear size (Lu et al. 2012). Interestingly, it has been shown that the SUN-1 proteins have a rather unique feature at the INM in that they are highly immobile proteins which can form oligomers in the form of dimers and tetramers and can also form heterodimers with SUN-2 proteins (Lu et al. 2008). The significance of the immobile and oligomer forming properties of the SUN-1 proteins at the INM includes providing mechanically stable platforms for the formation of various larger stable complexes traversing the nuclear envelope (Lu et al. 2008).

Interestingly, the relationship of the interaction between SUN-domain and KASH domain proteins is highly conserved across broad taxa (Lu et al. 2008; Schneider et al. 2008), which suggests that this system has been crucial for the functioning of the eukaryotic cell over evolutionary time and therefore the conservation of this structure and function is of great importance to all eukaryotes.
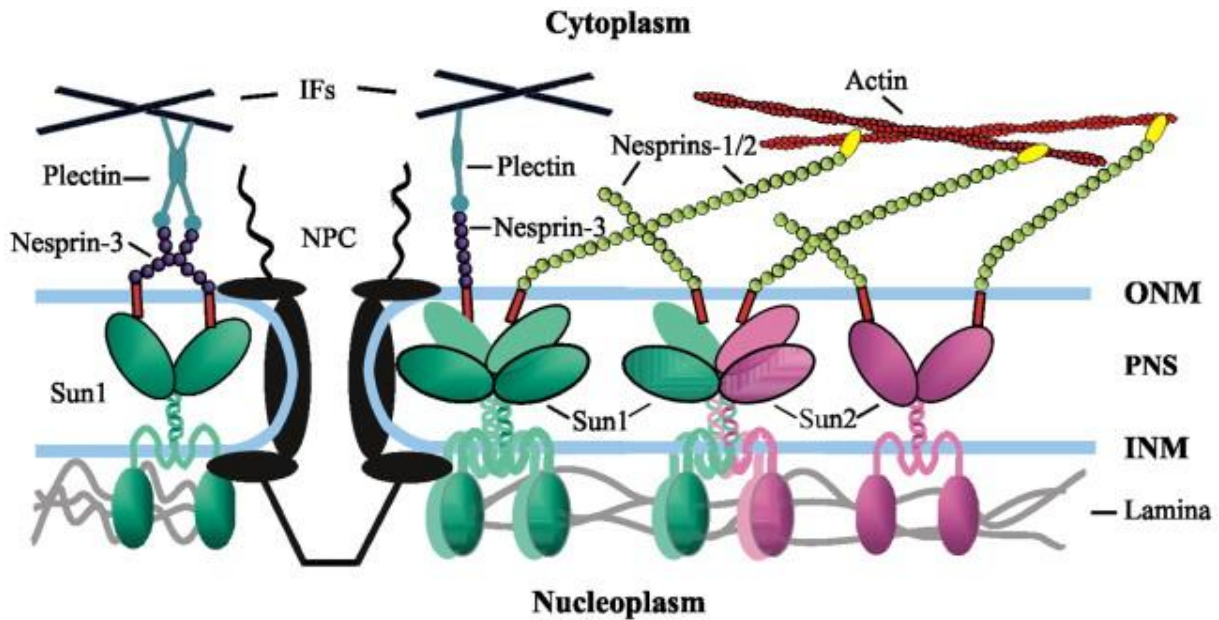
Figure 1.3. Detailed structure of the nuclear envelope. Showing components of the LINC complex including SUN-domain proteins in dimer and tetramer configurations bound with nesprins at the PNS thus bridging across to the cytoplasm. The NPC (nuclear pore complex) is also illustrated, visible in cross-section with three main ring structures depicted; the inner ring (forming the central pore) is connected with two outer rings, which are the nucleoplasmic ring (with nuclear basket extending to the nucleoplasm) at the INM (inner nuclear membrane); and the cytoplasmic ring (with cytoplasmic filaments extending to the cytoplasm) at the ONM (outer nuclear membrane). IFs (intermediate filaments), PNS (perinuclear space).
(Taken from Lu et al. 2008).

1.1.3 Transcription Factories

The transcription of genes is highly organised spatially by the presence of transcription factories which are distinct locations where mRNA transcripts are generated (Jackson 2005). These factories are composed of clusters of RNA polymerase molecules together with many other molecules required for transcription (Figure 1.4). A protein rich core is situated at the centre of transcription factories where the proteins required for transcription are present including transcription

factors, chromatin remodelers, ribonucleoproteins (RNPs) and histone modification enzymes, together with RNA polymerases at the surface of this core (Melnik et al. 2011; Rieder et al. 2012). Transcription factories have been estimated to contain between 4 and 30 RNA polymerase molecules and the number of these factories can range from about 100 to 8000 in a nucleus, and most commonly these clusters are known to contain RNA polymerase II but clusters of RNA polymerase I or III are also known to make up transcription factories (Rieder et al. 2012).

The configuration of the transcription machinery had been the subject of some debate and speculation from around the turn of the 21st century. Although transcription factories had been described some years earlier and known to contain concentrations of RNA polymerase molecules as transcription foci (Jackson et al. 1993; Wansink et al. 1993), the detailed architecture of transcription sites was not well established. The prevailing understanding of transcription involving RNA polymerase molecules moving along the DNA template as the new transcript grows were dominant and did not incorporate the findings on the presence of transcription factories as immobile centres of transcription (Cook 1999). Transcription factories have been intensively studied and it has been found that the clusters of immobile RNA polymerase molecules are part of a larger immobile protein complex, which is immobilised by contact with the nucleoskeleton or nuclear matrix (Iborra et al. 1996; Jackson 1997; Eskiw et al. 2008; Razin et al. 2011). Therefore, the configuration of transcription factories requires that mobility is that of the DNA template rather than a mobile RNA polymerase (Cook 1999; Papantonis et al. 2009; Eskiw and Fraser 2011; Papantonis and Cook 2011; Ghamari et al. 2013). This also highlights the significance of the requirement for active chromosome dynamics and mobility in the proper functioning of processes specifically occurring in the nucleus. Transcription factories and the associated transcription of genes have been visualised at high resolution by light and electron microscopy for example in murine erythroblasts (Eskiw and Fraser 2011). In this study which was ground breaking in that it was the first high resolution visual and quantitative demonstration of transcription in transcription factories, also suggested that transcription factories modify by growing in size according to the transcriptional load requirements of the subset of genes involved.

The fact that transcription occurs in preassembled transcription factories, where multiple genes assemble from different chromosomes, and different loci of the same chromosome, clearly demands an active and directed mechanism to move chromatin to these destinations of transcription centres. These chromatin movements are at the scale of whole chromosomes or chromosome domains as well as at the scale of gene loci. These dynamic movements of chromatin must and do involve the action of protein molecular motors, and the question is no longer 'if' molecular motors are involved, rather it is 'which' proteins are involved in the mechanism and 'how' do such mechanisms operate in the nucleus. These questions have been sought for many years now by several laboratories around the world and the pieces of this puzzle are accumulating to help build a clearer picture and to answer these questions, however there is still a long way to go before a full understanding of this very complex system can be obtained.
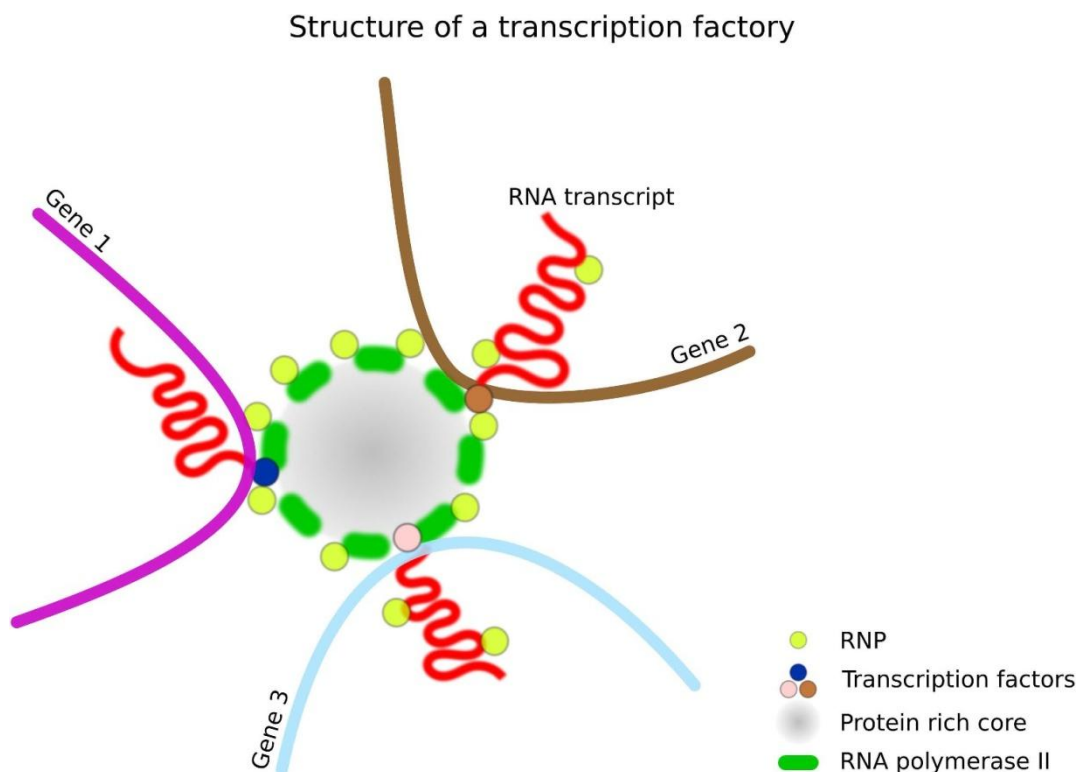

Figure 1.4. A schematic illustration of a transcription factory. Assembled at a protein rich core, ribonucleoproteins (RNP) are shown associated with RNA polymerase II enzymes and various transcription factors, as new RNA transcripts are produced from three different genes simultaneously at the transcription factory.
(Taken from Rieder et al. 2012).

1.1.4 Splicing Speckles

Within the nucleus there rather prominent irregularly shaped sites referred to as splicing speckles, SC35 domains or splicing factor compartments (SFC) (Hall et al. 2006). Estimates of the number of these sites in a nucleus vary from 10-30 (Hall et al. 2006) and 20-50 (Spector and Lamond 2011). This variation in the frequency range is probably due to the differences in the number of these speckles depending on cell type and differentiation state. Splicing speckles are involved with the processing of pre-mRNA molecules after they have been generated at transcription factories, therefore splicing speckles can be described as having a role in mRNA processing which follows 'downstream' after the role of transcription factories, then culminates in mature mRNA export (Hall et al. 2006). Indeed, splicing speckles are situated in close proximity to transcription factories and highly expressed genes are found to be associated with splicing speckles. Splicing speckles contain many pre-mRNA splicing factors as well as many other proteins including transcription factors, although it is important to note that splicing speckles are not directly involved in the process of transcription. This has led to the suggestion that splicing speckles are also involved with the recycling of splicing and transcription factors as part of the overall mechanisms of gene expression (Spector and Lamond 2011).

Splicing speckles have been shown to have dynamic behaviour in the nucleus, in that they show changes in shape, size and numbers, and speckle components/factors show directed motion as they detach from the speckle and shuttle to transcribed gene loci as needed and again reunite with the main speckle mass (Melcak et al. 2000; Spector and Lamond 2011; Zhang et al. 2016). In a very interesting finding by Zhang et al. (2016) where the authors researched the mechanism of the motion of speckle components in human mammary epithelial cells, it was found that the directed motion involves the action of ATP dependant processes. Although the specific molecules involved in bringing about this ATP dependant movement were not identified. The authors in this study did speculate that myosin motor proteins may be involved in this active process. They were able to show that the movement of small speckles towards larger speckles was significantly reduced when ATP was depleted and actin disrupted. This highlights the fact that protein molecular motors in the nucleus are utilized for many varied roles and may

be thought of as the actuators or engines of the nuclear environment allowing the highly dynamic nucleus to function correctly. It was also shown that the movement of small speckles may be occurring in the interchromatin channel regions which divide chromosome territories and where it had previously been shown that splicing speckles are found (Zhang et al. 2016).

1.1.5 PML Bodies

Another set of structures in the nucleus known as promyelocytic leukemia (PML) bodies due to consisting mainly of the tumor suppressor protein (PML), number between 5 and 20 and are highly active and dynamic structures associated with many different proteins (Palibrk et al. 2014). They have been shown to associate with the genome by direct contact with chromosomes and are also involved in responses to cellular stress, however they have also been assigned various other functions such as involvement in apoptosis and cell cycle regulation (Shiels et al. 2001; Ching et al. 2005; Palibrk et al. 2014). PML bodies selectively associate with some regions of chromosomes with high transcriptional activity, therefore it appears that they have quite specific locus dependant regulatory functions with regards to the genome (Ching et al. 2005). PML bodies have also been shown to associate with active transcription sites where they may function as scaffolds to allow assembly of various transcription factors (Kiesslich et al. 2002). The role of PML bodies as scaffolds has also been found in work by Chang et al. (2013), where the authors show that PML bodies function as scaffolds creating platforms for maintaining the integrity of telomeric chromatin, and thus play an important role in chromosome stability. They highlight that this genome stabilising role allows for accurate inheritance of epigenetic information at telomeres. Clearly PML bodies have several roles in the functioning of the nucleus and have been described as 'multi-faceted' in relation to their roles, which is reflected in the large variety of regulatory proteins they are composed of (Chang et al. 2013). The requirement of PML bodies to be recruited to gene loci and sites of active transcription suggests the activity of motor proteins since this movement must be very specific and directed with spatiotemporal

regulation, rather than random as diffusion processes would be insufficient as a mechanism to achieve this.

1.1.6 Cajal Bodies

Cajal bodies (CBs) are dynamic structures in nuclei and have a role in the synthesis of small nuclear ribonucleoproteins (snRNPs) through the action of small Cajal body specific RNAs (scaRNAs), as well as a role in the production of telomerase and the trafficking of this ribonucleoprotein complex to telomeres (Morris 2008; Li et al. 2014; Yuan et al. 2014). The snRNPs are components of the spliceosome although CBs do not contain other splicing factors or DNA and this has led to the suggestion that they are unlikely to be sites of transcription or pre-mRNA processing (Ogg and Lamond 2002). The mature snRNPs produced by CBs are either transported to splicing speckles or to sites of transcription (Li et al. 2014). More recently, CBs have also been linked with the process of microRNA (miRNA) production through association with miRNA gene clusters and regulatory interaction with the components of miRNA biogenesis (Logan et al. 2020). Therefore it appears that CBs are multi-faceted with regards to their roles in the nucleus, as is also the case with PML bodies, indicating that these nuclear bodies are very versatile and complex. Major components of CBs include coilin and the survival of motor neuron (SMN) protein as well as a protein called FAM118B which associates with coilin and SMN (Li et al. 2014). CBs are not present in all cell types and this is somewhat enigmatic since they have several crucial functions in cells. For example, CBs are absent in smooth and cardiac muscle cells as well as in skin cells (Young et al. 2000; Morris 2008). One explanation for this is that the CBs may aid to improve the efficiency of the various processes they are involved in, such that their absence in some cell types would not disrupt normal cellular functions (Stanek and Nuegebauer 2006). Perhaps in cells where CBs are not present, other nuclear bodies compensate for roles associated with CBs. Although much is known about CBs, they are among the nuclear substructures that have generated much speculation regarding their nature.

1.1.7 Nucleolus

In the nucleus there are usually 2-3 nucleoli though a range of 1-6 has also been cited (Shea and Leblond 1966). The nucleolus was first formally described by Rudolph Wagner in 1835 but it was not until 1898 that the first major study on the nucleolus was completed by Thomas Montgomery (Montgomery 1898; Pederson 2011). This work by Montgomery, first published in the *Journal of Morphology* was a groundbreaking and comprehensive comparative cytological study with particular emphasis on the nucleolus and was well over 300 pages long with the first 276 pages of text containing a description and discussion on cytology with emphasis on the nucleolus. This work further included over 300 individual illustrations of nuclei and nucleoli contained in 10 foldout multi-image figure pages together with figure explanation pages (Biodiversity Heritage Library website). The figures were drawn in colour on observing a wide range of tissues and demonstrating the diversity of nucleolar form (Figure 1.5).

Nucleoli are mainly known to be involved in the production of ribosomes where ribosomal RNA (rRNA) is produced and processed and combined with ribosomal proteins ready to be exported to the cytoplasm where protein synthesis takes place (Hernandez-Verdun et al. 2010). The synthesis of ribosomes begins with the production of 3 types of rRNA which are 18S, 5.8S and 28S rRNA, transcribed from the corresponding genes located in chromosomal domains referred to as Nucleolar Organiser Regions (NORs) making up the ribosomal DNA (rDNA), and It is these NORs around which the nucleoli form (Maiser et al. 2020). In a groundbreaking study, Maiser et al. (2020) used super-resolution microscopy to reveal in unprecedented detail the structural conformation of rDNA chromatin units in nucleoli of human fibroblast cells and mouse embryonic fibroblasts. In this study it was shown that active rDNA chromatin forms ring shaped structures in nucleoli and these rings of chromatin are clearly spatially separated from each other, with each ring constituting possibly one or two transcribed rRNA genes.

In addition to the main role of ribosome biosynthesis, further research has led to the discovery of other roles for nucleoli including control of the cell cycle (Tsai and Pederson 2014), and interestingly a putative role in translation in the nucleus where

protein synthesis specific to the nucleus may take place by functioning ribosomes (David et al. 2012; Reid and Nicchitta 2012; Mcleod et al. 2014; Theodoridis et al. 2021). This would allow nuclear specific proteins to be more readily and efficiently available than if they could only arrive from the cytoplasm following translation there. This example helps to highlight the fact that the cell nucleus and the substructures within it, together with the processes occurring there are far more complex and intricate than we have yet discovered.
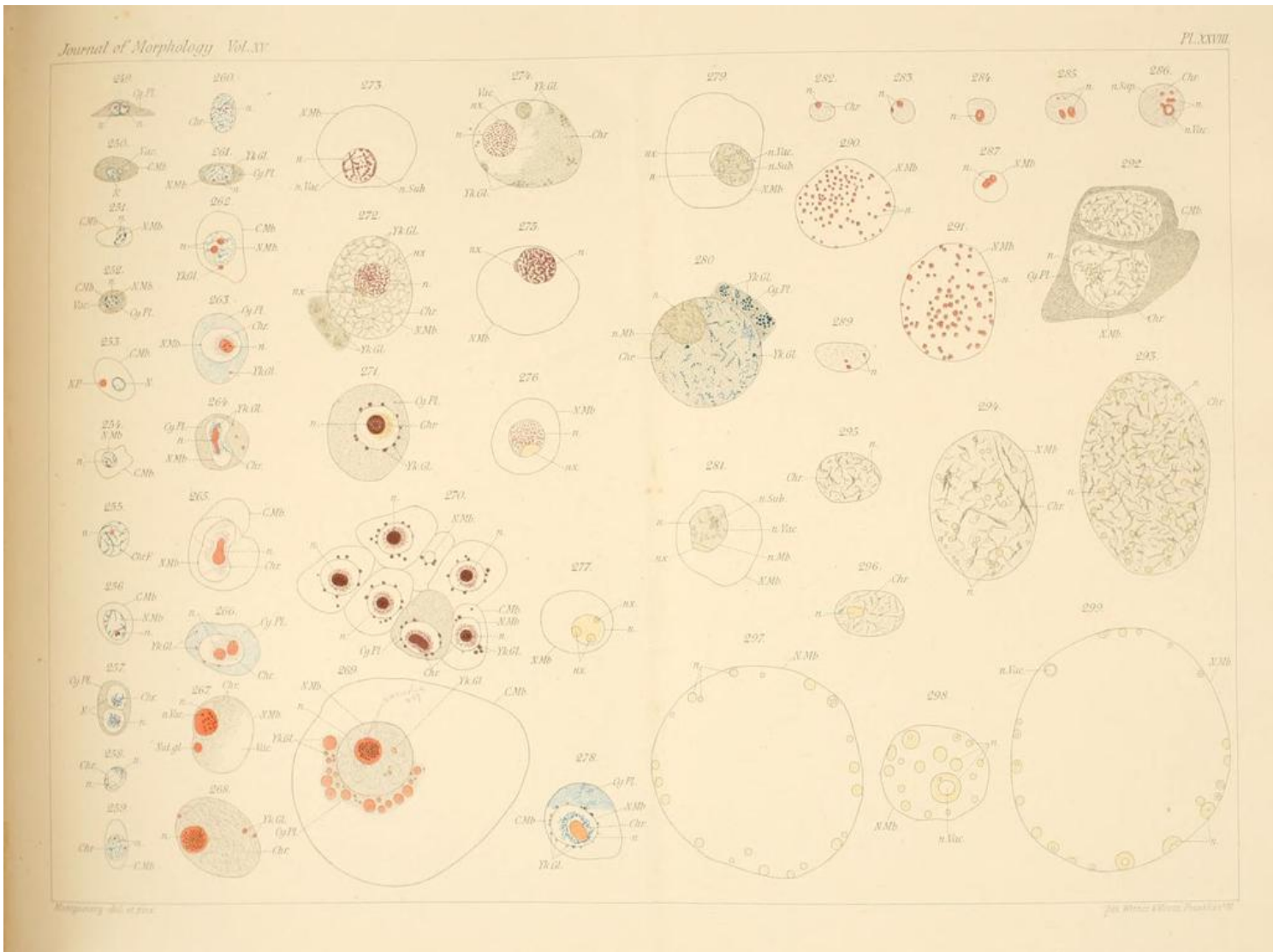
Figure 1.5. One of the illustration figure pages from the work by Thomas Montgomery in 1898 titled '*Comparative cytological studies, with especial regard to the morphology of the nucleolus*'. The page shown in this figure is Plate XXXVIII and includes drawings for egg development in *Polydora*, a genus of marine polychaetes (Plate Figures. 249-281). Also included, are drawings for egg development in *Tetrastemma elagans*, a species of marine nemertean, (Plate Figures. 282-299).

Labels in the drawings include *Chr* (chromatin); *C. Mb* (cell membrane); *Cy. Pl* (cytoplasm); *N* (nucleus); *N. Mb* (nuclear membrane); *n* (nucleolus); *n. Mb* (nucleolar membrane); *n. Sub* (nucleolar ground substance); *n. Vac* (nucleolar vacuole); *nx* (nucleolar body of unknown origin) (Montgomery 1898; Biodiversity Heritage Library website).

1.2 Chromosome Organisation and Dynamics

In interphase nuclei, chromosomes are situated in non-random locations known as chromosome territories (Cremer and Cremer 2001; Fritz et al. 2016) which are bordered by a perichromatin region at the very periphery of each chromosome territory. The structure of the perichromatin region of chromosome territories consists of chromatin in a decondensed state (Fakan and van Driel 2007). Separating the territories is the interchromatin compartment (IC) which is a network of channels that is mostly DNA free and contains various nuclear bodies and structures required for nuclear functions (Bridger et al. 1998; Reviewed by Foster and Bridger 2005; Albiez et al. 2006; Cremer and Cremer 2010) (Figures 1.6 and 1.7). The IC has also been shown to contain RNA transcripts which were described as residing in a reticular interchromosomal domain (ICD) compartment (Bridger et al. 2005). The description of the ICD compartment is the origin of the IC description and first appeared in work by Zirbel et al. (1993) where a model for the functional compartmentalisation of the nucleus was proposed, which included an interchromosomal network where transcription and splicing occurs (Figure 1.7). In very interesting work, Bridger et al. (1998) used *Xenopus* derived vimentin with an NLS to stably transfect human cells in order to further study the ICD compartment and found that the vimentin is detectable as speckles in the nucleus, and subsequently forms filamentous arrays which were associated with the ICD compartment and separate from the chromosome territories, thus further confirming the ICD compartment as a functional domain in the nucleus, and adding robustness to the existence of what we now refer to as the Interchromatin compartment (IC) which continues to be explored.

Some models of the organisation of chromosome territories exclude the IC and this is part of some controversy regarding the detailed architecture of chromosome territories in nuclei (reviewed by Cremer et al. 2006; Cremer and Cremer 2010). It comes as no surprise that the detailed architecture of chromatin organisation in relation to the layout of the rest of the nuclear structure has been difficult to establish conclusively. Such an endeavour is approaching the very limits of biological structure in terms of scale when we explore the detailed structural arrangement between the borders of chromosome territories. Interestingly, authors Rouquette et al. (2009) studied the detailed architecture of the nucleus using advanced electron microscopy

methods and were able to show that the 3-dimensional arrangement and distribution of chromatin in the nuclear space allows for a considerable volume for the interchromatin space which could be attributed to the IC.
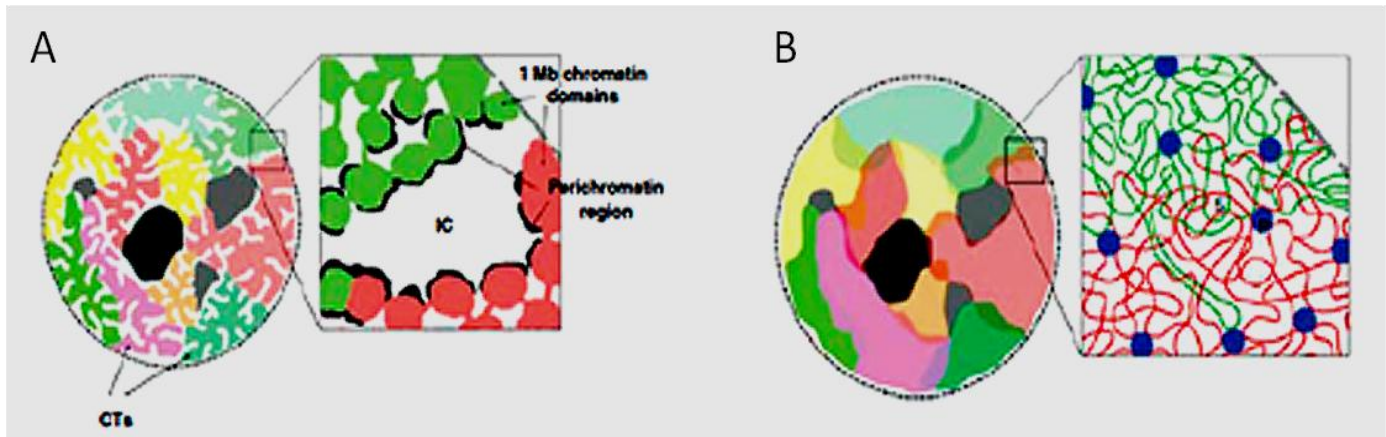
Figure 1.6. An illustration of the organisation of chromosomes in interphase nuclei. Two models of this organisation are shown in this figure. (A) This model includes the Interchromatin Compartment (IC) which separates the chromosome territories, which are bordered by the perichromatin region. (B) This model excludes the IC and instead consists of Interchromatin networks of intermingling chromatin including between adjacent chromosome territories (blue dots show areas of contact between chromosomes. (Taken from Cremer and Cremer (2010).
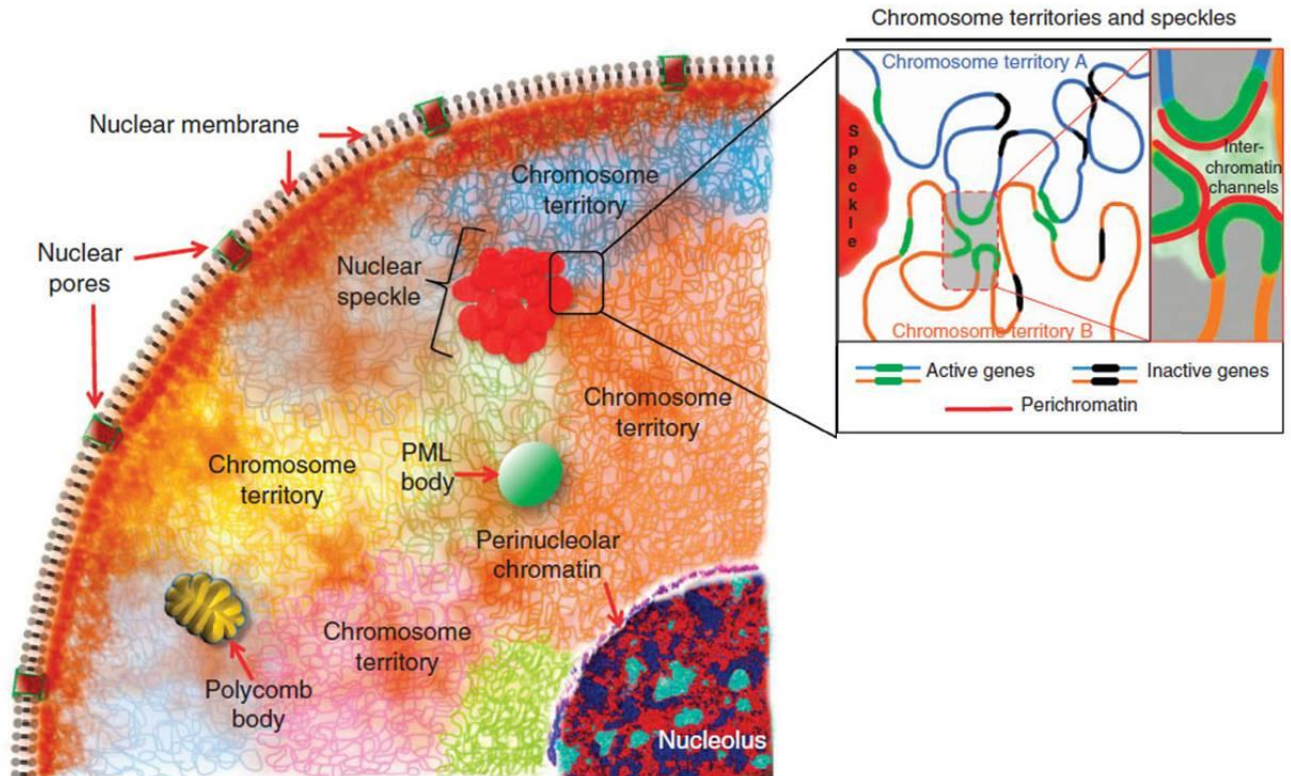
Figure 1.7. Illustration demonstrating the arrangement and organisation of chromosome territories. Also showing in more detail, the separation of two chromosome territories at regions of interchromatin channels, where active genes within the perichromatin regions are shown. These active genes are shown to be positioned in the vicinity of a nuclear speckle, where pre-mRNA splicing would occur after transcription at transcription factories, which are not shown in this illustration. (Taken from Botchkarev et al. 2012).

Chromosome territories are not permanently static, in fact chromosomes and specific gene loci within them can change location and are therefore dynamic structures (Reviewed by Bridger 2011). These chromosome and gene dynamics can be activated depending on a cell's physiological state (Bridger et al. 2000; Mehta et al. 2010), for example in proliferating and non-proliferating cells, or when cells are differentiating (Szczerbal et al. 2009). Also, in situations where a cell nucleus is affected by a genetic disease such that its architecture and function are altered, chromosome territories change compared to normal cells (Bridger et al. 2014). Mis-

19

localised chromosome territories are seen in the cell nuclei of individuals with the rare premature ageing disease, Hutchinson-Gilford Progeria Syndrome (HGPS), which is caused by a mutation in the *LMNA* gene, resulting in a mutant form of lamin A protein called Progerin (Mehta et al. 2011). It has also been shown that cells affected by infection show movements of specific gene loci as a result of the infection (Knight et al. 2011; Arican-Goktas 2014).

Considering chromosome and gene dynamics from a broader whole organism perspective, it is important to appreciate that despite all cells within an organism containing the same set of genes in their genome, gene expression is highly spatio-temporally dependant. Different cells within an organism express different sets of genes depending on their function and physiological state in specific tissues (Melé et al. 2015; Sonawane et al. 2017; Borsari et al. 2021). It is therefore crucial for the chromosomes in cell nuclei to be highly organised and regulated by control mechanisms. These regulatory systems function at many levels including dynamic changes in the 3-dimensional configurations of chromosomes under different physiological states. For this orchestration of gene expression to function, it is required for the genetic information in the chromosomes to be made available to transcription factories in a dynamic and highly reliable manner, particularly when a set of genes that may even be on different chromosomes need to be co-expressed in cells. Chromosome organisation has been found to consist of various chromatin compartments and domains at different scales pertaining to each chromosome. This adds further layers of order and compartmentalisation, and allows for gene regulation at the chromosome topological level to proceed. At the larger physical scale, this organisation within individual chromosomes, involves preferential long-range chromatin interactions, consisting of two compartment types. One is composed of open and active chromatin, referred to as "A" compartments. The second, referred to as "B" compartments, is composed of inactive chromatin in a closed state (Fortin and Hansen 2015; Szabo et al. 2019). At the smaller physical scale, in the region of tens to hundreds of kilobases, chromosome organisation is composed of domains which again involve preferential chromatin interactions. These domains are referred to as topologically associating domains (TADs) (Dixon et al. 2016; Szabo et al. 2019; Rajderkar et al. 2023). TADs are important features of chromosome organisation and have a major influence on the orchestration of gene

expression. The disruption of TADs leads to gene misexpression which can cause developmental disorders and disease states such as cancer (Hnisz et al. 2016; Lupiáñez et al. 2016).

The movement of certain gene loci, as chromatin loop extensions for example, may involve the association of those loci with transcription factories (Bridger et al. 2014). An example of interchromosomal interactions in relation to gene expression is work by Spilianakis et al. (2005) where it was found that the promoter region and the regulatory region of two cytokine gene loci situated on different chromosomes associate physically in the nucleus. In another work by Osborne et al. (2004) it was shown that widely separated genes on mouse chromosome 7 colocalise to the same transcription factories during transcription and demonstrated that movement of these genes away from transcription factories was linked with cease of transcription. This latter finding is particularly significant as it demonstrates that transcription is occurring at the foci of transcription factories only, rather than at individual gene loci independently of recognised transcription foci. Research showing specific gene loci extending from chromosomes as chromatin loops includes the work of Volpi et al. (2000) where using the major histocompatibility complex (MHC) genes and other gene loci on chromosome 6, they demonstrated large chromatin loops extending from chromosome 6 with a frequency dependant upon the level of transcription as regulated by interferon-gamma (IFN-γ). In another finding that demonstrates the extension of chromatin loops from a chromosomal territory in expressed gene complexes, the epidermal differentiation complex (EDC) on chromosome 1 was shown to be positioned away from the chromosome territory in keratinocytes where the EDC genes are highly expressed, but in lymphoblasts where the EDC genes are silent, a more peripheral or internal location was observed (Williams et al. 2002). In a study using cell differentiation in keratinocytes to study chromosome dynamics in relation to gene expression, it was found that during differentiation, significant changes occur in the radial arrangement and morphology of chromosomes 18 and 19, as well as interchromosomal associations between these chromosomes (Marella et al. 2009). Differentiating cells are very dynamic in their gene expression profiles and this work shows that chromosomal dynamics is directly related to gene expression dynamics, therefore highlighting a crucial role for 3-dimensional configuration of chromosomes in gene regulation.

1.3 Molecular Motors; Myosins

The generation of force at the cellular level in eukaryotic cells, involving for example the beating of flagella or cilia in protozoa (Roncaglia et al. 2017), leading to whole cell mobility, and chromosome segregation during mitosis, involves adenosine triphosphate (ATP) hydrolysing molecular motors. In the eukaryotic cell, molecular motor proteins interact with the dynamic cytoskeleton by association with actin and microtubules, and contribute to the overall cell structure and dynamics (Hartman et al. 2011). These dynamics for example include the transport of organelles by microtubules, by interaction with motor proteins, as well as the functional cooperation of microtubules and actin filaments in association with their motor proteins. These bring about various dynamic movements such as directed cell migration and nuclear migration (Goode et al. 2000; Schenk et al. 2009). There are three large superfamilies of molecular motor proteins which are classified as the myosins, dyneins and kinesins (Figure 1.8), associated with two different polymers, these being actin filaments or microtubules (Huitorel 1988; Woolley 2000; Richards and Cavalier-Smith 2005; Sperry 2007). Figure 1.8 demonstrates examples of these three types of protein motors which have been structurally and functionally studied extensively. Kinesin motors move towards the plus end of microtubules and the dynein motors move towards the minus end of microtubules, while the myosin motors move along actin filaments in the direction of the plus end, with the exception of myosin VI which moves towards the minus end (Mallik and Gross 2004; Hartman et al. 2011). Interestingly it has been found that in some organisms, two different classes of molecular motors function together to bring about the biomechanical motion. For example the flagella of *Chlamydomonas* function by the action of both dynein and various kinesins (Bernstein and Rosenbaum 1994). Our knowledge of these intracellular molecular motors had since before the 1970s been confined to the cytoplasm without any involvement of the nucleus, partly because the cytoplasm of the cell has been more accessible to research methods compared to the nucleus, which had been metaphorically described as a 'black box' due to the many unknowns regarding its structural organisation and functional details (van Driel et al. 1991).
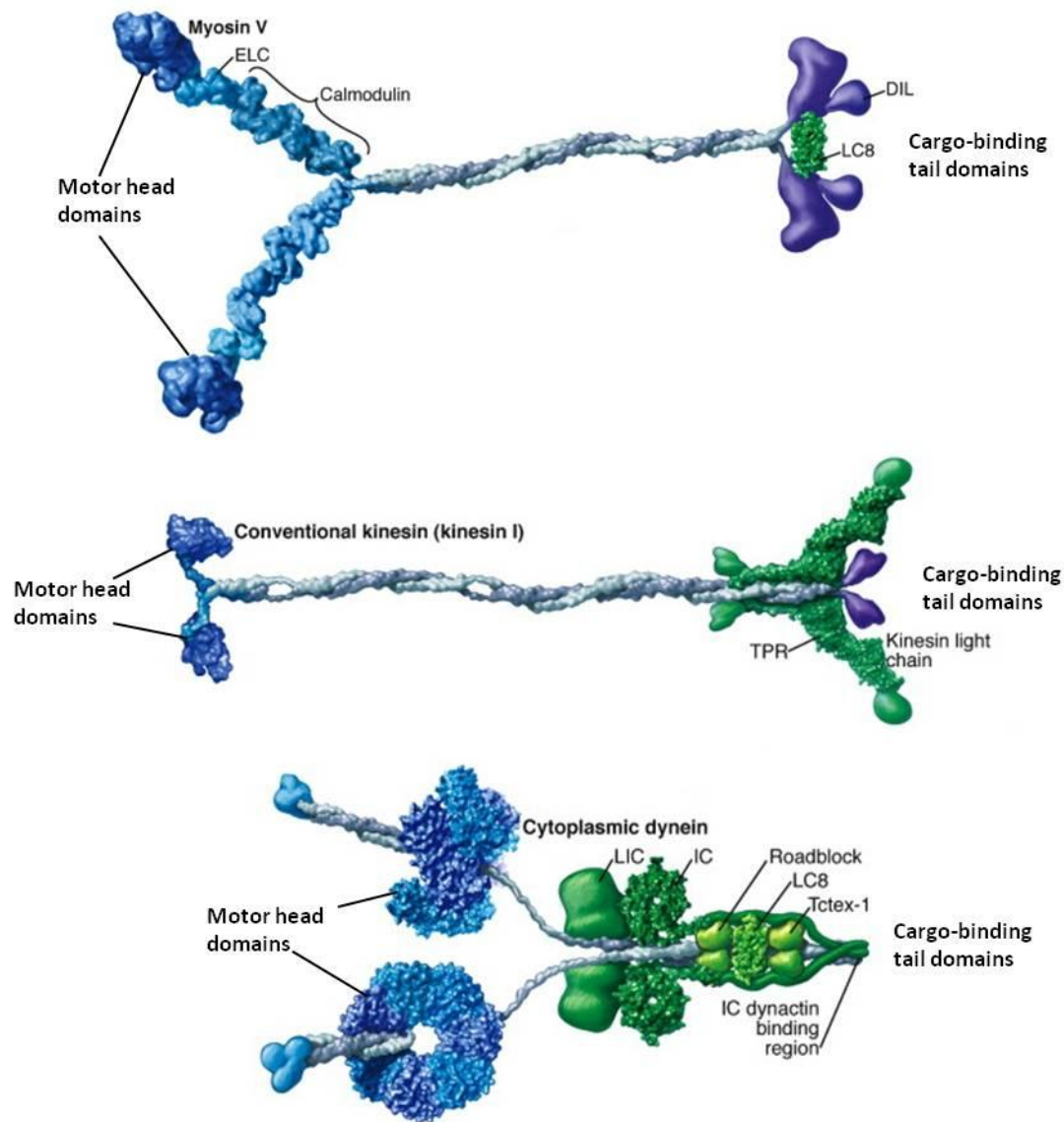
Figure 1.8. Examples of the three main types of molecular motors found in cells; myosins, kinesins and dyneins, represented here by myosin V, kinesin I and cytoplasmic dynein, respectively. Figure Abbreviations: DIL (dilute domain); LC8 (dynein light chain 8) which is also found in myosin 5a (Rapali et al. 2011); ELC (essential light chain) (Hernandez et al. 2007); TPR (tetratricopeptide repeat domain) (Kawano et al. 2012); IC (intermediate chain), LIC (light intermediate chain) (Mische et al. 2008). Roadblock and Tctex-1 are light chains. (Modified from Vale 2003; Phillips et al. 2012).

Increasing Interest in the possibility of active ATP dependant intranuclear mobility of various components gradually grew as the probability of this was realised to be high. This in part followed from the logical conclusions that although some mobility

processes known in the cytoplasm are due to Brownian motion, it is unlikely that this process can be in large part responsible for the orchestration of the myriads of dynamic molecular interactions occurring in the nucleus. The logic behind this stems partly from the knowledge of the compact nature of the nucleus resulting in macromolecular crowding. This makes reliance on simply Brownian motion which is random movement resulting from the thermal energy of molecules being translated to kinetic energy, as the main mode of molecular mobility, unfeasible and improbable (Carmo-Fonseca et al. 2002; Dion et al. 2010).

The myosins have been a crucial cellular component of eukaryotes since the origin and evolution of the first eukaryotic cells. The genome of the last eukaryotic common ancestor (LECA) has been estimated to have contained about six myosin genes (Sebé-Pedrós et al. 2014). Larger numbers of myosins are found in even primitive multicellular organisms such as the slime mould *Dictyostelium discoideum*, which is an important model organism for actin related motile processes, and has been estimated to contain thirteen myosin genes (Kollmar 2006). The myosin superfamily is composed of the conventional myosins (class 2 myosins) and the unconventional myosins. The conventional myosins were the first to be discovered and were found to be involved in muscle function, such as in the skeletal muscles and the cardiac muscles, but they were also found to have diverse non-sarcomeric functions in cells (Chantler et al. 2010). The conventional myosins have the characteristic feature of forming bipolar filaments by oligomerization (Woolner and Bement 2009). Myosins discovered subsequent to the initial discovery of the class 2 myosins were termed unconventional myosins, mainly for historical reasons (Woolner and Bement 2009). The myosins have been classified into over 30 classes and 12 of these classes are found in humans and comprising 40 genes, the majority of which encode unconventional myosin proteins (Richards and Cavalier-Smith 2005; Odronitz and Kollmar 2007; Fili and Toseland 2019). The general molecular structure of the myosin proteins consists of the motor head domain, a neck region domain and a tail domain. The highly conserved catalytic N-terminal actin binding head domain, contains the motor activity components of the protein (Figure 1.8). The neck region domain consists of a helical structure, and contains light chains of the calmodulin family (Figure 1.8). Thus the neck domain has a regulatory role and it also affects the physical and mechanical characteristics of the protein, in response to the activity of

the motor head domain (Batters and Veigel 2016; Fili and Toseland 2019). The C-terminal tail domain has cargo binding functions and also influences the oligomerization state of the myosin (Figure 1.8) (Krendel and Mooseker 2005).

Actin and myosin had been found in nuclei since the early studies of the nucleus, but it was not possible to confirm the presence of these molecules as intrinsic to the nucleus and they were considered as being artefacts of contamination from the cytoplasm, but with development of more advanced and powerful techniques including electron microscopy and fluorescence microscopy, the presence of these proteins in the nucleus has been firmly confirmed (Nowak et al. 1997; Dingova et al. 2009; Reviewed by Bridger 2011; de Lanerolle and Sererebrannyy 2011; de Lanerolle 2012; Falahzadeh et al. 2015; Percipalle and Vartiainen 2019; Maly and Hofmann 2020). The unconventional myosins that have been found in the nucleus include myosin I, nuclear myosin I (NMIβ), myosin Va, myosin Vb, myosin VI, myosin X, myosin XVI and myosin XVIIIB, with two conventional myosins known as non-muscle myosin IIA and non-muscle myosin IIB (Cook et al. 2020; Shahid-Fuente and Toseland 2023). Despite the confirmation of the presence of myosins in the nucleus, the assignment of function for these has understandably not been easy and subject to much speculation, for example as motors to power the elongation stage of pre-mRNA synthesis during transcription (de Lanerolle et al. 2005).

A considerable amount of evidence has been accumulating to indicate that the movement of whole chromosomes (Kuroda et al. 2004; Foster et al. 2005) and specific gene loci (Dundr et al. 2007) in nuclei at interphase, may involve motor proteins such as for example nuclear myosin 1β (NM1β) (Chuang et al. 2006; Hu et al. 2008; Mehta et al. 2010). This is within the framework of the many observations of the dynamic movements of whole chromosomes and gene loci in interphase nuclei as described in section 1.2 of this chapter. It is entirely reasonable to expect that directed and dynamic mobility of chromosomes and parts of chromosomes in the nucleus is brought about by ATP hydrolysing molecular motors, since as previously stated, intracellular mobility in general is known to involve the action of motor proteins. It has been shown that nuclear myosin 1β (NM1β) is indeed involved in chromosome mobility (Mehta et al. 2010) and is therefore a very interesting protein for investigations related to protein motor activity in nuclei. In the work by

Mehta et al. (2010) it was found that quiescent primary fibroblast cells which had been induced to quiescence by low serum (0.5% FCS) in their growth media, show repositioned chromosomes compared with proliferating primary fibroblast cells. Specifically, chromosomes 13 and 18 relocate to an interior position from a peripheral position in the nucleus, and chromosome 10 relocates to a peripheral position from an intermediate position in the nucleus. Some chromosomes did not change their location at all in response to low serum (0.5% FCS) media conditions, for example chromosomes X, 17 and 19 did not reposition. Interestingly it was found that the chromosome relocations took less than 15 minutes following exposure to low serum (0.5% FCS) media and this was an energy requiring process. Crucially this chromosome repositioning was inhibited by chemicals that affect the polymerisation of myosin and actin, and by inhibition of NM1β by RNA interference techniques (Mehta et al. 2010). The fibroblasts in this study were most probably responding to the change in growth conditions of their immediate environment following exposure to low serum (0.5% FCS) in their media.

The response of cells to a stimulus involves an alteration in the gene expression profile of those cells. Such alterations in gene expression are dependant upon the nature of the stimulus, which in turn induces the required specific genomic response. For example, in response to low serum (0.5% FCS) media conditions, only certain genes on particular chromosomes would be involved in the regulatory action which needs to be spatiotemporally precise and non-random. Other stimuli may induce a different set of chromosomes to relocate as part of the regulatory response.

1.4 Cellular Quiescence and Senescence

Cells are physiologically dynamic structures which can adopt various states depending on several environmental, as well as intrinsic factors such as cell type and age. Four main physiological states that are recognised in cells (Johnson and Cook 2023), both in vivo and in vitro are proliferation, quiescence, senescence and terminally differentiated. Proliferation is where cells are actively dividing and possibly differentiating, and quiescence is where cells exit the cell cycle and cease to divide, a phase referred to as G0 or resting phase in relation to the cell cycle (Figure 1.9). Quiescence can occur for example when cells are in a low nutrient environment or when contact inhibited (Abercrombie 1970; Gos et al. 2005), and it is also the state of stem cells (van Velthoven and Rando 2019). Quiescent cells may re-enter the cell cycle, leaving the G0 resting phase and become proliferating cells again, for example when nutrients become available again at sufficient levels. The third physiological state known as senescence is generally accepted to be when cells have permanently exited the cell cycle, and is also associated with cellular ageing (Baker et al. 2011). The fourth cellular state which is another permanent non-proliferative state, is the terminally differentiated cellular state, also involving cell cycle exit, which usually occurs at G0 (Figure 1.9 B). Terminally differentiated cells include for example neurons and keratinocytes (Fujiwara et al. 2016; Marescal and Cheeseman 2020; Smits et al. 2021). The senescence cell cycle arrest occurs mainly at G1 (gap 1) stage of the cell cycle but may also occur at the G0 stage, following a period of quiescence (Figure 1.9 B), and at G2 (gap 2) stage of the cell cycle (Mao et al. 2012; Gire and Dulic 2015). Quiescent cells also commonly exit the cell cycle at G1 to rest at G0 (Figure 1.9) but may also exit at G2 to rest at G0 (Johnson and Cook 2023). The quiescent cellular state and the senescent cellular state can broadly be categorised as non-proliferating cellular states, where cell cycle arrest has occurred, although there are significant differences between these two states.

Normal cells naturally have a finite lifespan and this is related to the number of cell replications that have occurred in the lifetime of the cell and is affected by progressive telomere shortening in the chromosomes. This type of senescence is referred to as replicative senescence and has a different cause to premature

senescence, also referred to as stress induced senescence (Bito et al. 2010; Beck et al. 2020; Kaur et al. 2021) which may be brought about by various external factors such as cellular stress damage (Kuilman et al. 2010; Maeda et al. 2015; Tai et al. 2017). The fact that cells naturally have a finite lifespan and eventually will stop dividing due to a senescence phase was hypothesized in the early 1960s by Leonard Hayflick and Moorhead (1961) and further elaborated by Leonard Hayflick in 1965.
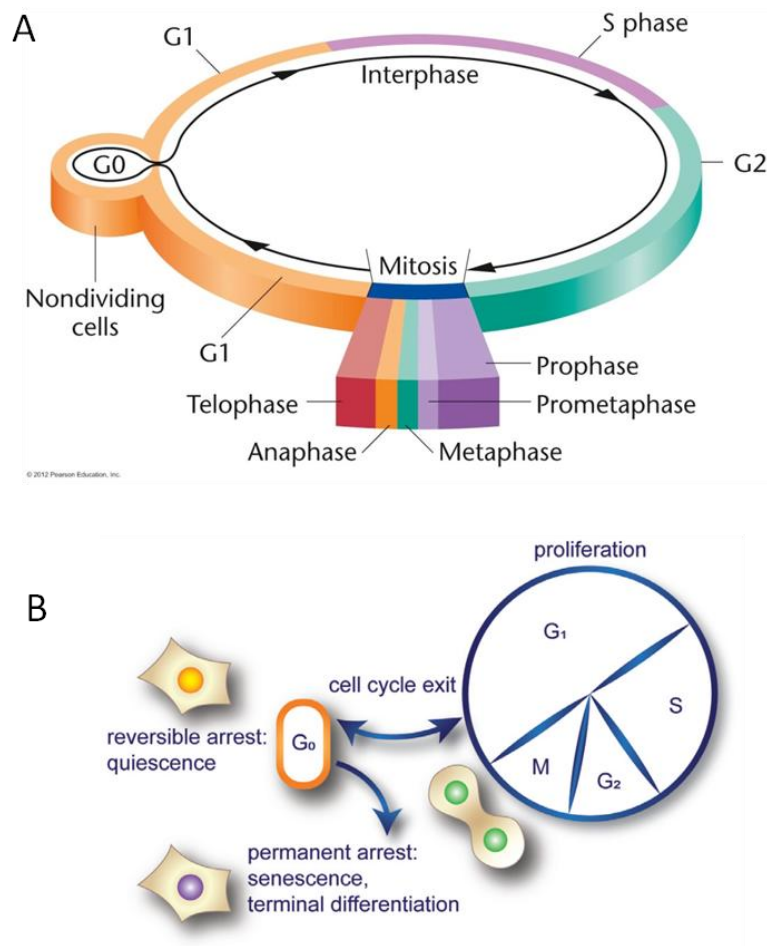

Figure 1.9. Schematic diagrams of the cell cycle and cellular states. (A) Showing the various stages of the cycle including those at interphase and the phases of mitosis. (B) Showing the various cellular states in relation to the cell cycle. G0 represents reversible cell cycle arrest, shown in this figure via G1, although this may also occur via G2. Senescent cells are shown to exit from G0 but this also usually occurs directly from G1 or G2 (Johnson and Cook 2023).
G1 (gap 1), G2 (gap 2), M (mitosis), S phase (synthesis phase).
A (Pearson Education Inc.) Taken from:
(https://www2.samford.edu/~djohnso2/jlb/333/(01)division.html).
B (Taken from Johnson and Cook 2023).

There are several biomarkers associated with the senescent state and these are useful and powerful molecular tools, to help determine senescence in cells. The activation of two main tumour suppressor pathways is associated with senescence and these are the p53/p21$^{WAF1/CIP1}$ pathway and the p16^{INK4A}/pRB pathway (Kumari and Jat 2021). Another biomarker used to determine senescence is senescence-associated-beta-galactosidase (SA-β-gal). It is important to note however that despite their usefulness, there are complications with regards to how these senescence biomarkers may be interpreted (Sharpless and Sherr 2015; Paramos-de-Carvalho et al. 2021). For example, one of the biomarkers considered among the most reliable indicators of senescence is the tumour suppressor protein p16^{INK4A} however, it has been shown that not all senescent fibroblast strains display altered RNA expression levels of this marker protein, and this is in keeping with the increasing realisation that some known senescence biomarkers are not universally applicable (Hernandez-Segura et al. 2017). Also, it has been found that some senescent cells can be SA-β-gal negative, and to further complicate matters, some cells that are SA-β-gal positive, do not show senescence related p21^{CIP1} expression. Therefore, SA-β-gal is not always a reliable indicator of senescence (Lee et al. 2006; Huang and Rivera-Pérez 2014). One of the major and well recognised characteristics of senescent cells is a complex and multifaceted secretory programme, referred to as the senescence associated secretory phenotype (SASP). This hypersecretory phenotype involves the secretion of a variety of signalling factors, which include cytokines, chemokines, growth factors, bioactive lipids, matrix metalloproteinases (MMPs) and other proteases, which can collectively also affect nearby cells and lead to a propagation of cellular senescence in a given tissue (Acosta et al. 2013; Ghosh and Capell 2016; Lopes-Paciencia et al. 2019; Kumari and Jat 2021).

It has been shown that quiescent cells maintain high metabolic activity despite not needing to undergo cell division (Lemons et al. 2010). This is also true with regards to senescent cells considering the SASP, and terminally differentiated cells such as neurons and keratinocytes, which have important functions in the organism. Clearly, all the non-proliferative cellular states need to maintain a certain degree of metabolic activity despite the lack of cell division. It is important to consider that different cell types will show different physiological characteristics depending on their cellular

state and the environment in which they are experimented with. This may be part of the reason for the debate and contradictions in defining senescence and quiescence (Blagosklonny 2011). Quiescence has been found to be comprised of heterogeneous cellular states, which result from the nature of the quiescence inducing stimulus, as well as the cell type involved (Coller et al. 2006; Johnson and Cook 2023). It has also been shown that quiescence can differ with respect to being in 'shallow' or 'deep' quiescent states, with the suggestion that deep quiescence may be a type of transition state prior to senescence (Figure 1.9 B) (Fujimaki et al. 2019). The depth of the quiescence state is for example affected by the length of time that the cells have been in a quiescent state (Kwon et al. 2017).

All cellular non-proliferative states have important roles in controlling and regulating cell proliferation in an organism, and therefore help to prevent uncontrolled cell division, which for example is associated with cancer (Collado and Serrano 2010). The dynamic nature of quiescent cells such as stem cells for example allows for mechanisms of tissue repair and regeneration, in response to tissue damage (Falanga 2012). Senescence also plays a crucial role in embryonic development, and in coordination with other processes such as apoptosis, helps to shape embryonic tissues and organ systems (Muñoz-Espín et al. 2013; Rhinn et al. 2019; Wanner et al. 2021). Although the nature of quiescence and senescence are debated, it is undeniable that for example the process of ageing is directly related to cellular senescence and that senescence is one of the outcomes of the ageing process, where cells slow down the renewal cycle and lose capacity for various functions (Baker et al. 2011; van Deursen 2014).

1.5 Aims of Project

Our group has previously shown that nuclear myosin 1b (NM1β) is involved in interphase chromosome mobility (Mehta et al. 2010), and as a result, this has generated a strong interest to further investigate other potential proteins, that may be related to protein motor activity in cell nuclei. In view of the need to further characterise the complexity of the nucleus, and demonstrate its modes of action in relation to genome regulation, this finding that NM1β is involved in nuclear motor activity, is largely the inspiration for this PhD project. A main aim in this project was to compare the presence and frequency of various nuclear located myosin proteins that may be involved in interphase chromosome dynamics, in proliferating and non-proliferating cells. Another main aim was to study the response of chromosomes, in proliferating and non-proliferating cells, to stress stimuli with regards to whole chromosome repositioning. Specifically, to investigate the ability of chromosomes in the interphase nuclei of fibroblast cells to relocate in response to low nutrient conditions and heat shock stimuli. These studies help to explore the hypothesis that in non-proliferating cells, chromosome repositioning does not occur, due to reduced functionality of the molecular motors involved. Also, another aim in this project, using bioinformatics, involved exploring and identifying other candidate proteins such as myosins, and various other proteins known to be located in the nucleus, and in some cases, possibly indirectly involved in the mechanisms that may play a role in active chromosome dynamics in the nucleus. It was also of interest to explore the possibility that the age of cells has an effect on their ability to relocate chromosomes in response to stimuli.

Chapter 2: Candidate nuclear motor proteins compared in proliferating and non-proliferating cells

2.1 Introduction.

2.2 Materials and methods.

2.3 Results.

2.3.1 Detection of candidate myosin motor proteins (antibody test phase) in nuclei of cells grown in high serum (15% FCS) media, by indirect immunofluorescence, using single primary antibodies.

2.3.2 Detection of candidate motor proteins in nuclei of proliferating and non-proliferating cells grown in high serum (15% FCS) media, by indirect immunofluorescence, by dual staining with primary antibodies including anti-Ki-67.

2.3.3 Detection of nuclear myosins in nuclei of quiescent cells grown in low serum (0.5% FCS) media.

2.3.4 Experiments to determine co-localisation of SC35 with nuclear myosins in cells grown in high serum (15% FCS) media.

2.4 Discussion.

2.1 INTRODUCTION

In order to investigate the involvement of possible candidate proteins in the movement of interphase chromosomes, it was decided to select and study a number of myosins known to be predominantly localised in the nucleus. This is clearly a logical approach as the involvement of such proteins that may have a role as molecular motors in the nucleus, is likely to include highly specific proteins and possibly with mechanisms quite separate from those found in the cytoplasm. Therefore myosins found equally in the cytoplasm and the nucleus would not be as interesting, although the involvement of even those proteins in any mechanisms of chromosome mobility could not be completely ruled out. There is extensive transport of many molecules across the nuclear envelope and it may be possible for proteins to carry out functions in the cytoplasm and be recruited to the nucleus when required for nuclear functions. The more feasible situation however in terms of the cell's energy expenditure for example and the requirement for dynamic chromosome movements to be closely and rapidly regulated would certainly suggest a nuclear location for the candidate proteins, possibly in an inactive conformation in a storage state such as granules which dynamically can switch between active and inactive forms as needed to carry out their functions. This level of spatiotemporal organisation of intranuclear components is crucial in the highly compact nucleus where space is limited and many combinations of processes are occurring, making the most efficient and coordinated organisation of the nucleus a necessity. Of course it would be expected that these nuclear proteins would have originated in the cytoplasm, however it may even be possible that some of these proteins may have originated in the nucleus, following the suggestion and considerable evidence that translation could be occurring within the nucleus, specifically in the nucleolus. This was briefly mentioned in the general introduction of this thesis (David et al. 2012; Reid and Nicchitta 2012; Mcleod et al. 2014; Theodoridis et al. 2021).

The candidate nuclear located myosins chosen to be studied in this chapter, that may be involved in chromosome mobility, include myosin 5b (MYO5B), myosin 16 (MYO16) and myosin 18b (MYO18B). These three myosins were selected primarily because they have been shown to be predominantly located in the nucleus (Salamon et al. 2003; Lindsay and McCaffrey 2009; Cameron et al. 2013). Although

there are a few other known nuclear located myosins in humans (see section 1.3), such as myosin 5a (Pranchevicius et al. 2008) and myosin 6 (Vreugde et al. 2006) for example, it was not feasible to study all the nuclear located myosins, and therefore only a subset was selected, with the view of studying all the other nuclear myosins in future work. MYO18B is a myosin heavy chain protein (Salamon et al. 2003) and when expressed in the nucleus, may be involved in the regulation of muscle related genes and is therefore very specific in its mode of action. MYO16 may be involved in cell cycle progression and proliferation, although the precise roles of MYO16 in the nucleus are not fully understood (Cameron et al. 2013). Generally, the expression of MYO16 is known to be mainly in the nervous system, where it may be involved in the development and physiology of the nervous system (Telek et al. 2020). MYO5B has been associated with various roles in the cell, and these include vesicle and membrane trafficking, involvement in transcription via RNA polymerase I interaction, and control of cell polarity (Lindsay and McCaffrey 2009; Thoeni et al. 2014).

In the initial experiments with these myosins it was desired to first confirm and demonstrate that using the selected specific antibodies, these myosins are in fact predominantly nuclear specific and that their staining patterns could be observed and characterised for subsequent experiments. The data for these initial experiments with the single antibodies were not quantified since this phase of the experiments was a testing phase, and of a qualitative nature with regards to confirmation of nuclear myosin staining observation, or the lack of such staining. Therefore, quantification was not deemed necessary. Also, as the staining patterns for these myosins are shown from subsequent experiments where dual staining experiments were performed using Ki-67 as marker of proliferation, it was not deemed necessary to show image figures of the test phase results, as this would be somewhat repetitious. The use of Ki-67 antibody was a very important aspect of the experiments performed for this chapter, since one of the key cellular principles relevant to this project, is that since proliferating and non-proliferating cells differ in their gene activity and therefore physiological states, this would require these distinct cellular states to have different gene expression requirements. These differences would in turn be reflected in the structures and mechanisms that regulate their chromosome organisation and dynamics at interphase. Therefore a main focus of

the experiments carried out was comparative in nature and aimed to determine the differences between the nuclei of proliferating and non-proliferating cells with regards to the levels of antibody staining, and therefore visible protein levels for the myosins studied.

In another aspect, a set of experiments for this chapter involved the comparison between the nuclei of proliferating and quiescent cells, which were induced to the quiescence state by growth in low serum (0.5% FCS) media conditions. It is important to note here that this was in contrast to the growth conditions used for the formerly mentioned experiments, which involved comparing proliferating cells with non-proliferating cells, since only high serum (15% FCS) media was used for growth of these cell cultures, and the only experimental variable being the effect of the cellular state on the nature of the myosin staining.

Experiments were also carried out to investigate the possible co-localisation of the myosins with SC35 to determine if the myosins may be associated with splicing speckles. This information would be of interest and would help shed light on the various functions of the nuclear myosins studied. It is important to highlight here that although some functions have been attributed to or suggested for the nuclear myosins, many of them have yet to be assigned clear and robustly studied functions in the nucleus.

Our group has previously shown that nuclear myosin 1β (NM1β) is involved in chromosome mobility (Mehta et al. 2010) and as a result, this has generated an interest to further investigate other nuclear myosins that may be involved in protein motor activity in nuclei, for the process of chromosome mobility. These other proteins may potentially be components of other active mechanisms of chromosome mobility separate from that involving NM1β. It is possible that several different molecular motors are involved in the movement of chromosomes.

2.2 MATERIALS AND METHODS

2.2.1 Cell culture and indirect immunofluorescence

The cells used in all experiments are human neonate foreskin fibroblast cells known as the NB1 (New Brunel 1) cell line developed by Fiona Bolland at Brunel University London (Bridger and Kill 2004). These are primary cells and have been maintained in plastic 10 cm cell culture dishes with Dulbecco's Modified Eagles Medium (DMEM) (supplemented with 15% foetal calf serum (FCS) for high serum media or 0.5% FCS for low serum media; and 2% Penicillin/Streptomycin), placed in a humidified incubator at 37°C and 5% CO_2. Cell cultures were passaged routinely twice a week by trypsinisation and new cultures were setup at a cell density of 2 x 10^5 in 10 ml of media in 10 cm plastic cell culture dishes. For cells grown on coverslips, round glass 1 cm coverslips were first placed inside the cell culture dishes before adding media and cells to the dishes. These cells were grown under the same conditions described above. These cultures grown on coverslips, were allowed to reach approximately 60-70% confluence regarding the cells attached to the coverslips, before being washed three times with PBS after media removal and fixed with ice-cold 1:1 (v/v) methanol:acetone for 10 minutes, with the cell culture dish placed on ice. Then the fixed cells on the coverslips were washed three times with PBS, followed by transfer of each coverslip using fine forceps (cells side facing up) to a moist chamber. This chamber consisting of damp filter paper inside a petri dish with a cover, and a numbered grid system to allow assignment of each coverslip, with fixed cells attached, for a given staining regime with regards to the antibody combinations to be applied, in preparation for antibody staining for indirect immuofluorescence.

The antibody staining for indirect immunofluorescence was as follows; 10 µl of Primary antibody diluted in 1% FCS/PBS, was added to each coverslip and incubation was for 1 hour at room temperature or overnight at 4°C. Then the coverslips were washed 27 times with PBS before the addition of 10 µl of the secondary antibody (diluted in 1% FCS/PBS) to the coverslips. Then incubation was carried out in the dark for 1 hour at room temperature, and the coverslips were washed a further 27 times with PBS followed by one final wash with ddH_2O. Staining

for visualisation of cell nuclei was carried out by 1.5 µg/ml 4', 6-Diamidino-2-phenylindole (DAPI), the DNA intercalator dye in the Vectashield mounting medium (Vector Laboratories). The mounting medium was applied as a drop to glass microscope slides prior to transfer of coverslips to the microscope slides, with cells side facing down and therefore in contact with the medium and microscope slide. For microscopy and image capture, slides were viewed and photographed in fluorescence mode using a Zeiss Axioskop 2 microscope (100x oil immersion objective lens selected), with attached Jenoptik ProgRes digital camera, or viewed and photographed in fluorescence mode using a Leica DM4000 microscope (100x oil immersion objective lens selected), with attached Leica digital camera. In some experiments, manual counts of the number of proliferating and non-proliferating cells with or without nuclear staining for the motor proteins were performed during observation by fluorescence microscopy. In other experiments, manual counts of the number of visible foci of motor protein staining in indivudual nuclei of proliferating and non-proliferating cells were performed during observation by fluorescence microscopy. The statistical analyses of these results were performed by unpaired t-test using the GraphPad Software.

2.2.2 Experiments to detect candidate myosin motor proteins in nuclei of cells in high serum (15% FCS) media, by indirect immunofluorescence, using single primary antibodies (antibody test phase)

NB1 cells were cultured in dishes, on coverslips in DMEM media as described in section 2.2.1, with FCS at 15% (high serum) before being fixed (section 2.2.1). The myosin antibodies planned to be used in the indirect immunofluorescence experiments for comparing proliferating and non-proliferating cells, were qualitatively tested to ensure that they show the nuclear localisation of the myosins and therefore could be used in the subsequent dual antibody experiments. If positive antibody detection in the nucleus was confirmed then the antibody test phase was concluded. MYO16 antibody was prepared to 2 µg/ml (dilution equivalents are given in Table 2.1) following manufacturer advice (Table 2.1). MYO5B and MYO18B antibodies were diluted to 1:100 (v/v). The secondary antibody used was donkey anti-rabbit conjugated with Tetramethylrhodamine (TRITC) and at 1:100 dilution (v/v). Each fixed coverslip culture was treated with a single primary and corresponding single secondary antibody. Primary antibody incubation was for 1 hour at room temperature and secondary antibody incubation was for 1 hour in the dark at room temperature.

Table 2.1. The myosin primary antibodies used. All antibody dilutions were made using 1% FCS in Phosphate Buffered Saline (PBS). Note that in these experiments only single primary antibodies were used, but in subsequent experiments Ki-67 antibody was also used. The manufacturer of each antibody is shown in brackets. Secondary antibody abbreviations: D = Donkey, R = Rabbit.

Myosin primary antibody (Rabbit host for all antibodies)	Dilution	Secondary antibody D anti-R (TRITC) (Stratech) dilution
MYO5B (Atlas Antibodies)	1:100	1:100
MYO16 (Novus Biologicals)	1:100	1:100
MYO18B (Biorbyt)	1:100	1:100

2.2.3 Experiments to detect candidate myosin proteins in nuclei of proliferating and non-proliferating cells grown in high serum (15% FCS) media, by indirect immunofluorescence, by dual staining with primary antibodies including anti-Ki-67

NB1 cells were cultured in dishes, on coverslips in DMEM media as described in section 2.2.1, with FCS at 15% (high serum) before being fixed (section 2.2.1). The same antibody dilutions used in the antibody test phase (section 2.2.2) experiments were used for the myosin primary antibodies in these experiments. Primary antibody against Ki-67 was also used as a marker of cell proliferation. For Ki-67 the secondary antibody used was conjugated with Fluorescein Isothiocyanate (FITC) (Table 2.2). The controls for these experiments were single primary antibody stained cells, but without Ki-67 primary antibody (Table 2.2). These controls were mainly setup to confirm successful staining with single primary antibodies, in case the dual staining did not work. Primary antibody incubation was overnight at 4°C and secondary antibody incubation was for 1 hour in the dark at room temperature. Manual counts of the number of proliferating and non-proliferating cells (Ki-67 +ve or Ki-67 -ve, respectively) with or without nuclear staining for the myosin proteins were performed. Manual counts of the number of visible foci of myosin protein staining in indivudual nuclei were also performed.

Table 2.2. Description of the primary and secondary antibody combinations with dilutions used, in the dual antibody staining experiments. For the main treatments (dual staining) each myosin primary antibody and Ki-67 primary antibody were mixed and applied combined, as were the secondary antibodies also mixed and applied combined. All antibody dilutions were carried out using 1% FCS in PBS.
Manufacturers of antibodies shown in brackets.
Secondary antibody abbreviations: D = Donkey, G = Goat, M = Mouse, R = Rabbit.

Myosin primary antibody (Rabbit host for all antibodies)	Myosin antibody dilution	Ki-67 primary antibody (Abcam) (Mouse host) dilution	Secondary antibodies (dilution 1:100) G anti-M (FITC) (Stratech) D anti-R (TRITC) (Stratech)
MYO5B (Atlas Antibodies)	1:100	1:25	G anti-M + D anti-R
MYO16 (Novus Biologicals)	1:100	1:25	G anti-M + D anti-R
MYO18B (Biorbyt)	1:100	1:25	G anti-M + D anti-R
CONTROLS (single stain primary antibody)			
MYO5B (Atlas Antibodies)	1:100	-	D anti-R
MYO16 (Novus Biologicals)	1:100	-	D anti-R
MYO18B (Biorbyt)	1:100	-	D anti-R

2.2.4 Experiments to study the staining patterns of nuclear myosins in quiescent cells grown in low serum (0.5% FCS) media

NB1 cells were cultured in dishes, on coverslips in DMEM media as described in section 2.2.1, with FCS at 15% (high serum) for 2 days, and then cultured in DMEM media with low serum (FCS at 0.5%) for 7 days in order to induce the cells into quiescence, before being fixed (section 2.2.1). These experiments were performed with MYO5B, MYO16 and MYO18B, all used at 1:100 (v/v) antibody dilution as had been used in previous experiments. Ki-67 (mouse host) antibody was used at 1:25 dilution as had been used in previous experiments (section 2.2.3). Ki-67 was used as a marker of cell proliferation and thus a useful indicator of whether the cells were quiescent or still proliferating. Secondary antibodies were used at 1:100 (v/v) dilution as had been used before; Goat anti-Mouse (FITC) + Donkey anti-Rabbit (TRITC). Both primary antibodies were mixed and applied combined. Secondary antibodies were also mixed and applied combined. Primary antibody incubation was overnight at 4ºC and secondary antibody incubation was for 1 hour in the dark at room temperature. Manual counts of the number of visible foci of myosin protein staining in indivudual nuclei were performed for both proliferating and non-proliferating cells for comparative purposes.

2.2.5 Experiments to determine co-localisation of SC35 with the nuclear myosins in cells grown in high serum (15% FCS) media

NB1 cells were cultured in dishes, on coverslips in DMEM media as described in section 2.2.1, with FCS at 15% (high serum) before being fixed (section 2.2.1). These experiments were performed with MYO5B, MYO16 and MYO18B, all used at 1:100 (v/v) antibody dilution as had been used in previous experiments, together with SC35 at an antibody dilution of 1:1000 (v/v). Each of these myosins was co-stained with SC35 (mouse host) (Abcam). Secondary antibodies were used at 1:100 dilution as had been used before; Goat anti-Mouse (FITC) + Donkey anti-Rabbit (TRITC). Both primary antibodies were mixed and applied combined. Secondary antibodies were also mixed and applied combined. Primary antibody staining was overnight at 4ºC and secondary antibody incubation was for 1 hour in the dark at room temperature.

2.3 RESULTS

2.3.1 Detection of candidate myosin motor proteins (antibody test phase) in nuclei of cells grown in high serum (15% FCS) media, by indirect immunofluorescence, using single primary antibodies

In order to test the myosin antibodies for confirmation of nuclear staining, this phase of the experiments was a preliminary qualitative study, and therefore quantitative results are not presented. In these experiments the observation of the presence of the myosin motor proteins in interphase cell nuclei, using single antibody staining was performed and qualitatively recorded as observed nuclear staining. Myosin antibody nuclear staining was successfully observed first for MYO18B only, but in subsequent experiments staining with MYO5B and MYO16 antibodies also worked successfully. Therefore, confirming that the available antibodies being used would be suitable for use in the subsequent experiments using dual primary antibody staining, including anti-Ki-67 as a marker of cell proliferation. Being the first immunofluorescence staining experiments in this project, the results were overall a successful demonstration of the technique and the efficacy of the antibodies used with the NB1 cell line, for the nuclear myosin proteins of interest.

2.3.2 Detection of candidate motor proteins in nuclei of proliferating and non-proliferating cells grown in high serum (15% FCS) media, by indirect immunofluorescence, by dual staining with primary antibodies including anti-Ki-67

In order to determine any differences in the presence of the candidate myosin motor proteins in interphase nuclei, between proliferating and non-proliferating cells, dual antibody staining for immunofluorescence detection was performed. Primary antibodies against Ki-67 were used as markers of cell proliferation. Dual staining with Ki-67 worked successfully for all three myosins selected; MYO16, MYO5B and MYO18B. Several visual examples of dual staining results for each of the nuclear myosin proteins of interest are shown in the following figures in this section, together with detailed description of the results for each myosin studied, in succession. Some of the images show more than one cell in the microscope field of view to highlight the differences in staining between nuclei and to demonstrate in a comparative and robust way, the visual results of the experiments. Presenting the visual results of staining differences with representative Ki-67 positive and Ki-67 negative nuclei in the same microscope field of view, is a useful format for demonstrating the comparison between proliferating and non-proliferating cells, and can be considered as forming a part of the evidence of the results. Also, some of the figures presented show more than one example of individual representative nuclei to demonstrate visually the staining variations in terms of foci, in both proliferating and non-proliferating cells and help the reader to gain a better visual appreciation of these variations in the results.

In order to quantify the differences in the presence of the different myosin proteins in proliferating and non-proliferating cells, manual replicate counts of the number of proliferating and non-proliferating cells with or without nuclear staining for the myosin proteins were performed during observation by fluorescence microscopy. Also, counts of the number of visible foci of myosin protein staining in nuclei were performed on the immunostained nuclei by manual counting during observation by fluorescence microscopy. These quantitative results for these experiments are shown in graphs in this section for each of the myosins. The average data for the number of foci was rounded to the nearest whole number to account for the fact that the raw data consists of whole numbers of foci only, and therefore describing the foci as fractions would suggest partial foci which would not be an accurate description.

Dual primary antibody staining with MYO16 + Ki-67 primary antibodies

Comparing high serum (15% FCS) media grown cells with regards to MYO16 staining in the nuclei of proliferating and non-proliferating cells, as shown by presence of Ki-67 staining, or absence of Ki-67 staining respectively, shows moderate to low frequency foci of staining, and in some nuclei with considerably larger aggregates (Figures 2.1 and 2.2). Therefore, there are foci of various sizes for MYO16 staining. By making visual comparative observations, it was clear that nuclei of non-proliferating cells show more MYO16 staining foci than the nuclei of proliferating cells as shown by Ki-67 proliferation marker staining. This trend in MYO16 staining in relation to cellular state was further corroborated by the nuclei of some proliferating cells showing no MYO16 staining at all, 22% of nuclei were MYO16 -ve Ki-67 +ve and only 7.3% of nuclei were MYO16 +ve Ki-67 +ve (Figure 2.3). The visual observations were confirmed by the quantitative data, collected by foci counts as shown in Figure 2.4 A, where MYO16 +ve Ki-67 –ve nuclei have the highest numbers of foci compared with MYO16 +ve Ki-67 +ve nuclei. When the average data are derived, the number of foci per nucleus, are estimated at 8 and 5.4 (rounded to 5) respectively (Figure 2.4 B). This difference was found to be statistically significant, with a P value of 0.0158. Although, the difference between 8 foci and 5 foci for these cellular states may seem small, the statistical analysis clearly shows there is a significant and therefore reliable difference in the number of foci for MYO16 protein expression in these cells. Another aspect of the data which may in some ways be more informative regarding the differences observed, is shown by the range of the numbers of foci as displayed in Figure 2.4 A. The data in Figure 2.4 A shows that only MYO16 +ve Ki-67 –ve nuclei show numbers of foci above 10, and furthermore show values of 12,13,16,17,19, 24 and a maximum of 33 foci per nucleus for these non-proliferating cells. Although the percentage occurrences of these higher numbers of foci are relatively low, they are nonetheless an important indicator of the differences between these cellular states of proliferation and non-proliferation.
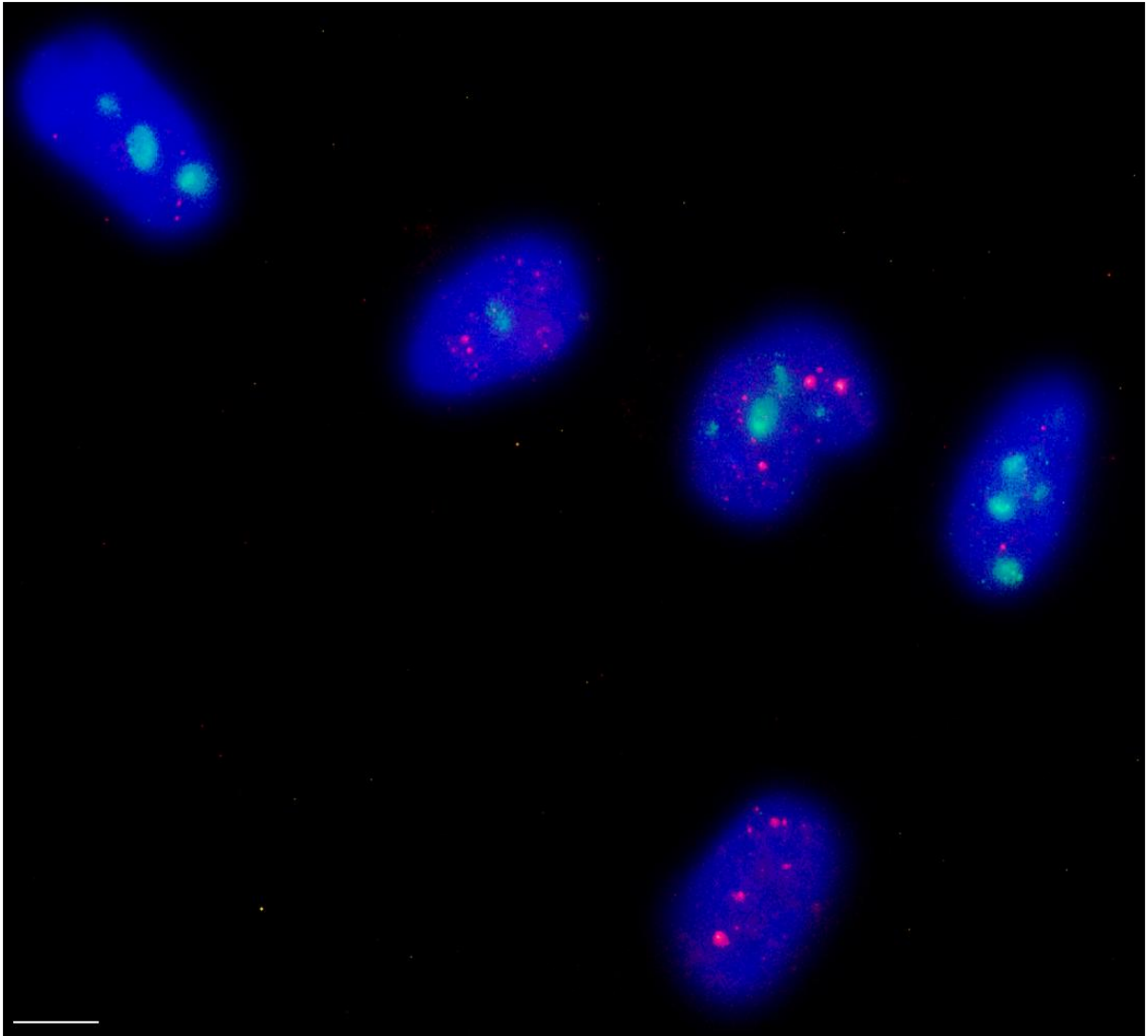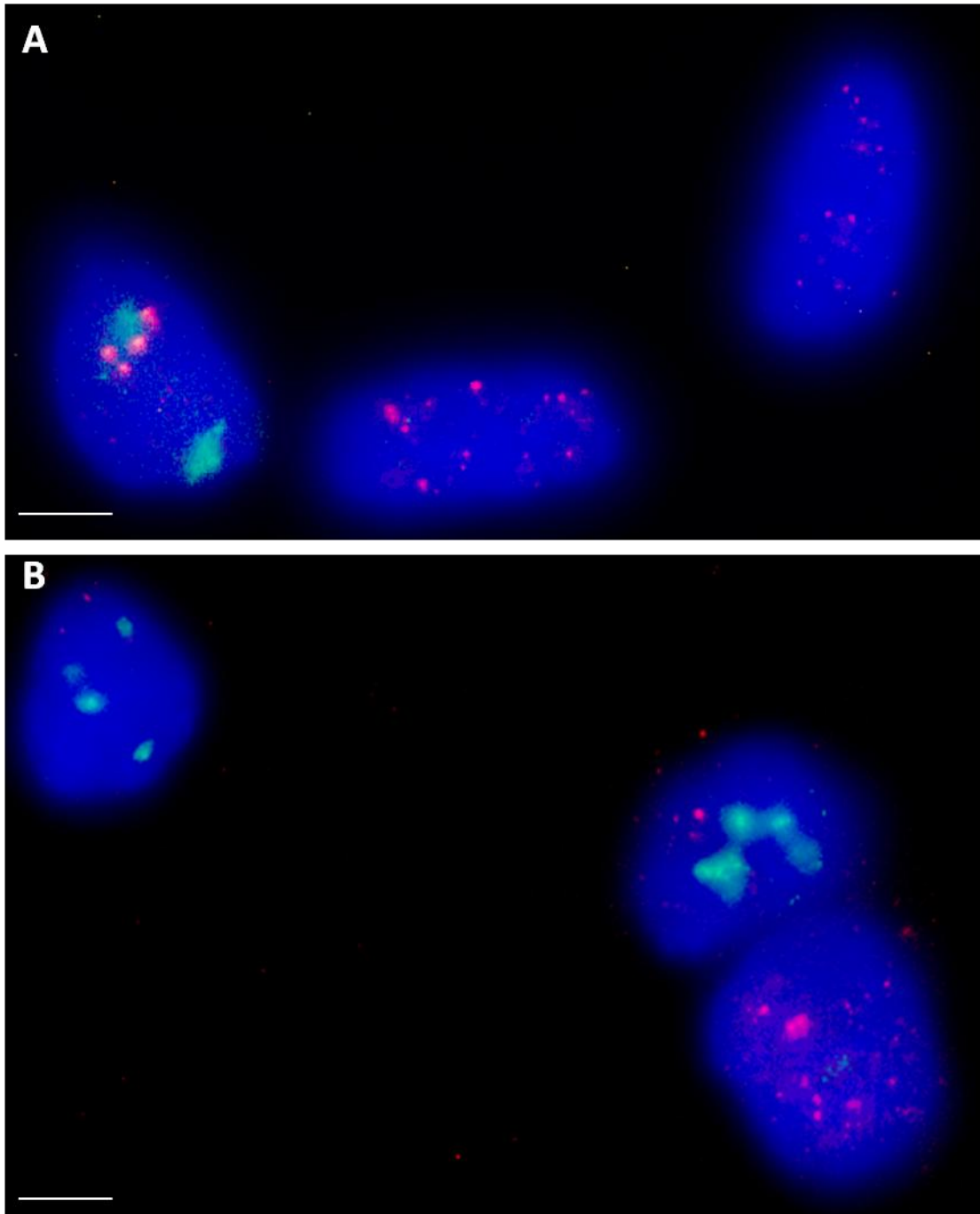
Figure 2.1. Nuclei of cells in the same microscope field of view, stained with DAPI (blue showing whole nucleus), MYO16 (red TRITC 2°) and Ki-67 (green FITC 2°) antibodies. In these nuclei there are varying levels of staining of both Ki-67 and MYO16 in four of the nuclei, and only MYO16 staining in one nucleus. Note that these are intact fixed cells and therefore, beyond the visible boundary of the nuclei is the cytoplasm of each cell, though it is not stained to be visible. Scale bar = 10μm.

Figure 2.2. Nuclei of cells in the same microscope field of view, stained with DAPI (blue showing whole nucleus), MYO16 (red TRITC 2°) and Ki-67 (green FITC 2°) antibodies. (A) Two nuclei showing MYO16 staining only and one nucleus showing both MYO16 and Ki-67 staining. (B) Two nuclei showing mostly Ki-67 staining and only minor MYO16 staining. Another nucleus showing only MYO16 staining, and with more foci compared with the Ki-67 +ve nuclei. Note that these are intact fixed cells and therefore, beyond the visible boundary of the nuclei is the cytoplasm of each cell, though it is not stained to be visible. Scale bar = 10μm.

MYO16 + Ki-67 dual stain
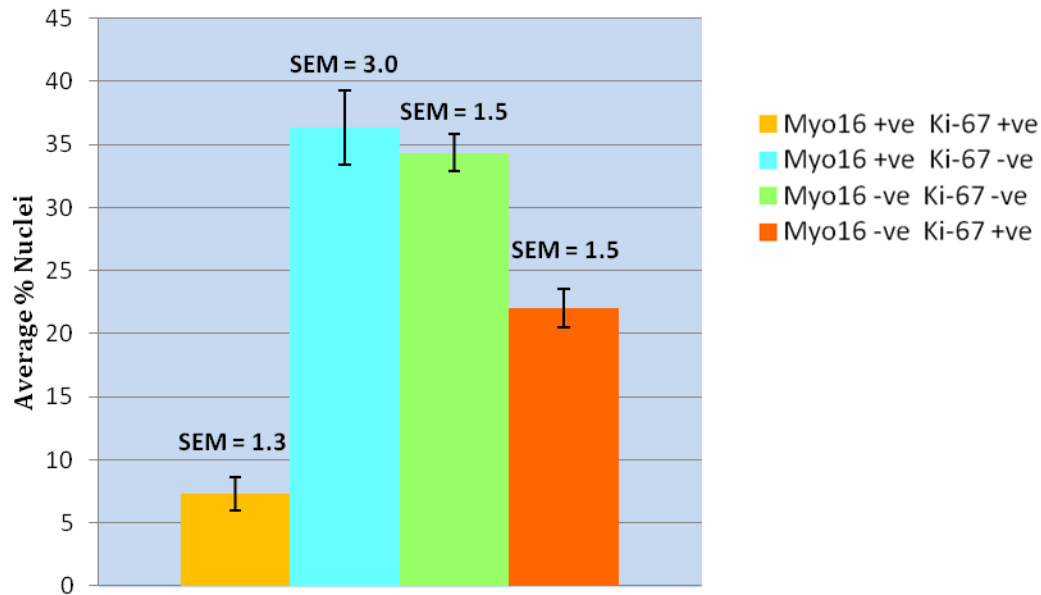
Figure 2.3. Graph displaying the quantitative results for immunofluorescence staining with MYO16 and Ki-67 in the nuclei of cells grown in high serum (15% FCS) media. This graph shows the average percentage of proliferating or non-proliferating cells with or without nuclear staining for MYO16. This average data is derived from 3 replicate counts of n = 291 nuclei, n = 437 nuclei, n = 356 nuclei (in each of these replicate counts the 4 variable states of staining as shown in the graph were counted). Error bars show the Standard Error of the Mean (SEM). t-test comparing Myo16 +ve Ki-67 +ve with Myo16 +ve Ki-67 -ve datasets gives: **P = 0.0009**.
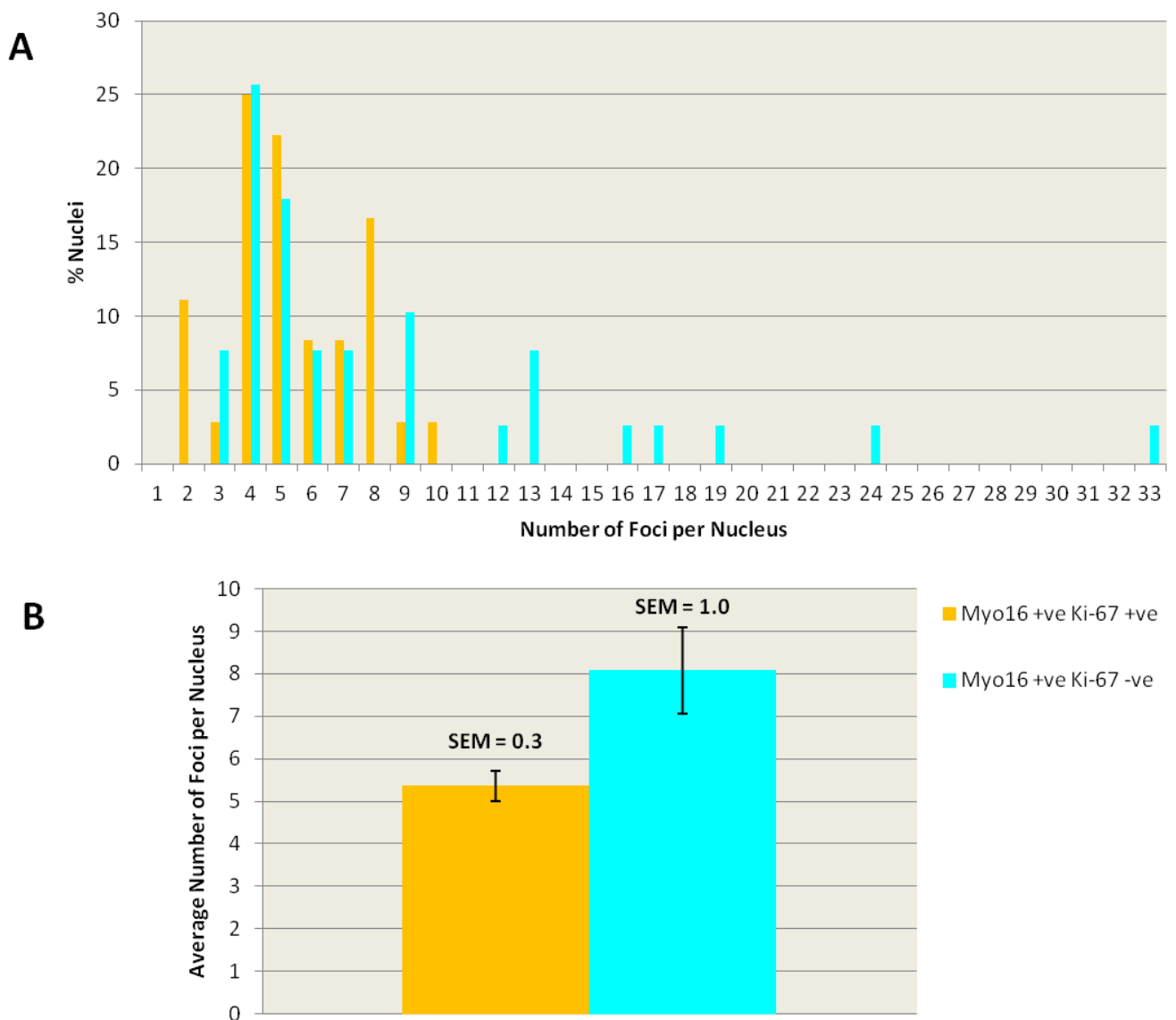
Figure 2.4. Graphs showing results of foci counts for immunofluorescence staining with MYO16 and Ki-67 in the nuclei of cells, grown in high serum (15% FCS) media, comparing proliferating and non-proliferating cells. For MYO16 +ve Ki-67 +ve n = 36 nuclei, for MYO16 +ve Ki-67 –ve n = 39 nuclei. (A) This graph shows the proportion of nuclei as percentages with different numbers of foci. (B) This graph shows the average numbers of foci per nucleus. SEM = Standard Error of the Mean. t-test **P = 0.0158.**

Dual primary antibody staining with MYO5B + Ki-67 primary antibodies

Comparing high serum (15% FCS) media grown cells with regards to the staining of MYO5B in the nuclei of proliferating and non-proliferating cells, as shown by presence of Ki-67 staining, or absence of Ki-67 staining respectively, shows rather large irregularly shaped foci of MYO5B as well as smaller foci of MYO5B (Figures 2.5 and 2.6). The quantitative data for MYO5B staining shows that the large majority of the nuclei were MYO5B +ve Ki-67 –ve (82%) and the remaining 18% were MYO5B +ve Ki-67 +ve, and there were no nuclei devoid of MYO5B staining (Figure 2.7). Again, nuclei of most non-proliferating cells had higher numbers of foci compared with those of proliferating cells (Figure 2.8 A), with average number of foci per nucleus of 17.6 (rounded to 18) and 11.8 (rounded to 12) respectively (Figure 2.8 B). This difference was found to be statistically significant, with a P value of <0.0001. Looking at the range of foci numbers for MYO5B (Figure 2.8 A), although the trend of higher foci in non-proliferating cells is supported, the difference is not as obvious when compared with the results for MYO16. For MYO5B the nuclei of proliferating cells can also have some high numbers of foci (see Figures 2.5 and 2.6), some as many as 24 foci (Figure 2.8 A), however still not as high as the maximum number of foci in the nuclei of non-proliferating cells which can be as high as 39, as shown in Figure 2.8 A. Apart from the MYO5B staining in the nuclei as described, it was also observed that some cells show considerable MYO5B staining in the cytoplasm (Figures 2.5 and 2.6), particularly in the vicinity of the nucleus, possibly within the region of the endoplasmic reticulum. The nature of this cytoplasmic staining was not investigated or quantified in this work, since the main focus was on the MYO5B protein presence in the nucleus. Although not a subject of investigation in this project, the observed cytoplasmic staining can be inferred to be related to the vesicular transport and membrane trafficking functions of MYO5B in the cytoplasm (Lapierre et al. 2001; Roland et al. 2011).
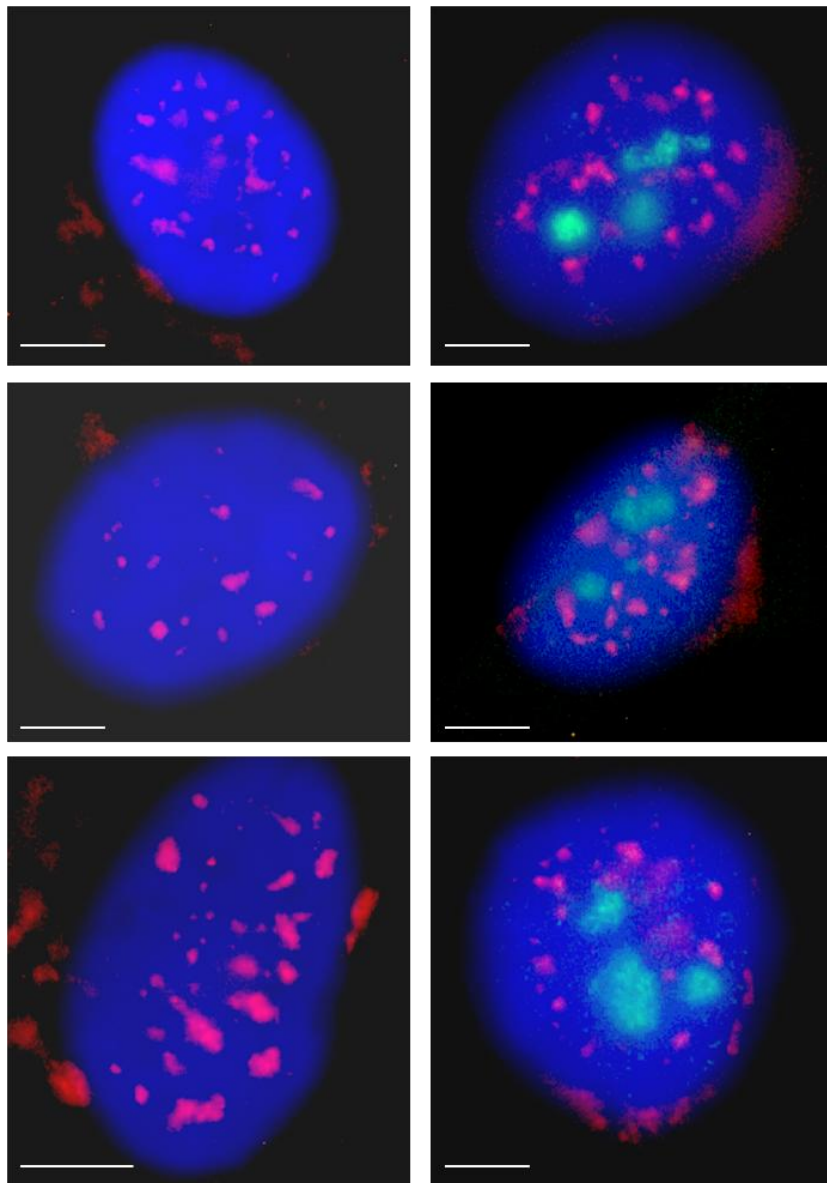
Figure 2.5. Nuclei of cells stained with DAPI (blue showing whole nucleus), MYO5B (red TRITC 2°) and Ki-67 (green FITC 2°) antibodies. Three nuclei (left column) show MYO5B staining only and three other nuclei (right column) show both MYO5B and Ki-67 staining. Note that these are intact fixed cells and therefore, beyond the visible boundary of the nuclei is the cytoplasm of each cell, though it is not stained to be visible. Cytoplasmic MYO5B staining is visible in the vicinity of the nuclei. Scale bar = 5µm.
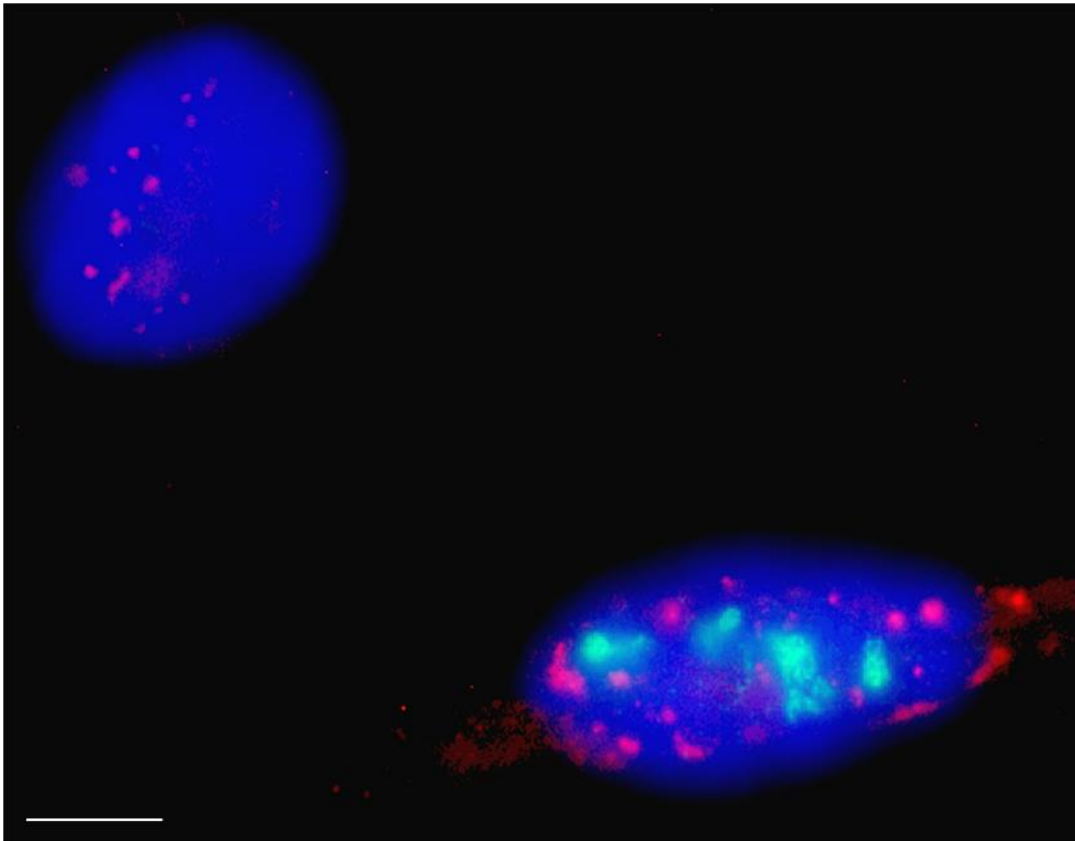
Figure 2.6. Nuclei of cells in the same microscope field of view, stained with DAPI (blue showing whole nucleus), MYO5B (red TRITC 2°) and Ki-67 (green FITC 2°) antibodies. One nucleus shows MYO5B staining only and the other nucleus shows both MYO5B and Ki-67 staining. Note that these are intact fixed cells and therefore, beyond the visible boundary of the nuclei is the cytoplasm of each cell, though it is not stained to be visible. Cytoplasmic staining is visible in the vicinity of the Ki-67 positive nucleus.

Scale bar = 5µm.
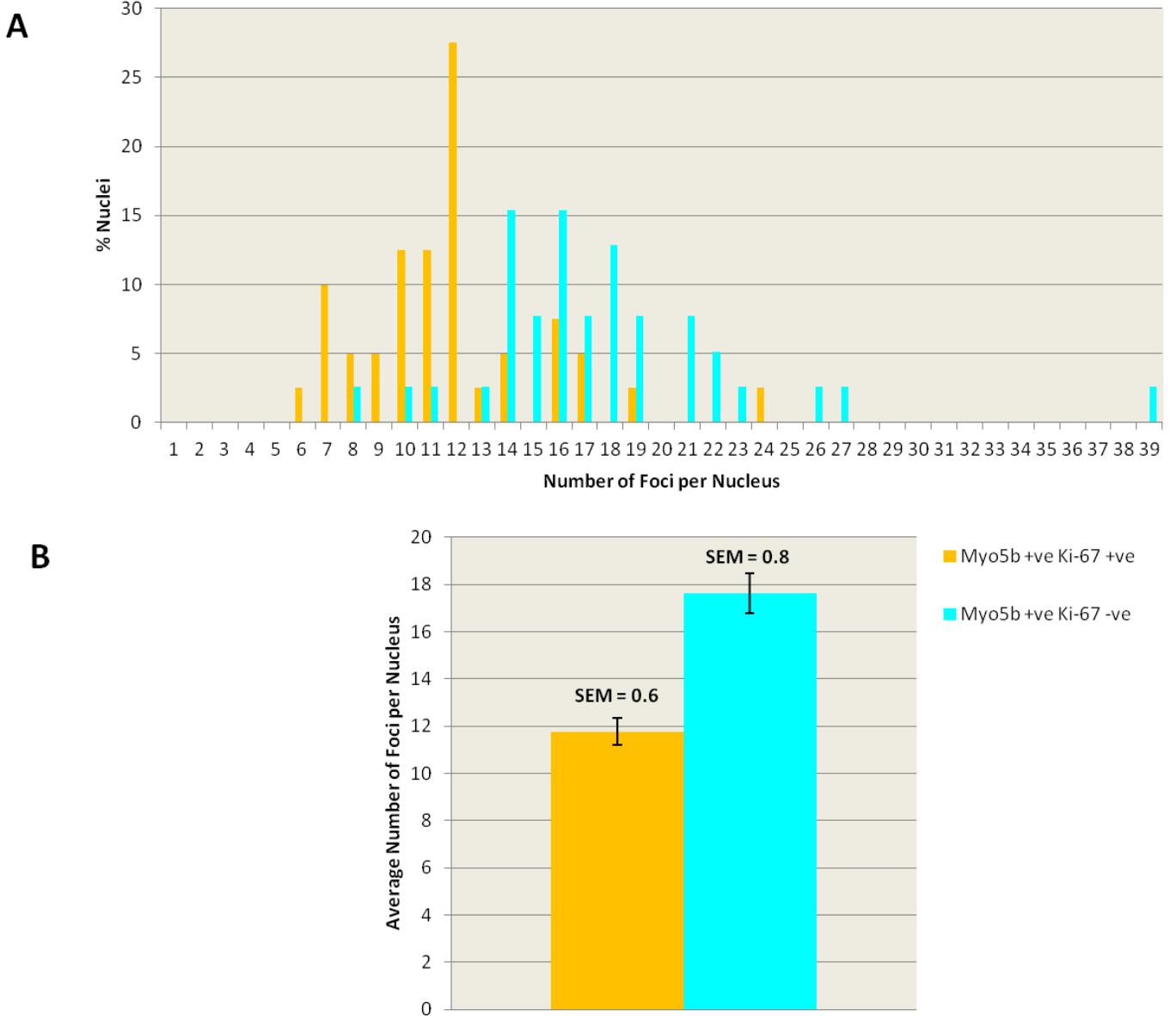
MYO5B + Ki-67 dual stain
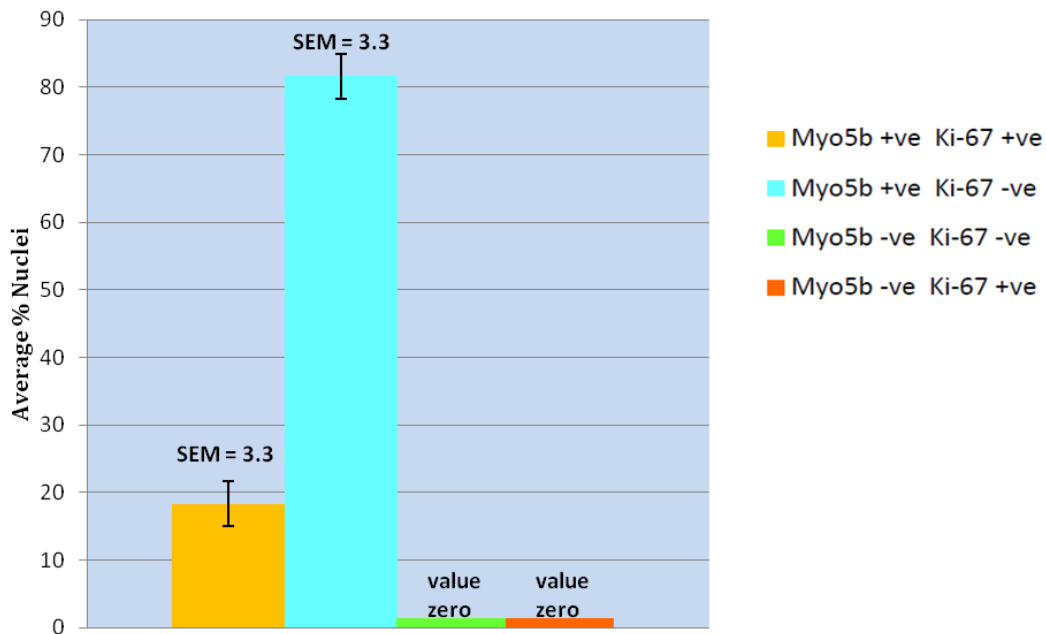
Figure 2.7. Graph showing the quantitative results for immunofluorescence staining with MYO5B and Ki-67 in the nuclei of cells grown in high serum (15% FCS) media. This graph shows the average percentage of proliferating or non-proliferating nuclei with or without nuclear staining for MYO5B. This average data is derived from 3 replicate counts of n = 212 nuclei; n = 496 nuclei; n = 519 nuclei (in each of these replicate counts the 4 variable states of staining as shown in the graph were counted). Error bars show the Standard Error of the Mean (SEM). Note that in this data for MYO5B there were no MYO5B –ve Ki-67 –ve and MYO5B –ve Ki-67 +ve nuclei found during counting, therefore these two data subsets are represented in the graph by the 'value zero' labels.

t-test comparing Myo5b +ve Ki-67 +ve with Myo5b +ve Ki-67 -ve datasets gives: **P = 0.0002.**

Figure 2.8. Graphs showing results of foci counts for immunofluorescence staining with MYO5B and Ki-67 in the nuclei of cells, grown in high serum (15% FCS) media, comparing proliferating and non-proliferating cells. For MYO5B +ve Ki-67 +ve n = 40, for MYO5B +ve Ki-67 –ve n = 39. (A) This graph shows the proportion of nuclei as percentages with different numbers of foci. (B) This graph shows the average numbers of foci per nucleus. SEM = Standard Error of the Mean. t-test **P<0.0001.**

Dual primary antibody staining with MYO18B + Ki-67 primary antibodies

Representative visual results comparing high serum (15% FCS) media grown cells with regards to MYO18B staining in the nuclei of proliferating and non-proliferating cells, as shown by presence of Ki-67 staining, or absence of Ki-67 staining respectively are shown in Figures 2.9 and 2.10. A feature which was noticed by visual observation was that the nuclei of some non-proliferating cells display a considerably large number of MYO18B foci when compared with the nuclei of proliferating cells (Figure 2.9). The quantitative data in Figure 2.11 shows that on average 20% of nuclei where MYO18B –ve Ki-67 +ve. As shown in Figure 2.11, only a small proportion of the nuclei (11%) show both MYO18B and Ki-67 staining, and visually it was clear that most of these had moderately lower frequency of MYO18B staining foci or much lower frequency of MYO18B staining foci, and these visual deductions were confirmed by the quantitative data shown in Figure 2.12 which clearly shows that most MYO18B +ve Ki-67 +ve nuclei had lower numbers of foci compared with MYO18B +ve Ki-67 –ve nuclei with an average number of foci per nucleus of 5.6 (rounded to 6) and 14 respectively. This is a relatively large difference and found to be statistically significant, with a P value of <0.0001. Furthermore, the majority (47%) of nuclei were MYO18B +ve Ki-67 –ve as shown in Figure 2.11. When comparing the range of the number of MYO18B foci, the results show that only the nuclei of non-proliferating cells had foci numbers above 18 with a maximum of 32 foci. These results strongly corroborate the trend seen in the results with MYO16 and MYO5B, that the nuclei of non-proliferating cells show higher numbers of foci when compared with the nuclei of proliferating cells.
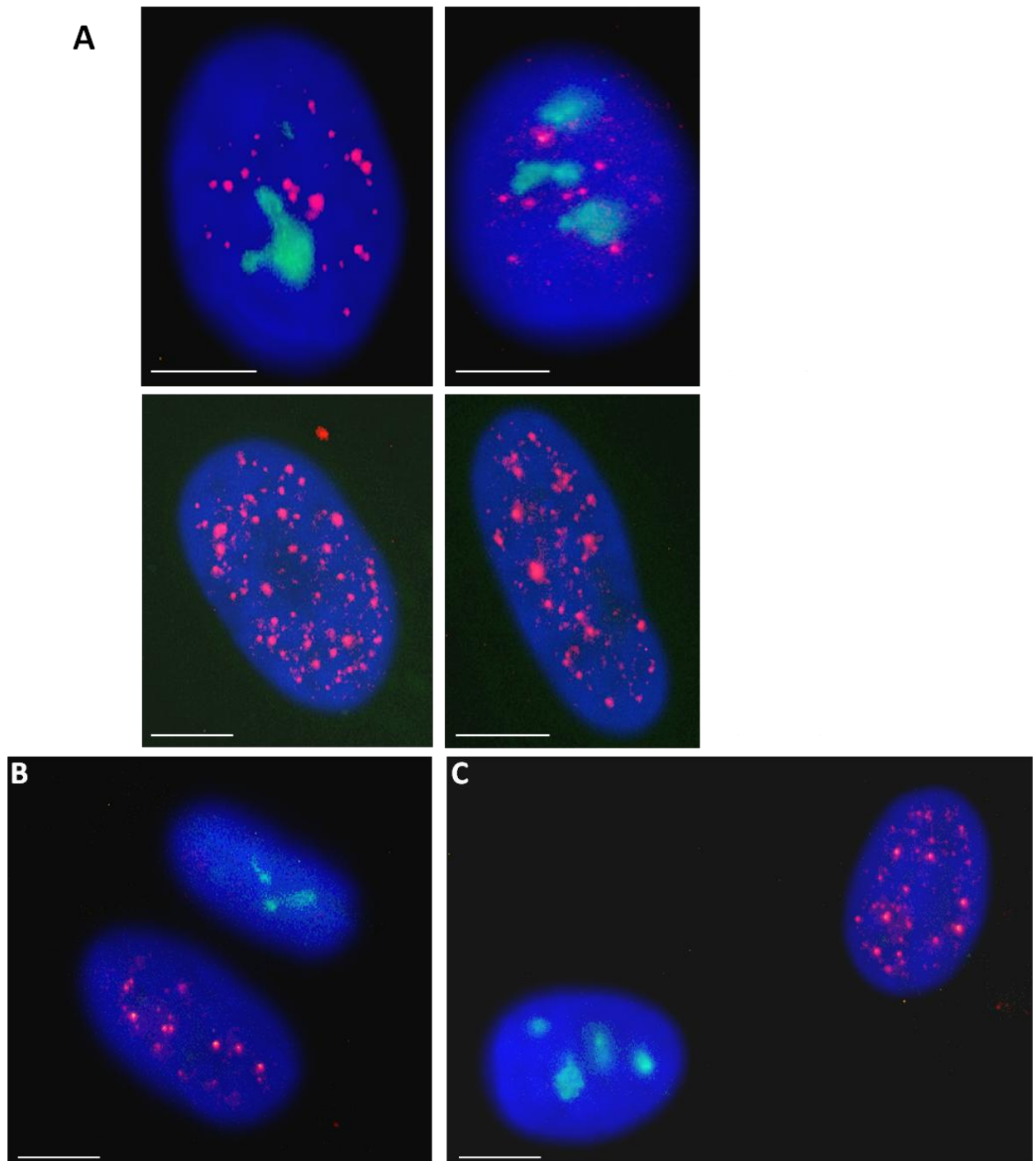
Figure 2.9. Nuclei of cells stained with DAPI (blue showing whole nucleus), MYO18B (red TRITC 2°) and Ki-67 (green FITC 2°) antibodies. (A) Two nuclei show both MYO18B staining and Ki-67 staining and two other nuclei show MYO18B staining only. Scale bar = 5μm. (B and C) Two nuclei in each, in the same microscope field of view, one showing only Ki-67 staining and the other showing MYO18B staining only. Note that these are intact fixed cells and therefore, beyond the visible boundary of the nuclei is the cytoplasm of each cell, though it is not stained to be visible. Scale bar = 10μm.
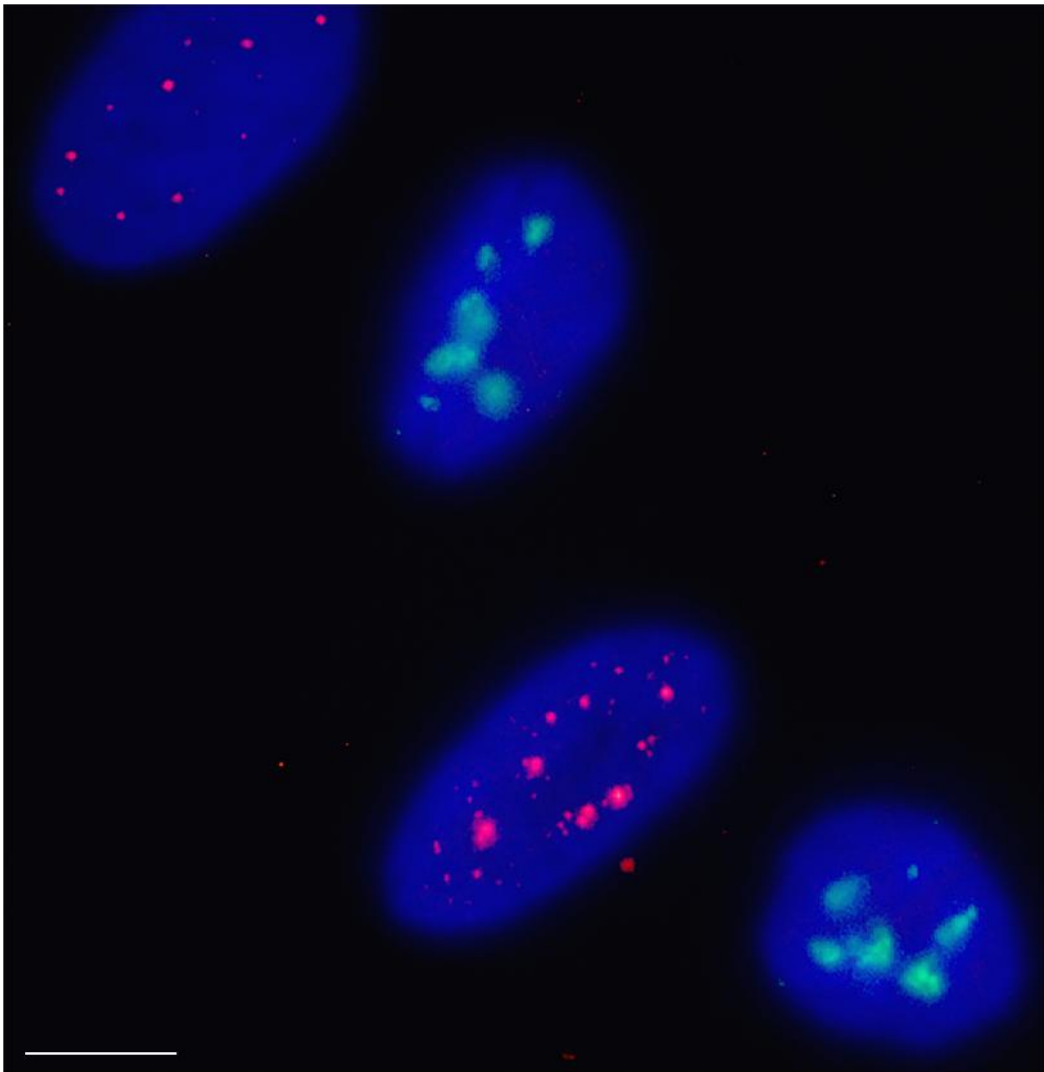
**Figure 2.10.** Nuclei of cells in the same microscope field of view, stained with DAPI (blue showing whole nucleus), MYO18B (red TRITC 2°) and Ki-67 (green FITC 2°) antibodies. In this image the nuclei that are MYO18B positive show relatively few foci compared to those in Figure 2.9 for example. This example together with the images in Figure 2.9 helps to visually demonstrate the range of foci numbers as quantified in Figure 2.12. Of the three nuclei fully visible in the field of view, two show Ki-67 staining only and one shows MYO18B staining only. Note that these are intact fixed cells and therefore, beyond the visible boundary of the nuclei is the cytoplasm of each cell, though it is not stained to be visible. Scale bar = 10μm.
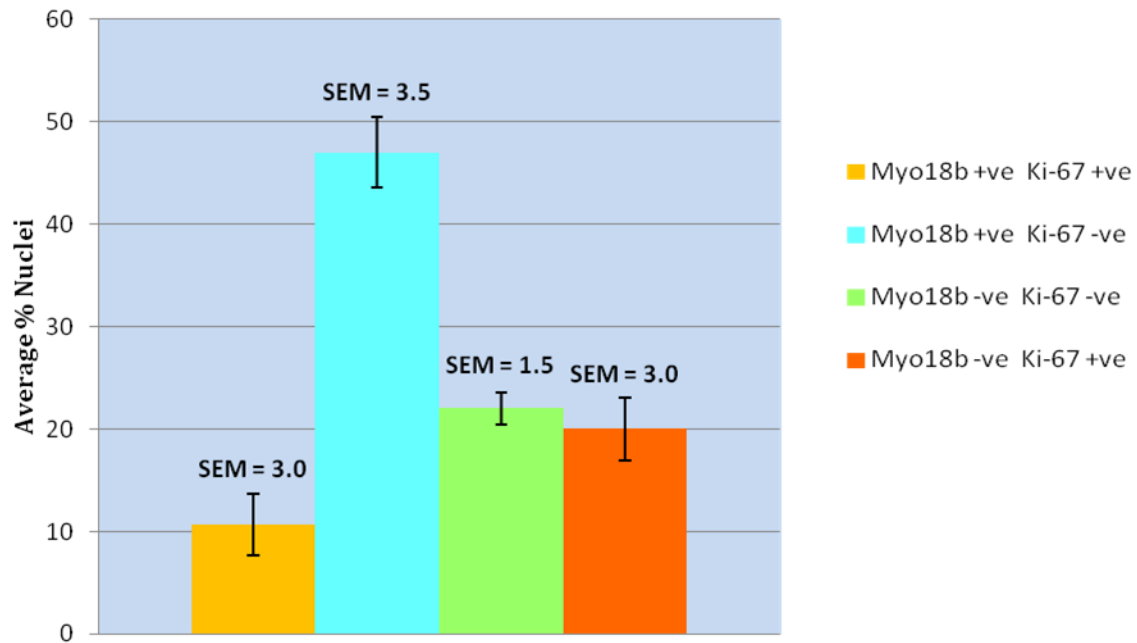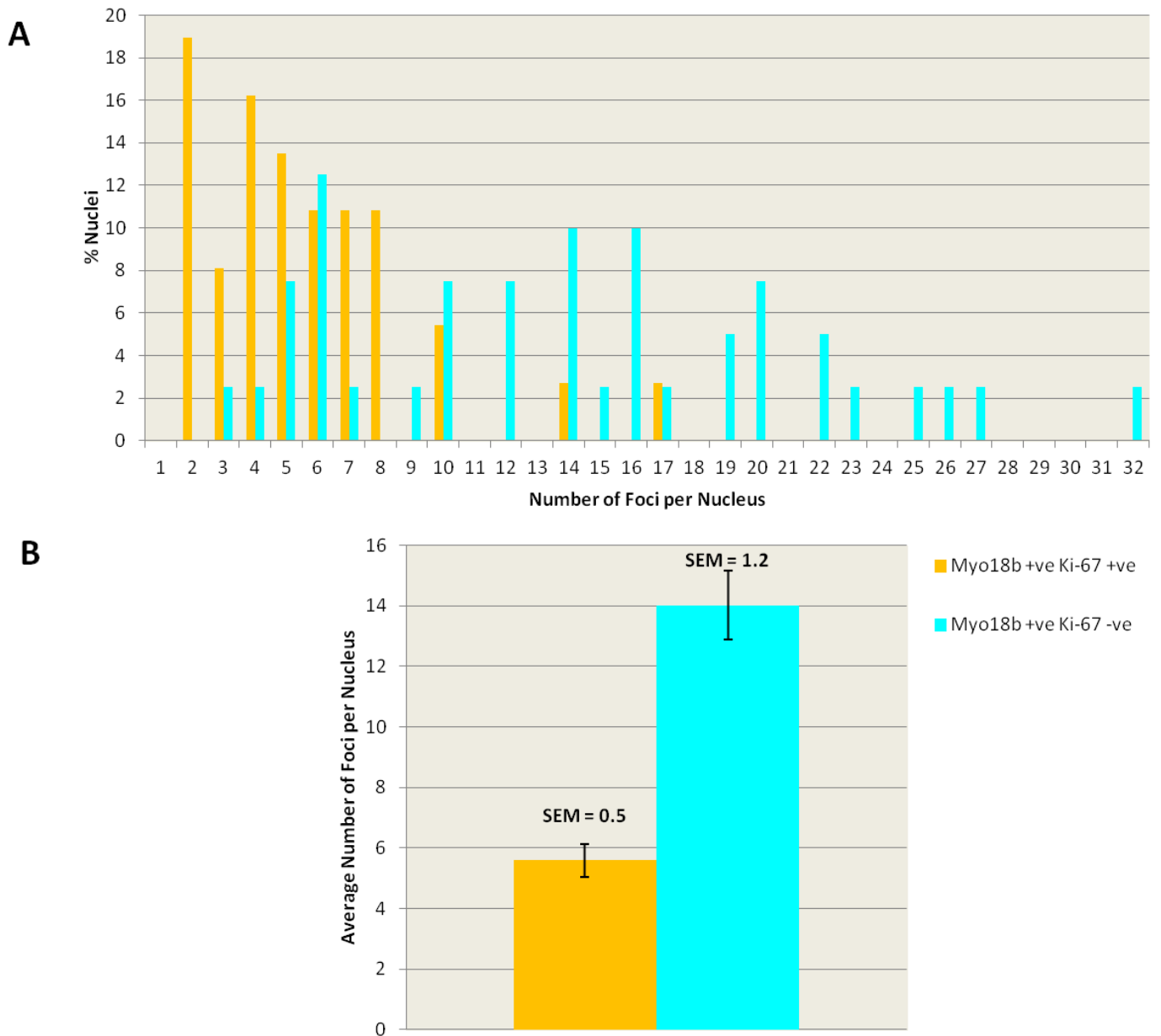
Figure 2.11. Graph showing the quantitative results for immunofluorescence staining with MYO18B and Ki-67 in the nuclei of cells grown in high serum (15% FCS) media. This graph shows the average percentage of proliferating or non-proliferating nuclei with or without staining for MYO18B. This average data is derived from 3 replicate counts of n = 181 nuclei; n = 301 nuclei; n = 369 nuclei (in each of these replicate counts the 4 variable states of staining as shown in the graph were counted). Error bars show the Standard Error of the Mean (SEM). t-test comparing Myo18b +ve Ki-67 +ve with Myo18b +ve Ki-67 -ve datasets gives: **P = 0.0014.**

Figure 2.12. Graphs showing results of foci counts for immunofluorescence staining with MYO18B and Ki-67 in the nuclei of cells, grown in high serum (15% FCS) media, comparing proliferating and non-proliferating cells. For MYO18B +ve Ki-67 +ve n = 37, for MYO18B +ve Ki-67 –ve n = 40. (A) This graph shows the proportion of nuclei as percentages with different numbers of foci. (B) This graph shows the average numbers of foci per nucleus. SEM = Standard Error of the Mean. t-test **P<0.0001.**

2.3.3 Detection of nuclear myosins in nuclei of quiescent cells grown in low serum (0.5% FCS) media

In order to investigate the staining of MYO5B, MYO16 and MYO18B in the nuclei of quiescent cells, cultures were induced to become quiescent by growth in low serum media conditions (media with 0.5% FCS) for 7 days, after prior growth in high serum media (media with 15% FCS) for 2 days, as described in section 2.2.4 in the materials and methods section of this chapter. Dual antibody staining for immunofluorescence detection was performed with each myosin including Ki-67 as a useful indicator of whether the cells were quiescent (lack of Ki-67 staining), or still proliferating as indicated by positive Ki-67 staining. Counts of the number of visible foci of myosin protein staining in indivudual nuclei were performed for MYO5B and MYO16 by manual counting during observation by fluorescence microscopy. These counts were performed for non-proliferating cells and the few still proliferating cells, both in low serum (0.5% FCS) media, for comparative purposes. The nature of the staining pattern for MYO18B was such that it was not suitable for foci counts due to being mainly hazy and homogenous with many punctate foci (Figures 2.18 and 2.19). This different type of staining was not comparable to the staining patterns obtained from the other two myosins (MYO5B and MYO16) used in these experiments, in terms of foci counts. The high density of a mixture of very fine stain points and hazy areas, combined with some larger foci was also not seen in the other experiments in section 2.3.2 with MYO18B. The Ki-67 proliferation marker worked well to give confidence that the large majority of the nuclei were quiescent, and only a small proportion of the nuclei were Ki-67 positive and therefore proliferating. The results of foci numbers in these experiments for nuclei of quiescent cells can be compared with those of the experiments in section 2.3.2 of this chapter, for nuclei of non-proliferating cells grown in high serum (15% FCS) media.

Detection of MYO5B in the nuclei of quiescent cells grown in low serum (0.5% FCS) media

Studying the staining for MYO5B in the nuclei of cells made quiescent (MYO5B +ve Ki-67 –ve), shows similar large accumulations of foci (Figures 2.13 and 2.14) as was observed in the nuclei of cells grown in high serum (15% FCS) media and stained for MYO5B (section 2.3.2). The cytoplasmic staining for MYO5B was clearly present in the cells grown in low serum (0.5% FCS) media in this section, as was also observed in the cells grown in high serum (15% FCS) media conditions (section 2.3.2). The position of these cytoplasmic MYO5B areas were in the vicinity of the nucleus but also extending further in the cytoplasm in some cells, as clearly seen in Figure 2.13. Since the main focus of this project was the nuclear myosin staining, again these cytoplasmic MYO5B areas were not further investigated or quantified. However, by inference, they may be related to the vesicular transport and membrane trafficking functions of MYO5B in the cytoplasm (Lapierre et al. 2001; Roland et al. 2011). The quantitative results in Figure 2.15 show that there was a statistically significant difference (P = 0.0054) in the numbers of MYO5B foci per nucleus, when the quiescent cells were compared with the few still proliferating cells (13.8%, MYO5B +ve Ki-67 +ve) (Figure 2.14 A and C), in the same cell cultures. The actual average numbers of foci being 21.64 (rounded to 22) for the quiescent cells and 18.125 (rounded to 18) for the few proliferating cells. Although the actual difference in numbers of foci between these averages is not very high, there is clearly a real difference as confirmed by the statistical analysis. This difference is also clear to see in Figure 2.15 A, where the range and percentage frequency distribution of the two datasets can be compared. Thus the trend that the nuclei of non-proliferating cells show higher numbers of foci when compared with the nuclei of proliferating cells is again supported. Looking at the range of foci more closely, only the quiescent cells show numbers of foci per nucleus at 30 and above, these being 30, 32, 36, 38 and 40) however, the lowest number of foci per nucleus in the data is also found in the quiescent cells at 12 albeit at very low frequency (Figure 2.15 A) and therefore possibly an anomaly.
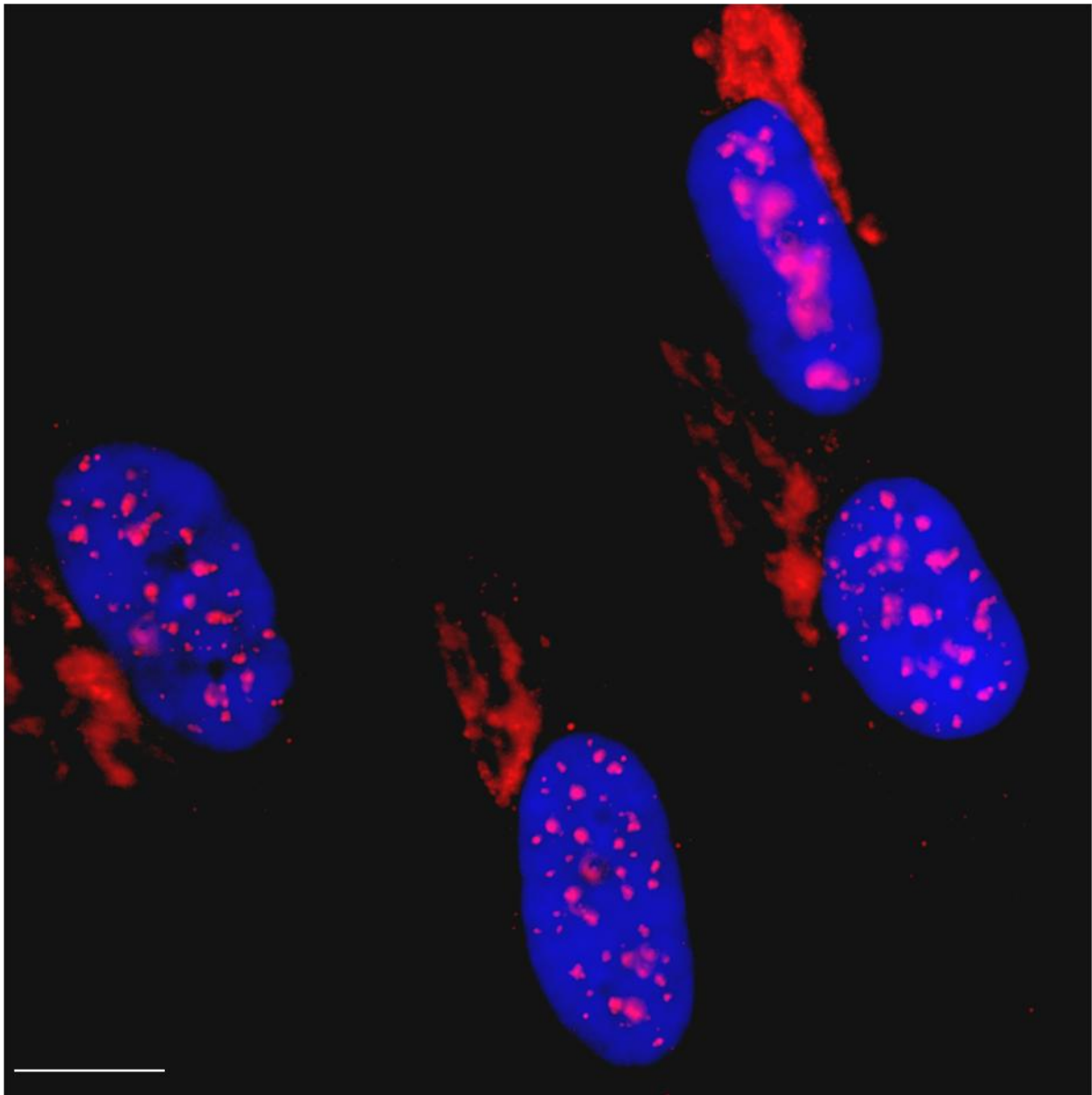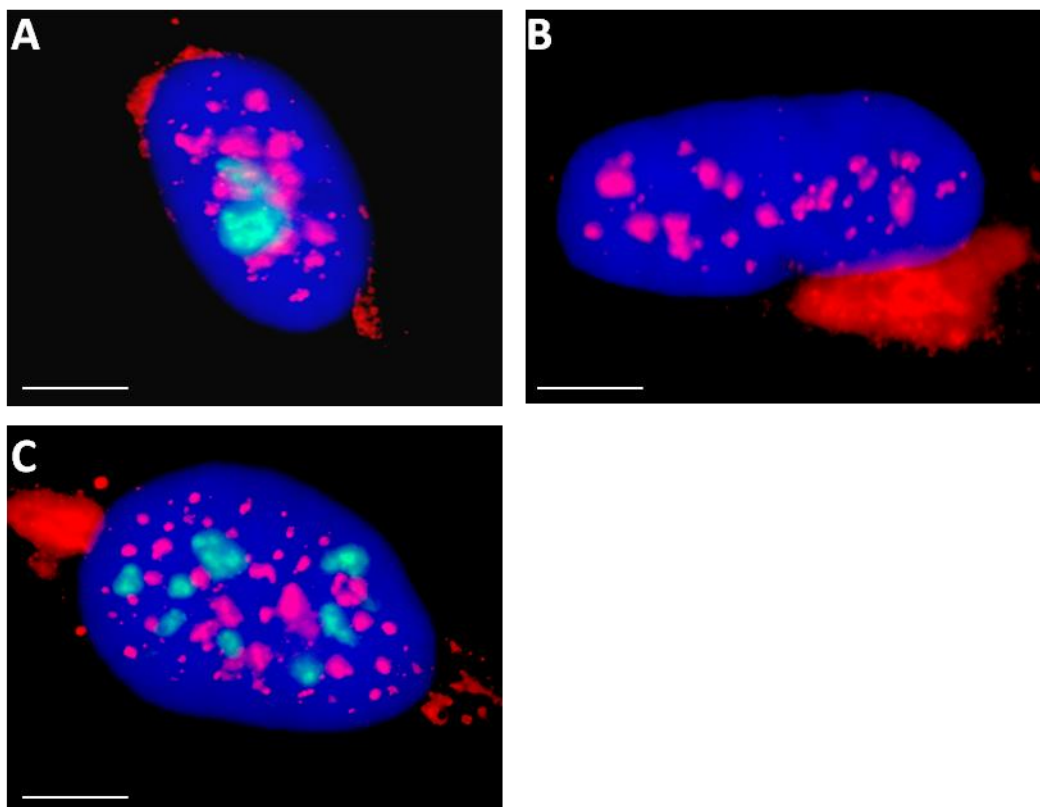
Figure 2.13. Nuclei of cells in the same field of view, stained with DAPI (blue showing whole nucleus), MYO5B (red TRITC 2°) and Ki-67 (green FITC 2°) antibodies (note no Ki-67 + nuclei in this field of view). Note that these are intact fixed cells and therefore, beyond the visible boundary of the nuclei is the cytoplasm of each cell, though it is not stained to be visible. There is extensive cytoplasmic MYO5B staining in the vicinity of the nuclei and further in the cytoplasm as clearly visible outside of the DAPI stained region. Scale bar = 10µm.

Compared with the results obtained in the previous section (2.3.2) with cells grown in high serum (15% FCS) media, it was similarly found that nuclei of non-proliferating cells had higher numbers of foci compared with those of proliferating cells, with the average number of foci per nucleus of 18 and 12 respectively (Figure 2.8 B). These

numbers also show that overall, the cells grown to quiescence in low serum conditions, the majority of which are quiescent and a minority still proliferating, show on average more MYO5B nuclear foci compared to cells grown in high serum (15% FCS) media conditions. This difference was confirmed by statistical analysis, thus when the low serum data for MYO5B +ve Ki-67 +ve are compared with high serum data for MYO5B +ve Ki-67 +ve, the difference in the numbers of foci was found to be statistically significant (P = <0.0001). Also, when the low serum data for MYO5B +ve Ki-67 -ve are compared with high serum data for MYO5B +ve Ki-67 -ve, the difference in the numbers of foci was again found to be statistically significant (P = <0.0001).

Figure 2.14. Nuclei of cells stained with DAPI (blue showing whole nucleus), MYO5B (red TRITC 2°) and Ki-67 (green FITC 2°) antibodies. Nuclei in (A) and (C) are proliferating as shown by Ki-67 Staining, and they also show MYO5B staining. Note that these are intact fixed cells and therefore, beyond the visible boundary of the nuclei is the cytoplasm of each cell, though it is not stained to be visible. Cytoplasmic MYO5B staining is visible in the vicinity of the nuclei. Scale bar = 5µm.
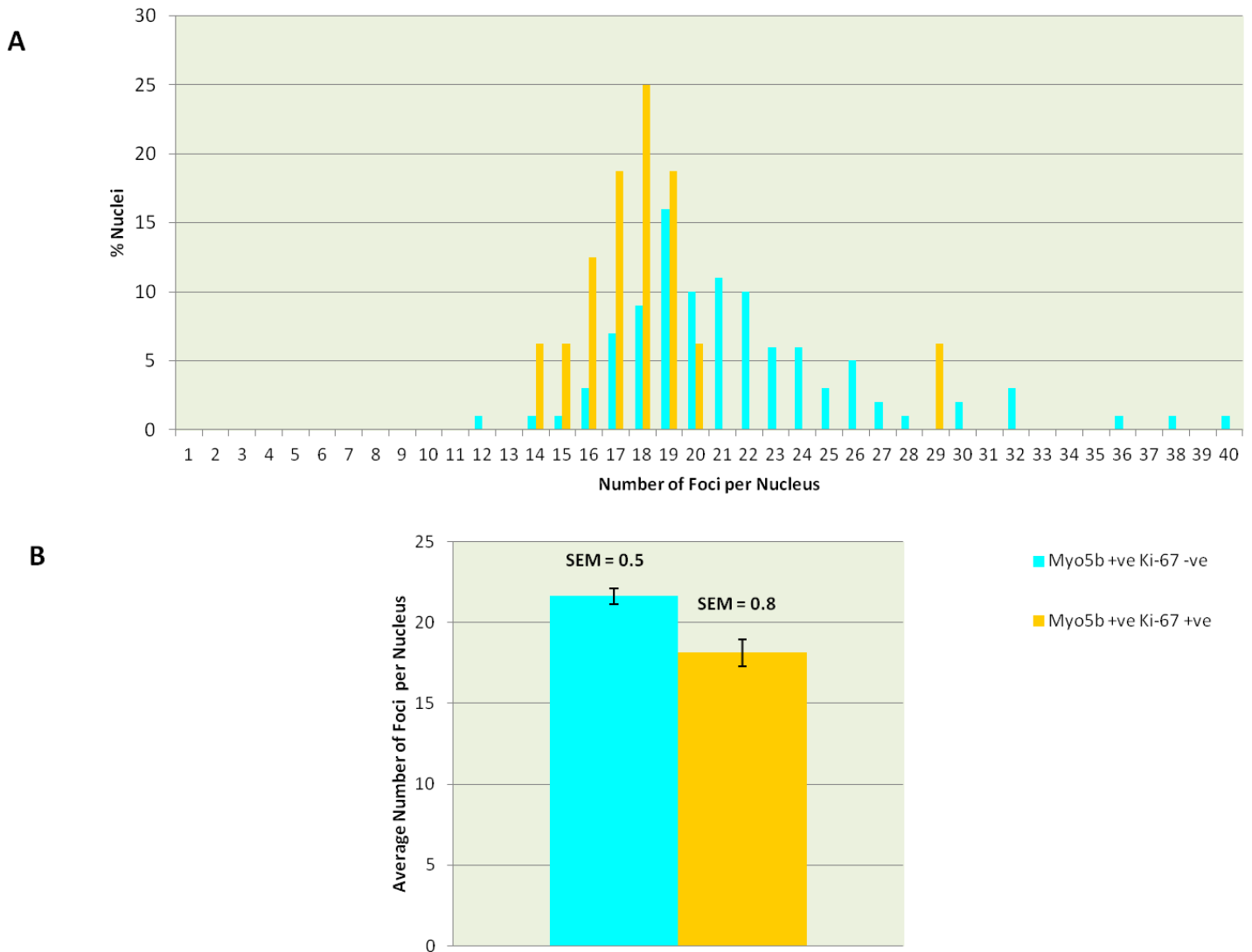
61

Figure 2.15. Graphs showing results of foci counts for immunofluorescence staining with MYO5B and Ki-67 in the nuclei of quiescent cells, grown in low serum (0.5% FCS) media, comparing proliferating and non-proliferating cells. For MYO5B +ve Ki-67 +ve n = 16, for MYO5B +ve Ki-67 –ve n = 100. (A) This graph shows the proportion of nuclei as percentages with different numbers of foci. (B) This graph shows the average numbers of foci per nucleus. SEM = Standard Error of the Mean. t-test **P = 0.0054.**

Detection of MYO16 in the nuclei of quiescent cells grown in low serum (0.5% FCS) media

The staining of MYO16 in the nuclei of cells made quiescent (MYO16 +ve Ki-67 –ve) by growth in low serum (0.5% FCS) media, showed considerably higher numbers of foci (Figures 2.16 and 2.17) when compared with the nuclei of cells grown in high serum (15% FCS) media and stained for MYO16, shown in the previous section (2.3.2). This higher number of foci was also seen when the nuclei of the few cells that were still proliferating (16.7%, MYO16 +ve Ki-67 +ve), despite growth in low serum (0.5% FCS) conditions, were compared with proliferating cells grown in high serum (15% FCS) media in section 3.2.3. The average numbers of MYO16 foci in the nuclei of quiescent cells were found to be 16.69 (rounded to 17) and average number of MYO16 foci in the nuclei of the few cells that were still proliferating was 14.1 (rounded to 14) (Figure 2.17). Compared with the average numbers of MYO16 foci in the nuclei of cells grown in high (15% FCS) serum conditions, these were 8 for non-proliferating cells and 5 for proliferating cells (section 2.3.2). As also found for MYO5B in this section, this difference was confirmed by statistical analysis to be significant. Therefore, when the low serum data for MYO16 +ve Ki-67 +ve are compared with high serum data for MYO16 +ve Ki-67 +ve, the difference in the numbers of foci was found to be statistically significant ($P = <0.0001$). Also, when the low serum data for MYO16 +ve Ki-67 -ve are compared with high serum data for MYO16 +ve Ki-67 -ve, the difference in the numbers of foci was again found to be statistically significant ($P = <0.0001$).

The quantitative results presented in Figure 2.17 did not show a statistically significant difference in the number of MYO16 foci, when the quiescent cells are compared with cells that were still proliferating, in the same low serum media culture. Therefore, the difference between 16.69 foci and 14.1 foci was not deemed to be a reliable difference in the data. The t-test P value of 0.1243 obtained for this comparison is considerably higher than the $P = 0.05$ statistically significant threshold. However, studying the range distribution of the number of MYO16 foci as presented in Figure 2.17 A, it was found that only the nuclei of quiescent cells had numbers of MYO16 foci higher than 27 with numbers being 28, 31, 32, 35 and 36. These numbers were however not sufficiently higher than the 27 maximum observed for

proliferating cells to be significantly different, as supported by the outcome of the statistical analysis.
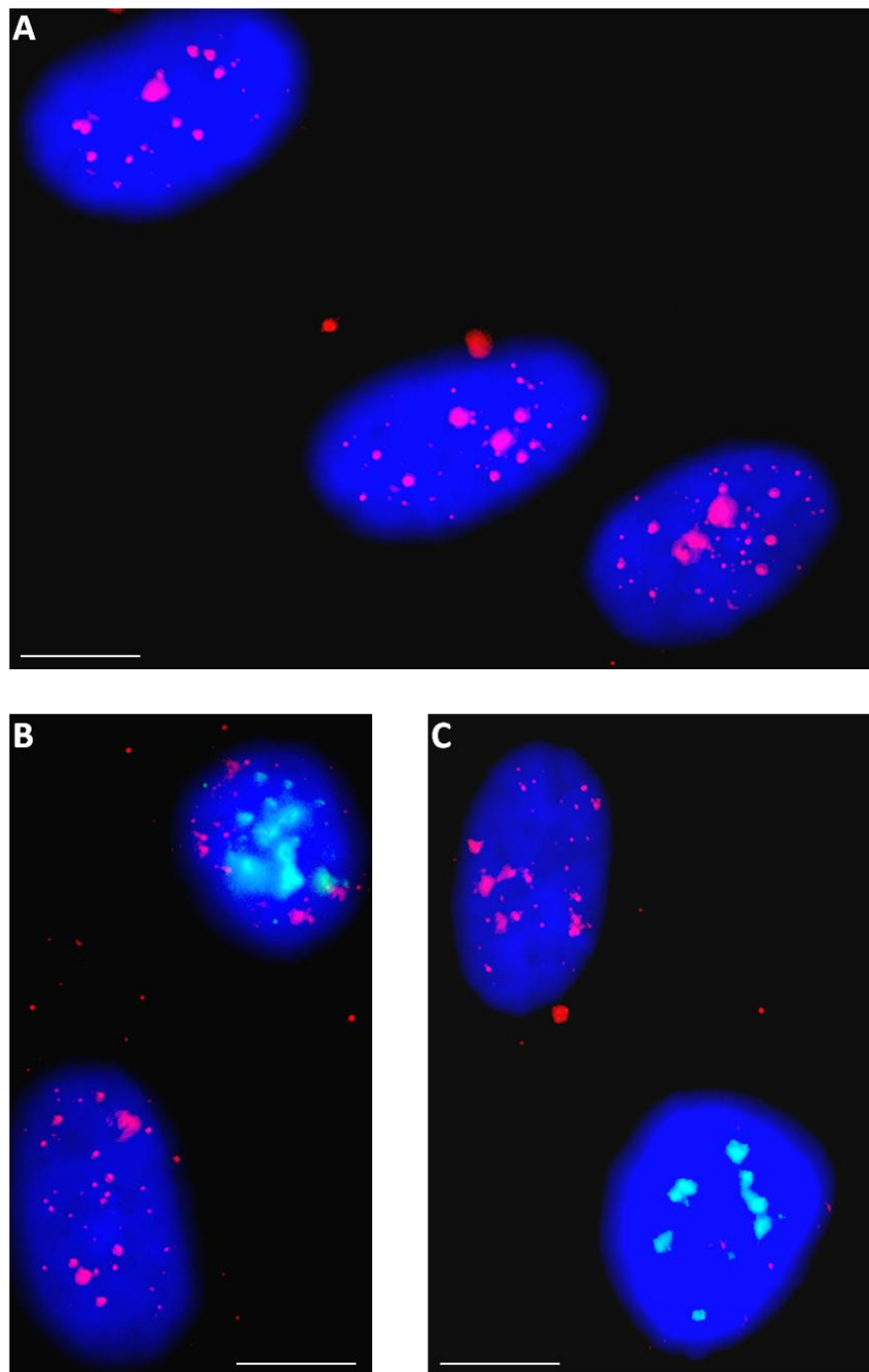

Figure 2.16. Nuclei of cells stained with DAPI (blue showing whole nucleus), MYO16 (red TRITC 2°) and Ki-67 (green FITC 2°) antibodies. (A) All nuclei show MYO16 staining only. (B) One nucleus showing MYO16 staining only and one nucleus showing both MYO16 and Ki-67 staining. (C) One nucleus showing MYO16 staining only and one nucleus showing mainly Ki-67 staining, but also showing 4 very small MYO16 foci. Scale bar = 10µm.
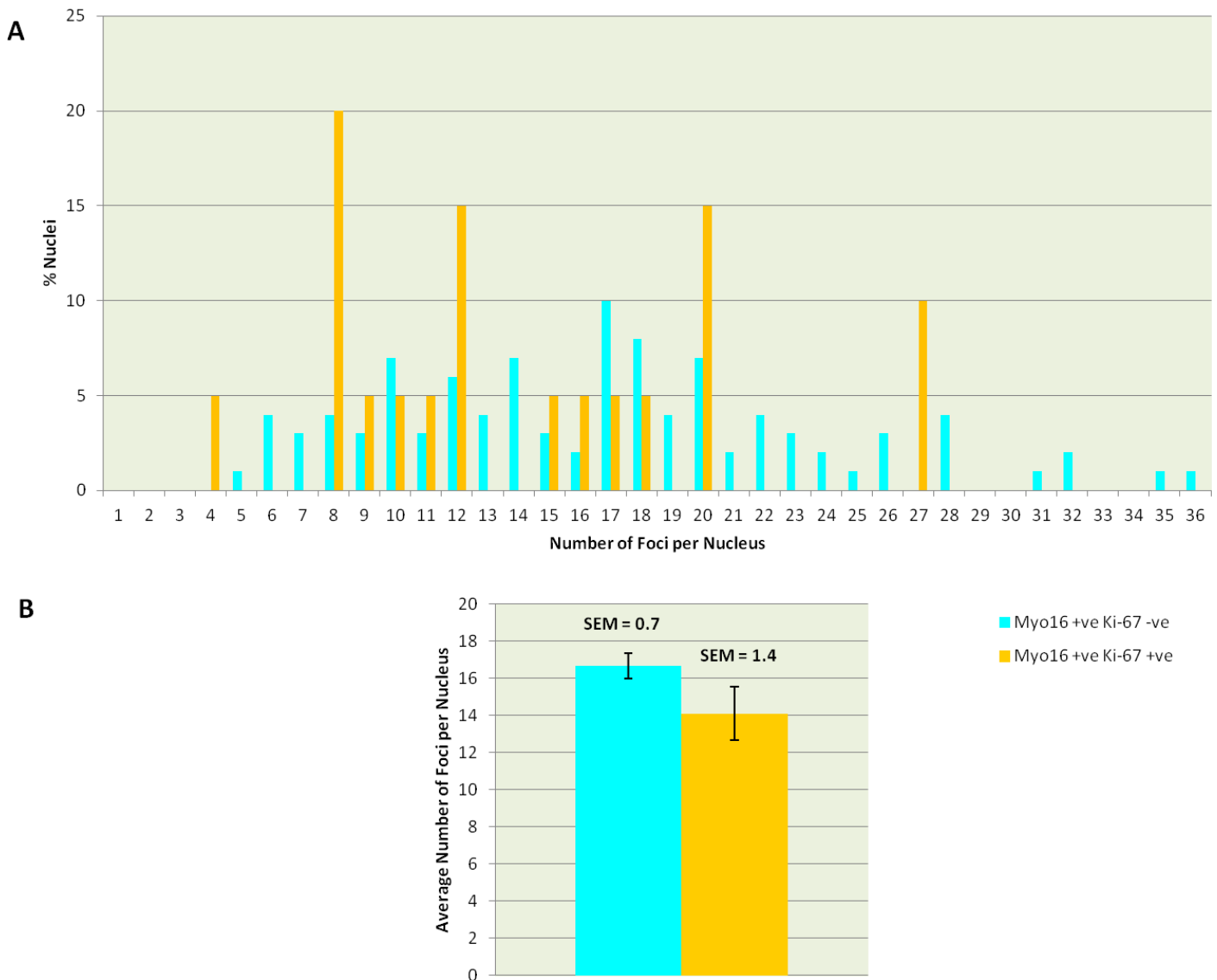
Figure 2.17. Graphs showing results of foci counts for immunofluorescence staining with MYO16 and Ki-67 in the nuclei of quiescent cells, grown in low serum media, comparing proliferating and non-proliferating cells. For MYO16 +ve Ki-67 +ve n = 20 nuclei, for MYO16 +ve Ki-67 –ve n = 100 nuclei. (A) This graph shows the proportion of nuclei as percentages with different numbers of foci. (B) This graph shows the average numbers of foci per nucleus. SEM = Standard Error of the Mean. t-test **P = 0.1243**.

Detection of MYO18B in the nuclei of quiescent cells grown in low serum (0.5% FCS) media

The staining of MYO18B in the nuclei of cells made quiescent was quite different compared with the staining obtained with MYO5B and MYO16. Representative images of the results are shown in Figures 2.18 and 2.19. This staining covers most of the visible area of the nucleus in the quiescent cells, and consists mostly of hazy homogenous areas, combined with many very fine punctate foci. It was decided that the nature of staining obtained for MYO18B was not suitable for foci counts in a comparative manner, with regards to the other two myosins studied in this section. As a consequence, there was no quantification of the data for MYO18B in this section, and only qualitative results are presented. As can be seen in Figure 2.19 A, the nuclei which were quiescent, as shown by lack of Ki-67 staining had visibly much higher levels of staining compared with nuclei which were still proliferating. Therefore, the trend that the nuclei of non-proliferating cells show more foci than the nuclei of proliferating cells is again supported in principle, though without the benefit of full quantification.
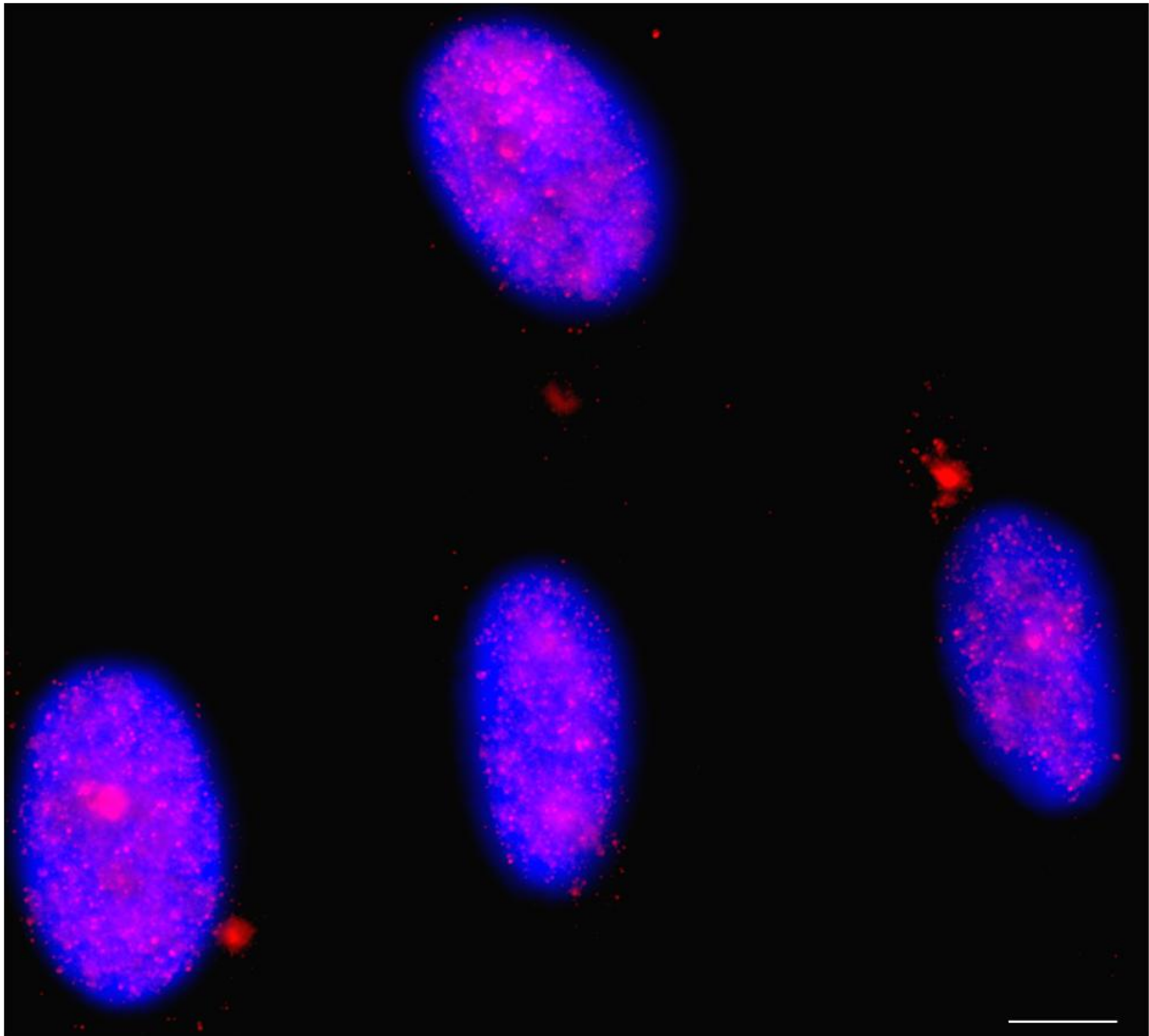
Figure 2.18. Nuclei of cells stained with DAPI (blue showing whole nucleus), MYO18B (red TRITC 2°) and Ki-67 (green FITC 2°) antibodies (note no Ki-67 +ve nuclei in this figure). This staining for MYO18B is described as consisting of hazy homogenous areas combined with many very fine punctate foci, and was quite unusual compared to the staining for MYO5B and MYO16. Scale bar = 10µm.
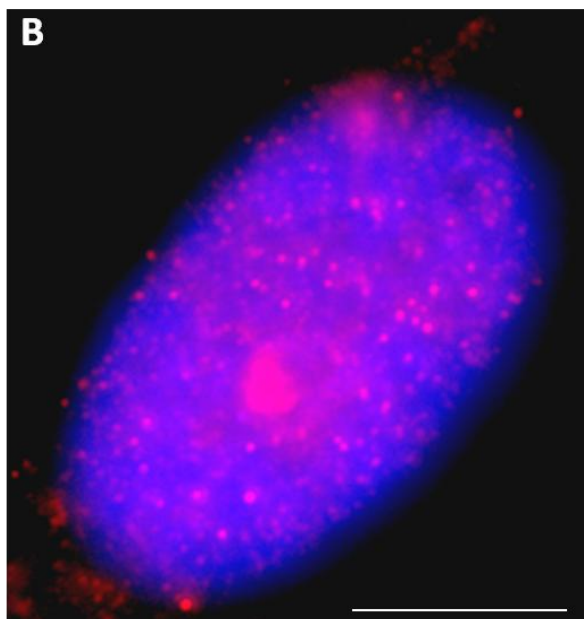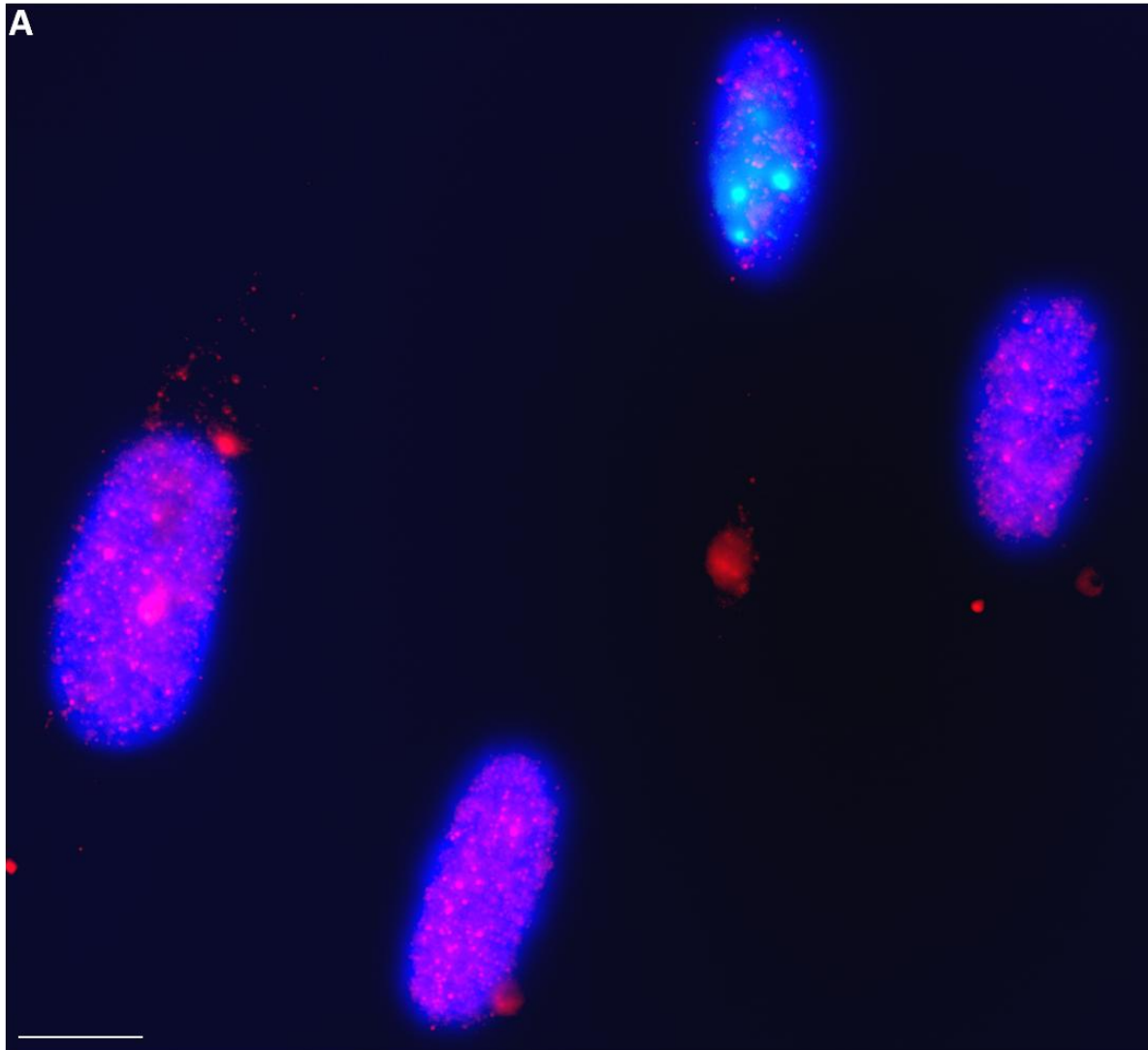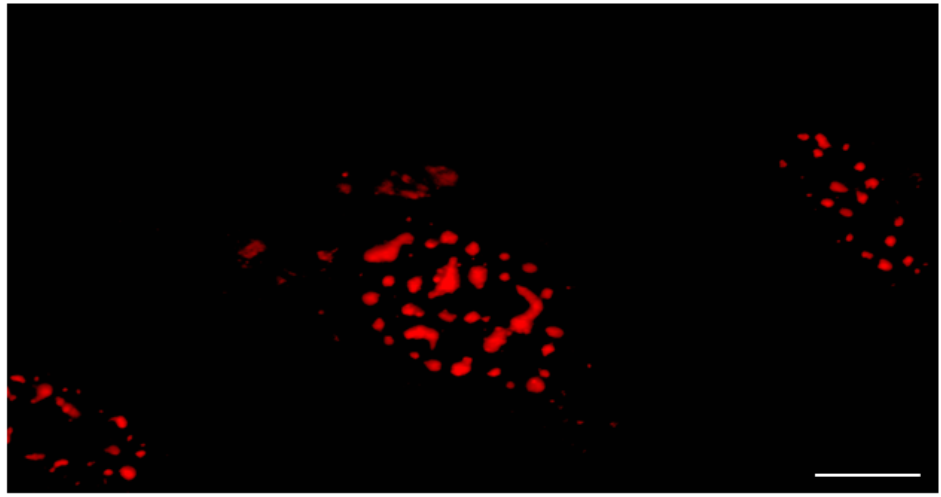
Figure 2.19. Nuclei of cells stained with DAPI (blue showing whole nucleus), MYO18B (red TRITC 2°) and Ki-67 (green FITC 2°) antibodies. (A) Three nuclei showing MYO18B staining only and one nucleus showing both MYO18B staining and Ki-67 staining, though with considerably less MYO18B foci than in the Ki-67 negative nuclei. (B) Larger image of a nucleus with MYO18B staining only. Scale bar = 10µm.

2.3.4 Experiments to determine co-localisation of SC35 with nuclear myosins in cells grown in high serum (15% FCS) media

In order to help further determine the nature of the possible interactions of the nuclear myosins studied, with other known proteins in the nucleus that may have a similar distribution, immunofluorescence dual staining was performed with MYO5B, MYO16 and MYO18B, each co-stained with SC35, which is known to be associated with splicing speckles. Particularly, as the staining patterns for MYO5B carried out in previous experiments looked similar to splicing speckles, it was of interest to investigate the possibility that MYO5B was co-localised with SC35. Indeed this postulation proved correct and unequivocal co-localisation was found in the nucleus between MYO5B and SC35 only. This is a new finding, since this co-localisation has not been reported in the literature. The other myosins (MYO16 and MYO18B) used in these experiments did not co-localise with SC35. Results are shown only for the novel co-localisation of MYO5B with SC35 (Figure 2.20). The lack of co-localisation of SC35 with MYO16 and MYO18B was not imaged and was only qualitatively recorded as negative for co-localisation in the raw data. For MYO5B co-stained with SC35 It was found that after observing over 200 cells by fluorescence microscopy, all the nuclei viewed display this complete co-localisation (100%) and although some very minor parts of very few individual structures in the nucleus were not completely co-localised (see Figure 2.20 for example), every MYO5B stained structure in the nucleus was co-localised with SC35. Due to this complete positive result for co-localisation, it was not deemed necessary to present a graph for this outcome.
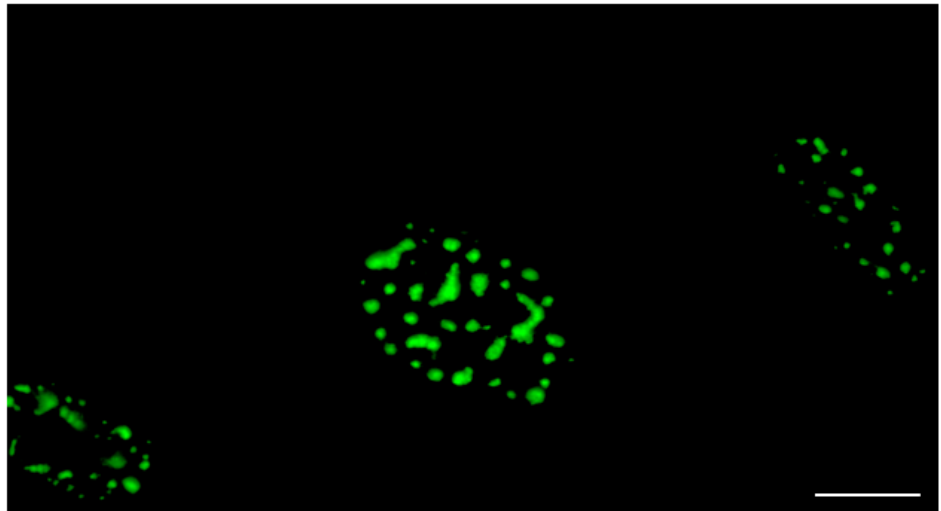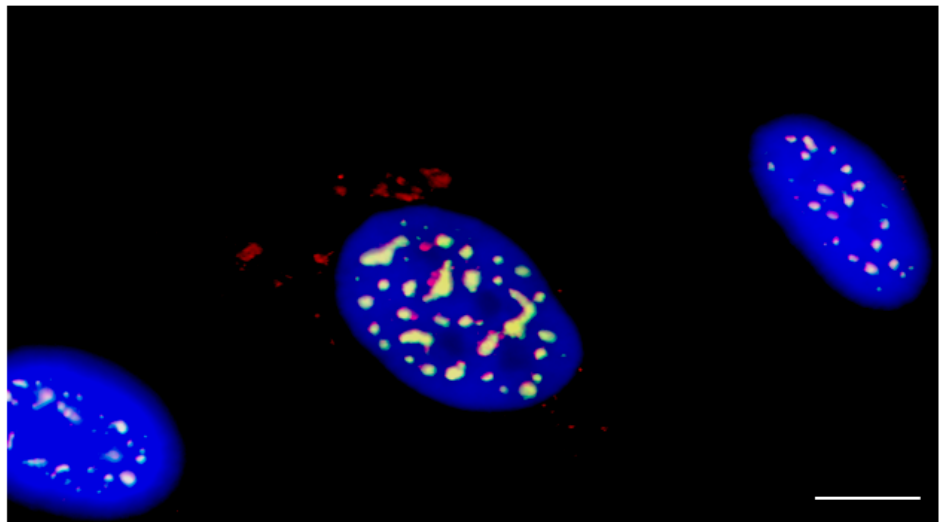
Figure 2.20. Three cell nuclei stained with DAPI (blue showing whole nucleus), MYO5B (red TRITC 2°) and SC35 (green FITC 2°) antibodies. Separate images are shown for each antibody and the merged image clearly shows that MYO5B and SC35 are colocalised in the nucleus. Note that these are intact fixed cells and therefore, beyond the visible boundary of the nuclei is the cytoplasm of each cell, though it is not stained to be visible. Some cytoplasmic MYO5B staining can be seen in the vicinity of one nucleus. Scale bar = 10um.

2.4. DISCUSSION

A comparative study was performed using proliferating and non-proliferating fibroblast cells, in order to gain some insight into differences in the staining patterns of various nuclear myosins under these cellular states, with a view to obtain extrapolated information concerning the expression patterns and frequency of these proteins under such conditions. This information would allow the deduction of the cellular environment with regards to these potential molecular motor proteins which may, or may not be involved in chromosome mobility. The relevance of this information stems from a key principle of this project, that in non-proliferating cells the mobility of chromosomes is affected, and this may be due to the possibility that the active myosin molecular motors located in the nucleus have reduced functionality in this cellular state. These concepts and lines of research are important in helping to shed light on the relationships between the cell nucleus with regards to structure, function and dynamics, and the physiological states and processes that affect for example, cellular and organismal ageing.

Having successfully obtained results for the myosin primary antibodies in the initial antibody test phase experiments involving use of single primary antibodies, showing staining in the nucleus, the dual staining experiments were designed to include Ki-67 staining to help interpret the results in the context of cell proliferation or non-proliferation. The results obtained from the dual staining experiments demonstrated clearly that proliferating and non-proliferating cells show differences in nuclear staining for the myosins studied in this project. The observed trend in the results for cells grown in high serum (15% FCS) media was that in non-proliferating cells the nuclei show more myosin foci compared with the nuclei of proliferating cells. This difference in the results was found to be strongly supported by the statistical analyses, and corroborated by all the myosin proteins studied in this chapter. In particular this difference was very strongly supported by the statistical analysis for MYO5B and MYO18B, and less strongly supported for MYO16 though still statistically significant (this point has relevance to the discussion which follows).

When cells grown in low serum (0.5% FCS) media, for the purpose of inducing quiescence were investigated, the results were rather more complex and two other

71

trends emerged when this data was compared with the data for high serum (15% FCS) media grown cells. Firstly, looking at the low serum media results for MYO5B, they did confirm the trend of non-proliferating cells showing more nuclear myosin foci than in proliferating cells, however this difference although still statistically significant, was less so when compared with the high serum MYO5B results, on the basis of the P value obtained from the t-test. The low serum media results for MYO16 did show more nuclear foci for non-proliferating cells when compared to the proliferating cells, but this difference was not supported by the statistical analysis as being significant, and importantly in terms of trend, note that with the high serum media results, MYO16 was the protein with less strong statistical support for the trend of more nuclear foci in non-proliferating cells compared with MYO5B and MYO18B. This point reveals the first trend of the low serum media results, which is that in low serum media grown cells, the difference between the numbers of myosin foci comparing proliferating and non-proliferating cell, becomes less statistically significant when compared with the situation where cells are grown in high serum media. This suggests that under low nutrient conditions, the differences are less pronounced with regards to the frequency of nuclear myosin foci. The second trend emerging from the low serum media results, is that growth in low serum conditions correlates with a higher number of nuclear foci overall for MYO5B and MYO16, both in the non-proliferating cells and the proliferating cells, compared with cells grown in high serum media. This difference was most pronounced for MYO16, but for both MYO5B and MYO16 the difference was also very strongly supported statistically. Clearly the nutrient level in the media is an important variable, affecting the presence of visible nuclear myosin foci. The low serum media results for MYO18B were unusual and found not to be suitable for the same foci count method of quantification, as had been applied to the other two myosins studied. The nature of the MYO18B staining which covered most of the nuclear area was hazy and homogenous, with many very fine punctate foci. With regards to the second trend discussed here, that cells in low serum conditions show more nuclear myosin foci than those in high serum conditions, this result obtained for MYO18B does adhere to this trend, since the staining is more intense and covers more of the nuclear space. Interestingly, the staining pattern for MYO18B in low serum conditions shows similarities to that seen for NM1β in senescent cells, in the work by Mehta et al. (2021). The authors described this staining pattern as comprised of aggregates, and correlated this type

72

of staining with the lack of chromosome relocation in response to stimuli. Therefore, in principle the findings in this chapter, that in non-proliferating cells there is a trend of increased nuclear myosin staining foci, and that this trend is more pronounced when cells are grown in low nutrient conditions, are in agreement with the findings of Mehta et al. (2021). Thus this trend seems to be a characteristic pattern of non-proliferating cells and may be an indicator of the cellular changes that occur with regards to nuclear myosins, when proliferating cells become quiescent or senescent.

The precise molecular reasons leading to this trend was beyond the scope of this work, however by way of postulation it may be inferred that, the nuclear myosin proteins studied may exist as visible storage granules at interphase in the nuclei of non-proliferating cells where they may be largely inactive in terms of their active functions. Thus, they are present in visually larger numbers of foci of varying sizes. However, in the nuclei of proliferating cells, these nuclear proteins may exist mostly in an active form, and therefore not visible as storage granules to the same extent seen in non-proliferating cells. In the active form, the proteins would be more dispersed carrying out their functions where needed, however some will still remain as inactive granules such the supply of these crucial proteins would not be exhausted at anytime. It has been found that the myosin proteins are very dynamic with regards to molecular conformation and can alter between active and inactive forms (Carragher et al. 1998; Taylor 2007; Porter et al. 2020).

The results of the co-localisation experiments of the myosins with SC35 led to a new find with the clear co-localisation of SC35 with MYO5B. It has previously been shown that MYO5A co-localises with SC35 (Pranchevicius et al. 2008), but the co-localisation of MYO5B with SC35 has not been previously reported. Splicing speckles are involved with the processing of pre-mRNA and are involved with mature mRNA export. Interestingly, highly expressed genes are found to be associated with splicing speckles and so potentially, there may be a requirement for molecular motor activity in this gene locus specific translocation during gene regulation. It may be possible that MYO5B could be involved in this process, as part of a molecular motor complex together with MYO5A. Equally interesting is the possibility that MYO5B has a role in the mobility of splicing speckles, a possibility which is related to a finding described in chapter 1, section 1.1.4, Zhang et al. (2016). Although the authors

postulated that myosins may be involved in the mobility of splicing speckles, the identity of the myosin has not been discovered. Therefore this is potentially a significant find which will need further investigation in future.

The process of cellular ageing has also been associated with the effects of reactive oxygen species (ROS) (Klimova et al. 2009; Shimi and Goldman 2014; Roger et al. 2021), though this relationship may be rather complex, and positive correlation is not always observed (Miwa et al. 2004; Magwere et al. 2006). It has been suggested that ROS can have both harmful and beneficial effects with regards to ageing (Shields et al. 2021). Unravelling the details of the ageing process at a cellular level is a multifaceted and multifactorial endeavour, and may include effects of cellular biochemistry, as well as changes to the dynamic mechanisms related to cellular and genome functions (Vijg and Suh 2023). Increased understanding of the differences between proliferating and non-proliferating cells and how these differences may affect cellular processes, may also help inform regarding aspects of disease states, where the control of cell proliferation has been disrupted, thus leading to uncontrolled cell division, for example in cancer.

Chapter 3: Bioinformatics to further explore myosin proteins studied and to identify other proteins which may be involved in chromosome mobility

3.1 Introduction.

3.2 Materials and methods.

3.3 Results: Bioinformatics data analysis.

3.4 Discussion.

3.1 INTRODUCTION

In silico analyses and bioinformatics data searching and mining were used, firstly in order to gain more insight into the candidate myosin proteins that had been initially selected for this study, as described in chapter 2 (MYO5B, MYO16 and MYO18B). Further to the analyses performed for the myosins studied in chapter 2, the same analyses were also performed for NM1β which has previously been shown to be directly involved in chromosome mobility (Mehta et al. 2010), and for two actin related proteins (ARPs), these being ACTR6 and BAF53A. The ARP ACTR6 also known as ARP6 is part of the snf-2 related CBP activator protein (SRCAP) complex, which is involved in chromatin remodeling (Oma and Harata 2011). The ARP BAF53A is a component of the BAF complex (BRG1/brm-Associated Factor) complex. BAF53A was the first vertebrate ARP found to be expressed in the nucleus, and in humans there are two isoforms, BAF53A which is expressed in all tissues, and BAF53B which is expressed in brain tissue only (Oma and Harata 2011). BAF53A is involved in transcriptional activation by ATP-dependant chromatin remodeling (Oma and Harata 2011). The results of the core analyses (MYO5B, MYO16, MYO18B, NM1β, ACTR6 and BAF53A) with regards to interaction networks were then utilised to explore other possible candidate proteins that may be involved in chromosome mobility processes. Further to this and as a continuation of this investigation, additional bioinformatics tools were utilised to study the conserved domains of the proteins that were studied in the core analyses. Other bioinformatics resources were used to gain some insight from aspects of the phylogenetic evolutionary history of these proteins.

Bioinformatics offers a large array of powerful tools to perform various types of analyses on biological data. This opportunity to further explore the selected myosin proteins studied in chapter 2, and additionally NM1β and two ARPs, and to further hunt for other possible candidates, was an exciting prospect and considered very beneficial. This would help shed light on the various proteins that may have a role in chromosome dynamics. Some of the advantages of the bioinformatics approach include the organisation of vast amounts of biological data into standard formats, which are made available to researchers in a reliable and easily accessible way (Hagen 2000; Hogeweg 2011; Gauthier et al. 2019). The computational power of

bioinformatics programmes and databases allows such data mining and investigations to be carried out relatively rapidly, although it is important to select the most suitable and informative tools, following a wider consideration of the available resources and their relative informational or analytical attributes.

The use of bioinformatics resources also allows a comparative approach such that proteins and genes can be studied in a broader context in terms of their occurrence, similarity and functions in other taxa. This would help shed light on conserved structures and functions, thus highlighting important functional roles in living systems (Marsden et al. 2006; Yang et al. 2012). This stems from the key principles of evolutionary theory that those structures and functions, be they at the molecular, cellular or organismal level, which are necessary for life processes and impart a survival advantage, will be conserved through evolutionary time and across taxa through the action of natural selection (Sharan et al. 2005; Richards and Cavalier-Smith 2005; Laurent et al. 2010). Although there will be some mutational drift and alteration, for example when comparing a class of proteins in different taxa, several key features will be conserved, and it is those features which characterise the specific functional aspects of the protein (Jez 2017).

Considering the vast information generation in recent biological research which may be described as 'information overload', it is clear that bioinformatics is a necessary tool in most areas of bioscience research. With this realisation together with the desire to further reveal candidate proteins involved with chromosome mobility, bioinformatics was considered as a useful and productive addition to this project. Using bioinformatics for this project has been beneficial, and has helped to further determine the likelihood of whether the myosins initially selected for study in this project, may or may not be involved in chromosome mobility. In addition, other possible candidate proteins which may potentially be involved in chromosome mobility have been suggested, as a result of interaction networks. These include other myosins as well as ARPs including those of the actin related protein 2/3 (ARP2/3) complex, and other proteins such as actin nucleation factors.

3.2 MATERIALS AND METHODS

The 'Search Tool for the Retrieval of Interacting Genes/Proteins' (STRING) online resource was used to determine interaction networks (Snel et al. 2000; von Mering et al. 2005; Szklarczyk et al. 2019; Szklarczyk et al. 2021) for the candidate myosin proteins which had been selected at the start of this project, as well as for NM1β, ACTR6 and BAF53A. These analyses generated diagrams and lists of predicted functional partners for these proteins. The settings for the minimum interaction scores and maximum number of interactors were adjusted accordingly for each protein, to allow for proteins with mostly low interaction scoring partners, such that a sizable network diagram and interaction list could be generated for those proteins also.

Diagrams for co-expression of the members of each generated network were also studied to gain more insight on any possible interaction, or inferred common function in humans as well as in other taxa. Comparisons with other taxa help to shed light on conservation of molecular interactions across evolutionary scales, indicating crucial associations with regards to networks. The co-expression diagrams are determined by RNA expression patterns, and information on protein co-regulation which is obtained from the ProteomeHD online database. In addition to this, the functional domains of each candidate protein was characterised using the Conserved Domains Database (CDD) resource on the National Centre for Biotechnology Information (NCBI) website. This level of information is useful for gaining more knowledge about the structure of the proteins as well as identifying potential regions on the corresponding gene sequence for possible future projects, involving site-directed mutagenesis experiments for example, to generate knockout or partially functional transgenes. This would help identify both crucial proteins in mechanisms under study, as well as further identify the specific important residues required for proper function of the protein, and therefore possibly aid any future gene repair strategies.

Phylogenetic trees generated following a protein BLAST (Basic Local Alignment Search Tool) analysis were also studied to gain more information regarding the taxon wide conservation of the proteins of interest, thus indicating the functional and structural conservation over evolutionary scales. This mode of analysis via

highlighting conservation of structure and function over evolutionary time and across taxa helps to add robustness to any inferences regarding crucial functions.

The STRING analysis network prediction diagrams are generated based on the algorithms of the programme and an important note to consider is that the distances between the protein nodes is not proportional to the interaction scores. Therefore, it should not be attempted to derive information regarding the level of confidence of the interaction between the proteins of interest by this visual method (STRING website; Szklarczyk et al. 2021). According to the developers of the STRING algorithm, the shape of the interaction network is mainly influenced by a spring model, where the protein nodes are masses held together by springs, and the tendency of this layout is set to minimize the energy of the system. High scoring interactions are given higher spring strengths and generally are drawn closer together and therefore in this respect, there is some visual information to be gained from the overall structure of the network (STRING website; Szklarczyk et al. 2021). The generated list of predicted functional partners together with information on the types of evidence for the interaction computation clearly and informatively displays the strength of interactions in descending order of interaction score. The types of evidence used to determine the interaction scores include co-occurrence (in terms of gene families in other species); co-expression (based on RNA and protein data); experiments (based on known protein-protein interaction data); databases (based on biochemical pathways and protein complexes from curated databases) and text-mining (based on scientific literature) (STRING website). The closer the interaction score is to 1 the higher the confidence level of interaction (scores of 0.7 and above are categorised as high confidence and scores of 0.9 and above are categorised as highest confidence). The results generated by these lists were very useful and were used to help identify other potential candidate proteins of interest which may be involved in aspects of chromosome mobility. The selection procedure for these additional candidates involved assessing the interaction score, the nature of the protein and any known information regarding functions.

3.3 RESULTS

3.3.1 MYO5B bioinformatics analyses

The results of the STRING analysis for MYO5B do not associate this protein with other myosins or ARPs. However, a rather interesting association with relevance to the nucleus was made with two other interactors following the STRING analysis (Figure 3.1). These proteins are SPIRE1 (Protein spire homolog 1) and SPIRE2 (Protein spire homolog 2) which although not classified as ARPs, are closely involved with actin function, both in the cytoplasm and in the nucleus, and referred to as actin nucleation factors (Belin et al. 2015). In humans these proteins are encoded by the genes; spire type actin nucleation factor 1 and spire type actin nucleation factor 2, respectively. The spire protein was first identified in *Drosophila* (Quinlan et al. 2005). The interaction score for SPIRE1 is 0.871 and the interaction score for SPIRE2 is 0.875, showing both interactions to be considerably above the high confidence level of 0.7 in the criteria of the STRING analysis settings. The three highest confidence interactions with MYO5B were shown with two members of the Ras related proteins, and a RAB11 interacting protein, specifically RAB11A, RAB11B and RAB11FIP2 (Rab11 family interacting protein 2). Other members of the Ras related proteins showing high confidence interactions with MYO5B are RAB8A, RAB25, RAB10 and RAB8B.

The co-expression chart for the MYO5B network in humans shows low level confidence co-expression with RAB25 (Figure 3.2). There are various low level confidence co-expression data between other members of the generated network, though not involving MYO5B, with the strongest being between RAB11B and RAB10. In other taxa there is very low level confidence co-expression between Myo5b and all other members of the generated network except for Spire1.
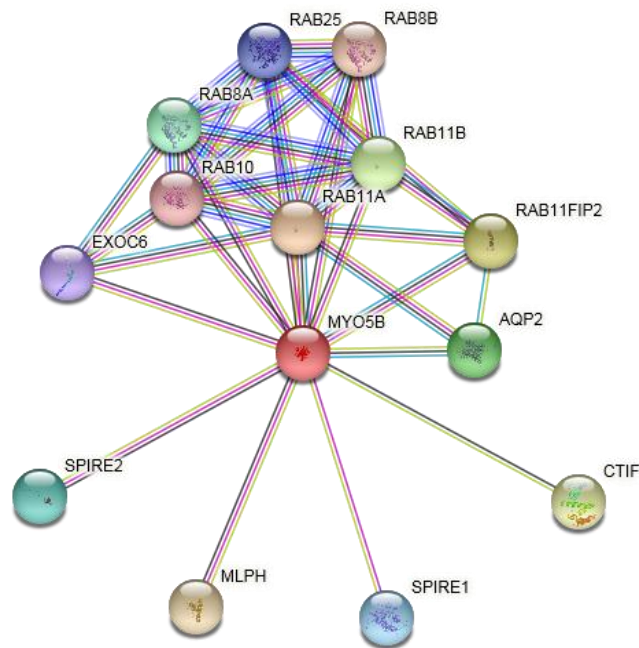
Your Input:

● MYO5B	Unconventional myosin-Vb; May be involved in vesicular trafficking via its association with the CART complex. The CART complex is necessary for efficient transferrin receptor recycling but not for EGFR degradation. Required in a complex with RAB11A and RAB11FIP2 for the transport of NPC1L1 to the plasma membrane. Together with RAB11A participates in CFTR trafficking to the plasma membrane and TF (transferrin) recycling in nonpolarized cells. Together with RAB11A and RAB8A participates in epithelial cell polarization. Together with RAB25 regulates transcytosis; Belongs to the TRAFAC cla [...] (1848 aa)

Predicted Functional Partners:

		Neighborhood	Gene Fusion	Cooccurence	Coexpression	Experiments	Databases	Textmining	[Homology]	Score
● RAB11A	Ras-related protein Rab-11A; The small GTPases Rab are key regulators of intracellular membrane trafficking, from the fo...				●	●	●			0.999
● RAB11FIP2	Rab11 family-interacting protein 2; A Rab11 effector binding preferentially phosphatidylinositol 3,4,5-trisphosphate (PtdI...				●	●	●			0.993
● RAB11B	Ras-related protein Rab-11B; The small GTPases Rab are key regulators of intracellular membrane trafficking, from the fo...				●		●			0.969
● AQP2	Aquaporin-2; Forms a water-specific channel that provides the plasma membranes of renal collecting duct with high per...					●	●			0.939
● RAB8A	Ras-related protein Rab-8A; The small GTPases Rab are key regulators of intracellular membrane trafficking, from the for...				●		●			0.933
● SPIRE2	Protein spire homolog 2; Acts as an actin nucleation factor, remains associated with the slow-growing pointed end of the...				●		●			0.875
● SPIRE1	Protein spire homolog 1; Acts as an actin nucleation factor, remains associated with the slow-growing pointed end of the...					●	●			0.871
● RAB25	Ras-related protein Rab-25; Involved in the regulation of cell survival. Promotes invasive migration of cells in which it fun...				●	●	●			0.865
● EXOC6	Exocyst complex component 6; Component of the exocyst complex involved in the docking of exocytic vesicles with fusi...				●	●	●			0.794
● RAB10	Ras-related protein Rab-10; The small GTPases Rab are key regulators of intracellular membrane trafficking, from the for...				●	●	●			0.737
● RAB8B	Ras-related protein Rab-8B; The small GTPases Rab are key regulators of intracellular membrane trafficking, from the for...				●	●	●			0.708
● MLPH	Melanophilin; Rab effector protein involved in melanosome transport. Serves as link between melanosome-bound RAB27...				●	●	●			0.704
● CTIF	CBP80/20-dependent translation initiation factor; Specifically required for the pioneer round of mRNA translation mediat...						●			0.703

Your Current Organism:

Homo sapiens

NCBI taxonomy Id: 9606
Other names: H. sapiens, Homo sapiens, human, man

Figure 3.1. MYO5B network prediction with settings at minimum of 0.7 interaction score (high confidence) and maximum of 20 interactors for the generated network. The highest confidence interactions are shown with two the Ras related proteins and a RAB11 interacting protein. The high confidence interactions with SPIRE1 and SPIRE2 are interesting since these are actin nucleation factors.
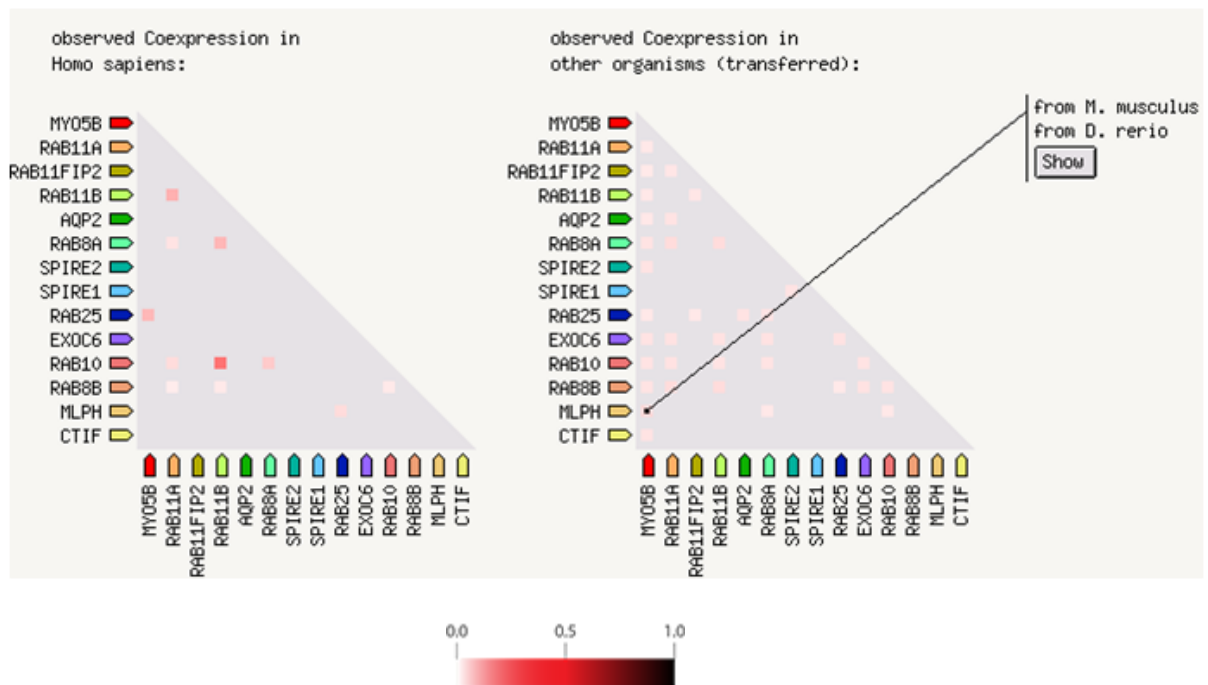
Figure 3.2. MYO5B network co-expression based on RNA expression patterns and protein co-regulation. In humans, the co-expression chart for MYO5B shows low level confidence co-expression with RAB25 only. In other taxa, the co-expression of MYO5B with most other members of the network shows very low level confidence. The intensity of the square box colour represents the level of confidence as shown by the red bar scale.

The conserved domains analysis for MYO5B shows the positions of several features on the protein including characteristic class V myosin motor and a cargo binding domain, as well as the ATP binding site residues. There are also 3 calmodulin binding motifs (see Figure 3.3).

The phylogenetic tree generated by BLAST shows MYO5B to be well conserved in mammals (Figure 3.4), with the outgroup sequence representing the most basal sequence for this tree, belonging to *Chrysochloris asiatica* (Cape Golden Mole). It is important to note that this phylogenetic tree only shows the most similar sequences and so for this protein, the tree shows only mammalian species. There are certainly more distant homologous proteins to MYO5B in more primitive taxa outside of the mammals.
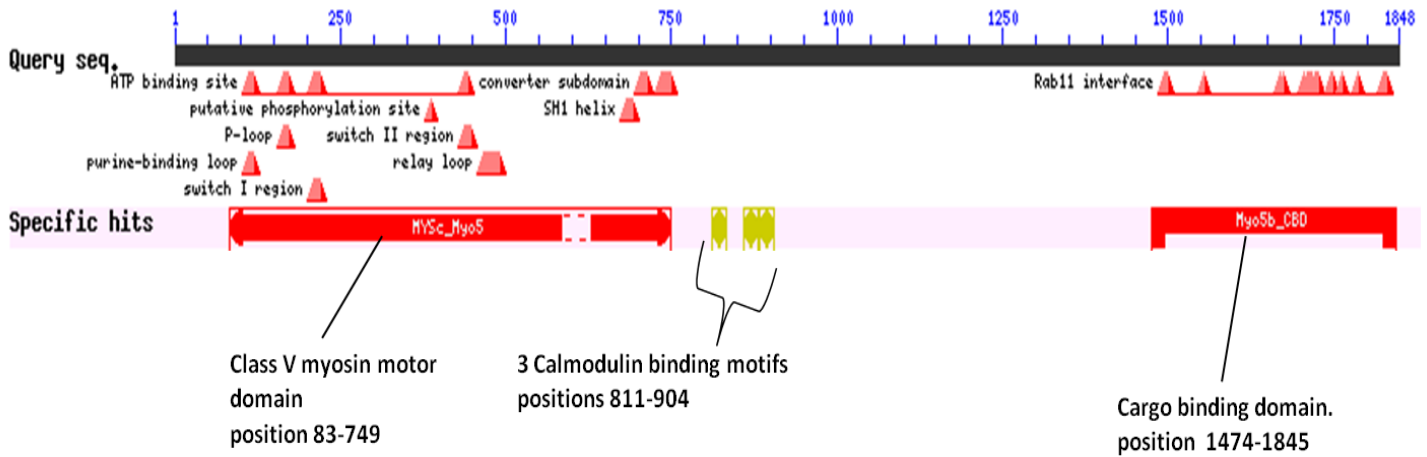
Figure 3.3. Results of the conserved domains analysis for MYO5B. The NCBI Conserved Domains Database (CDD) tool was used to generate the data in this figure. Specific hits show class V myosin motor domain, calmodulin binding motifs and the cargo binding domain. Within the region of the motor domain, more information on the positions of residues are given such as the ATP binding site.
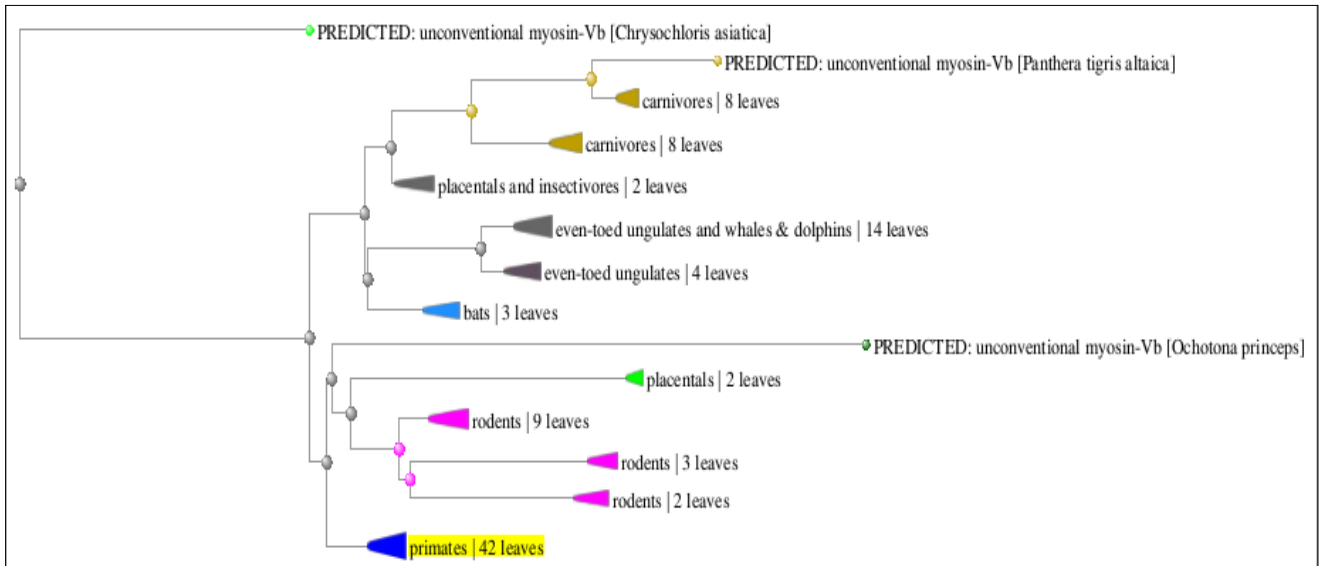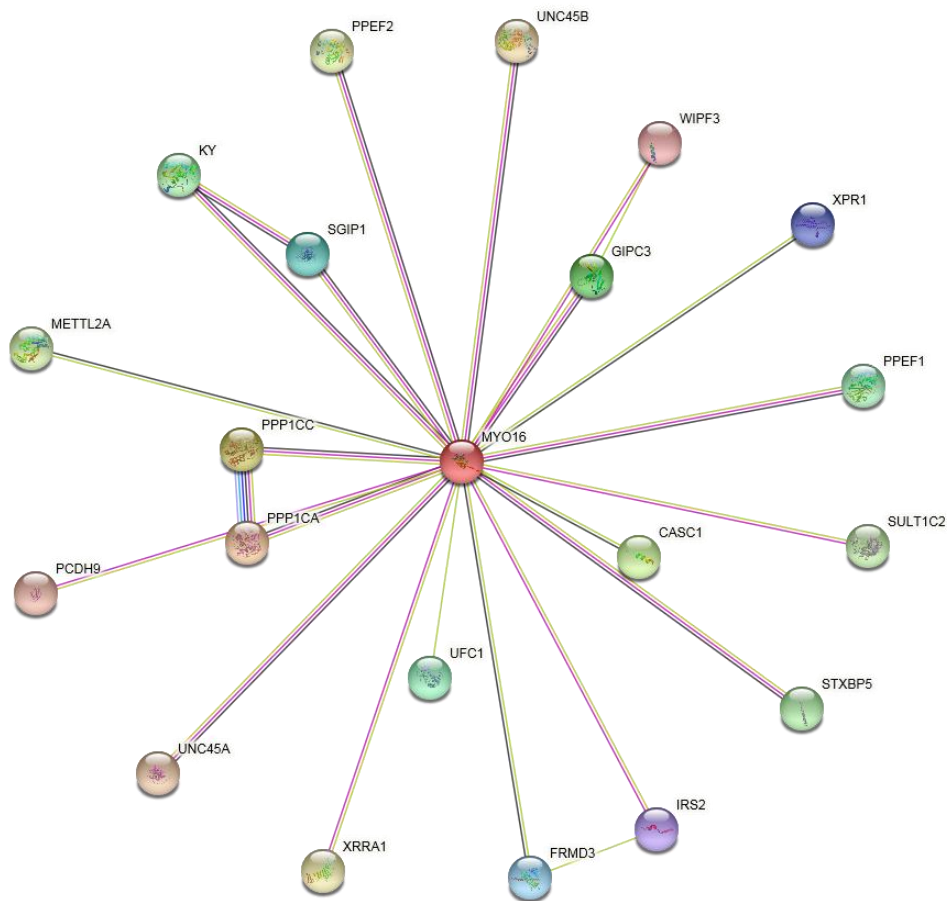

Figure 3.4. Phylogenetic tree of the BLAST results for MYO5B. Tree method is fast minimum evolution with pairwise alignment between query sequence (Homo sapiens) which is within the yellow highlighted cluster (Primates), and the sequences searched in the database (BLAST website). Tree settings are with Max sequence difference 0.85 and Grishin (Protein) distance method.

83

3.3.2 MYO16 bioinformatics analyses

The STRING analysis results for MYO16 did not produce any high confidence interactions for the network. It was therefore necessary to set the minimum interaction score parameter to a minimum of 0.4 (medium confidence) in order to allow for an interaction network to be generated (Figure 3.5). In addition to this, there were no myosin or ARP interactors identified by the network. The co-expression chart for humans shows low level confidence co-expression of MYO16 with SH3-containing GRB2-like protein 3-Interacting Protein-1 (SGIP1) only (Figure 3.6). In other taxa there are several more low confidence expression data between Myo16 and other network proteins.

The conserved domains analysis shows the expected class XVI myosin motor domain and various other features including the ATP binding region, however there does not seem to be a cargo binding domain identified (Figure 3.7).

The BLAST phylogenetic tree for MYO16 shows that the protein is well conserved in mammals (Figure 3.8) and interestingly the outgroup branch of the tree, representing the most basal sequences in the tree include reptiles, including *Chrysemys picta bellii* (Western painted turtle).

Figure 3.5. MYO16 network prediction with settings at minimum 0.4 interaction score (medium confidence) and maximum 20 interactors. For this protein there were no high level confidence interactions, with the highest score being only 0.583.
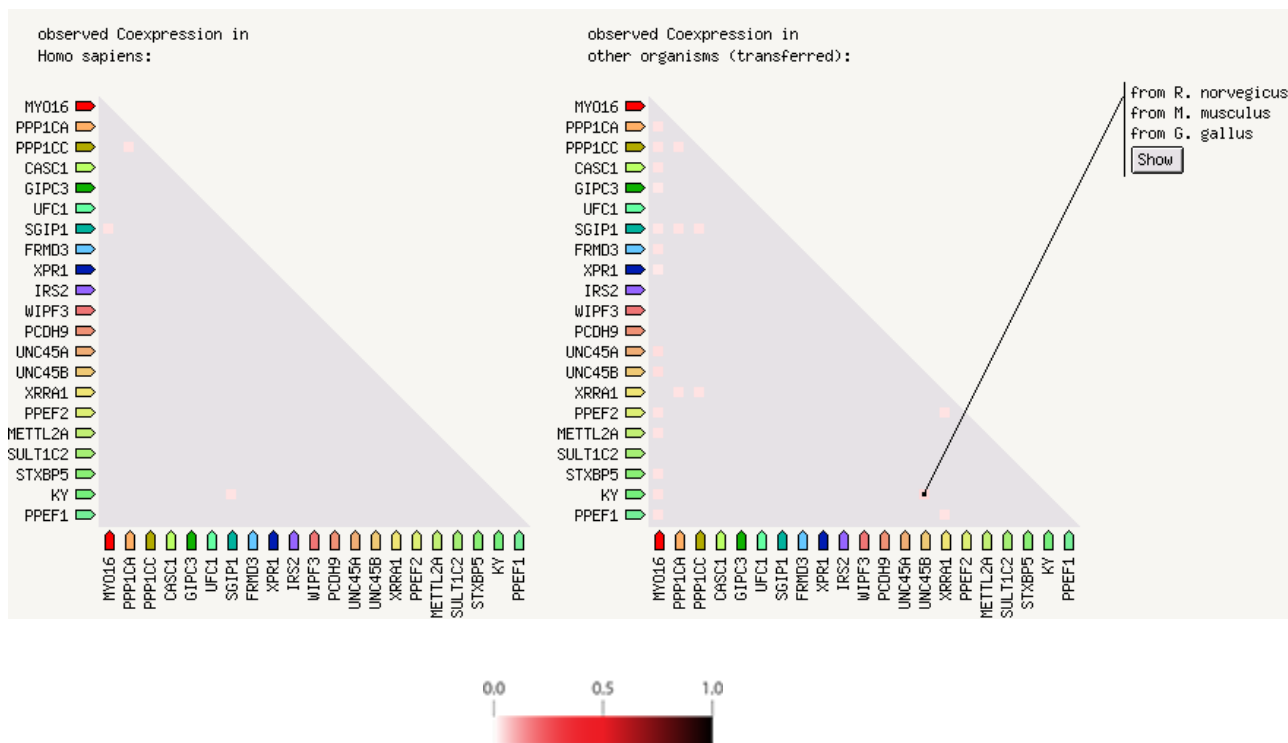
Figure 3.6. MYO16 network co-expression based on RNA expression patterns and protein co-regulation. In humans, only very low level confidence co-expression is shown with SGIP1. In other taxa some very low level confidence co-expression are shown. The intensity of the square box colour represents the level of confidence as shown by the red bar scale.

.
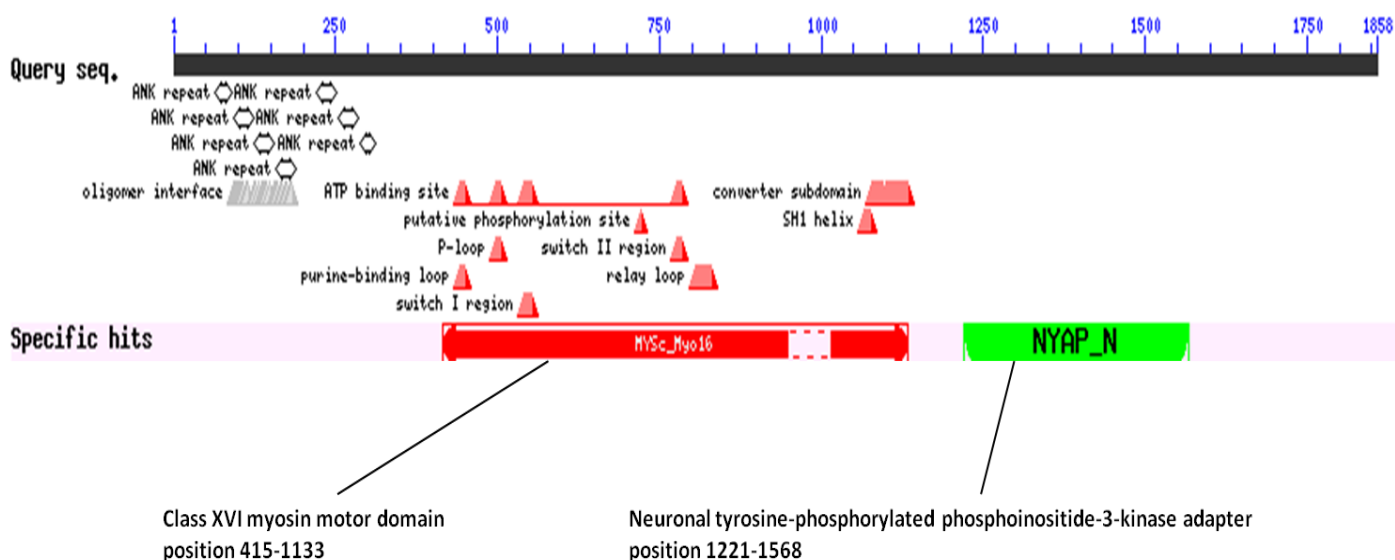
Figure 3.7. Results of the conserved domains analysis for MYO16. The NCBI Conserved Domains Database (CDD) tool was used to generate the data in this figure. Specific hits include class XVI myosin motor domain including position of the ATP binding site.
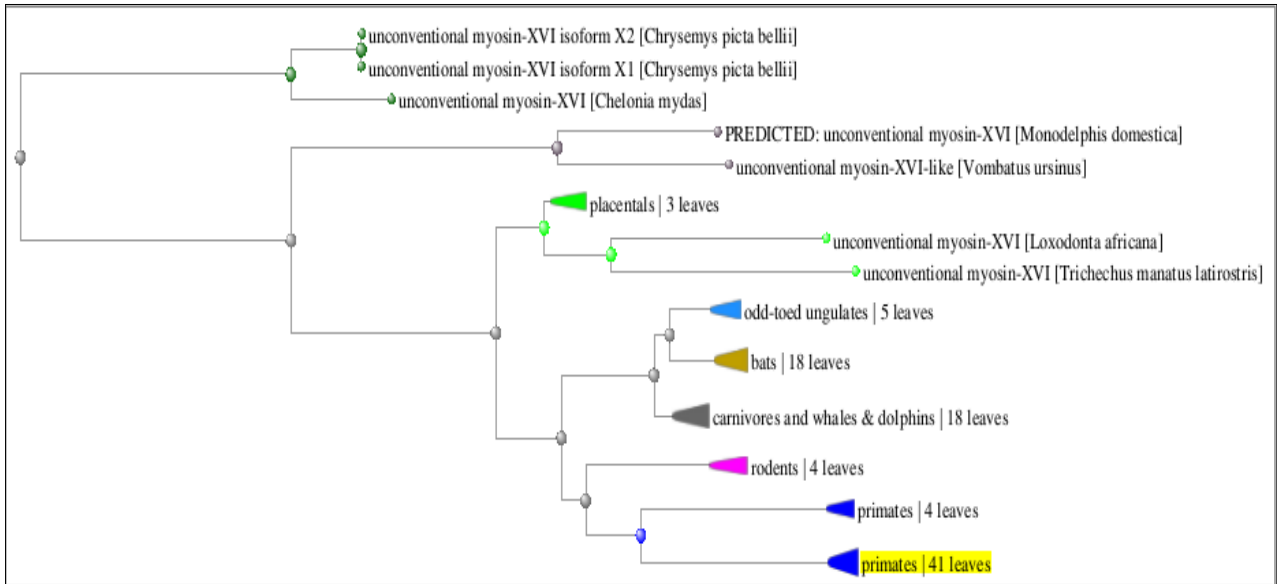
Figure 3.8. Phylogenetic tree of the BLAST results for MYO16. Tree method is fast minimum evolution with pairwise alignment between query sequence (*Homo sapiens*) which is within the yellow highlighted cluster (Primates), and the sequences searched in the database (BLAST website). Tree settings are with Max sequence difference 0.85 and Grishin (Protein) distance method.

3.3.3 MYO18B bioinformatics analyses

The STRING analysis results for MYO18B show highest confidence (above 0.9 score) interactions with several myosins and medium confidence interactions with two other myosins and ACTB (actin beta) (Figure 3.9). The highest confidence interactions are with MYO1F, MYO1C (NM1β), MYO9A and MYO6. MYO5A and MYO7A show medium confidence interaction with MYO18B. Clearly MYO18B is very active in several cellular processes, including those involving a number of other myosins. This makes MYO18B an interesting candidate, particularly considering its very high confidence interaction with MYO1C. The myosin I family of proteins consists of eight members in the higher vertebrates, named (Myo1a to Myo1h) (Sherr et al. 1993; McIntosh and Ostap 2016). The *MYO1C* gene products include a nuclear located isoform which is nuclear myosin 1 beta (NM1β) (Nowak et al. 1997; Pestic-Dragovich et al. 2000; Hofmann et al. 2006).

The co-expression chart for humans does not show MYO18B to be co-expressed with any of the network members (Figure 3.10) which is somewhat surprising considering the strong interaction data. However, it is important to consider that interactors and functional partners need not always be co-expressed, since many proteins may be available in excess as highly stable molecules or possibly in an inactive storage state (Carragher et al. 1998). It is also important to realise the limitations of the STRING resource, as the data utilisation of the STRING software is mainly based on known results and various types of predictions, therefore the information output is limited by current knowledge and predictive methods. The co-expression chart for other taxa shows low confidence level co-expression between Myo18b and Myo9a in several species including *C. elegans* and *D. melanogaster* (Figure 3.10).

The conserved domains analysis for MYO18B shows several features of the motor domain (Figure 3.11). The BLAST phylogenetic tree shows MYO18B to be well conserved in the mammals (Figure 3.12) and the outgroup sequence of the tree belongs to the Florida Manatee (*Trichechus manatus latirostris*).

MYO18B network with nodes labeled: NRIP3, SLC15A5, TIAF1, HOMER2, AHCYL2, ANKRD20A2, AHCYL1, MYO1F, MYO9A, UNC45B, TTC29, ERICH4, MYO18B, MYO1C, MYO6, DYNLL2, MYO7A, MYL6, MYL6B, MYO5A, OR51G2, KIF26B, ACTB, OR3A3, ADRBK2, CAP1, OR4K17, OR3A2, SEZ6L, CCDC36, C3orf62
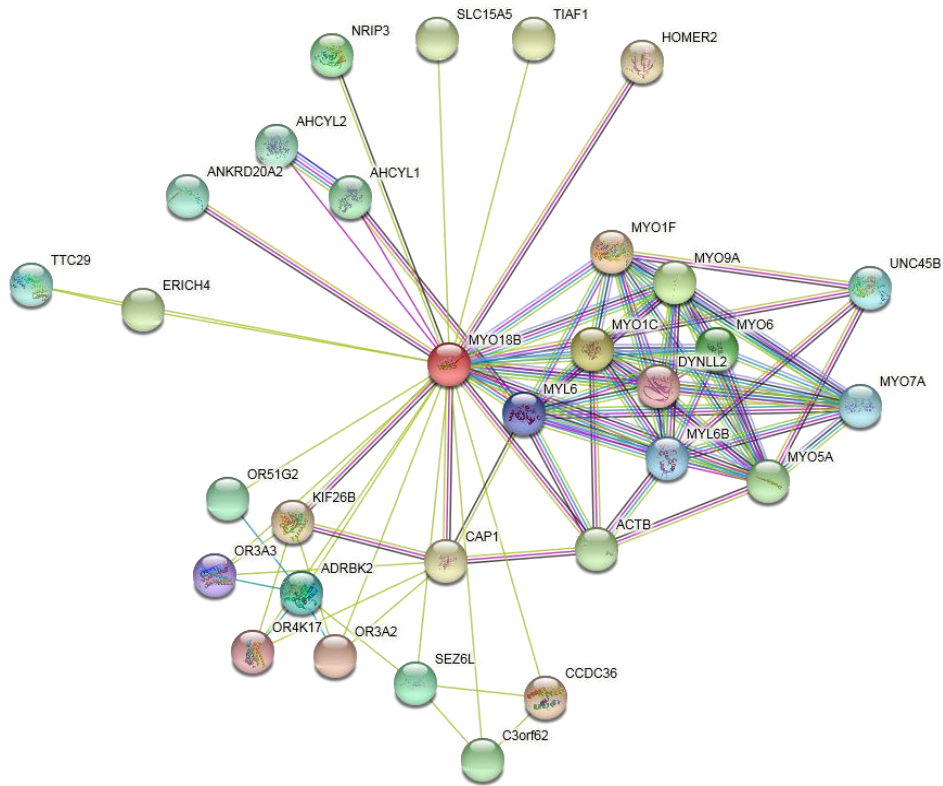
		Neighborhood	Gene Fusion	Cooccurrence	Coexpression	Experiments	Databases	Textmining	[Homology]	Score
● MYO18B	Unconventional myosin-XVIIIb; May be involved in intracellular trafficking of the muscle cell when in the cytoplasm, whereas entering the nucleus, may be involved in the regulation of muscle specific genes. May play a role in the control of tumor development and progression; restored MYO18B expression in lung cancer cells suppresses anchorage-independent growth; Belongs to the TRAFAC class myosin-kinesin ATPase superfamily. Myosin family (2567 aa)									

Predicted Functional Partners:

		Neighborhood	Gene Fusion	Cooccurrence	Coexpression	Experiments	Databases	Textmining	[Homology]	Score
MYO1F	Unconventional myosin-If; Myosins are actin-based motor molecules with ATPase activity. Unconventional myosins ser...					●	●	●	●	0.916
MYO1C	Unconventional myosin-Ic; Myosins are actin-based motor molecules with ATPase activity. Unconventional myosins ser...					●	●	●	●	0.914
MYO9A	Unconventional myosin-IXa; Myosins are actin-based motor molecules with ATPase activity. Unconventional myosins s...				●	●	●	●	●	0.912
MYO6	Unconventional myosin-VI; Myosins are actin-based motor molecules with ATPase activity. Unconventional myosins se...					●	●	●	●	0.906
SEZ6L	Seizure 6-like protein; May contribute to specialized endoplasmic reticulum functions in neurons; Sushi domain contain...							●		0.905
ADRBK2	Beta-adrenergic receptor kinase 2; Specifically phosphorylates the agonist-occupied form of the beta-adrenergic and cl...							●		0.901
MYL6B	Myosin light chain 6B; Regulatory light chain of myosin. Does not bind calcium; EF-hand domain containing (208 aa)				●	●				0.805
MYL6	Myosin light polypeptide 6; Regulatory light chain of myosin. Does not bind calcium; EF-hand domain containing (151 aa)				●	●				0.805
OR3A3	Olfactory receptor 3A3; Odorant receptor; Olfactory receptors, family 3 (321 aa)							●		0.794
OR4K17	Olfactory receptor 4K17; Odorant receptor; Olfactory receptors, family 4 (343 aa)							●		0.781
DYNLL2	Dynein light chain 2, cytoplasmic; Acts as one of several non-catalytic accessory components of the cytoplasmic dynei...				●	●				0.765
OR3A2	Olfactory receptor 3A2; Odorant receptor; Olfactory receptors, family 3 (321 aa)							●		0.760
CCDC36	Interactor of HORMAD1 protein 1; Required for DNA double-strand breaks (DSBs) formation in unsynapsed regions duri...							●		0.677
KIF26B	Kinesin-like protein KIF26B; Essential for embryonic kidney development. Plays an important role in the compact adhesi...				●	●		●		0.661
HOMER2	Homer protein homolog 2; Postsynaptic density scaffolding protein. Binds and cross-links cytoplasmic regions of GRM...				●	●		●		0.649
CAP1	Adenylyl cyclase-associated protein 1; Directly regulates filament dynamics and has been implicated in a number of co...				●	●		●		0.645
TIAF1	TGFB1-induced anti-apoptotic factor 1; Inhibits the cytotoxic effects of TNF-alpha and overexpressed TNF receptor ada...							●		0.644
SLC15A5	Solute carrier family 15 member 5; Proton oligopeptide cotransporter; Solute carriers (579 aa)							●		0.558
ERICH4	Glutamate-rich protein 4; Glutamate rich 4 (130 aa)							●		0.551
ACTB	Actin, cytoplasmic 1; Actins are highly conserved proteins that are involved in various types of cell motility and are ubiq...					●		●		0.551
MYO5A	Unconventional myosin-Va; Processive actin-based motor that can move in large steps approximating the 36-nm pseud...				●	●	●	●	●	0.534
C3orf62	Uncharacterized protein C3orf62; Chromosome 3 open reading frame 62 (267 aa)							●		0.529
NRIP3	Nuclear receptor interacting protein 3 (241 aa)				●			●		0.522
AHCYL1	S-adenosylhomocysteine hydrolase-like protein 1; Multifaceted cellular regulator which coordinates several essential ce...					●				0.507
OR51G2	Olfactory receptor 51G2; Odorant receptor; Olfactory receptors, family 51 (314 aa)							●		0.507
AHCYL2	Adenosylhomocysteinase 3; May regulate the electrogenic sodium/bicarbonate cotransporter SLC4A4 activity and Mg(...					●				0.507
ANKRD20A2	Ankyrin repeat domain-containing protein 20A2; Ankyrin repeat domain 20 family member A2 (823 aa)							●		0.505
TTC29	Tetratricopeptide repeat domain containing (501 aa)							●		0.497
UNC45B	Protein unc-45 homolog B; Acts as a co-chaperone for HSP90 and is required for proper folding of the myosin motor do...				●	●		●		0.493
MYO7A	Unconventional myosin-VIIa; Myosins are actin-based motor molecules with ATPase activity. Unconventional myosins s...				●	●	●	●	●	0.490

Your Current Organism:

Homo sapiens

NCBI taxonomy Id: 9606
Other names: H. sapiens, Homo sapiens, human, man

Figure 3.9. MYO18B network prediction with settings at minimum 0.4 interaction score (medium confidence) and maximum 30 interactors. The top 4 highest level confidence interactions of MYO18B are with other myosins.
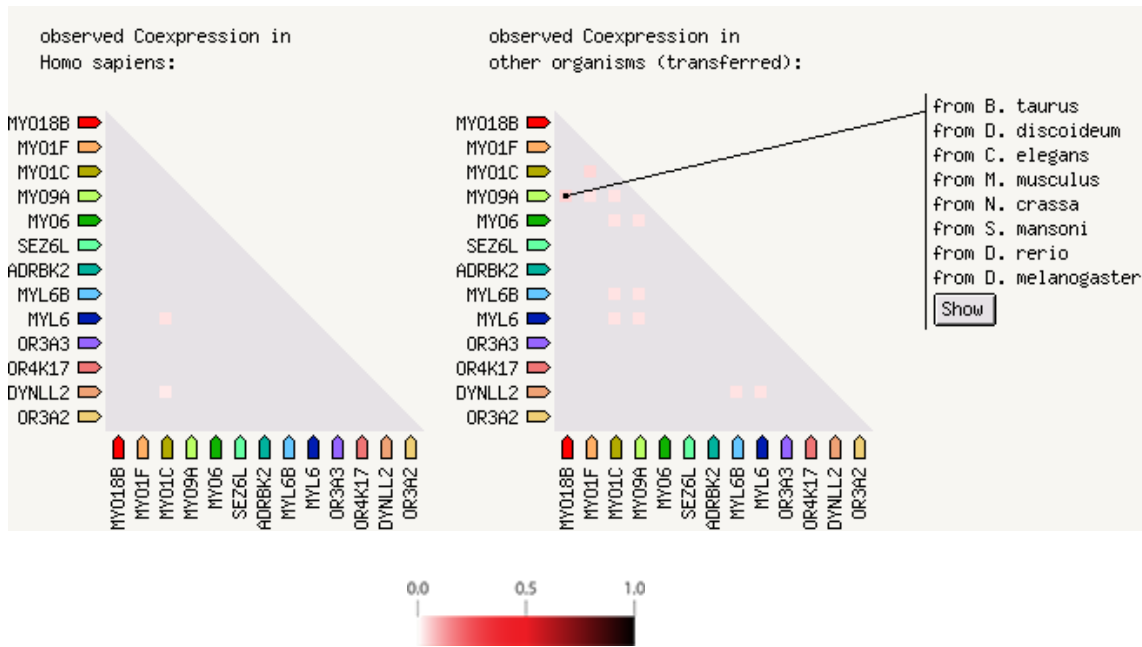
Figure 3.10. MYO18B network co-expression based on RNA expression patterns and protein co-regulation. In humans, no co-expression is shown with MYO18B. In other taxa only very low level confidence co-expression is shown with MYO9A. The intensity of the square box colour represents the level of confidence as shown by the red bar scale.

Figure 3.11. Results of the conserved domains analysis for MYO18B. The NCBI Conserved Domains Database (CDD) tool was used to generate the data in this figure. Specific hits show details of the class XVIII myosin motor domain.

Figure 3.12. Phylogenetic tree of the BLAST results for MYO18B. Tree method is fast minimum evolution with pairwise alignment between query sequence (Homo sapiens) which is within the yellow highlighted cluster (Primates), and the sequences searched in the database (BLAST website). Tree settings are with Max sequence difference 0.85 and Grishin (Protein) distance method.

3.3.4 MYO1C bioinformatics analyses

The STRING analysis results for MYO1C show highest level confidence (above 0.9 score) interactions with several ARPs and two myosins (Figure 3.13). These include ARPC1A, ARPC1B, ARPC2, ARPC3 and ARPC4 all of which are subunits of the actin related protein 2/3 (ARP2/3) complex. ACTR2 and ACTR3, also components of the (ARP2/3) complex, are also found in the generated network. The two myosins in this network are MYO5A, and a conventional non-muscle myosin, MYH9. MYO1C differs from MYO18B with regards to the classes of interactor proteins, since many of the functional partners of the latter are myosins and many interactors of the former are ARPs.

The co-expression data for MYO1C with other members of the network is very low confidence (Figure 3.14). Human co-expression data for some of the other members of the generated network show very strong confidence co-expression, including among the ARPs, thought not including MYO1C. The co-expression chart for other taxa shows low level confidence co-expression for many of the network members including Myo1c.

Figure 3.13. MYO1C network prediction with settings at minimum 0.9 interaction score (highest confidence) and maximum 30 interactors. Highest confidence interactions with many proteins are shown, including with several ARPs and two myosins.
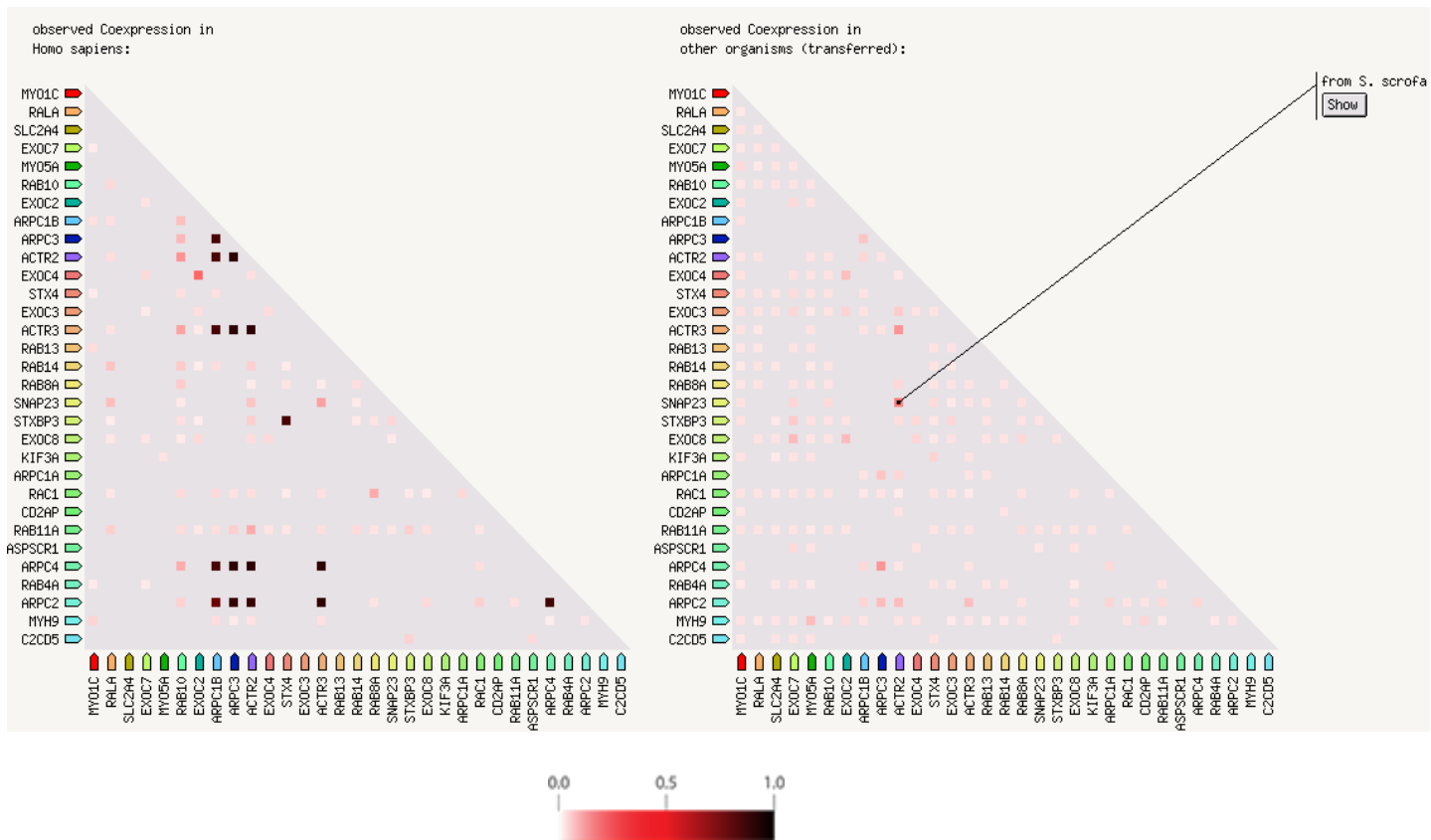
Figure 3.14. MYO1C network co-expression based on RNA expression patterns and protein co-regulation. No high confidence level co-expression is shown in humans for MYO1C. Several very low level confidence co-expressions are shown in other taxa with MYO1C. The intensity of the square box colour represents the level of confidence as shown by the red bar scale.
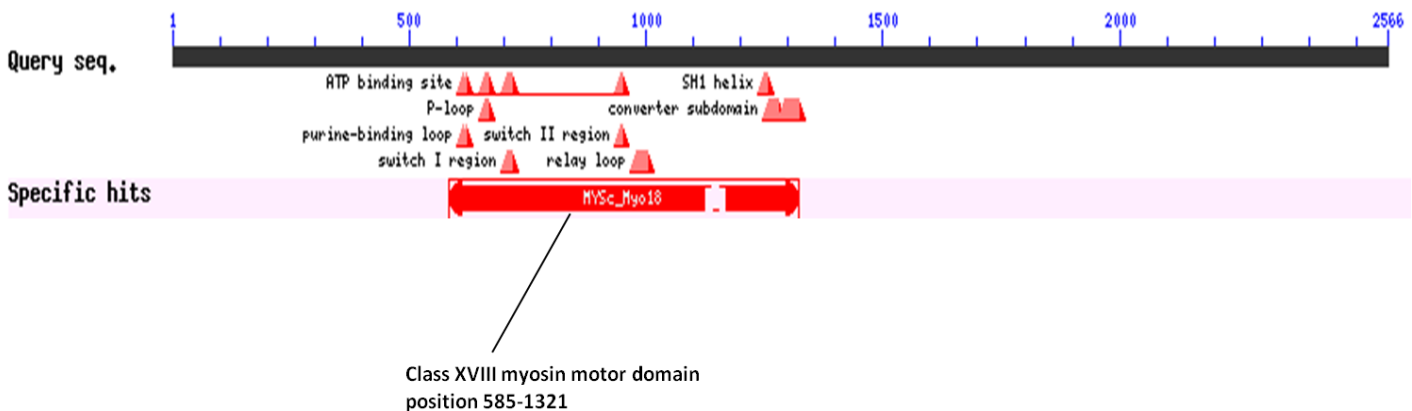
The conserved domains analysis for MYO1C shows the locations of several features including the myosin head motor domain and the myosin tail (Figure 3.15). The BLAST phylogentic tree for MYO1C shows high conservation in the mammals, and the outgroup in this tree is *Elephantulus edwardii* (Cape elephant shrew) (Figure 3.16). As with the other BLAST phylogenetic trees generated for these results, only the highest similarity sequences in other taxa are shown in the tree and there are certainly more primitive homologues in more distantly related organisms.
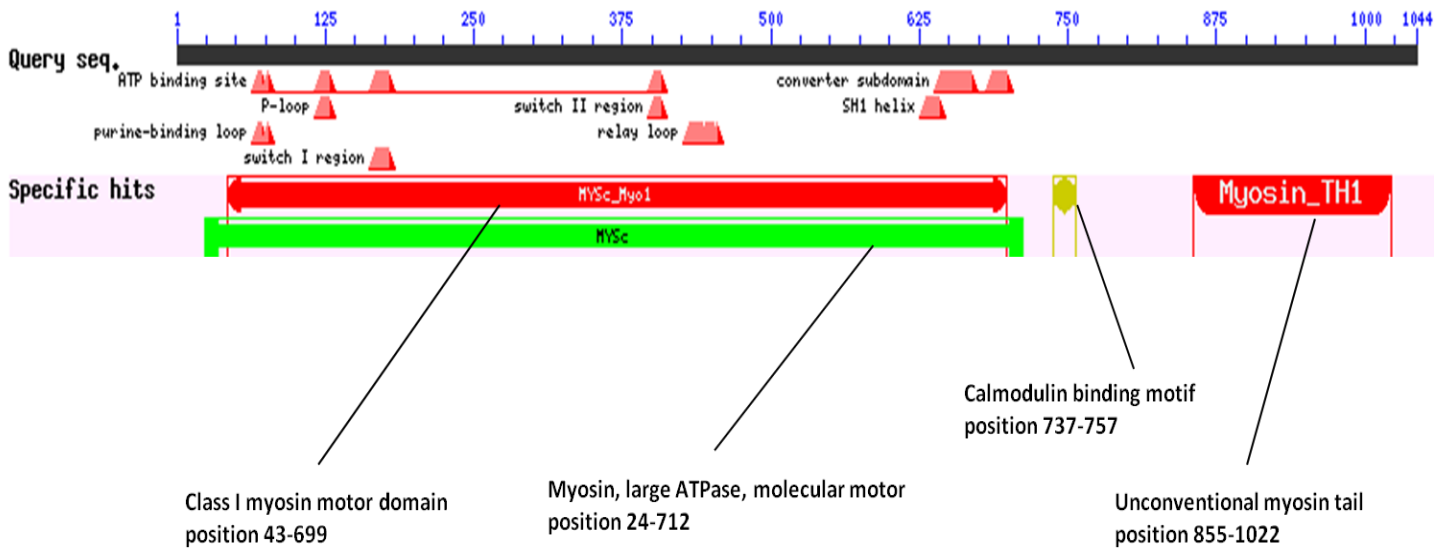
Figure 3.15. Results of the conserved domains analysis for MYO1C. The NCBI Conserved Domains Database (CDD) tool was used to generate the data in this figure. Specific hits include class I myosin motor domain, a calmodulin binding motif and the unconventional myosin tail domain.
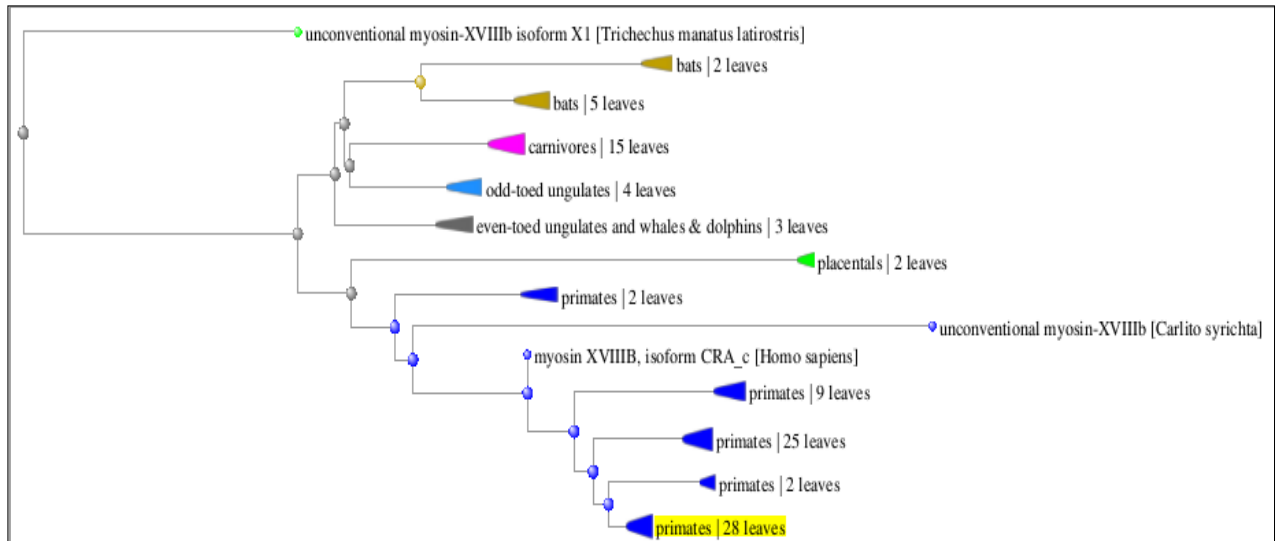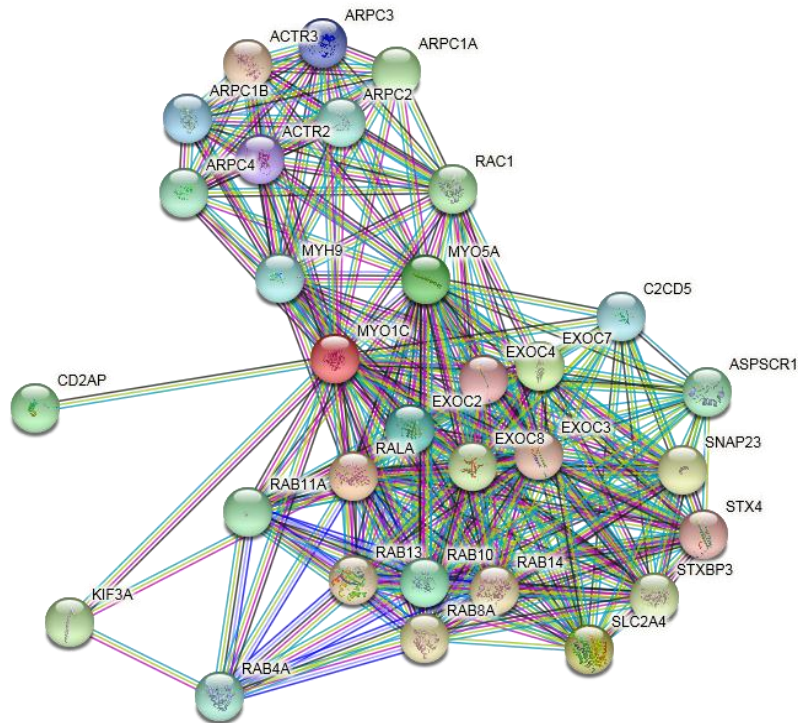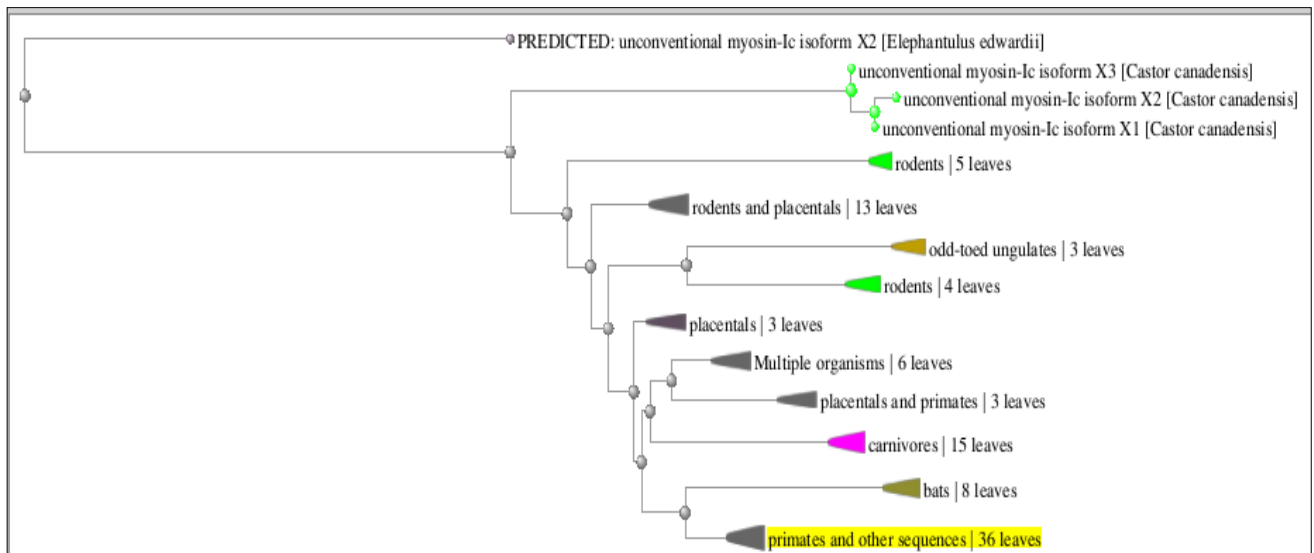

Figure 3.16. Phylogenetic tree of the BLAST results for MYO1C. Tree method is fast minimum evolution with pairwise alignment between query sequence (Homo sapiens) which is within the yellow highlighted cluster (Primates), and the sequences searched in the database (BLAST website). Tree settings are with Max sequence difference 0.85 and Grishin (Protein) distance method.

95

3.3.5 BAF53A (ACTL6A) bioinformatics analyses

The STRING analysis results for BAF53A (ACTL6A) show many high level confidence (above 0.9 score) interactions (Figure 3.17). Several of these interactors are subunits of the SWI/SNF complex, which is involved in chromatin remodeling. The highest level confidence interactor of these is SMARCB1 which has an interaction score of 0.999 and is an actin-dependant chromatin regulator subunit of the complex. Another interactor in the generated network is ACTR5 which is an ARP shown to be nuclear localised, but also shuttled between the nucleus and the cytoplasm (Kitayama et al. 2009). Both of these proteins are involved in chromatin remodeling and therefore based on these results, a role for BAF53A in chromosome mobility is not supported. According to the STRING network generated for BAF53A, this protein is clearly interacting with many other proteins and the number of high level confidence interactors is far more than the 30 shown, which was limited by the STRING network prediction settings of maximum 30 interactors.

The co-expression data for BAF53A in humans shows moderate level confidence co-expression with RUVBL1 and RUVBL2, and lower level confidence co-expression with various other network members, although the highest confidence co-expression in the network is between RUVBL1 and RUVBL2 (Figure 3.18). In other taxa Baf53a shows only low level confidence co-expression with other network members.

The conserved domains analysis for BAF53A which is an ARP, shows actin and actin related domains as well as a nucleotide binding domain of a sugar kinase/HSP70 (Figure 3.19). The phylogenetic tree for BAF53A shows this protein to be well conserved across a broad range of vertebrate taxa, including the reptiles and birds which are more primitive and ancient vertebrate taxa (Figure 3.20). Interestingly, the outgroup for this tree is a very primitive amphibian called a caecilcian, of the species *Rhinatrema bivittatum* (Two lined caecilian).
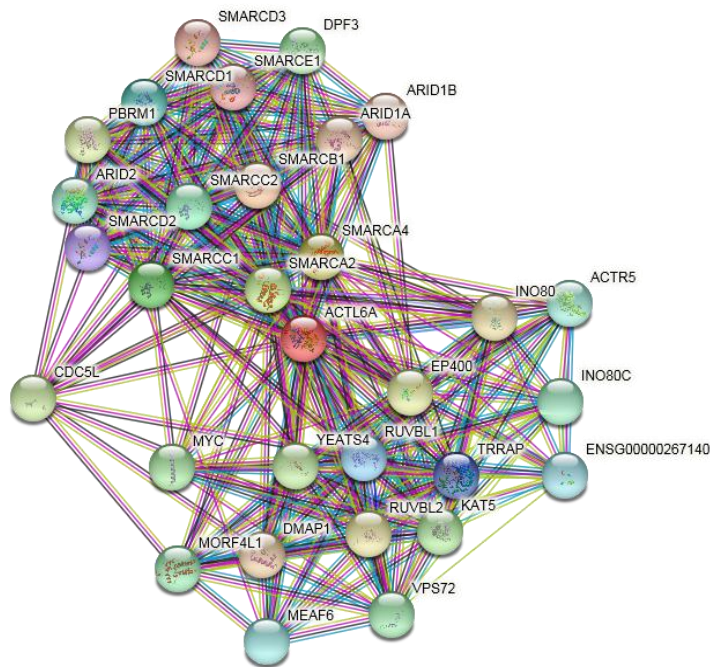
		Neighborhood	Gene Fusion	Cooccurence	Coexpression	Experiments	Databases	Textmining	[Homology]	Score
● ACTL6A	Actin-like protein 6A; Involved in transcriptional activation and repression of select genes by chromatin remodeling (alteration of DNA-nucleosome topology). Component of SWI/SNF chromatin remodeling complexes that carry out key enzymatic activities, changing chromatin structure by altering DNA-histone contacts within a nucleosome in an ATP-dependent manner. Required for maximal ATPase activity of SMARCA4/BRG1/BAF190A and for association of the SMARCA4/BRG1/BAF190A containing remodeling complex BAF with chromatin/nuclear matrix. Belongs to the neural progenitors- specific chromatin rem [...] (429 aa)									

Predicted Functional Partners:

		Neighborhood	Gene Fusion	Cooccurence	Coexpression	Experiments	Databases	Textmining	[Homology]	Score
SMARCB1	SWI/SNF-related matrix-associated actin-dependent regulator of chromatin subfamily B member 1; Core compon...				○	●	●	●		0.999
SMARCA4	Transcription activator BRG1; Involved in transcriptional activation and repression of select genes by chromatin...				○	●	●	●		0.998
SMARCA2	Probable global transcription activator SNF2L2; Involved in transcriptional activation and repression of select ge...				○	●	●	●		0.998
SMARCC1	SWI/SNF complex subunit SMARCC1; Involved in transcriptional activation and repression of select genes by ch...				○	●	●	●		0.998
SMARCC2	SWI/SNF complex subunit SMARCC2; Involved in transcriptional activation and repression of select genes by ch...				○	●	●	●		0.998
SMARCD1	SWI/SNF-related matrix-associated actin-dependent regulator of chromatin subfamily D member 1; Involved in tr...				○	●	●	●		0.997
RUVBL1	RuvB-like 1; May be able to bind plasminogen at cell surface and enhance plasminogen activation; AAA ATPases...	○		○	○	●	●	●		0.997
TRRAP	Transformation/transcription domain-associated protein; Adapter protein, which is found in various multiprotein...				○	●	●	●		0.997
SMARCD2	SWI/SNF-related matrix-associated actin-dependent regulator of chromatin subfamily D member 2; Involved in tr...				○	●	●	●		0.997
SMARCE1	SWI/SNF-related matrix-associated actin-dependent regulator of chromatin subfamily E member 1; Involved in tr...				○	●	●	●		0.996
SMARCD3	SWI/SNF-related matrix-associated actin-dependent regulator of chromatin subfamily D member 3; Involved in tr...				○	●	●	●		0.995
ARID1B	AT-rich interactive domain-containing protein 1B; Involved in transcriptional activation and repression of select g...					●	●	●		0.994
ARID1A	AT-rich interactive domain-containing protein 1A; Involved in transcriptional activation and repression of select g...					●	●	●		0.993
DMAP1	DNA methyltransferase 1-associated protein 1; Involved in transcription repression and activation. Its interaction...				○	●	●	●		0.992
INO80	DNA helicase INO80; DNA helicase and probable main scaffold component of the chromatin remodeling INO80 c...				○	●	●	●		0.992
RUVBL2	RuvB-like 2; Involved in the endoplasmic reticulum (ER)-associated degradation (ERAD) pathway where it negativ...	○		○	○	●	●	●		0.990
EP400	E1A-binding protein p400; Component of the NuA4 histone acetyltransferase complex which is involved in transc...				○	●	●	●		0.989
PBRM1	Protein polybromo-1; Involved in transcriptional activation and repression of select genes by chromatin remodeli...				○	●	●	●		0.983
CDC5L	Cell division cycle 5-like protein; DNA-binding protein involved in cell cycle control. May act as a transcription act...				○	●				0.981
YEATS4	YEATS domain-containing protein 4; Component of the NuA4 histone acetyltransferase (HAT) complex which is i...				○	●	●	●		0.980
KAT5	Histone acetyltransferase KAT5; Catalytic subunit of the NuA4 histone acetyltransferase complex which is invol...				○	●	●	●		0.979
MYC	Myc proto-oncogene protein; Transcription factor that binds DNA in a non-specific manner, yet also specifically r...				○	●	●	●		0.973
DPF3	Zinc finger protein DPF3; Belongs to the neuron-specific chromatin remodeling complex (nBAF complex). During...				○	●	●	●		0.973
VPS72	Vacuolar protein sorting-associated protein 72 homolog; Deposition-and-exchange histone chaperone specific fo...				○	●	●	●		0.972
MORF4L1	Mortality factor 4-like protein 1; Component of the NuA4 histone acetyltransferase (HAT) complex which is invol...				○	●	●	●		0.967
INO80C	Chromosome 18 open reading frame 37, isoform CRA_a; Proposed core component of the chromatin remodeling...				○	●	●	●		0.967
ARID2	AT-rich interactive domain-containing protein 2; Involved in transcriptional activation and repression of select ge...				○	●	●	●		0.967
ACTR5	Actin-related protein 5; Proposed core component of the chromatin remodeling INO80 complex which is involved...				○	●	●	●	●	0.965
MEAF6	Chromatin modification-related protein MEAF6; Component of the NuA4 histone acetyltransferase complex whic...				○	●	●	●		0.963
ENSG00000267140	INO80 complex subunit C; Proposed core component of the chromatin remodeling INO80 complex which is invol...				○	●	●	●		0.961

Your Current Organism:

Homo sapiens

Figure 3.17. BAF53A (ACTL6A) network prediction with settings at minimum 0.7 interaction score (high confidence) and maximum 30 interactors. Many highest level confidence interactions are shown including chromatin remodelers of the SWI/SNF complex, and ACTR5 which is nuclear localised but also found in the cytoplasm.
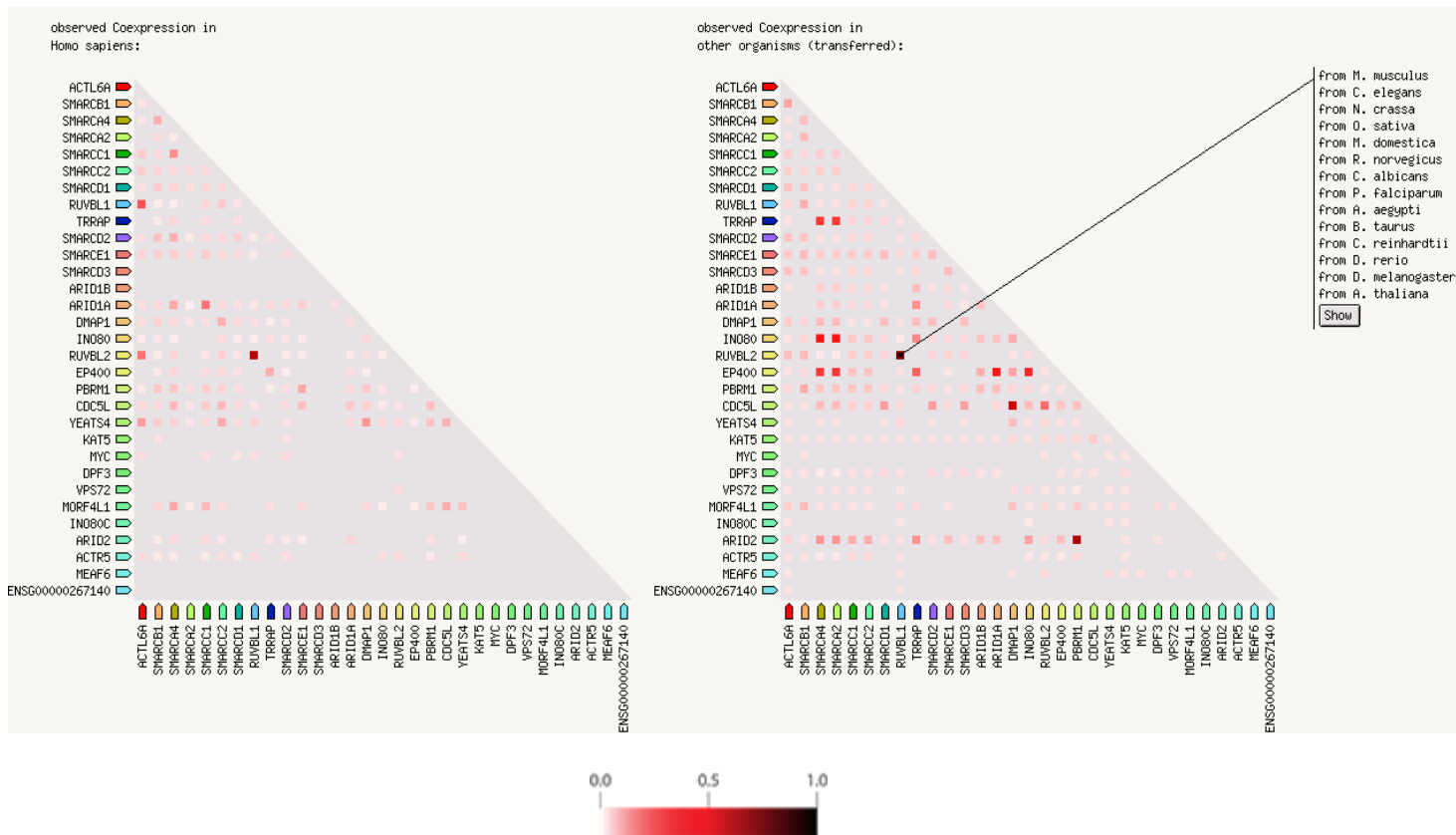
Figure 3.18. BAF53A (ACTL6A) co-expression based on RNA expression patterns and protein co-regulation. In humans, moderate level confidence co-expression is shown between BAF53A and both RUVBL1 and RUVBL2, and lower level confidence co-expression with several other members of the network including proteins of the SWI/SNF complex. In other taxa very low level confidence co-expression is shown between BAF53A and nearly all members of the network with SMARCB1 showing the highest of these. The intensity of the square box colour represents the level of confidence as shown by the red bar scale.
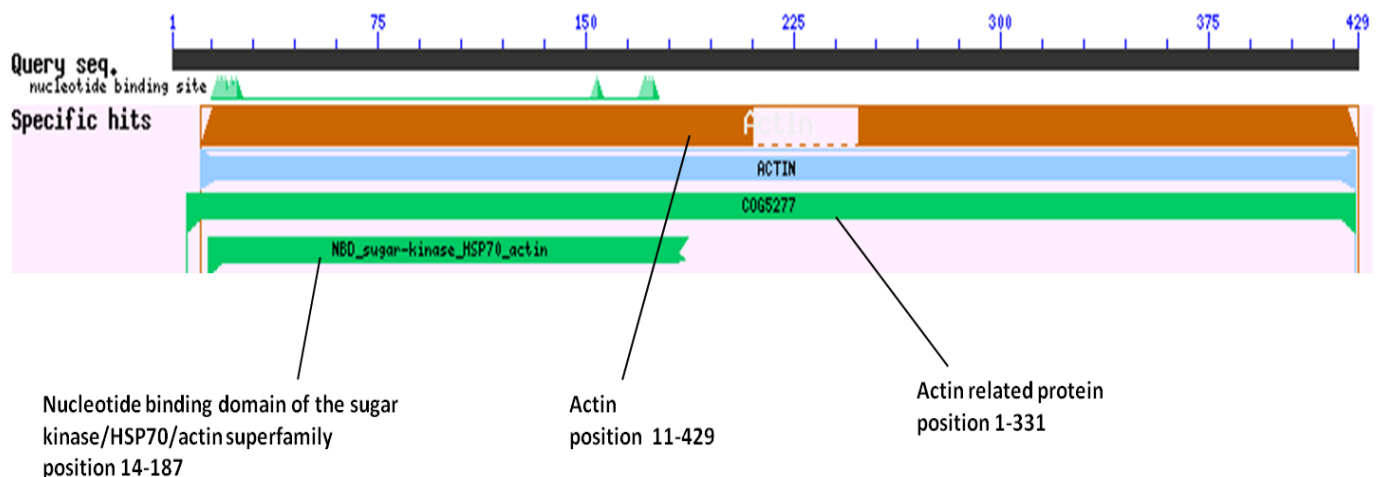
Figure 3.19. Results of the conserved domains analysis for BAF53A (ACTL6A). The NCBI Conserved Domains Database (CDD) tool was used to generate the data in this figure. Specific hits show the nucleotide binding domain of the sugar kinase/HSP70/actin superfamily, related to the nucleotide binding site on this protein. Domains related to the ARPs and actin, are also shown in the specific hits.

98
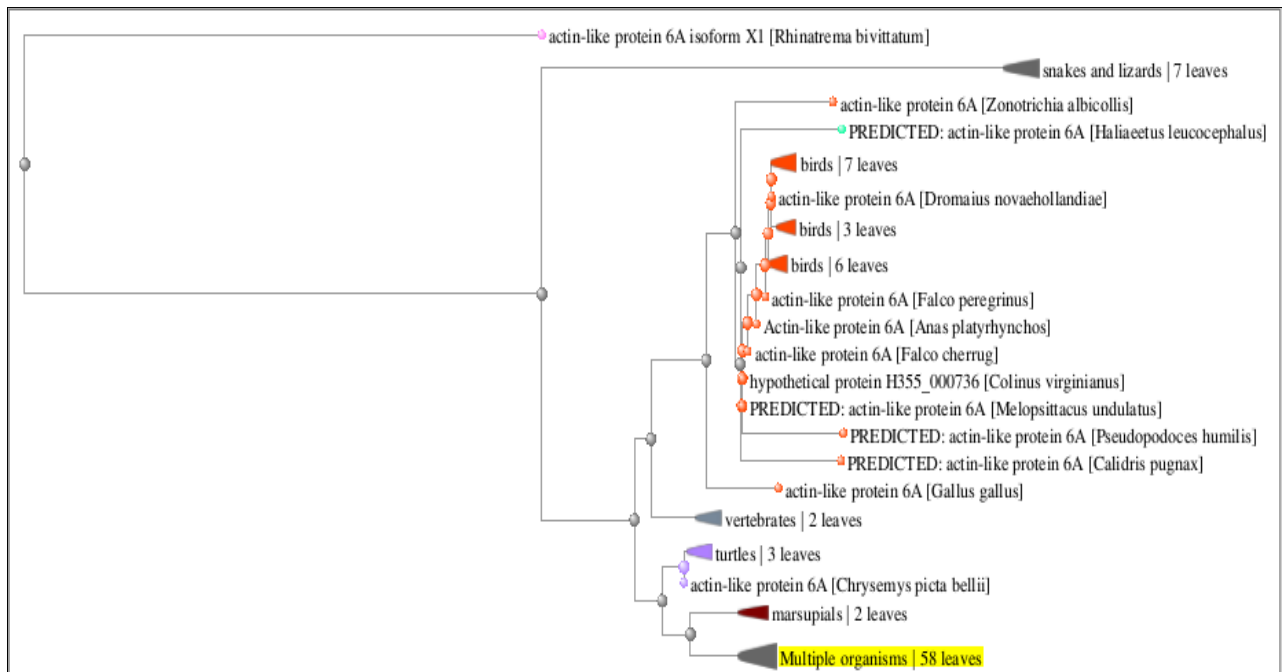
Figure 3.20. Phylogenetic tree of the BLAST results for BAF53A (ACTL6A). Tree method is fast minimum evolution with pairwise alignment between query sequence (Homo sapiens) which is within the yellow highlighted cluster (Primates), and the sequences searched in the database (BLAST website). Tree settings are with Max sequence difference 0.85 and Grishin (Protein) distance method.

3.3.6 ACTR6 bioinformatics analyses

The STRING analysis network for ACTR6 shows the highest confidence interaction with Helicase SRCAP of the chromatin remodeling SRCAP complex (Figure 3.21). It also shows high level confidence interaction with ACTR8 which is involved with mitotic chromosome organisation, and moderately low level confidence interaction with ACTR3C. The co-expression data for ACTR6 shows only low level confidence co-expression with BAF53A, CETN3 and YEATS4 in humans (Figure 3.22). In other taxa Actr6 shows low level confidence co-expression with CETN3. The conserved domains analysis for ACTR6 shows very similar features to BAF53A, including a nucleotide binding domain (3.23). The phylogenetic tree for ACTR6 shows conservation among the mammalian taxa, with the outgroup of the tree being the *Octodon degus* (Common degu) a small rodent (Figure 3.24).

Figure 3.21. ACTR6 network prediction with settings at minimum 0.4 interaction score (medium confidence) and maximum 20 interactors. Only four highest level confidence interactions are shown, and a high level confidence interaction with ACTR8 which is involved in mitotic chromosome organisation. Lower level confidence interaction is shown with ACTR3C.
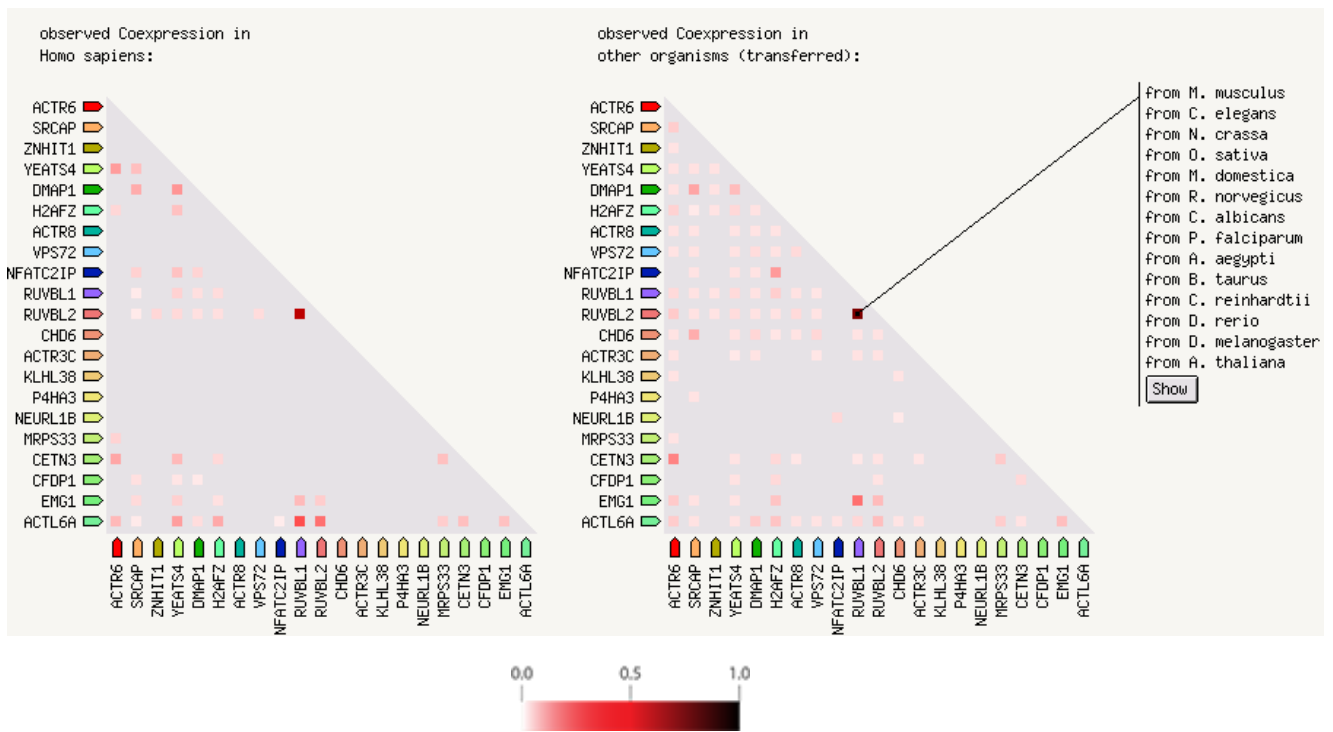
Figure 3.22. ACTR6 co-expression based on RNA expression patterns and protein co-regulation. In humans, low level confidence co-expression is shown between ACTR6 and ACTL6A (BAF53A), CETN3 and YEATS4. Very low level confidence co-expression is shown with MRPS33 and H2AFZ. In other taxa, low level confidence co-expression is shown between ACTR6 and CETN3, and very low level confidence co-expression with nearly all members of the network. The intensity of the square box colour represents the level of confidence as shown by the red bar scale.
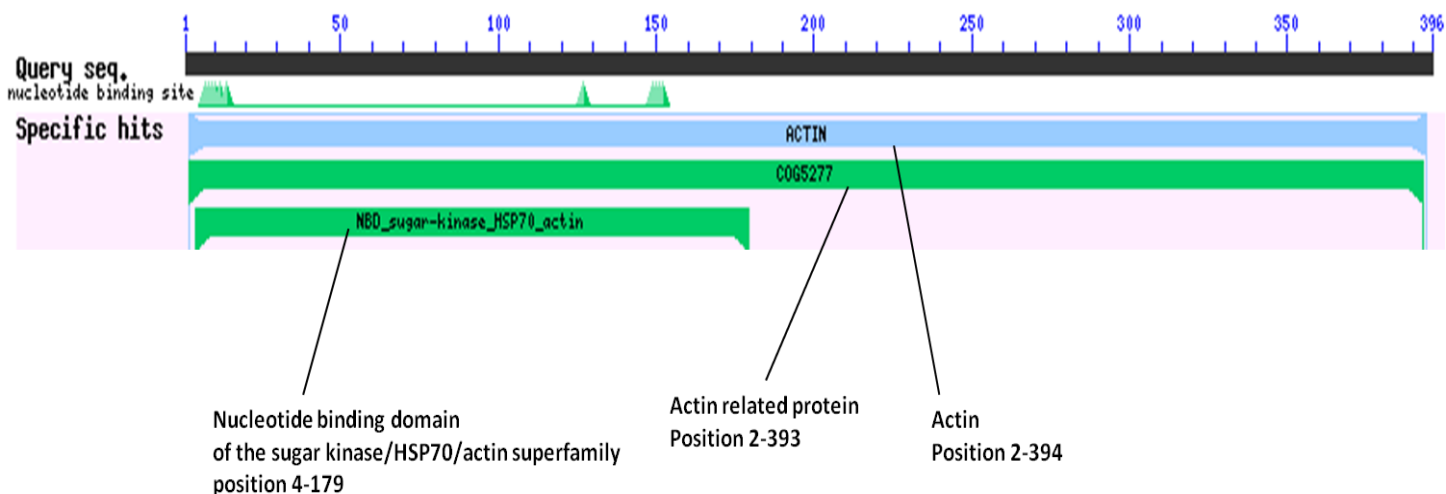
Figure 3.23. Results of the conserved domains analysis for ACTR6. The NCBI Conserved Domains Database (CDD) tool was used to generate the data in this figure. Specific hits show the nucleotide binding domain of the sugar kinase/HSP70/actin superfamily, related to the nucleotide binding site on this protein. Domains related to the ARPs and actin, are also shown in the specific hits.
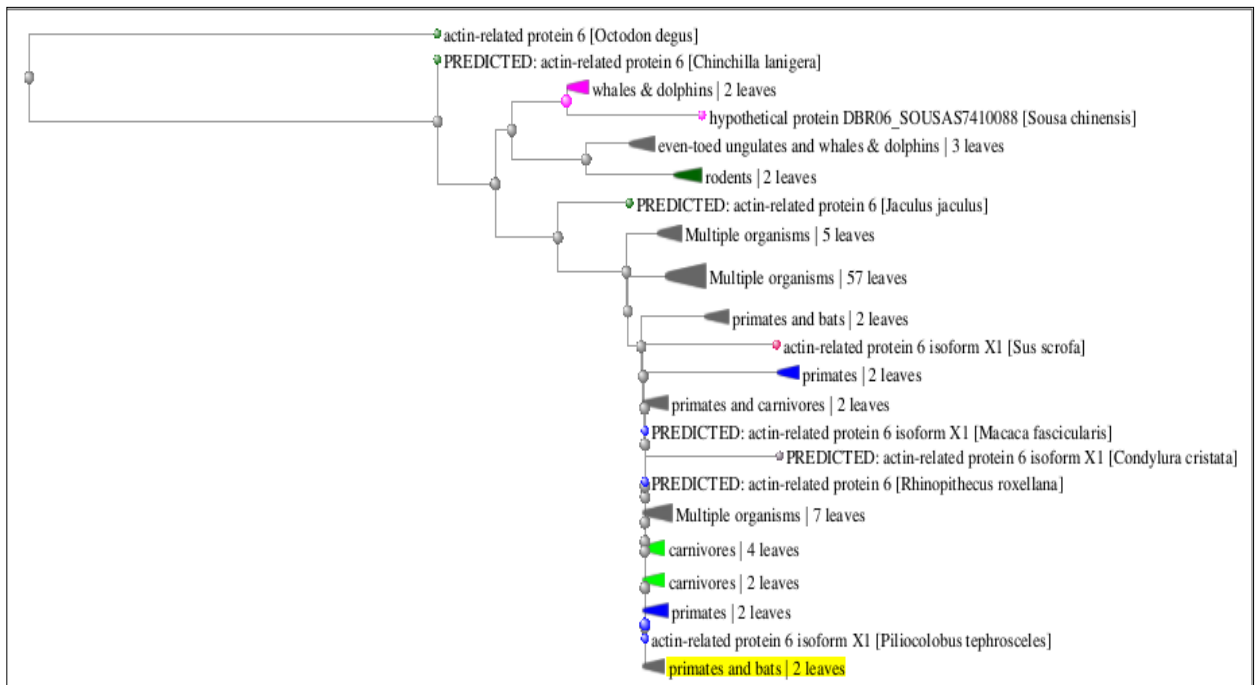
Figure 3.24. Phylogenetic tree of the BLAST results for ACTR6. Tree method is fast minimum evolution with pairwise alignment between query sequence (Homo sapiens) which is within the yellow highlighted cluster (Primates), and the sequences searched in the database (BLAST website). Tree settings are with Max sequence difference 0.85 and Grishin (Protein) distance method.

3.4 DISCUSSION

In silico bioinformatics methods were utilised to explore other possible proteins which may be directly or indirectly involved in chromosome dynamics. In addition to this, insight was gained into some structural features of the various proteins of interest, specifically highlighting the residue positions of key features and domains. This information is relevant for example, to any future work involving site-directed mutagenesis for knockout experiments. Phylogenetic analysis by tree output helped to show the level of conservation across taxa for each protein of interest, thus indicating functional importance. The power bioinformatics based explorations was demonstrated by the ability of this approach to reveal other interesting proteins and interactions, which may potentially play a role in active chromosome dynamics. The fact that these proteins and interactions were not considered for this project prior to the use of the STRING analysis is evidence of the usefulness of this resource. With living systems being highly complex and multifactorial in terms of interaction networks, a systems level approach is under certain conditions a preferred one, that leads to discovery of individual or multiple factors in the complex processes occurring in cells.

Some of the proteins revealed by the STRING analysis were not myosins or ARPs and interestingly included the actin nucleation factors, SPIRE1 and SPIRE2. Also included were proteins of the ARP2/3 complex, which is involved with actin nucleation and polymerization (Mullins and Pollard 1999). The work in this chapter has also helped to confirm that one of the myosin proteins selected for study in this project, is indeed interesting and a strong candidate for involvement in chromosome dynamics. Specifically, MYO18B is the myosin protein that needs to be further investigated for possible involvement with chromosome mobility, particularly due to the high confidence interaction with MYO1C (NM1β). The other myosins showing highest level confidence interaction with MYO18B are potentially of interest in relation to chromosome mobility, these being MYO1F, MYO9A and MYO6. Following the bioinformatics analyses in this work, MYO1C (NM1β) has also been confirmed to be highly relevant to chromosome dynamics, corroborating the work of Mehta et al. (2010) which experimentally show that this protein is indeed involved in interphase chromosome mobility. Highest level confidence interactions of MYO1C (NM1β) with

members of the (ARP2/3) complex, and two myosins, including a conventional myosin, MYH9 which is known to be located in the nucleus (Ye et al. 2020), reveals other potential proteins of interest for further investigations related to chromosome mobility. MYO16 was not confirmed by the bioinformatics analyses in this work to be an interesting candidate for involvement in chromosome mobility, however this does not definitely rule out MYO16 for further investigation, since in-silico bioinformatics findings are only one aspect of biological research tools. MYO5B appears not be involved in chromosome dynamics and its role in vesicular transport is supported by the high level confidence interaction with the SPIRE1 and SPIRE2 actin nucleation factors, which are also involved in vesicular transport. Other interactors of MYO5B, with highest level confidence interaction, were RAB11A, RAB11B and RAB11FIP2, which are also involved with vesicular transport. However, SPIRE1 and SPIRE2 are also found in the nucleus, where they have been shown to be involved in the DNA damage response, which includes the movement of chromatin and repair factors (Belin et al. 2015). Therefore, the SPIRE proteins may yet prove to have some relevance to interphase chromosome mobility. Perhaps this suggests that MYO5B could also have a role in DNA damage repair. The outcome of the bioinformatics analyses for the ARPs, BAF53A and ACTR6 included for the core analyses in this work did not reveal them to be very promising with regards to possible involvement in chromosome mobility. The high level confidence interaction of ACTR6 with only a few proteins, including Helicase SRCAP of the SRCAP complex, which is involved with chromatin remodeling, and with ACTR8 which is involved in mitotic chromosome organisation, suggest that this ACTR6 may possibly have a role in mitosis, and therefore functionally distant to interphase chromosome mobility. The outcome of the bioinformatics results for BAF53A also confirm that it is unlikely to be involved in chromosome mobility, since its high level confidence interactions are with proteins involved with chromatin remodeling, which is the assigned function of this protein (Krasteva et al. 2012).

One of the aspects that the work in this chapter has highlighted is that biological systems are indeed multifactorial systems. It is very rarely the case, if ever that a process is orchestrated by a single protein or even a small group of proteins. (Jansen 2003). There are nearly always several proteins that need to be considered when attempting to decipher the mechanisms of any given cellular process, such as

chromosome dynamics. Of course, these components of the whole would occupy different positions upstream or downstream in relation to the other components of the system. Although it is possible that disruption in even a single one of those factors could severely affect the process, or bring it to a halt completely, there could also be biological/genetic redundancy (Nowak et al. 1997) for a given protein in the process. In this case, the lost function could be continued by another related protein however, this may be rare, unless biological systems have evolved to allow genetic redundancy as a kind of biological backup system for crucial cellular processes.

Chapter 4: Studies on chromosome relocation: Novel chromosome relocation assay by heat shock and novel demonstration of chromosome 11 relocation; Confirmation of lack of chromosome movement in non-proliferating cells

4.1 Introduction.

4.2 Materials and methods.

4.3 Results.

4.3.1 Chromosome relocation assays: Initial experiments for low serum (0.5% FCS) media assay (passage 20 and 25 NB1 cells) and initial experiments for heat shock assay (passage 20 NB1 cells) with anti-Ki-67 proliferation marker.

4.3.2 Chromosome 10 low serum (0.5% FCS) media assay (passage 19 NB1 cells) with anti-Ki-67 proliferation marker.

4.3.3 Novel chromosome relocation assay: Chromosome 11 heat shock assay with anti-Ki-67 proliferation marker using passage 12 NB1 cells.

The work in section 4.3.3 has been included in a publication:

Mehta IS, Riyahi K, Pereira RT, Meaburn KJ, Figgitt M, Kill IR, Eskiw CH and Bridger JM. (2021). Interphase Chromosomes in Replicative Senescence: Chromosome Positioning as a Senescence Biomarker and the Lack of Nuclear Motor-Driven Chromosome Repositioning in Senescent Cells. *Front. Cell Dev. Biol*. May 24;9:640200.

4.4 Discussion.

4.1 INTRODUCTION

The compact and intricate nature of the nucleus with regards to the structures and processes existing therein, require a highly organised and regulated dynamic environment, in which some structures must be allowed to alter their spatiotemporal locations depending on the requirements of the cell. These dynamics are dependent upon the conditions and physiological state that the cell is exposed to, in the context of immediate tissues and the organism as a whole. In principle, it is logical to expect this scenario to be a necessity of any highly complex system with very limited space, which must self regulate in response to varying conditions. This is especially true of living systems where the principles of changeability and dynamics are inherent.

Interphase chromosome territories are in very close proximity to each other, and only separated by the interchromatin region, or possibly in contact with adjacent territories by the outer border regions of chromatin (Cremer and Cremer 2010, Cremer et al. 2020). The arrangement of interphase chromosomes in the form of chromatin consisting of highly condensed heterochromatin, and the more uncoiled and open conformation of euchromatin, has long been recognised as seen by electron microscopy, showing the ultrastructure of eukaryotic cells. With the electron microscope, the heterochromatin appears as darkly stained regions and the euchromatin appearing only lightly stained as a result of the density of the staining material, corresponding to the chromatin density (Figure 4.1). This level of ultrastructural observation helps to visually show just how compact the nucleus is in terms of space availability. This ultrastructural view of the nucleus, although not informative in terms of individual chromosomes, is informative in terms of overall nuclear architecture (Liu et al. 2020).

The ultrastructural view of nuclei as seen by the methods of electron microscopy had in part been responsible for a lack of appreciation of the territorial organisation of interphase chromosomes. Indeed up to the 1980s many had rejected the idea of chromosome territories, as a result of electron microscope imaging of nuclei, which did not have the capability to distinguish the separation of individual territories, beyond the distinction of euchromatin from heterochromatin (Liu et al. 2020), see Cremer and Cremer (2010) for review. Although electron microscopy would in theory

be expected to show such detail due to the high resolving power and the extremely high magnifications possible, in region of tens to hundreds of thousands of times magnification. However, it is logical that perhaps in large part the reason for this failure was due to the compact nature of chromosome territories, combined with the standard preparation techniques of electron microscopy. The sample preparation methods for transmission electron microscopy can be quite harsh to cells, and therefore distort the architecture sufficiently to visually abolish the very fine borders consisting of the perichromatin region and the interchromatin compartments. However, later developed and current specialised techniques for electron microscopy do allow for visualisation of the perichromatin regions in nuclei (Masiello et al. 2018).
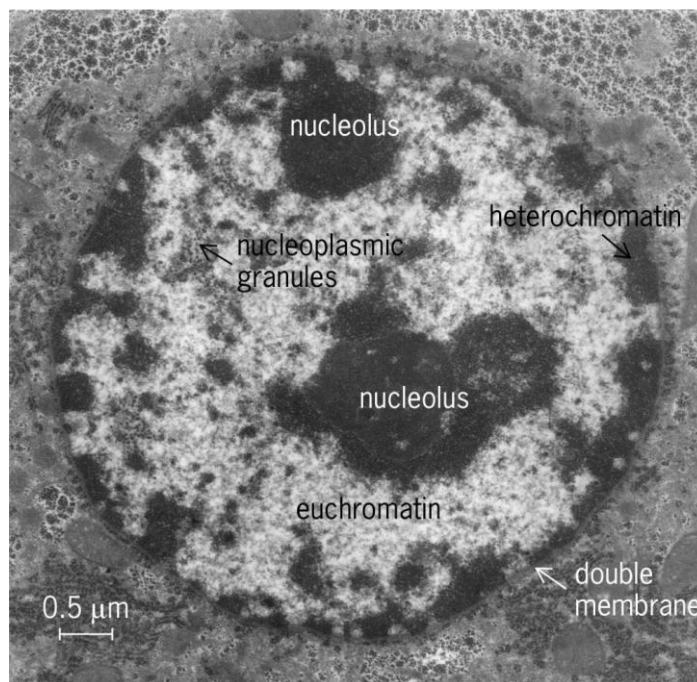
Figure 4.1. Nucleus of a rat liver cell as viewed by transmission electron microscopy. The distinction between euchromatin and heterochromatin are readily visible, however chromosome territories are not revealed. Image taken from McGraw-Hill Concise Encyclopedia of Bioscience (2002).

Subsequent studies including the use of fluorescence microscopy and FISH techniques clearly demonstrated the arrangement of individual interphase chromosomes into chromosome territories, and therefore the compact and highly organised nature of the nucleus was corroborated by these methods with increased detail (Figure 4.2).
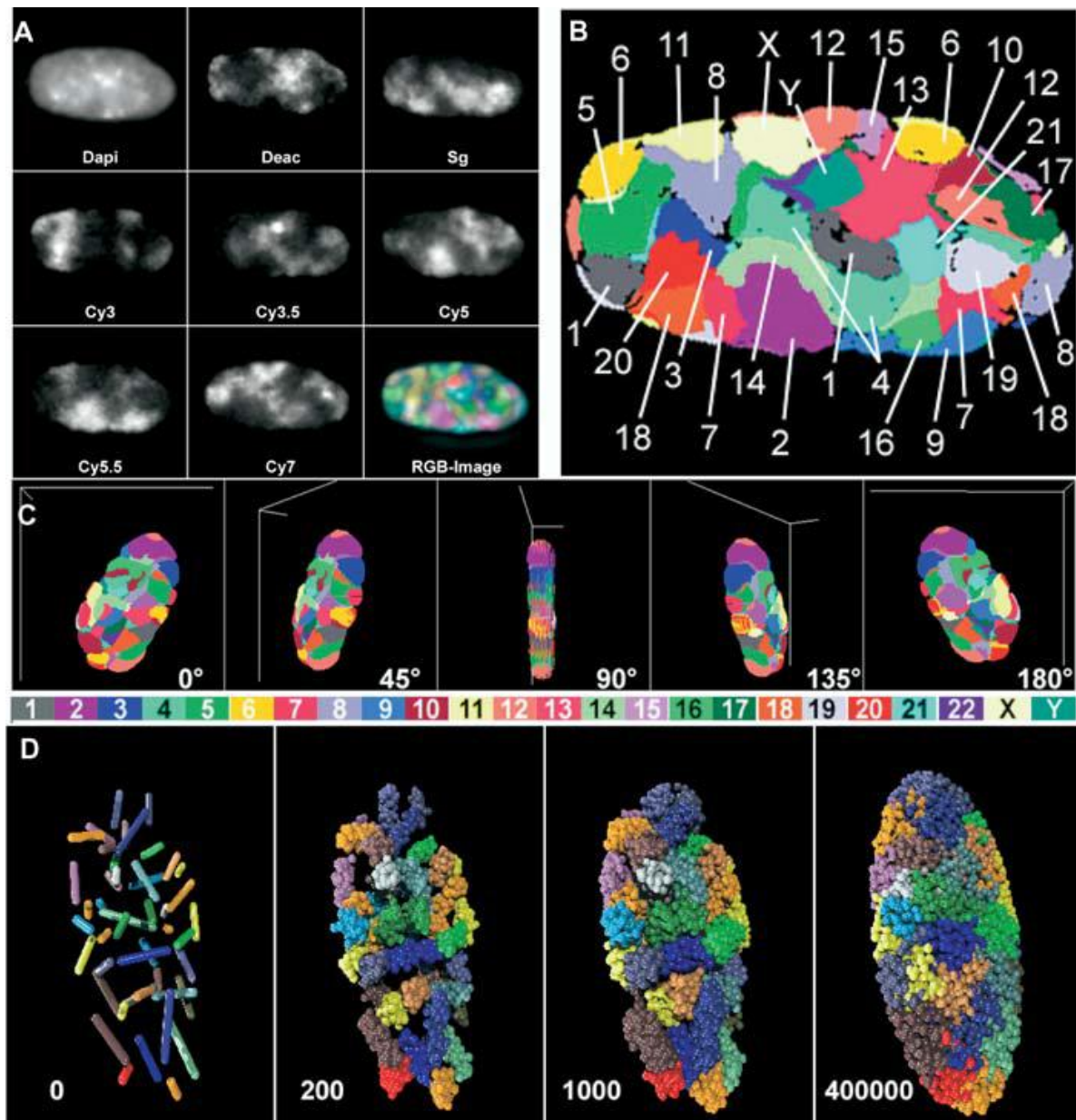
Figure 4.2. A detailed representation of interphase chromosomes in the human fibroblast cell nucleus, including 3D reconstruction and simulated model. The detailed organisation of the chromosome territories are revealed by fluorescence microscopy and FISH techniques as shown in (A) and mapped in (B), together with advanced 3D positional mapping and reconstruction methods as shown in (C), and modelling methods as shown in (D) with simulated decondensation of chromosomes, increasing left to right panels to show territories.

Image taken from Bolzer et al. (2005).

Generally, in normal proliferating cells the organisation of interphase chromosomes in their respective territories has been shown to correspond to the number of genes they contain, such that low gene number chromosomes are located at the periphery of the nucleus, and high gene number chromosomes are located in a more interior location in the nucleus (Boyle et al. 2001; Cremer et al. 2003; Mehta et al. 2007). In addition to this organisation, the level of genomic activity of chromosomes is correlated with their dynamic positioning in the nucleus, where a position at the nuclear periphery is associated with low activity and a closed conformation, and a more interior position is associated with high genomic activity and a more open chromatin conformation. See Foster and Bridger (2005) and Fritz et al. (2016) for reviews.

The physiological activity of cells is directly related to their state with regards to the cell cycle, such that proliferating cells which are actively dividing and continuing to expand and/or renew the tissues they are a part of, will have a different gene expression profile, as well as other cellular characteristics compared with non-proliferating cells, which have exited the cell cycle, either temporarily as in quiescent cells or permanently as in senescent cells (Aguilar and Fajas 2010; Cai and Tu 2012). This makes studies comparing proliferating and non-proliferating cells especially important to research into ageing for example, particularly the senescent cellular state is strongly associated with the process of ageing, where the tissue renewal mechanisms of the organism become diminished as part of the ageing process. Integral to this, is the increasing proportions of senescent cells which in turn, are the result of the altered genomic and cellular circumstances found in the cells of ageing organisms (Macieira-Coelho and Taboury 1982; Franceschi 1989; Di Micco et al. 2021).

In the work for this chapter, the responses of interphase chromosomes 10, 11, and 15 to two separate external stimuli in the form of reduced serum media conditions (chromosomes 10 and 15) and heat shock (chromosome 11) were studied in a comparative manner, between proliferating and non-proliferating cells. This work also involved comparing such responses in young, low passage number cells with older, moderately higher passage number cells. These three chromosomes were selected for this study mainly because they were known to relocate from previous

studies (Mehta et al. 2010) and therefore they were suitable for assays which test the relocation of chromosomes, under different conditions. In addition to this, chromosome 11 was selected for the heat shock assay because it was known to contain the HSP73 heat shock gene (Tavaria et al. 1995; Tavaria et al. 1996). Importantly, in this chapter, a chromosome relocation assay has been established based on the heat shock stimulus using chromosome 11. In addition to establishing an assay for chromosome relocation, this heat shock assay has demonstrated a novel chromosome 11 relocation in response to heat shock. Importantly, the results of this work also indicate that in non-proliferating cells, chromosome relocation does not occur after stimulus, in contrast to the situation with proliferating cells. This supports one of the key hypotheses of this project, which postulates that in non-proliferating cells the prospective molecular motors involved in chromosome relocation are working with much reduced functionality, therefore not allowing chromosomes to relocate as they would in proliferating cells. The chromosome 11 relocation found in this work occurs in the nuclei of proliferating cells only, and is from the nuclear periphery to the nuclear interior in response to heat shock stimulus at 42°C for 1 hour. The results of the work in this chapter are included in a recent publication (Mehta et al. 2021). Previously, Mehta et al. (2010) had shown that in cells made quiescent by serum removal (low serum conditions), and therefore had entered a reversible non-proliferative state, the positions of specific interphase chromosomes were altered, and that the repositioning in response to serum removal was rapid and involved an active process by the action nuclear myosin 1β (NM1β).

4.2 MATERIALS AND METHODS

4.2.1 Low serum assay for chromosome relocation: for cells exposed to low serum (0.5% FCS) conditions

Using the low serum assay, the movement of whole chromosomes in the interphase nuclei of NB1 human neonate foreskin fibroblast cells, maintained in high serum media (as described in section 2.2.1), was investigated by exposure to low serum media conditions and 2D FISH. Low serum media (DMEM media with 0.5% FCS) exposed cells were compared with cells grown in high serum media (DMEM media with 15% FCS), and not exposed to low serum media conditions, as a control. For this procedure, NB1 cells were cultured in high serum (15% FCS) for 3 days and then were exposed to low serum media by change of media, for 1 hour before being harvested by trypsinisation and pelleted by centrifugation at 800 rpm. The 1 hour incubation period in low serum media was selected to provide adequate time for the response to the stimulus. The harvested pellets were fixed for FISH procedure as described below in section 4.2.3.

4.2.2 Heat shock procedure for chromosome relocation assay

The cells used were NB1 human neonate foreskin fibroblast cells, maintained in plastic 10 cm cell culture dishes with DMEM media (supplemented with 15% FCS, 2% Penicillin/Streptomycin), placed in a humidified incubator at 37°C and 5% CO_2. Cell cultures were passaged routinely twice a week by trypsinisation, and new cell cultures were then setup at a cell density of 2×10^5 in 10 ml of media in 10 cm plastic cell culture dishes, and allowed to grow until approximately 70% confluent, ready for heat shock experiments. Heat shock was carried out on cells growing in 10 cm plastic dishes placed inside a separate humidified cell culture incubator maintained at 42°C and 5% CO_2. The plates used for main treatment and control were initially observed to ensure approximate equal density of cells in all plates to avoid any bias due to cell density effects on cellular state. The duration of the heat shock was 1 hour. Control cell plates from the same passage continued to be

maintained at standard conditions of 37°C and 5% CO_2. Following the heat shock procedure, both heat shocked and control cells were harvested by trypsinisation and then pelleted immediately by centrifugation at 800 rpm, and care was taken to minimise exposure of cells to ambient temperatures following heat shock. The harvested pellets were fixed for FISH procedure as described below in section 4.2.3.

4.2.3 Chromosome relocation assay with 2D FISH procedure

Pelleted cells were re-suspended and disrupted by adding a hypotonic solution of KCL (0.075 M) dropwise with regular agitation, and left at room temperature for 15 minutes and then centrifuged at 800 rpm for 5 minutes. Then the pelleted disrupted cells were resuspended and fixed by adding ice cold 3:1 (v/v) methanol:acetic acid dropwise with regular agitation. The resuspended disrupted cells were left on ice for 1 hour. At this stage a drop of the sample on a damp slide, was observed using a phase contrast microscope (Hund Wetzlar Wilovert) to see what proportion of the nuclei were separated from the contents of the cell cytoplasm, and to determine the approximate concentration of nuclei visually on the slide. The aim was to have approximately 90% of the nuclei clear of cytoplasm surrounding them, and to have a density of nuclei such that they were not clumped together. After centrifugation of the main sample, again at 800 rpm for 5 minutes, the fixation procedure with 3:1 (v/v) methanol:acetic acid was repeated 4-8 times until approximately 90% of the nuclei were clear of cytoplasm, and the final fixative volume was adjusted to give the desired density (non-clumped) of nuclei, when a drop of the sample was again observed on a damp slide using a microscope. Then samples were dropped onto damp slides, allowed to dry and baked for 1 hour at 70°C in preparation for dehydration by an ethanol row (concentration series) for 5 minutes in each of 70%, 90% and 100% ethanol solution, after which they were dried and incubated for 5 minutes at 70°C. To denature the DNA, the slides were then incubated in a denaturing solution for 2 minutes (70% formamide, 2x saline sodium citrate (SSC), pH 7.0) and then put through an ethanol row again, starting with 70% ice cold ethanol followed by 90% and 100% ethanol both at room temperature. The slides were dried on a warm plate in preparation for hybridisation with the chromosome painting probes.

A whole chromosome painting probe for the relevant chromosome was made from a previously stored collection/library of whole chromosome secondary templates, which had been produced from microdissected chromosome arms (sequence pools) by degenerate oligonucleotide primed polymerase chain reaction (DOP-PCR) (Telenius et al. 1992) amplification. This secondary template was used to produce a tertiary amplified template by DOP-PCR, and this template was in turn used to produce the Biotin-16dUTP labelled quaternary probe by DOP-PCR.

The reaction mix (50 μl) for producing the tertiary template by DOP-PCR amplification contained: (10 μl 5 x DOP-PCR buffer; 5 μl dACGTP (2 mM); 5 μl dTTTP (2 mM); 5 μl DOP primer (20 μM); 1 μl Taq (1U/μl); 23 μl sterile water and 1 μl template).

The reaction mix for producing the quaternary probe included Biotin-16dUTP in addition to the above components given for producing the tertiary template.

The reaction mix (50 μl) for producing the Biotin-16dUTP labelled quaternary probe by DOP-PCR amplification contained: (10 μl 5 x DOP-PCR buffer; 5 μl dACGTP (2 mM); 2 μl dTTTP (2 mM); 10 μl Biotin-16dUTP; 5 μl DOP primer (20 μM); 1 μl Taq (1U/μl); 12 μl sterile water and 5 μl template).

PCR settings for DOP-PCR reaction producing tertiary template: 1 cycle at 95ºC for 3 minutes then 31 cycles at 98ºC for 20 seconds, 62ºC for 1 minute and 72ºC for 30 seconds, then 1 cycle at 72ºC for 5 minutes).

PCR settings for DOP-PCR reaction producing Biotin-16dUTP labelled quaternary probe: 1 cycle at 95ºC for 3 minutes then 34 cycles at 98ºC for 20 seconds, 62ºC for 1 minute and 72ºC for 30 seconds, then 1 cycle at 72ºC for 5 minutes).

Then per slide, 8μl of probe was mixed with 7μl of Cot1 DNA, 3μl of herring sperm, 3M sodium acetate (1/10th volume) and 2 volumes of ice cold ethanol. This mixture was incubated at -80°C for more that 30 minutes and then centrifuged at 13000 rpm for 30 minutes, and the resulting pellet washed with 200 μl of ice cold ethanol, followed by centrifugation, again at 13000 rpm for 30 minutes. Then the pellet was dried on a hot block at 45°C until it became transparent, and then 12μl of hybridisation mix (50% formamide, 10% dextran sulphate, 10% 20X SSC, 1% Tween 20, in aqueous solution) was added to the pellet, which was incubated at 37°C for 2 hours to dissolve. Next, the probe was denatured at 75°C for 10 minutes, followed by incubation at 37°C for up to 2 hours to allow re-annealing of repetitive sequences.

Then 12 µl of probe was added to each slide for hybridisation, and coverslips were placed over the slides and sealed with rubber cement and the slides were placed in a moist chamber at 37°C overnight.

Following the incubation for hybridisation, the coverslips were removed from the slides. The slides were then washed in wash buffer A (50% formamide 2x SSC in aqueous solution, pH 7) at 45°C, 3 times with buffer changes for 5 minutes each wash. Then the slides were washed in wash buffer B (0.1% SSC in aqueous solution) at 60°C, 3 times with buffer changes for 5 minutes each wash. The slides were then placed in 4X SSC and then the slides were blocked using 100 µl 4% bovine serum albumen (BSA) for 10 minutes at room temperature. Then the slides were incubated with 100 µl 1:200 dilution streptavidin-cyanine 3 (Cy3) (Thermo Fisher) for 1 hour at room temperature and then washed 3 times with buffer changes for 5 minutes each wash, with 4x SSC with 0.05% Tween 20 at 42°C. The slides were covered with coverslips after applying Vectashield mounting medium (Vector Laboratories) in preparation for fluorescence microscopy. Following observation of the slides by fluorescence microscopy (Leica DM4000 microscope with 100x oil immersion objective lens selected) and confirmation that the FISH procedure had worked, it was then necessary to stain the slides with Ki-67 antibody in order to visually determine the proliferating and non-proliferating nuclei on the slides by immunofluorescence. This was performed by first washing off the Vectashield mounting medium from the FISH slides, with three 30 minute washes in PBS followed by one final wash in ddH$_2$O. Then the slides were incubated with 100 µl of 1:25 dilution Ki-67 primary antibody (Abcam) overnight at 4°C, then washed three times (5 minutes each wash) with PBS, followed by incubation with 100 µl of 1:100 dilution secondary antibody (Goat-anti-Mouse FITC) (Stratech) for 1 hour, in the dark at room temperature, followed by three PBS washes (5 minutes each wash) and one final ddH$_2$O wash. The slides were again covered with coverslips after applying Vectashield mounting medium in preparation for fluorescence microscopy and image capture on a Leica DM4000 microscope (100x oil immersion objective lens selected) with attached Leica digital camera.

Images were prepared for analysis by the IPLab computer software (Croft et al. 1999; Boyle et al. 2001) which carries out an erosion analysis by dividing each

image of nuclei into 5 concentric shells with 1 being the most peripheral and 5 being most interior (Figure 4.3). This is a long and well established method for analysing chromosome position used by various laboratories. Firstly, it was necessary to convert the red colour of the Cy3 in the images to green colour by digital image processing, since this is the colour the programme detects as chromosome territory. Also, it was necessary to remove the Ki-67 signal from the images of proliferating nuclei to prevent interference with the erosion analysis of the computer software. The proliferating and non-proliferating datasets had first been recorded and separated and therefore were designated prior to removal of the Ki-67 signal. The programme then measures the intensity of the DAPI signal and the signal from the chromosome territories. The signal from the chromosome territory staining was normalised using the DAPI signal for each shell of the nucleus (the chromosome territory signal value was divided by the DAPI signal value, to give the normalised value). The averages of the normalised values for each shell were plotted as graphs, which could then be used to compare any differences between chromosome positions.

It is important to note here that the graphs generated in this method do not show absolute positions in terms of occupancy for a given chromosome. Therefore, there will always be signal, albeit to a lesser extent compared with the main determined occupancy, in all the nuclear shells. The main factor is the highest occupancy, and supported by the statistical analysis, that informs regarding determined chromosome position. The statistical analyses of FISH results are by unpaired t-test using GraphPad Software. Statistical results are displayed as compiled from the output of the software.
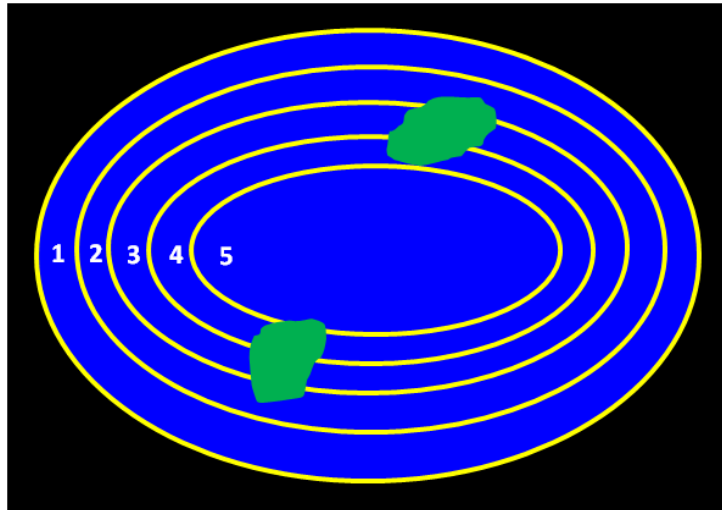
Figure 4.3. A schematic illustrating the nucleus (blue), divided into five nuclear shells, used by the IPLab computer software analysis to determine chromosome position. Shells are numbered 1-5 and separated by the yellow lines as shown in the illustration. Two stained chromosomes (green) are depicted as a demonstration.

4.3 RESULTS

4.3.1 Chromosome relocation assays: Initial experiments for low serum (0.5% FCS) media assay (passage 20 and 25 NB1 cells) and initial experiments for heat shock assay (passage 20 NB1 cells) with anti-Ki-67 proliferation marker

Chromosome positioning assays with low serum (0.5% FCS) media and heat shock stimulus were performed with chromosomes 10, 11 and 15. Low serum (0.5% FCS) assay was performed with chromosome 10 and 15, comparing high serum (15% FCS) media maintained cells with cells exposed to low serum conditions in the growth media for 1 hour. Heat shock assay was performed with chromosome 11 comparing proliferating cells and non-proliferating cells exposed to heat shock at 42°C for 1 hour. These experiments were a good starting point for studies on chromosome relocation in this project, and indicated the importance of cell age (passage number) in interpreting results obtained in chromosome relocation assay experiments. In the initial, low serum (0.5% FCS) media experiments, Ki-67 antibody was not used and therefore the data does not rely on confirmation of proliferation or non-proliferation state using this marker. In subsequent experiments using the low serum assay, Ki-67 antibody was used and higher sample size datasets were analysed, and cells at a lower passage number were used for the experiments. The initial heat shock experiments were a useful preparation for the larger major heat shock experiment using much larger sample size datasets and younger cells at passage number 12.

With these experiments, an interesting outcome was the implication of a trend that with older cells at moderately higher passage numbers, the responses to stimuli may be diminished, since for these cells, stimuli did not induce chromosome repositioning, such that there were no statistically significant differences between the control datasets and the main treatment datasets. Initially this was of some concern, however it was later found to be very interesting and informative when compared to results with moderately younger cells, albeit with larger sample sizes.

In order to gauge the growth characteristics of the NB1 cell line being used for these experiments and under the conditions maintained, in relation to viability, cell culture growth curve graphs were generated for NB1 cells from passage numbers 16-19 and 16-20 (Figure 4.4). These growth curves, showing the rate of accumulated population doublings (APD) confirmed that the NB1 cell line being used remained viable, and continued to grow vigorously up to and beyond passage number 20. This confirmed that these cell cultures were suitable for experiments, and would generate reliable data, not biased by diminished overall replication potential. It is however important to note that in even a vigorously growing cell culture, there will always be a proportion of non-proliferating cells that have exited the cell cycle. This is clearly shown when the Ki-67 proliferation marker is used, and shows that some cells are no longer in proliferation, even in cell cultures maintained in high serum media. Ki-67 staining is a powerful and reliable biomarker of cell proliferation, and the absence of Ki-67 staining is equally a powerful tool for confirming non-proliferation.

Statistical analyses by t-test were performed using the GraphPad Software and the output generated by the software is displayed in tabulated form, in the results sections showing the details of the calculations and parameters. This is considered desirable, as the statistical analysis is especially central to the interpretation of the results of the chromosome positioning data, such that each nuclear shell, as designated by the erosion script software, must be individually analysed to determine the significance of the difference if any between data sets. It is just as important to determine that a pair of data sets for a given nuclear shell show no statistically significant difference as it is important to determine if a pair of datasets do show a statistically significant difference. By this logic a repositioning event can be confirmed.
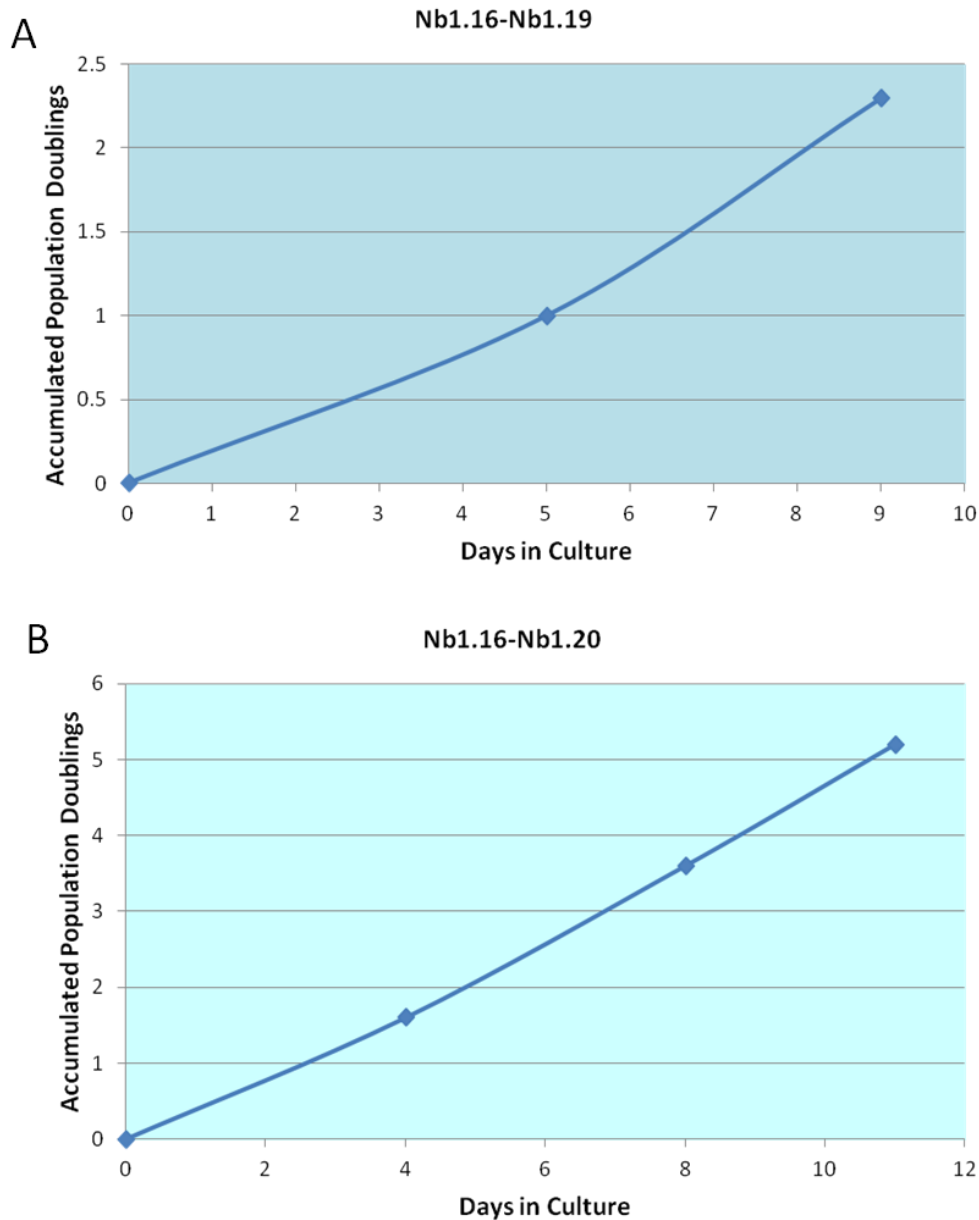
Figure 4.4. Examples of graphs showing growth curves, with the rate of Accumulated Population Doubling (APD) for two separate NB1 fibroblast cell cultures. Both cultures demonstrate vigorous growth, thus corroborating the growth characteristics. (A) Passage numbers 16-19; this culture was used for a heat shock experiment at passage 18 (Nb1.18). (B) Passage numbers 16-20; this culture was not used in an experiment. These graphs were generated to help confirm that the NB1 cell cultures used were viable and therefore suitable for experiments. Formula below used for calculation of population doubling.

Population doubling =

(*log* no. of cells harvested per dish - *log* no. of cells set up at previous passage per dish) / *log* 2.0

Low serum assay with chromosome 10 (passage 25 NB1 cells)

Chromosome 10 was used in a low serum (0.5% FCS) assay to observe the effect of this stimulus on chromosome position. The NB1 cells used were at passage number 25 and therefore these cells represent moderate age cells, and thus the findings would inform regarding the response in relation to cell age when compared to similar experiments with younger cells. Representative images of the nuclei stained for chromosome 10 positions are shown in Figures 4.5 and 4.6. These images are examples of the digital data used by the computer erosion analysis to determine the positions of chromosome 10. The graph in Figure 4.7 shows that in both the high serum maintained control cells and the low serum exposed cells, the position of chromosome 10 is mostly towards the interior (nuclear shells 4 and 5) of the nucleus, although as also shown in the graph, there are lesser amounts of chromosome 10 signal at an intermediate position in the nucleus (nuclear shell 3). This is also shown by the images in Figures 4.5 and 4.6 where some nuclei show intermediate and peripheral positions. The cells exposed to low serum (0.5% FCS) media for 1 hour, would not be induced to quiescence, since they would need to be in low serum media for at least 4 days to exit the cell cycle as a result of reduced nutrient conditions. Therefore, the stimulus of a low nutrient environment for 1 hour may only induce chromosome relocation as a response, and not alter the cellular state of the cells. According to the statistical analyses (Tables 4.1-4.5) there is no statistically significant difference between the high serum (15% FCS) media maintained cells and the low serum (0.5% FCS) media exposed cells in the positions of chromosome 10. This result indicates that there was no chromosome 10 relocation in response to the low serum media exposure for 1 hour. Though it is important to note the conditions of this experiment with regards to age of cells and sample size both of which will affect the outcome of the results.
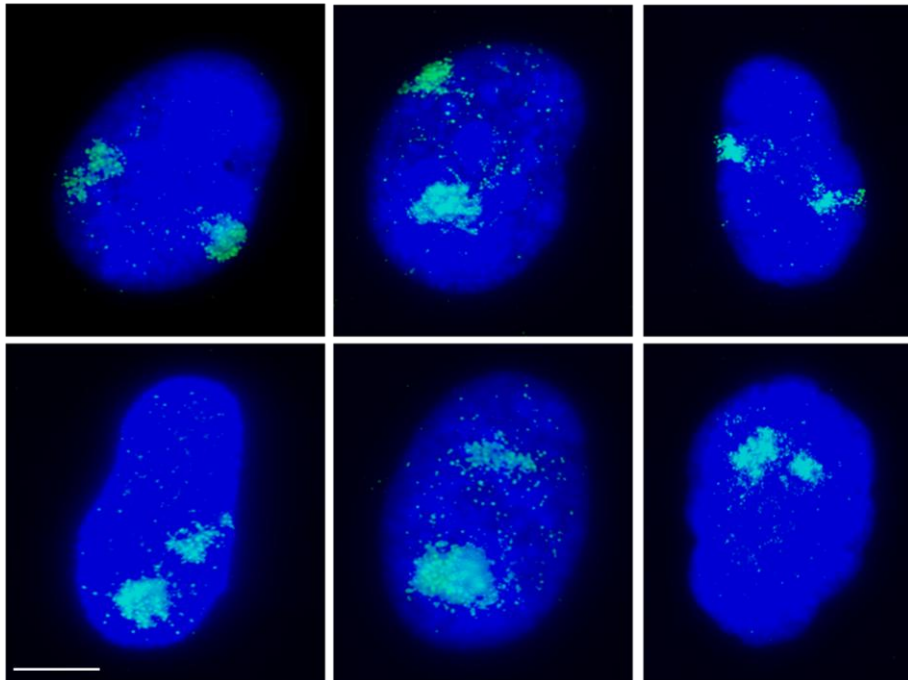
Figure 4.5. Representative images used for the computer erosion analysis, showing nuclei of high serum maintained control cells, stained for chromosome 10 territories by 2D FISH. Scale bar = 10 µm.
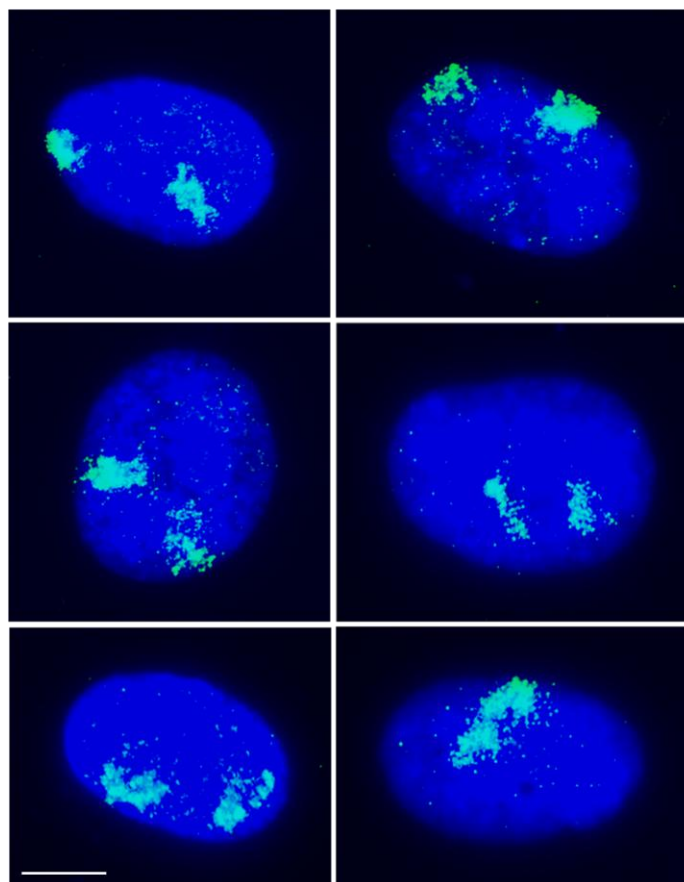
Figure 4.6. Representative images used for the computer erosion analysis, showing nuclei of low serum (0.5% FCS) media exposed cells (for 1 hour), stained for chromosome 10 territories by 2D FISH. Scale bar = 10 µm.
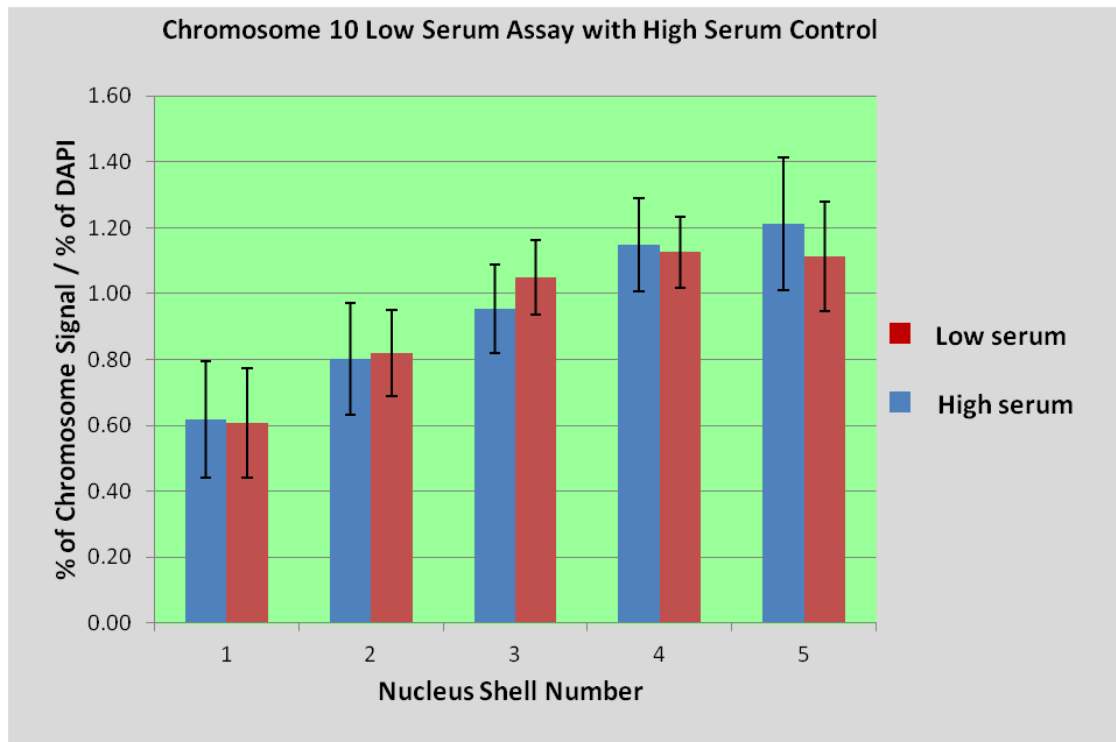
Figure 4.7. Results of low serum (0.5% FCS) assay for chromosome positioning. Shell number 1 is most peripheral and shell number 5 is most interior. The graph shows that chromosome 10 positions (mostly interior) in nuclei of high serum maintained control cells and low serum exposed cells are very similar, indicating a lack of chromosome 10 relocation in response to low serum media exposure for 1 hour. For both datasets n = 15. Error bars show SEM. The statistical analysis found no significant difference when the data for low serum exposed cells are compared with the data for high serum maintained cells. See tables 4.1-4.5 for statistical calculation and analysis.

Statistical analysis: chromosome 10 low serum assay with high serum (15% FCS) maintained control cells

Low serum exposed cells compared with high serum maintained control cells for each nucleus shell

Table 4.1. HS = high serum control, LS = low serum exposed.

Nucleus Shell 1		
P value and statistical significance:		
The two-tailed P value equals **0.9674**		
This difference is **not statistically significant**.		
Intermediate values used in calculations:		
t = 0.0412		
df = 28		
standard error of difference = 0.243		
Group	**One ch10 HS**	**One ch10 LS**
Mean	0.620	0.610
SD	0.688	0.639
SEM	0.177	0.165
N	15	15

Table 4.2. HS = high serum control, LS = low serum exposed.

Nucleus Shell 2		
P value and statistical significance:		
The two-tailed P value equals **0.9264**		
This difference is **not statistically significant**.		
Intermediate values used in calculations:		
t = 0.0932		
df = 28		
standard error of difference = 0.214		
Group	**Two ch10 HS**	**Two ch10 LS**
Mean	0.800	0.820
SD	0.658	0.506
SEM	0.169	0.130
N	15	15

Table 4.3. HS = high serum control, LS = low serum exposed.

Nucleus Shell 3		
P value and statistical significance:		
The two-tailed P value equals **0.5743**		
This difference is **not statistically significant**		
Intermediate values used in calculations:		
t = 0.5683		
df = 28		
standard error of difference = 0.176		
Group	**Three ch10 HS**	**Three ch10 LS**
Mean	0.950	1.050
SD	0.522	0.436
SEM	0.135	0.112
N	15	15

Table 4.4. HS = high serum control, LS = low serum exposed.

Nucleus Shell 4		
P value and statistical significance:		
The two-tailed P value equals **0.9112**		
This difference is **not statistically significant**.		
Intermediate values used in calculations:		
t = 0.1126		
df = 28		
standard error of difference = 0.178		
Group	**Four ch10 HS**	**Four ch10 LS**
Mean	1.150	1.130
SD	0.548	0.415
SEM	0.141	0.107
N	15	15

Table 4.5. HS = high serum control, LS = low serum exposed.

Nucleus Shell 5		
P value and statistical significance:		
The two-tailed P value equals **0.7040**		
This difference is **not statistically significant**.		
Intermediate values used in calculations:		
t = 0.3838		
df = 28		
standard error of difference = 0.261		
Group	**Five ch10 HS**	**Five ch10 LS**
Mean	1.210	1.110
SD	0.778	0.642
SEM	0.201	0.165
N	15	15

Low serum assay with chromosome 15 (passage 20 NB1 cells) and anti-Ki-67 proliferation marker

NB1 cells at passage 20 were used to study the effect of exposure to low serum conditions for 1 hour, by the low serum (0.5% FCS) media assay, on chromosome 15 positioning. Ki-67 proliferation marker was used to distinguish between proliferating and non-proliferating cells. This added more reliability and robustness to the data collection stage, such that the difference between proliferating and non-proliferating cells could be determined with more confidence. This is particularly important when using cell cultures still showing vigorous growth, as a considerable proportion of cells in such cultures would be proliferating. In data presented here, the positions of chromosome 15 in the nuclei of proliferating and non-proliferating cells following exposure to low serum media conditions were compared, in order to determine if chromosome 15 relocation had occurred. Also in the data, the position of chromosome 15 in the nuclei of high serum (15% FCS) maintained non-proliferating cells (Ki-67 –ve) are included. Representative images of the nuclei stained for chromosome 15 positions are shown in Figures 4.8-4.10. These images are examples of the digital data used by the computer erosion analysis to determine the positions of chromosome 15. As had been described in section 4.2.3 of this chapter, the Ki-67 signal had been removed from the images in order to allow for the computer analysis of the images for chromosome territory determination without interference. The results of this work under the conditions performed and with the cells used at given passage number, show that there is was no statistically significant difference in the positions of chromosome 15 after 1 hour exposure to low serum (0.5% FCS) media conditions, when proliferating and non-proliferating cells are compared. Chromosome 15 position in the nuclei of the non-proliferating cells maintained in high serum media, also show the same nuclear location as the low serum exposed cells. This suggests that the chromosome 15 position of proliferating and non-proliferating cells after exposure low nutrient conditions are similar, and that chromosome relocation had not occurred. The graph in Figure 4.11 shows clearly that the position of chromosome 15 is mostly at the nuclear interior (nuclear shell 5) and this is corroborated by some the sample images of nuclei used in the analysis as shown in Figures 4.8-4.10. This position is in agreement with previous findings of the position of chromosome 15 in quiescent cells (Mehta et al. 2010).

Figure 4.8. Representative images used for the computer erosion analysis, showing low serum (0.5% FCS) media exposed Ki-67 negative nuclei stained for chromosome 15 territories by 2D FISH. Scale bar = 10 µm.
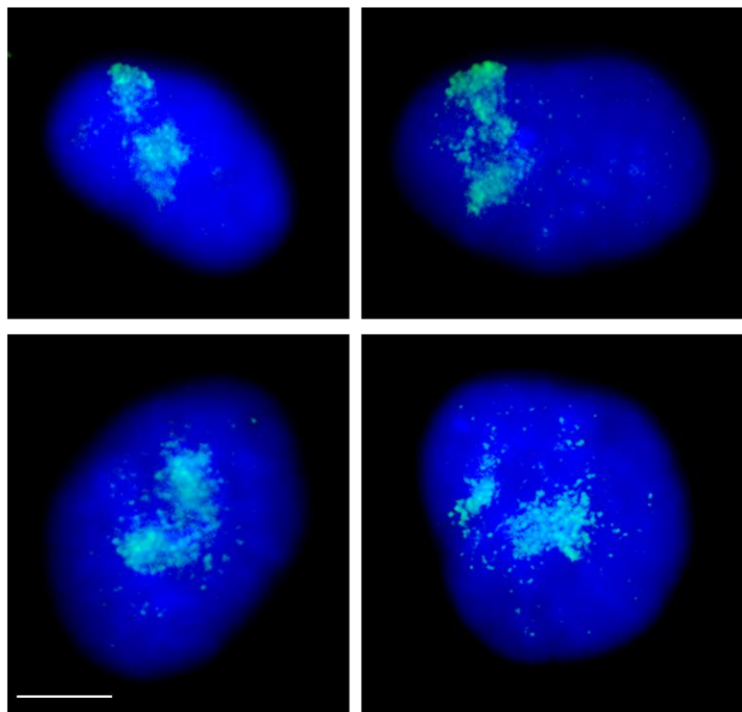
Figure 4.9. Representative images used for the computer erosion analysis, showing low serum (0.5% FCS) media exposed Ki-67 positive nuclei stained for chromosome 15 territories by 2D FISH. Note that the Ki-67 signal has been removed in order to allow for the computer analysis of the images for chromosome territory determination. Scale bar = 10 µm.
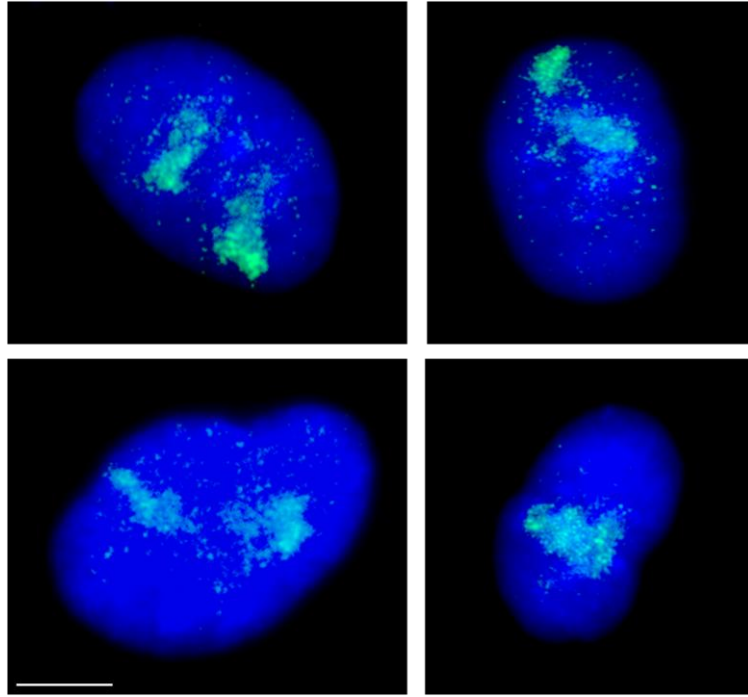
Figure 4.10. Representative images used for the computer erosion analysis, showing high serum (15% FCS) maintained Ki-67 negative nuclei stained for chromosome 15 territories by 2D FISH. Scale bar = 10 µm.
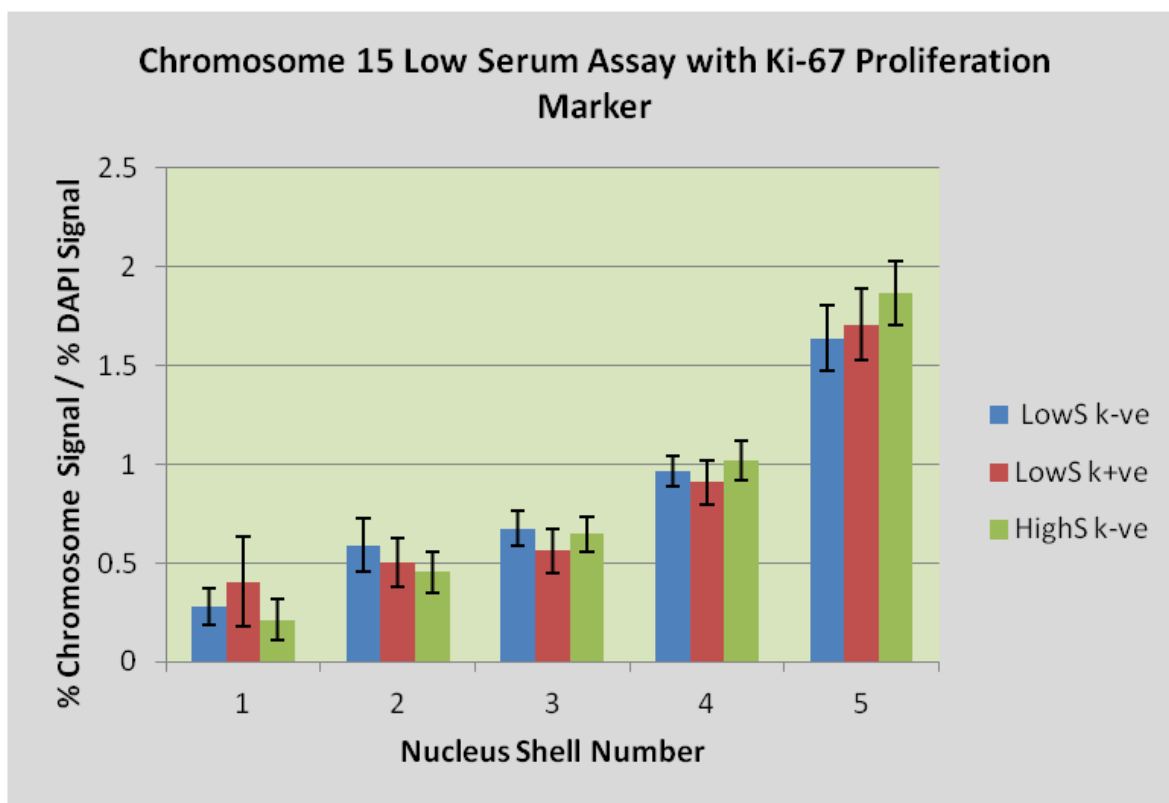
Figure 4.11. Results of the low serum (0.5% FCS) assay for chromosome positioning with Ki-67 proliferation marker. Shell number 1 is most peripheral and shell number 5 is most interior. The graph shows that the nuclear positions of chromosome 15 are mostly interior for both Ki-67 positive and Ki-67 negative nuclei exposed to low serum media, and for Ki-67 negative nuclei maintained in high serum (15% FCS). This indicates a lack of chromosome 15 relocation in response to low serum conditions. n = 32 for low serum exposed Ki-67 –ve, n = 26 for low serum exposed Ki-67 +ve, n = 15 for high serum (15% FCS) maintained Ki-67 –ve. Error bars show SEM. The statistical analysis found no significant difference when the data for proliferating and non-proliferating cells are compared. See tables 4.6-4.15 for statistical analysis and calculation.

Statistical analysis: chromosome 15 low serum assay

Low serum assay main treatment Ki-67 -ve compared with Ki-67 +ve

Table 4.6. LS = low serum exposed.

Nucleus Shell 1		
P value and statistical significance:		
The two-tailed P value equals **0.5842**		
This difference is **not statistically significant**.		
Intermediate values used in calculations:		
t = 0.5504		
df = 56		
standard error of difference = 0.228		
Group	**One ch15 LS k-**	**One ch15 LS k+**
Mean	0.278	0.403
SD	0.517	1.157
SEM	0.091	0.227
N	32	26

Table 4.7. LS = low serum exposed.

Nucleus Shell 2		
P value and statistical significance:		
The two-tailed P value equals **0.6340**		
This difference is **not statistically significant**.		
Intermediate values used in calculations:		
t = 0.4788		
df = 56		
standard error of difference = 0.185		
Group	**Two ch15 LS k-**	**Two ch15 LS k+**
Mean	0.590	0.502
SD	0.758	0.616
SEM	0.134	0.120
N	32	26

Table 4.8. LS = low serum exposed.

Nucleus Shell 3		
P value and statistical significance:		
The two-tailed P value equals **0.4313**		
This difference is **not statistically significant.**		
Intermediate values used in calculations:		
t = 0.7928		
df = 56		
standard error of difference = 0.141		
Group	**Three ch15 LS k-**	**Three ch15 LS k+**
Mean	0.673	0.562
SD	0.496	0.573
SEM	0.087	0.112
N	32	26

Table 4.9. LS = low serum exposed.

Nucleus Shell 4		
P value and statistical significance:		
The two-tailed P value equals **0.6756**		
This difference is **not statistically significant.**		
Intermediate values used in calculations:		
t = 0.4207		
df = 56		
standard error of difference = 0.133		
Group	**Four ch15 LS k-**	**Four ch15 LS k+**
Mean	0.964	0.908
SD	0.439	0.575
SEM	0.077	0.112
N	32	26

Table 4.10. LS = low serum exposed.

Nucleus Shell 5		
P value and statistical significance: The two-tailed P value equals **0.7828** This difference is **not statistically significant**.		
Intermediate values used in calculations: t = 0.2771 df = 56 standard error of difference = 0.247		
Group	**Five ch15 LS k-**	**Five ch15 LS k+**
Mean	1.639	1.707
SD	0.949	0.921
SEM	0.167	0.180
N	32	26

Low serum exposed Ki-67 +ve compared high serum maintained Ki-67 -ve

Table 4.11. HS = high serum control, LS = low serum exposed.

Nucleus Shell 1		
P value and statistical significance: The two-tailed P value equals **0.5395** This difference is **not statistically significant.**		
Intermediate values used in calculations: t = 0.6190 df = 39 standard error of difference = 0.311		
Group	**One ch15 LS k+**	**One ch15 HS k-**
Mean	0.403	0.211
SD	1.157	0.402
SEM	0.227	0.103
N	26	15

Table 4.12. HS = high serum control, LS = low serum exposed.

Nucleus Shell 2		
P value and statistical significance:		
The two-tailed P value equals **0.7919**		
This difference is **not statistically significant.**		
Intermediate values used in calculations:		
t = 0.2657		
df = 39		
standard error of difference = 0.178		
Group	**Two ch15 LS k+**	**Two ch15 HS k-**
Mean	0.502	0.454
SD	0.616	0.406
SEM	0.120	0.104
N	26	15

Table 4.13. HS = high serum control, LS = low serum exposed.

Nucleus Shell 3		
P value and statistical significance:		
The two-tailed P value equals **0.6082**		
This difference is **not statistically significant**.		
Intermediate values used in calculations:		
t = 0.5168		
df = 39		
standard error of difference = 0.162		
Group	**Three ch15 LS k+**	**Three ch15 HS k-**
Mean	0.562	0.646
SD	0.573	0.329
SEM	0.112	0.085
N	26	15

Table 4.14. HS = high serum control, LS = low serum exposed.

Nucleus Shell 4		
P value and statistical significance:		
The two-tailed P value equals **0.5107**		
This difference is **not statistically significant.**		
Intermediate values used in calculations:		
t = 0.6639		
df = 39		
standard error of difference = 0.167		
Group	**Four ch15 LS k+**	**Four ch15 HS k-**
Mean	0.908	1.019
SD	0.575	0.387
SEM	0.112	0.100
N	26	15

Table 4.15. HS = high serum control, LS = low serum exposed.

Nucleus Shell 5		
P value and statistical significance:		
The two-tailed P value equals **0.5555**		
This difference is **not statistically significant.**		
Intermediate values used in calculations:		
t = 0.5946		
df = 39		
standard error of difference = 0.268		
Group	**Five ch15 LS k+**	**Five ch15 HS k-**
Mean	1.707	1.866
SD	0.921	0.622
SEM	0.180	0.160
N	26	15

Heat shock assay with chromosome 11 (passage 20 NB1 cells) and anti-Ki-67 proliferation marker

The response of chromosome 11 to a heat shock stimulus at 42°C for 1 hour, with regards to nuclear position was studied using NB1 cells at passage 20. The Ki-67 proliferation marker was also used as a useful marker of cell proliferation. It was of interest to study the response to this assay in particular with chromosome 11, as it is known to contain the HSP73 heat shock protein gene (Tavaria et al. 1995; Tavaria et al. 1996). As shown in Figure 4.14, the results of this work under the conditions performed, and with the cells used at given passage number, did not show a statistically significant difference in the positions of chromosome 11 in response to heat shock, when the proliferating and non-proliferating cells are compared, before and after the heat shock stimulus for 1 hour at 42°C. Representative images of the nuclei stained for chromosome 11 positions are shown in Figures 4.12 and 4.13. These images are examples of the digital data used by the computer erosion analysis to determine the positions of chromosome 11. Figure 4.14 shows that the position of chromosome 11 as analysed in this work is mostly at the nuclear periphery (nuclear shells 1 and 2) and this is corroborated by some of the images shown in Figures 4.12 and 4.13. The heat shock assay with chromosome 11, when subsequently performed at a larger scale and with younger cells at considerably lower passage number of 12, did show chromosome 11 relocation as presented in section 4.3.3.
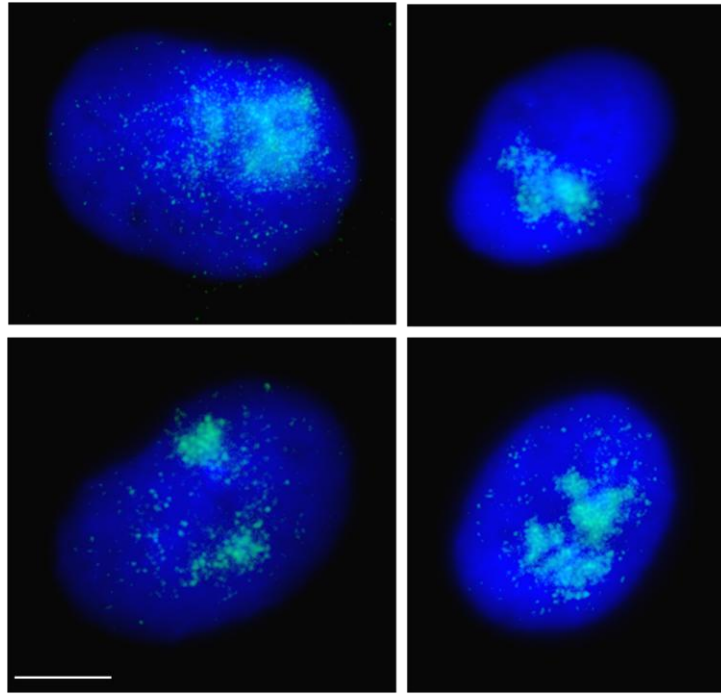
Figure 4.12. Representative images used for the computer erosion analysis, showing control (not heat shocked) Ki-67 negative nuclei stained for chromosome 11 territories by 2D FISH. Scale bar = 10 μm.

Figure 4.13. Representative images used for the computer erosion analysis, showing heat shocked (42°C for 1 hour) Ki-67 negative nuclei stained for chromosome 11 territories by 2D FISH. Scale bar = 10 μm.
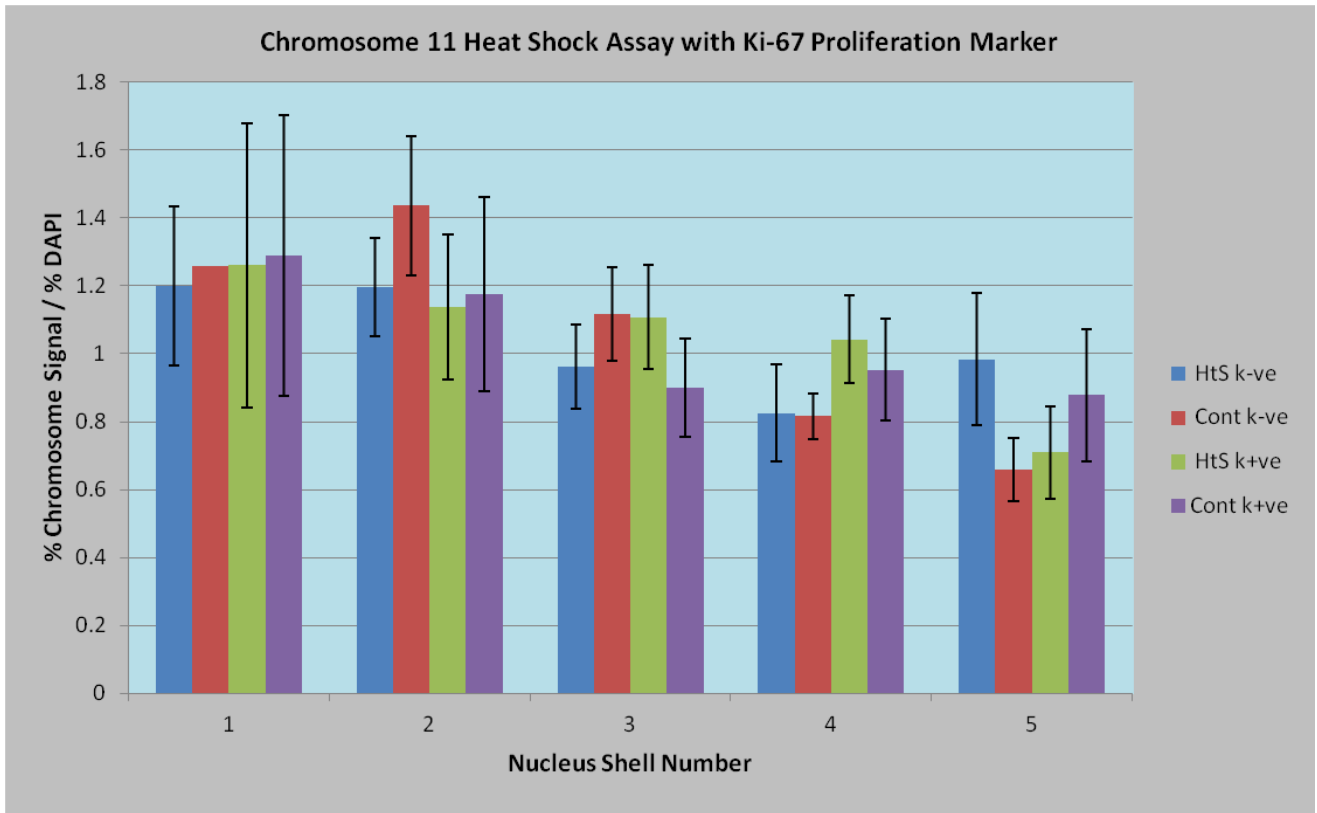
Figure 4.14. Results of the heat shock assay (42°C for 1 hour) for chromosome positioning with Ki-67 proliferation marker. Shell number 1 is most peripheral and shell number 5 is most interior. The graph and statistical analysis show no significant difference in the positions of chromosome 11 in response to heat shock when the proliferating and non-proliferating cells are compared, before and after the heat shock stimulus for 1 hour at 42°C. This indicates a lack of chromosome 11 relocation in response to this heat shock. The graph also shows that the nuclear position of chromosome 11 is mainly at a peripheral location. n = 42 for control Ki-67 –ve, n = 21 for heat shock Ki-67 –ve, n = 15 for heat shock Ki-67 +ve, n = 18 for control Ki-67 +ve. Error bars show SEM. See tables 4.16-4.25 for statistical analysis and calculation.

Statistical Analysis:
Initial heat shock assay with chromosome 11

Heat shock Ki-67 -ve compared with heat shock Ki-67 +ve for each nucleus shell

Table 4.16. HtS = heat shock.

Nucleus Shell 1	
P value and statistical significance: The two-tailed P value equals **0.8949** This difference is **not statistically significant**.	
Intermediate values used in calculations: t = 0.1331 df = 34 standard error of difference = 0.448	

Group	One ch11 HtS k-	One ch11 HtS k+
Mean	1.200	1.260
SD	1.071	1.622
SEM	0.233	0.418
N	21	15

Table 4.17. HtS = heat shock.

Nucleus Shell 2	
P value and statistical significance: The two-tailed P value equals **0.8201** This difference is **not statistically significant**.	
Intermediate values used in calculations: t = 0.2292 df = 34 standard error of difference = 0.249	

Group	Two ch11 HtS k-	Two ch11 HtS k+
Mean	1.195	1.138
SD	0.667	0.827
SEM	0.145	0.213
N	21	15

Table 4.18. HtS = heat shock.

Nucleus Shell 3		
P value and statistical significance: The two-tailed P value equals **0.4555** This difference is **<u>not statistically significant</u>**.		
Intermediate values used in calculations: t = 0.7548 df = 34 standard error of difference = 0.195		
Group	**Three ch11 HtS k-**	**Three ch11 HtS k+**
Mean	0.960	1.107
SD	0.566	0.591
SEM	0.123	0.152
N	21	15

Table 4.19. HtS = heat shock.

Nucleus Shell 4		
P value and statistical significance: The two-tailed P value equals **0.2874** This difference is **<u>not statistically significant</u>**.		
Intermediate values used in calculations: t = 1.0807 df = 34 standard error of difference = 0.201		
Group	**Four ch11 HtS k-**	**Four ch11 HtS k+**
Mean	0.825	1.042
SD	0.655	0.498
SEM	0.142	0.128
N	21	15

Table 4.20. HtS = heat shock.

Nucleus Shell 5		
P value and statistical significance: The two-tailed P value equals **0.2957** This difference is **not statistically significant**.		
Intermediate values used in calculations: t = 1.0622 df = 34 standard error of difference = 0.258		
Group	**Five ch11 HtS k-**	**Five ch11 HtS k+**
Mean	0.984	0.710
SD	0.891	0.527
SEM	0.194	0.136
N	21	15

Heat shock Ki-67 +ve compared with control Ki-67 +ve for each nucleus shell

Table 4.21. HtS = heat shock, Cont = not heat shocked.

Nucleus Shell 1		
P value and statistical significance:		
The two-tailed P value equals **0.9612**		
This difference is **not statistically significant**.		
Intermediate values used in calculations:		
t = 0.0490		
df = 31		
standard error of difference = 0.593		
Group	**One ch11 HtS k+**	**One ch11 Cont k+**
Mean	1.260	1.289
SD	1.622	1.754
SEM	0.418	0.413
N	15	18

Table 4.22. HtS = heat shock, Cont = not heat shocked.

Nucleus Shell 2		
P value and statistical significance:		
The two-tailed P value equals **0.9234**		
This difference is **not statistically significant.**		
Intermediate values used in calculations:		
t = 0.0970		
df = 31		
standard error of difference = 0.370		
Group	**Two ch11 HtS k+**	**Two ch11 Cont k+**
Mean	1.138	1.174
SD	0.827	1.214
SEM	0.213	0.286
N	15	18

Table 4.23. HtS = heat shock, Cont = not heat shocked.

Nucleus Shell 3		
P value and statistical significance: The two-tailed P value equals **0.3315** This difference is **_not statistically significant_**.		
Intermediate values used in calculations: t = 0.9866 df = 31 standard error of difference = 0.211		
Group	**Three ch11 HtS k+**	**Three ch11 Cont k+**
Mean	1.107	0.899
SD	0.591	0.615
SEM	0.152	0.145
N	15	18

Table 4.24. HtS = heat shock, Cont = not heat shocked.

Nucleus Shell 4		
P value and statistical significance: The two-tailed P value equals **0.6604** This difference is **_not statistically significant._**		
Intermediate values used in calculations: t = 0.4437 df = 31 standard error of difference = 0.202		
Group	**Four ch11 HtS k+**	**Four ch11 Cont k+**
Mean	1.042	0.953
SD	0.498	0.634
SEM	0.128	0.149
N	15	18

Table 4.25. HtS = heat shock, Cont = not heat shocked.

Nucleus Shell 5		
P value and statistical significance:		
The two-tailed P value equals **0.5007**		
This difference is **not statistically significant.**		
Intermediate values used in calculations:		
t = 0.6814		
df = 31		
standard error of difference = 0.246		
Group	**Five ch11 HtS k+**	**Five ch11 Cont k+**
Mean	0.710	0.878
SD	0.527	0.821
SEM	0.136	0.193
N	15	18

4.3.2 Chromosome 10 low serum (0.5% FCS) media assay (passage 19 NB1 cells) with anti-Ki-67 proliferation marker

In this work NB1 cells at passage 19 were used to study the effect of exposure to low serum conditions for 1 hour, by the low serum (0.5% FCS) media assay, on chromosome 10 positioning. In the initial low serum assays performed previously with chromosome 10, the Ki-67 proliferation marker was not used (section 4.3.1) therefore with the use of Ki-67 marker for this work it was possible to distinguish between proliferating and non-proliferating cells. This low serum media assay was performed with moderately younger cells (passage 19) compared to the work presented in section 4.3.1 for the chromosome 10 low serum assay, which was performed with cells at passage number 25. Although this difference in passage number is not very large, there may still be a sufficient distance in cell age between the passage numbers, to be relevant for a comparison. Representative images of the nuclei stained for chromosome 10 positions are shown in Figures 4.15 and 4.16. These images are examples of the digital data used by the computer erosion analysis to determine the positions of chromosome 10. According to the results of this work as shown in Figure 4.17, in proliferating cells exposed to low serum (0.5% FCS) media, chromosome 10 has a mostly intermediate-interior position (nucleus shells 3 and 4 peaking at 3) in the nucleus, as demonstrated by some of the images in Figure 4.16. In non-proliferating cells exposed to low serum (0.5% FCS) media chromosome 10 has a more peripheral position (nucleus shell 2) in the nucleus, as demonstrated by some of the images in Figure 4.15. According to the statistical analysis there are statistically significant differences in the positions of chromosome 10 in the nuclei of proliferating cells (Ki-67 +ve), exposed to low serum media when compared to chromosome 10 positions in the nuclei of non-proliferating cells (Ki-67 – ve), exposed to low serum (0.5% FCS) media. Specifically these differences are seen in nucleus shell 2 (P = 0.0494) and nucleus shell 4 (P = 0.0080). These differences may indicate chromosome 10 relocation.
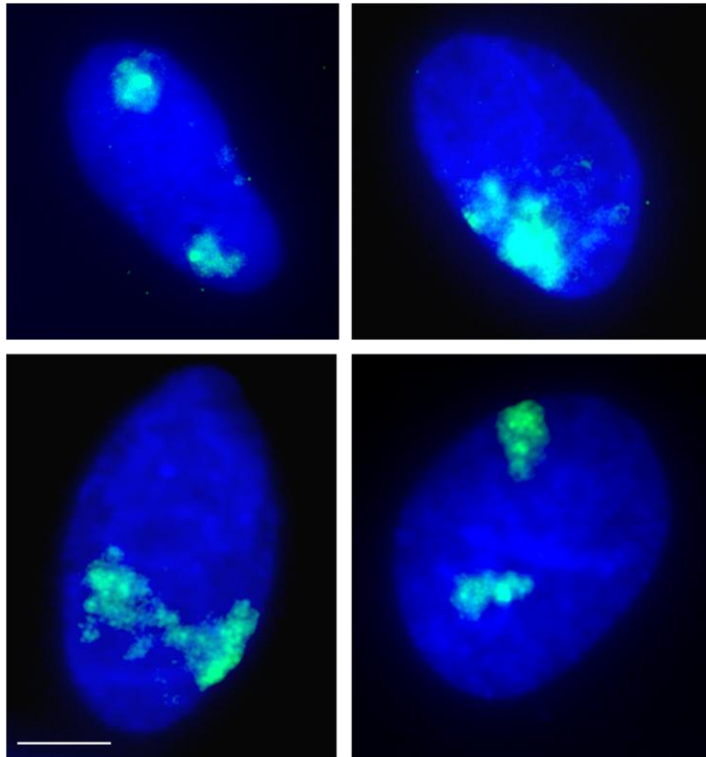
Figure 4.15. Representative images used for the computer erosion analysis, showing Ki-67 negative nuclei stained for chromosome 10 territories by 2D FISH. Scale bar = 10 μm.

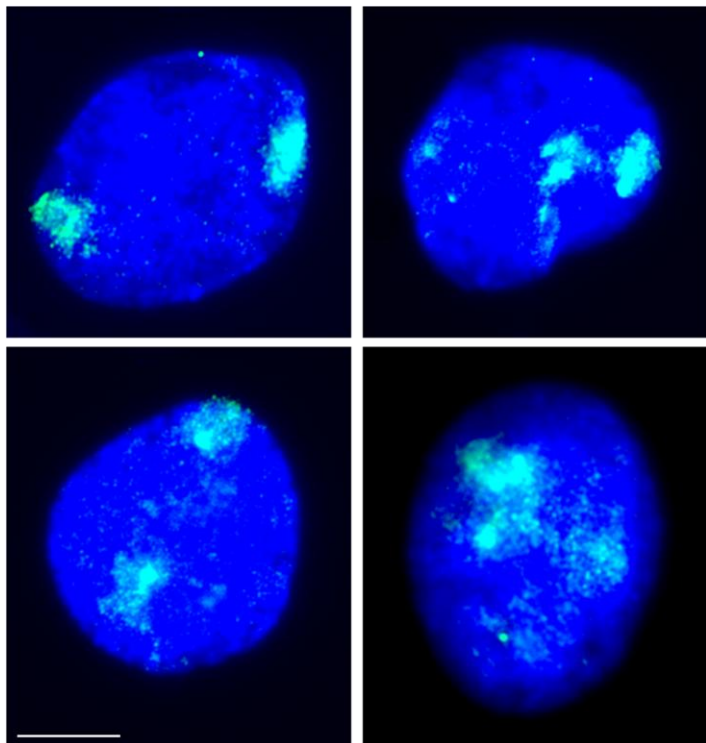**Figure 4.16.** Representative images used for the computer erosion analysis, showing Ki-67 positive nuclei stained for chromosome 10 territories by 2D FISH. Note that the Ki-67 signal has been removed in order to allow for the computer analysis of the images for chromosome territory determination. Scale bar = 10 μm.
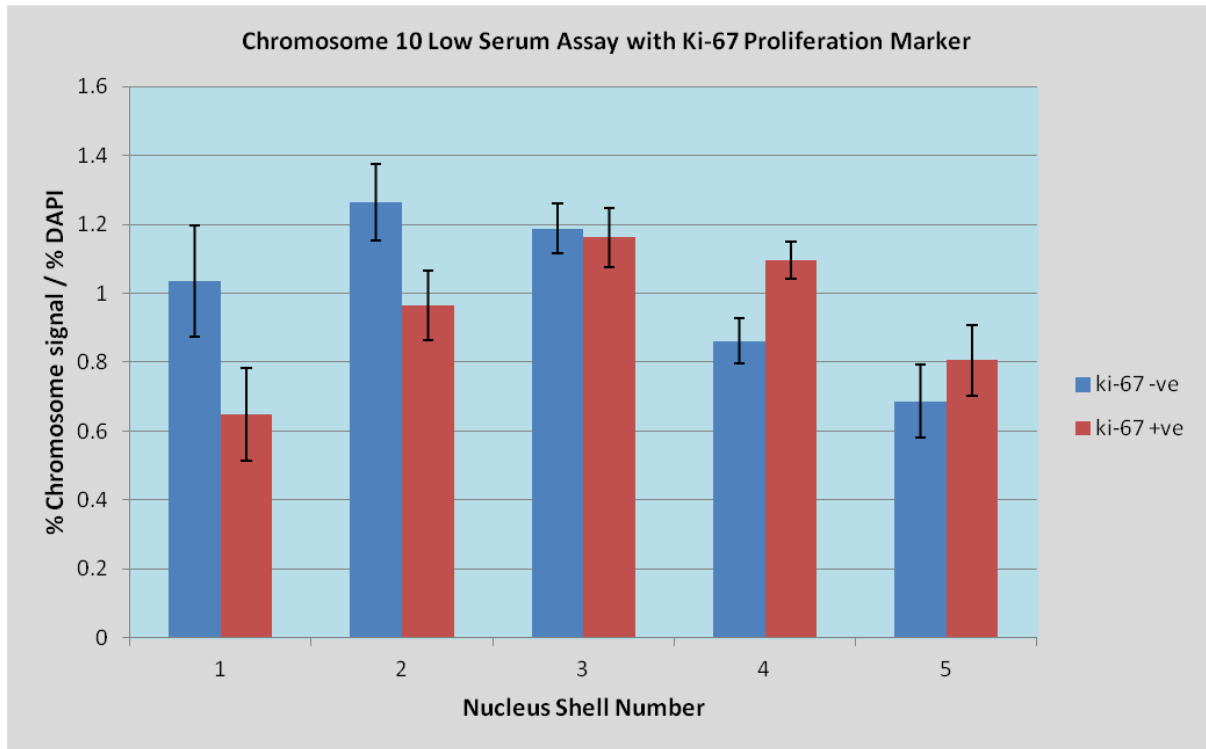
Figure 4.17. Results of the low serum (0.5% FCS) media assay for chromosome 10 positioning with Ki-67 proliferation marker. Shell number 1 is most peripheral and shell number 5 is most interior. These results show a statistically significant difference in shell 2 (**P = 0.0494**) for chromosome 10 position between proliferating and non-proliferating cells. The difference in shell 4 is also statistically significant (**P = 0.0080**). The graph shows that, following exposure to low serum conditions for 1 hour, chromosome 10 positions for the Ki-67 positive nuclei are mostly intermediate-interior and those for Ki-67 negative nuclei are more towards the periphery in comparison. n = 57 for Ki-67 –ve, n = 52 for Ki-67 +ve. Error bars show SEM. See tables 4.26-4.30 for statistical analysis and calculation.

Statistical analysis: chromosome 10 low serum assay with Ki-67; Ki-67 –ve compared with Ki67+ve for each nucleus shell

Table 4.26. LS = low serum exposed.

Nucleus Shell 1		
P value and statistical significance: The two-tailed P value equals **0.0701** This difference is **not statistically significant.**		
Intermediate values used in calculations: t = 1.8297 df = 107 standard error of difference = 0.213		
Group	**one ch10 LS k-**	**one ch10 LS k+**
Mean	1.036	0.648
SD	1.219	0.970
SEM	0.161	0.134
N	57	52

Table 4.27. LS = low serum exposed.

Nucleus Shell 2		
P value and statistical significance: The two-tailed P value equals **0.0494** This difference is **statistically significant**.		
Intermediate values used in calculations: t = 1.9880 df = 107 standard error of difference = 0.150		
Group	**Two ch10 LS k-**	**Two ch10 LS k+**
Mean	1.263	0.964
SD	0.837	0.722
SEM	0.110	0.100
N	57	52

Table 4.28. LS = low serum exposed.

Nucleus Shell 3		
P value and statistical significance:		
The two-tailed P value equals **0.8104**		
This difference is **not statistically significant**.		
Intermediate values used in calculations:		
t = 0.2405		
df = 107		
standard error of difference = 0.111		
Group	**Three ch10 LS k-**	**Three ch10 LS k+**
Mean	1.188	1.161
SD	0.536	0.622
SEM	0.071	0.086
N	57	52

Table 4.29. LS = low serum exposed.

Nucleus Shell 4		
P value and statistical significance:		
The two-tailed P value equals **0.0080**		
This difference is **statistically significant**.		
Intermediate values used in calculations:		
t = 2.7038		
df = 107		
standard error of difference = 0.086		
Group	**Four ch10 LS k-**	**Four ch10 LS k+**
Mean	0.861	1.095
SD	0.502	0.385
SEM	0.066	0.053
N	57	52

Table 4.30. LS = low serum exposed.

Nucleus Shell 5		
P value and statistical significance:		
The two-tailed P value equals **0.4215**		
This difference is **not statistically significant**.		
Intermediate values used in calculations:		
t = 0.8069		
df = 107		
standard error of difference = 0.148		
Group	**Five ch10 LS k-**	**Five ch10 LS k+**
Mean	0.686	0.805
SD	0.797	0.741
SEM	0.105	0.102
N	57	52

4.3.3 Novel chromosome relocation assay: Chromosome 11 heat shock assay with anti-Ki-67 proliferation marker using passage 12 NB1 cells

In this major work, large datasets were used to thoroughly investigate the response of chromosome 11 to a heat shock stimulus at 42°C for 1 hour, to determine the nuclear positions of chromosome 11, before and after heat shock, in the nuclei of proliferating and non-proliferating cells, using young NB1 cells at passage 12. Ki-67 was used as a marker of proliferation. By a thorough comparison of the obtained data for both the heat shocked cells and control cells, proliferating and non-proliferating for both (Figures 4.22-4.25), the aim was to provide robust results for this investigation. Chromosome 11 is known to contain the HSP73 heat shock protein gene (Tavaria et al. 1995; Tavaria et al. 1996) and is therefore of particular relevance for performing heat shock assays. Representative images of the nuclei stained for chromosome 11 positions for the four datasets generated are shown in Figures 4.18-4.21. These images help to corroborate the data in the graphs. The representative images are examples of the digital data used by the computer erosion analysis to determine the positions of chromosome 11. The analyses of the data are shown in graphs and associated statistical calculations in the following pages. The graph in Figure 4.22 which is one of the key presentations of the data, shows a difference in the nuclear locations of chromosome 11 between control proliferating and heat shocked proliferating cells. Importantly, this graph indicates chromosome relocation from nucleus shell 2 to 4 after heat shock. Another key presentation of the data is the graph in Figure 4.23 which compares the nuclear locations of chromosome 11 between control non-proliferating cells and heat shocked non-proliferating cells. This clearly and importantly shows that in non-proliferating cells, heat shock has not affected chromosome 11 position, suggesting a lack of relocation in non-proliferating cells. The graphs in Figures 4.24 and 4.25 show a different comparison of the data, which also confirm these findings. This work has established a chromosome relocation assay based on the heat shock stimulus using chromosome 11. In addition to establishing an assay for chromosome relocation, this work has demonstrated a novel chromosome relocation in response to heat shock, in a robust manner for chromosome 11.
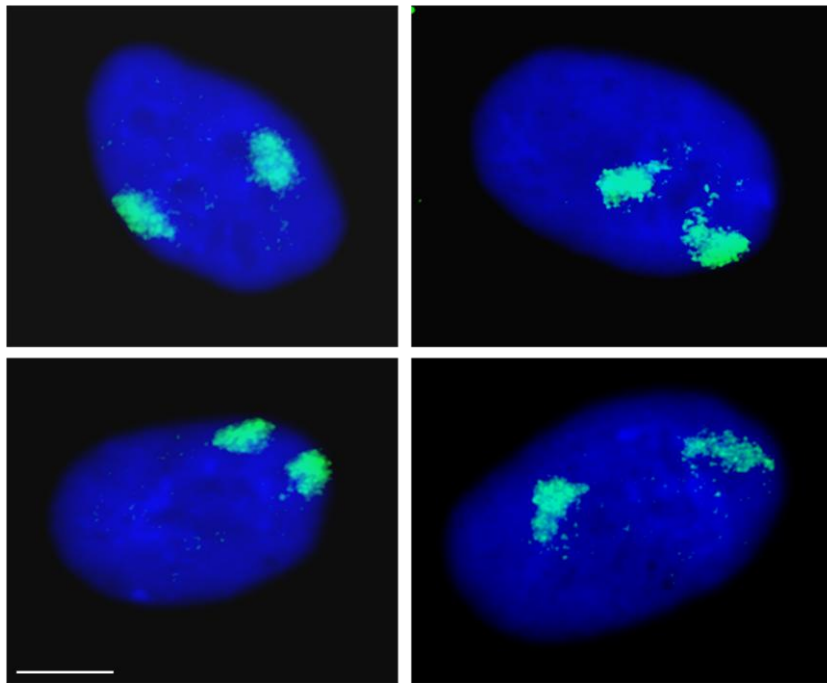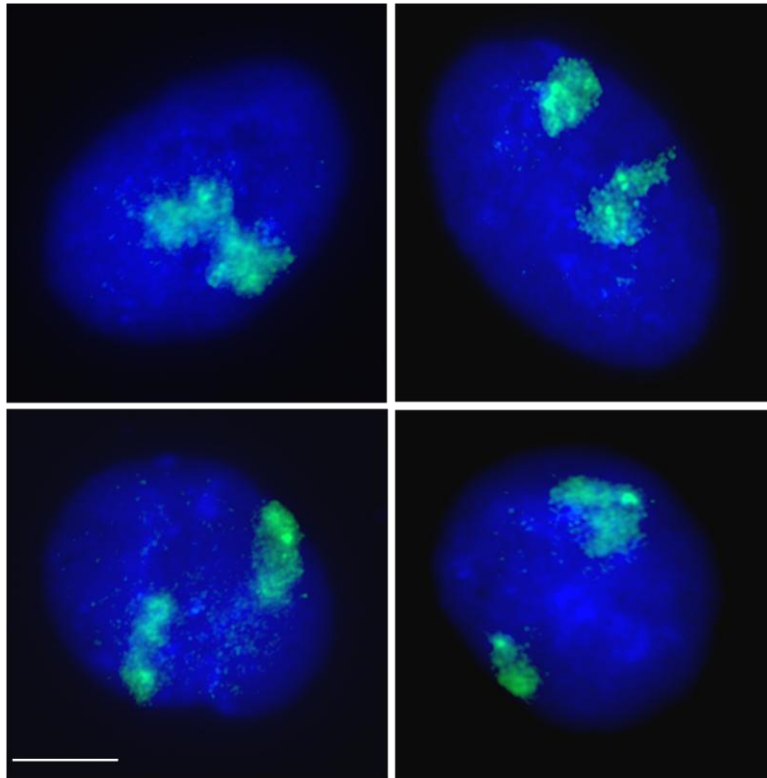
Figure 4.18. Representative images used for the computer erosion analysis, showing control Ki-67 negative nuclei stained for chromosome 11 territories by 2D FISH. Scale bar = 10 µm.
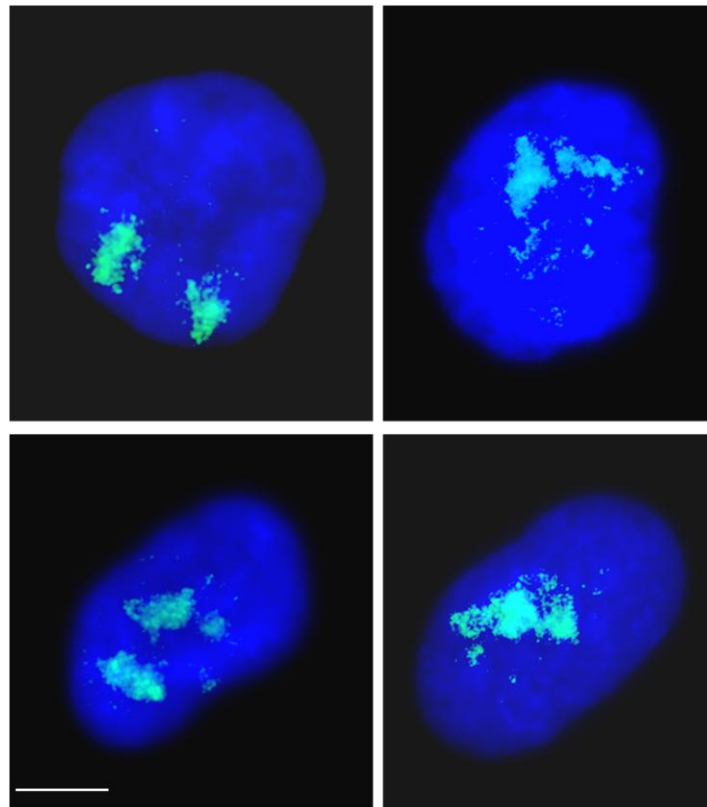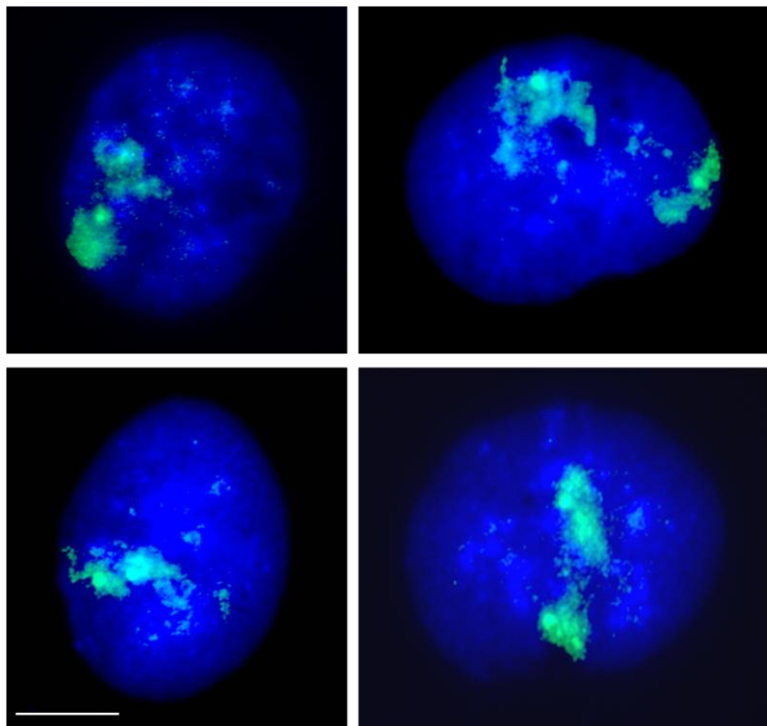

Figure 4.19. Representative images used for the computer erosion analysis, showing control Ki-67 positive nuclei stained for chromosome 11 territories by 2D FISH. Note that the Ki-67 signal has been removed in order to allow for the computer analysis of the images for chromosome territory determination. Scale bar = 10 µm.
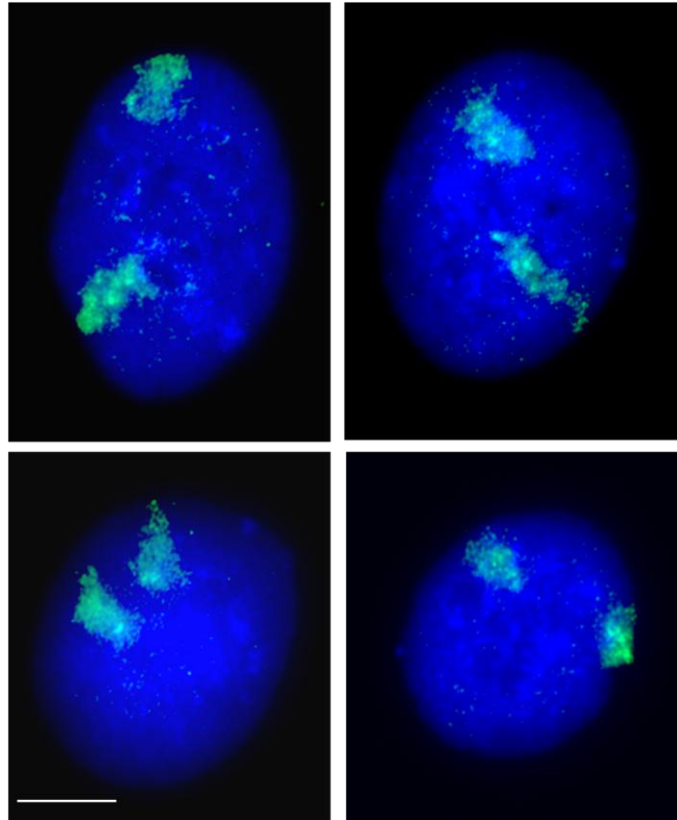
Figure 4.20. Representative images used for the computer erosion analysis, showing heat shocked Ki-67 negative nuclei stained for chromosome 11 territories by 2D FISH. Scale bar = 10 µm.
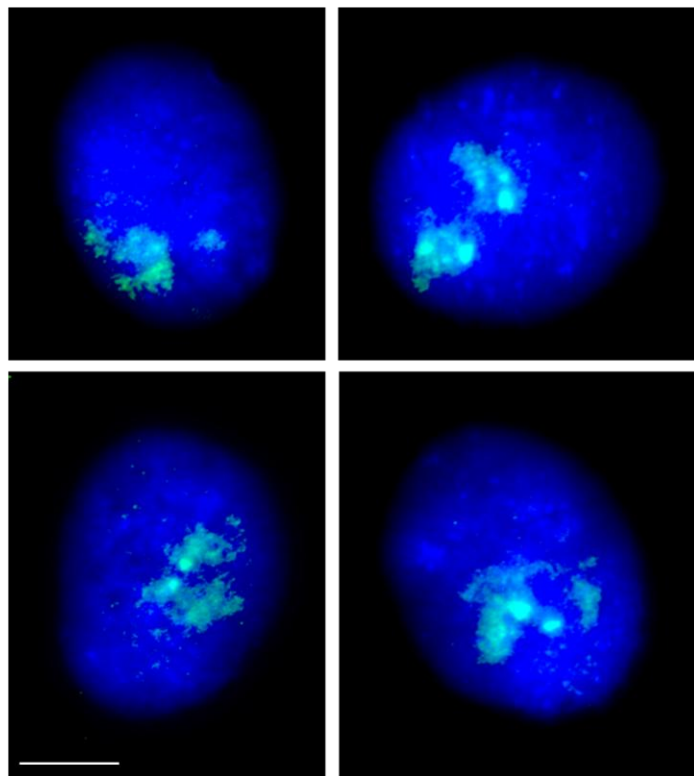
Figure 4.21. Representative images used for the computer erosion analysis, showing heat shocked Ki-67 positive nuclei stained for chromosome 11 territories by 2D FISH. Note that the Ki-67 signal has been removed in order to allow for the computer analysis of the images for chromosome territory determination. Scale bar = 10 µm.
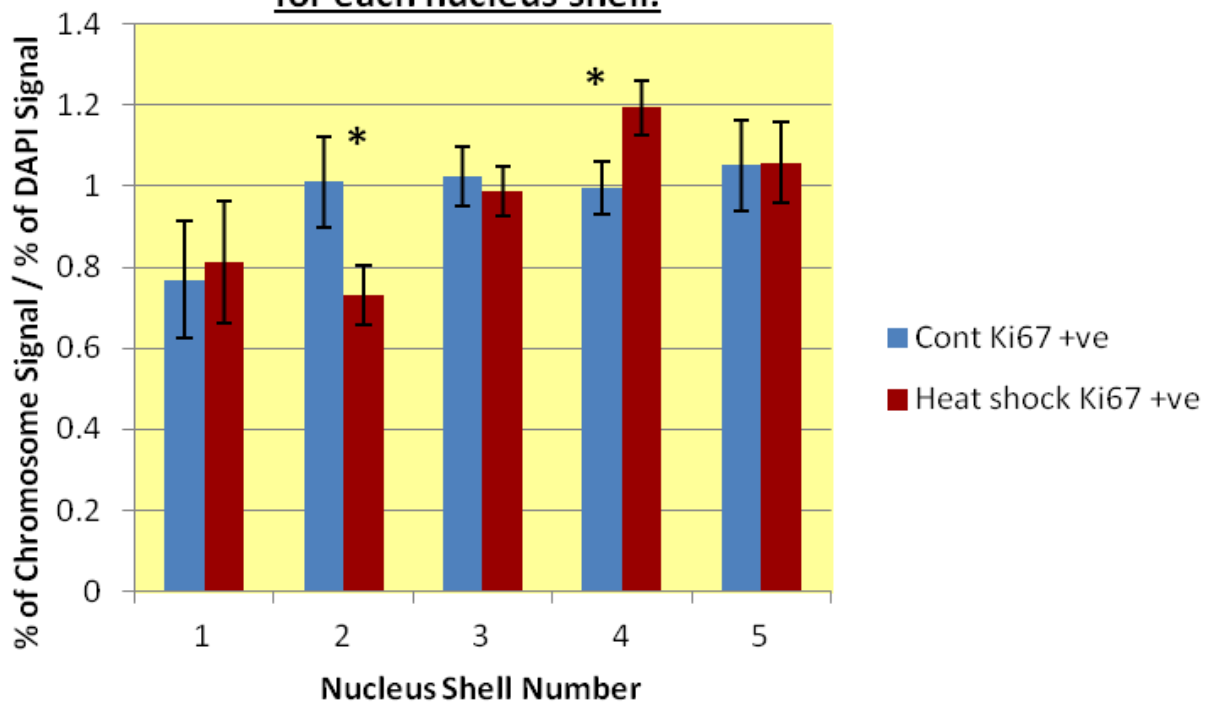
Figure 4.22. Results of heat shock assay (42°C for 1 hour) for chromosome positioning with Ki-67 proliferation marker. Nucleus shell number 1 is most peripheral location and nucleus shell number 5 is most interior location. This graph shows a difference in the nuclear locations of chromosome 11 between control proliferating and heat shocked proliferating cells. Importantly, this graph indicates chromosome relocation from nucleus shell 2 to 4 after heat shock. The differences between control proliferating cells, and heat shocked proliferating cells, in nucleus shell 2 (**P = 0.0317**) and nucleus shell 4 (**P = 0.0385**) are statistically significant. Error bars show SEM. See tables 4.31-4.35 for statistical analysis and calculation.

Statistical analysis: major heat shock assay with chromosome 11

Control Ki-67 +ve compared with heat shock Ki-67 +ve for each nucleus shell

Table 4.31. HeatS = heat shock, Cont = not heat shocked.

Nucleus Shell 1		
P value and statistical significance:		
The two-tailed P value equals **0.8368**		
This difference is **not statistically significant**.		
Intermediate values used in calculations:		
t = 0.2064		
df = 119		
standard error of difference = 0.214		
Group	**One Cont Ki-67 +ve**	**One HeatS ki-67 +ve**
Mean	0.768	0.812
SD	1.064	1.247
SEM	0.144	0.152
N	54	67

Table 4.32. HeatS = heat shock, Cont = not heat shocked.

Nucleus Shell 2		
P value and statistical significance:		
The two-tailed P value equals **0.0317**		
This difference is **statistically significant.**		
Intermediate values used in calculations:		
t = 2.1734		
df = 119		
standard error of difference = 0.129		
Group	**Two Cont Ki-67 +ve**	**Two HeatS Ki-67 +ve**
Mean	1.010	0.730
SD	0.819	0.596
SEM	0.111	0.072
N	54	67

Table 4.33. HeatS = heat shock, Cont = not heat shocked.

Nucleus Shell 3		
P value and statistical significance:		
The two-tailed P value equals **0.6978**		
This difference is **not statistically significant.**		
Intermediate values used in calculations:		
t = 0.3893		
df = 119		
standard error of difference = 0.095		
Group	**Three Cont Ki-67 +ve**	**Three HeatS Ki-67 +ve**
Mean	1.023	0.986
SD	0.539	0.504
SEM	0.073	0.061
N	54	67

Table 4.34. HeatS = heat shock, Cont = not heat shocked.

Nucleus Shell 4		
P value and statistical significance:		
The two-tailed P value equals **0.0385**		
This difference is **statistically significant.**		
Intermediate values used in calculations:		
t = 2.0927		
df = 119		
standard error of difference = 0.095		
Group	**Four Cont Ki-67 +ve**	**Four HeatS Ki-67 +ve**
Mean	0.995	1.194
SD	0.472	0.552
SEM	0.064	0.067
N	54	67

Table 4.35. HeatS = heat shock, Cont = not heat shocked.

Nucleus Shell 5		
P value and statistical significance:		
The two-tailed P value equals **0.9644**		
This difference is **not statistically significant.**		
Intermediate values used in calculations:		
t = 0.0448		
df = 119		
standard error of difference = 0.150		
Group	**Five Cont Ki-67 +ve**	**Five HeatS Ki-67 +ve**
Mean	1.051	1.058
SD	0.815	0.819
SEM	0.110	0.100
N	54	67
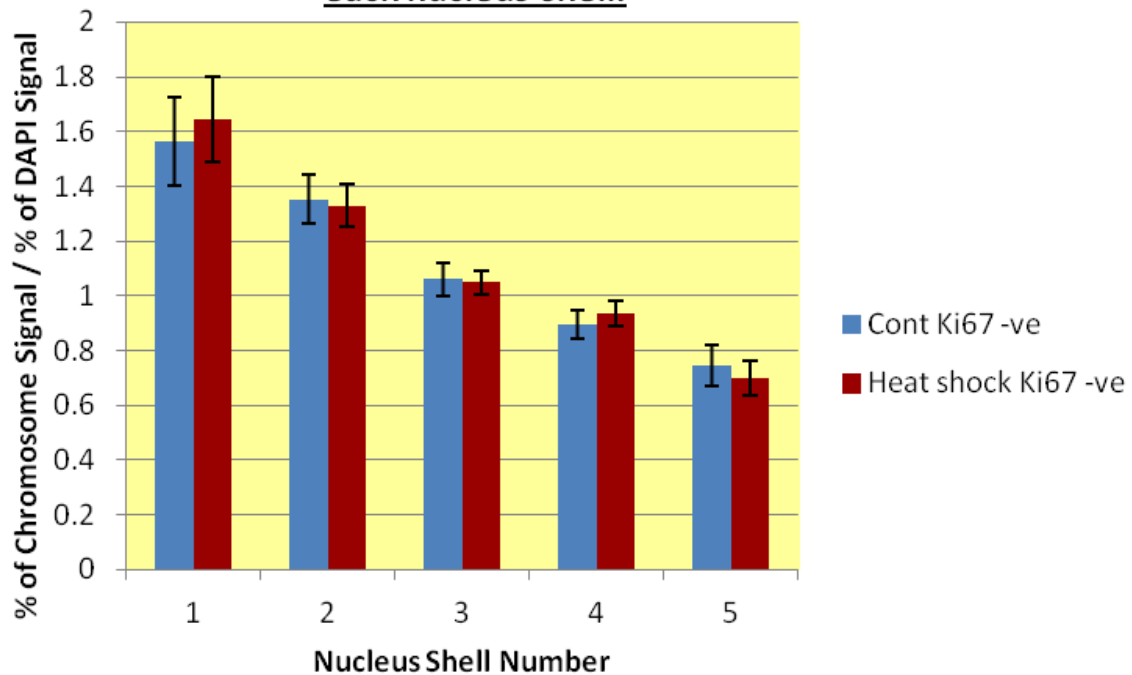
Figure 4.23. Results of heat shock assay (42°C for 1 hour) for chromosome positioning with Ki-67 proliferation marker. Nucleus shell number 1 is most peripheral location and nucleus shell number 5 is most interior location. This graph compares the nuclear locations of chromosome 11 between control non-proliferating cells and heat shocked non-proliferating cells, and shows that there is no statistically significant difference in the nuclear locations of chromosome 11. Importantly, this shows that in non-proliferating cells, heat shock has not affected chromosome position, suggesting a lack of relocation. Error bars show SEM. See tables 4.36-4.40 for statistical analysis and calculation.

Control Ki-67 –ve compared with heat shock Ki-67 –ve for each nucleus shell

Table 4.36. HeatS = heat shock, Cont = not heat shocked.

Nucleus Shell 1		
P value and statistical significance:		
The two-tailed P value equals **0.7272**		
This difference is **not statistically significant.**		
Intermediate values used in calculations:		
t = 0.3492		
df = 226		
standard error of difference = 0.228		
Group	**One Cont ki-67 -ve**	**One HeatS Ki-67 -ve**
Mean	1.562	1.642
SD	1.604	1.769
SEM	0.162	0.155
N	98	130

Table 4.37. HeatS = heat shock, Cont = not heat shocked.

Nucleus Shell 2		
P value and statistical significance:		
The two-tailed P value equals **0.8468**		
This difference is **not statistically significant**.		
Intermediate values used in calculations:		
t = 0.1934		
df = 226		
standard error of difference = 0.119		
Group	**Two Cont Ki-67 -ve**	**Two HeatS Ki-67 -ve**
Mean	1.352	1.329
SD	0.888	0.889
SEM	0.089	0.078
N	98	130

Table 4.38. HeatS = heat shock, Cont = not heat shocked.

Nucleus Shell 3		
P value and statistical significance:		
The two-tailed P value equals **0.8770**		
This difference is **not statistically significant**.		
Intermediate values used in calculations:		
t = 0.1550		
df = 226		
standard error of difference = 0.071		
Group	**Three Cont Ki-67 -ve**	**Three HeatS Ki-67 -ve**
Mean	1.060	1.049
SD	0.580	0.493
SEM	0.058	0.043
N	98	130

Table 4.39. HeatS = heat shock, Cont = not heat shocked.

Nucleus Shell 4		
P value and statistical significance:		
The two-tailed P value equals **0.5772**		
This difference is **not statistically significant**.		
Intermediate values used in calculations:		
t = 0.5583		
df = 226		
standard error of difference = 0.073		
Group	**Four Cont Ki-67 -ve**	**Four HeatS Ki-67 -ve**
Mean	0.894	0.934
SD	0.531	0.551
SEM	0.053	0.048
N	98	130

Table 4.40. HeatS = heat shock, Cont = not heat shocked.

Nucleus Shell 5		
P value and statistical significance: The two-tailed P value equals **0.6282** This difference is **not statistically significant**.		
Intermediate values used in calculations: t = 0.4850 df = 226 standard error of difference = 0.096		
Group	**Five Cont Ki-67 -ve**	**Five HeatS Ki-67 -ve**
Mean	0.746	0.699
SD	0.727	0.710
SEM	0.073	0.062
N	98	130
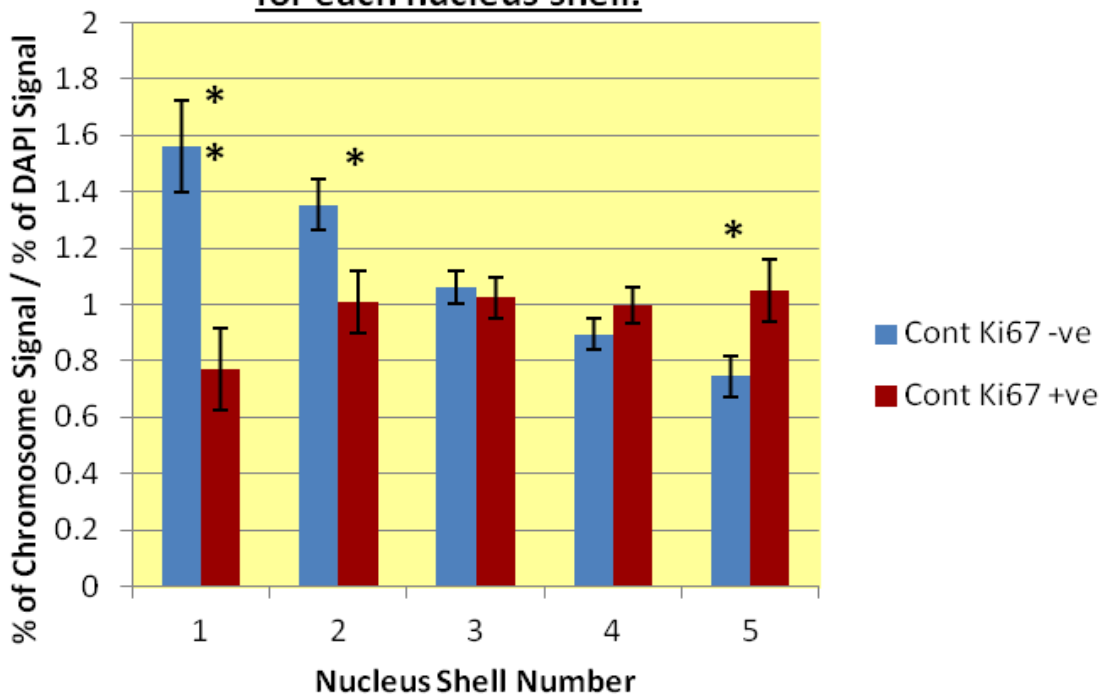
Figure 4.24. Results of heat shock assay (control) for chromosome positioning with Ki-67 proliferation marker. Nucleus shell number 1 is most peripheral location and nucleus shell number 5 is most interior location. This graph shows a difference in the nuclear locations of chromosome 11 between control non-proliferating cells and control proliferating cells. Importantly, this graph shows that chromosome 11 occupies a different nuclear location in non-proliferating cells (more peripheral) compared with proliferating cells (intermediate-interior). The differences between proliferating and non-proliferating cells in nucleus shells 1 (**P = 0.0014**), 2 (**P = 0.0207**) and 5 (**P = 0.0190**) are statistically significant. Error bars show SEM. See tables 4.41-4.45 for statistical analysis and calculation.

Control Ki-67 –ve compared with control Ki-67 +ve for each nucleus shell

Table 4.41. Cont = not heat shocked.

Nucleus shell 1		
P value and statistical significance: The two-tailed P value equals **0.0014** This difference is **statistically significant**.		
Intermediate values used in calculations: t = 3.2605 df = 150 standard error of difference = 0.244		
Group	**One Cont Ki-67 -ve**	**One Cont Ki-67 +ve**
Mean	1.562	0.768
SD	1.604	1.064
SEM	0.162	0.144
N	98	54

Table 4.42. Cont = not heat shocked.

Nucleus Shell 2		
P value and statistical significance: The two-tailed P value equals **0.0207** This difference is **statistically significant.**		
Intermediate values used in calculations: t = 2.3374 df = 150 standard error of difference = 0.147		
Group	**Two Cont Ki-67 -ve**	**Two Cont Ki-67 +ve**
Mean	1.352	1.010
SD	0.888	0.819
SEM	0.089	0.111
N	98	54

Table 4.43. Cont = not heat shocked.

Nucleus Shell 3		
P value and statistical significance:		
The two-tailed P value equals **0.7027**		
This difference is **not statistically significant**.		
Intermediate values used in calculations:		
t = 0.3823		
df = 150		
standard error of difference = 0.096		
Group	**Three Cont Ki-67 -ve**	**Three Cont Ki-67 +ve**
Mean	1.060	1.023
SD	0.580	0.539
SEM	0.058	0.073
N	98	54

Table 4.44. Cont = not heat shocked.

Nucleus shell 4		
P value and statistical significance:		
The two-tailed P value equals **0.2436**		
This difference is **not statistically significant**.		
Intermediate values used in calculations:		
t = 1.1706		
df = 150		
standard error of difference = 0.087		
Group	**Four Cont Ki-67 -ve**	**Four cont Ki-67 +ve**
Mean	0.894	0.995
SD	0.531	0.472
SEM	0.053	0.064
N	98	54

Table 4.45. Cont = not heat shocked.

Nucleus Shell 5		
P value and statistical significance:		
The two-tailed P value equals 0.0190		
This difference is **statistically significant**.		
Intermediate values used in calculations:		
t = 2.3719		
df = 150		
standard error of difference = 0.129		
Group	**Five Cont Ki-67 -ve**	**Five Cont Ki-67 +ve**
Mean	0.746	1.051
SD	0.727	0.815
SEM	0.073	0.110
N	98	54

Heat Shock Ki-67 +ve compared with Heat Shock Ki-67 -ve for each nucleus shell.
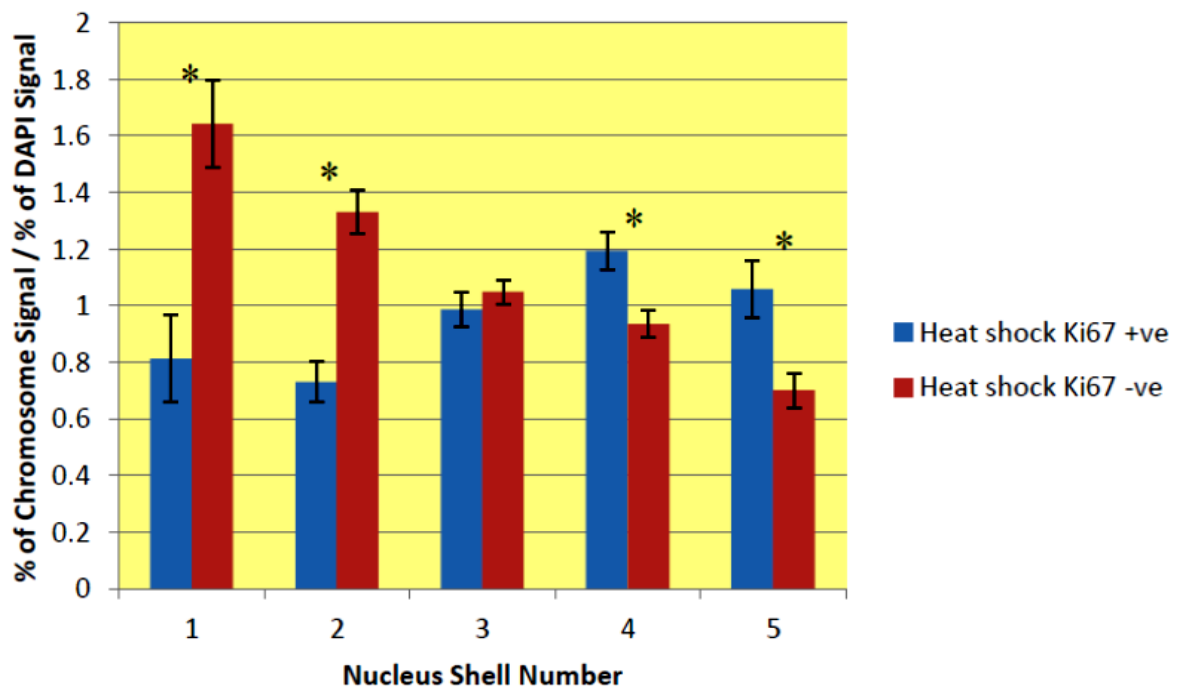
Figure 4.25. Results of heat shock assay (42°C for 1 hour) for chromosome positioning with Ki-67 proliferation marker. Nucleus shell number 1 is most peripheral location and nucleus shell number 5 is most interior location. This graph shows a difference in the nuclear locations of chromosome 11 between heat shocked proliferating and heat shocked non-proliferating cells. Importantly, this graph indicates chromosome relocation (from the periphery to interior) in proliferating cells after heat shock, and no relocation in non-proliferating cells. The differences between heat shocked proliferating cells and heat shocked non-proliferating cells in nucleus shells 1 (**P = 0.0008**), 2 (**P = 0.0001**), 4 (**P = 0.0021**) and 5 (**P = 0.0017**) are statistically significant. See tables 4.46-4.50 for statistical analysis and calculation.

Heat shock Ki-67 +ve compared with heat shock Ki-67 -ve for each nucleus shell.

Table 4.46. HeatS = heat shock.

Nucleus Shell 1		
P value and statistical significance: The two-tailed P value equals **0.0008** This difference is **statistically significant**.		
Intermediate values used in calculations: t = 3.4227 df = 195 standard error of difference = 0.242		
Group	**One HeatS Ki-67 +ve**	**One HeatS Ki-67 -ve**
Mean	0.812	1.642
SD	1.247	1.769
SEM	0.152	0.155
N	67	130

Table 4.47. HeatS = heat shock.

Nucleus shell 2		
P value and statistical significance: The two-tailed P value is less than **0.0001** This difference is **statistically significant**.		
Intermediate values used in calculations: t = 4.9665 df = 195 standard error of difference = 0.121		
Group	**Two HeatS Ki-67 +ve**	**Two HeatS Ki-67 -ve**
Mean	0.730	1.329
SD	0.596	0.889
SEM	0.072	0.078
N	67	130

Table 4.48. HeatS = heat shock.

Nucleus Shell 3		
P value and statistical significance:		
The two-tailed P value equals **0.4029**		
This difference is **not statistically significant**.		
Intermediate values used in calculations:		
t = 0.8383		
df = 195		
standard error of difference = 0.075		
Group	**Three HeatS Ki-67 +ve**	**Three HeatS Ki-67 -ve**
Mean	0.986	1.049
SD	0.504	0.493
SEM	0.061	0.043
N	67	130

Table 4.49. HeatS = heat shock.

Nucleus Shell 4		
P value and statistical significance:		
The two-tailed P value equals **0.0021**		
This difference is **statistically significant**.		
Intermediate values used in calculations:		
t = 3.1226		
df = 195		
standard error of difference = 0.083		
Group	**Four HeatS Ki-67 +ve**	**Four HeatS Ki-67 -ve**
Mean	1.194	0.934
SD	0.552	0.551
SEM	0.067	0.048
N	67	130

Table 4.50. HeatS = heat shock.

Nucleus Shell 5
P value and statistical significance:
The two-tailed P value equals **0.0017**
This difference is **statistically significant**.
Intermediate values used in calculations:
t = 3.1824
df = 195
standard error of difference = 0.113

Group	Five HeatS Ki-67 +ve	Five HeatS Ki-67 -ve
Mean	1.058	0.699
SD	0.819	0.710
SEM	0.100	0.062
N	67	130

4.4 DISCUSSION

The dynamics of various interphase chromosomes in response to two separate stimuli have been studied. These two stimuli in the form of biotic (low nutrient) and abiotic (heat shock) stress conditions have been studied with a comparative approach, investigating proliferating and non-proliferating cells. One objective was also partly directed towards developing an assay for chromosome movement, and to observe the nature of the response by the chromosomes studied, to the stress stimuli and therefore help to shed light on the natural processes that may occur at cell physiological level, when cells are challenged under stress related conditions. In addition, it was of interest to gain some insight into how this response may be related to the age of the cells. The relevance of comparisons between proliferating and non-proliferating cells in relation to the ability to respond to various stimuli is important for several reasons. One central aspect is that, it informs regarding the physiological effects of the ageing process at the cellular level, and this can be extrapolated to effects at the tissue and organismal levels (Mylonas and O'Loghlen 2022). Also, factoring in the age of the cells being compared in responses to stimuli, is important to help gain further insight into which specific processes are functionally compromised when cells age. An understanding of the specific processes affected in ageing cells can allow for the development of clinical strategies, to ameliorate the general health demise that may be associated with, and resulting from the ageing process for example. Though it is also important to note that such demise with age is also under the influence of other factors such as lifestyle choices (Rizzuto et al. 2012) and congenital tendencies (Daelman and Moons 2023), which may synergistically interact with the physiological factors of ageing, and may therefore render individuals more prone to the undesirable health outcomes with of the ageing process.

The results of this chapter, in addition to confirming that in non-proliferating cells chromosome 11 relocation has diminished functionality, and therefore this relocation is not observed (Mehta et al. 2021), possibly as a result of the loss of functionality of the molecular motor proteins involved (Mehta et al. 2010), has also suggested that when cells are old due to replicative accumulated effects, they may also have diminished ability to relocate chromosomes in response to stimuli. This was indirectly

evident from the comparison of the low serum media assay performed with NB1 cells at passage 25 compared with low serum media assay performed with cells at passage 19, where chromosome 10 relocation was found only with the passage 19 cells. Therefore it may be possible that at passages above 20 cells begin to display some age related deficiencies in function. Although the comparison between passage 19 and 25 cells is not a very robust approach, due to the small difference between these, it may lead the way to more thorough and better designed investigations in future, to shed light on this topic. Chromosome 15 at passage 20 also did not show chromosome relocation in response to the low serum media assay. Chromosome 11 in proliferating cells in response to heat shock, relocated with considerably young NB1 cells at passage 12, but with passage 20 NB1 cells chromosome 11 relocation in response to heat shock was not observed. The difference between passage 12 and passage 20 cells is more considerable and possibly adds more credence to this postulation, regarding the relationship between cell age as inferred by passage number, and chromosome relocation potential in response to stimuli. In order to confirm the possibility that old NB1 cells regardless of being in proliferation or non-proliferation state, as confirmed by the presence or absence of Ki-67 staining respectively, may start to show diminished chromosome mobility, further future experiments would need to be performed with larger datasets. This possible relationship may be explained by suggesting that older cells are unable to relocate due to reduced functionality of the relocation mechanism, which would involve molecular motor proteins. This is in keeping with a main focus of the line of inquiry in this project, that in non-proliferating cells the molecular motor proteins may have reduced function. This may possibly also be true in older cells as a separate factor affecting the ability of cells to respond to stimuli.

The low serum assay work in this chapter, with passage 19 cells, shows that in proliferating cells exposed to low serum media, chromosome 10 has a mostly intermediate position in the nucleus and this agrees with previous observations regarding chromosome 10 in proliferation (Mehta et al. 2010). In non-proliferating cells exposed to low serum media, chromosome 10 was found to have a more peripheral position in the nucleus, again in agreement with previous findings (Mehta et al 2010). In their work, Mehta et al. (2010) show that chromosome 10 relocates from an intermediate position to a peripheral position when induced to quiescence by

low serum media conditions. The authors also demonstrated that in normal proliferating cells, chromosome 10 is at an intermediate position in the nucleus. Interestingly, it was shown by Mehta et al. (2021) that chromosome 10 shows differing positions in senescent cells compared with quiescent cells, such that in senescent cells the position of chromosome 10 is at the interior of the nucleus compared with a peripheral position in quiescent cells. The lack of chromosome 15 relocation in response to the low serum media under the conditions performed in the current study, suggests that the chromosome 15 position and behaviour of proliferating and non-proliferating cells after exposure to low nutrient conditions are similar. It was found that the position of chromosome 15 is at the nuclear interior. This position is in agreement with previous findings of the position of chromosome 15 in quiescent cells (Mehta et al. 2010).

In the initial heat shock assay with chromosome 11, it was found that chromosome 11 position is mainly at the nuclear periphery, though also tending towards the margins of the intermediate position. This is somewhat comparable to previous findings (Meaburn et al. 2008; Mehta et al. 2010) where chromosome 11 was found to be located at an intermediate position in proliferating cells, and at a peripheral position in quiescent cells. The major finding in this chapter was the successful completion of a heat shock assay using NB1 passage 12 fibroblast cells, which has generated high quality and interesting results and has established a chromosome relocation assay based on the heat shock stimulus using chromosome 11. In addition to establishing an assay for chromosome relocation, this work has demonstrated a novel chromosome relocation in response to heat shock, in a robust manner using chromosome 11. Importantly, the results of this work also indicate that in non-proliferating cells, chromosome relocation does not occur after stimulus, in contrast to the situation with proliferating cells. This supports the main hypothesis of this project regarding the lack of interphase chromosome relocation in non-proliferating cells due to reduced functionality of molecular motors. The chromosome relocation found in this work occurs in the nuclei of proliferating cells only and is from the nuclear periphery to the interior in response to heat shock stimulus at 42°C for 1 hour.

Among the most important features of living things is the ability to respond to various biotic and abiotic stimuli, such that all organisms have sensory ability to gauge the conditions of the environment with which they interact (Kaas 1989; Oteiza and Baldwin 2021). This ability to respond to stimuli has evolved to allow organisms to survive and flourish in their natural habitat, and function at the organismal level as well as at the tissue, cellular and sub-cellular level. Just as an organism has sensory systems and mechanisms to interact with the conditions found in the ecosystem it inhabits, a cell has mechanisms to respond to the conditions it is exposed to. These mechanisms also involve cellular signalling cascades, ultimately leading to changes in gene expression, and a physiological effect to meet the biological requirements induced by the original stimulus. The different scales of response are not always exclusive in living systems, in that the stimuli/conditions at the organismal level are conveyed at the tissue and cellular level to elicit a response, which may in turn translate at the organismal level (Abouheif et al. 2014; Gilbert et al. 2015). Although studying such dynamics in vitro sheds light on such processes, the situation in vivo will be more complex. However, in vitro studies are a powerful tool to allow a reductionist approach to help unravel the complexities that exist in vivo.

Chapter 5: General Discussion

The cell nucleus and the molecular processes that occur in this highly complex structure, which are crucial to the cell and the organism as a whole, are without doubt among the most important and pivotal components of life in all eukaryotic organisms, both unicellular and multicellular. Importantly, the chromosomes contained in the nucleus in collaboration with the various nuclear substructures, have a most crucial role of orchestrating the complex gene expression profile of an organism, through gene regulatory networks in a highly accurate, efficient and dynamic manner for the duration of its lifespan, from fertilization to early development, morphogenesis and growth, all the way to reproduction and old age (Davidson and Levine 2008; Peng and Han 2018). The spatiotemporal and dynamic nature of genomic expression (Sato et al. 2020) allows for the genetic information contained within the chromosomes to be utilized by cells, and therefore the organism according to physiological needs, under various conditions. As living systems are in a constant state of sensing and responding to conditions they are exposed to, the ability to continue these dynamics efficiently is important throughout the life of the organism (Bowsher and Swain 2014).

The work in this thesis has taken the aspect of a rather broad approach, to address the exploration of chromosome dynamics, and a search for the possible associated proteins, in proliferating and non-proliferating cells. This exploration has involved both extensive laboratory work, and in silico analyses, investigating a fairly large number of possible candidate proteins, the roles of which in chromosome dynamics may be inferred and lead to further investigative work, to determine the possibility of involvement in the process of chromosome mobility. The novel demonstration that the myosin proteins studied in the work of this thesis, show distinct and significant differences in staining patterns when compared in proliferating and non-proliferating cells, is an important find. This compels further investigation and exploration in future work. The confirmation in this thesis, that chromosome mobility in non-proliferating

175

cells is functionally halted to a large extent as demonstrated by heat shock non-response, and furthermore, the establishment of a heat shock assay for chromosome mobility, together with the relocation of human chromosome 11 in response to a heat shock stimulus in primary fibroblast cells, are major finds and contributions. In addition to these, the results of this work may suggest that possibly in older cells at higher passage numbers, the chromosomes may have diminished ability for relocation in response to stimuli, though this postulation is not strongly confirmed in this work, and will require further investigation and may possibly lead to interesting finds. Another interesting and significant find is that MYO5B may possibly be involved in the process of splicing speckle mobility, due to the novel observation of unequivocal colocalisation, discovered in this work, and by extrapolation to previous findings by other labs that have demonstrated directed and active mobility in parts of splicing speckles (Zhang et al. 2016).

Studies on the dynamics of chromosomes and the molecular mechanisms involved in this process are inherently very complex and multifactorial. By exploring possible protein candidates that may be involved in this mechanism, more insight will be gained regarding the multifactorial nature of active chromosome mobility. The observation of chromosome dynamics in response to stimuli under various biotic and abiotic stress conditions, as well as the realisation of cellular states that halt such dynamics, is crucial to shedding light on understanding this aspect of genomic regulation, and how this regulatory mechanism can be controlled or altered both in disease conditions, and in cellular ageing. Clearly, the evolution of this regulatory mechanism of whole chromosome dynamics and directed mobility, allowing complex orchestration of large genome based gene expression profiles, would have been crucial to the functioning of the eukaryotes. The emergence and evolution of this regulatory process, in the early eukaryotes and allowing for the evolution of multicellularity was without doubt, among the most important and pivotal events in the history of life on Earth.

REFERENCES

Abercrombie M. (1970). Contact inhibition in tissue culture.
In Vitro. Sep-Oct;6(2):128-42.

Abouheif E, Favé MJ, Ibarrarán-Viniegra AS, Lesoway MP, Rafiqi AM, Rajakumar R. (2014). Eco-evo-devo: the time has come. *Adv Exp Med Biol*. 781:107-25.

Acosta JC, Banito A, Wuestefeld T, Georgilis A, Janich P, Morton JP, Athineos D, Kang TW, Lasitschka F, Andrulis M, Pascual G, Morris KJ, Khan S, Jin H, Dharmalingam G, Snijders AP, Carroll T, Capper D, Pritchard C, Inman GJ, Longerich T, Sansom OJ, Benitah SA, Zender L, Gil J. (2013). A complex secretory program orchestrated by the inflammasome controls paracrine senescence.
Nat Cell Biol. Aug;15(8):978-90.

Albiez H, Cremer M, Tiberi C, Vecchio L, Schermelleh L, Dittrich S, Küpper K, Joffe B, Thormeyer T, von Hase J, Yang S, Rohr K, Leonhardt H, Solovei I, Cremer C, Fakan S, Cremer T. (2006). Chromatin domains and the interchromatin compartment form structurally defined and functionally interacting nuclear networks*.
Chromosome Res. 14(7):707-33.

Allen TD, Cronshaw JM, Bagley S, Kiseleva E, Goldberg MW. (2000). The nuclear pore complex: mediator of translocation between nucleus and cytoplasm.
J Cell Sci. May;113 (Pt 10):1651-9.

Andrä K, Nikolic B, Stöcher M, Drenckhahn D, Wiche G. (1998). Not just scaffolding: plectin regulates actin dynamics in cultured cells. *Genes Dev*. Nov 1;12(21):3442-51

Aguilar V, Fajas L. (2010). Cycling through metabolism.
EMBO Mol Med. Sep;2(9):338-48.

Arican-Goktas HD. (2013). Parasitic Influences on the Host Genome Using the Molluscan Model Organism *Biomphalaria glabrata. PhD Thesis*.

Arican-Goktas HD, Ittiprasert W, Bridger JM, Knight M. (2014). Differential Spatial Repositioning of Activated Genes in Biomphalaria glabrata Snails Infected with Schistosoma mansoni. *PLoS Negl Trop Dis*. Sep 11;8(9):e3013.

Baker DJ, Wijshake T, Tchkonia T, LeBrasseur NK, Childs BG, van de Sluis B, Kirkland JL, van Deursen JM. (2011). Clearance of p16Ink4a-positive senescent cells delays ageing-associated disorders. *Nature*. Nov 2;479(7372):232-6.

Batters C, Veigel C. (2016). Mechanics and Activation of Unconventional Myosins.
Traffic. Aug;17(8):860-71.

Beck J, Horikawa I, Harris C. (2020). Cellular Senescence: Mechanisms, Morphology, and Mouse Models. *Vet Pathol*. Nov;57(6):747-757.

Beck M, Hurt E. (2017). The nuclear pore complex: understanding its function through structural insight. *Nat Rev Mol Cell Biol*. Feb;18(2):73-89.

Belin BJ, Lee T, Mullins RD. (2015). DNA damage induces nuclear actin filament assembly by Formin -2 and Spire-½ that promotes efficient DNA repair. [corrected]. *Elife.* Aug 19;4:e07735.

Belmont A. (2003). Dynamics of chromatin, proteins, and bodies within the cell nucleus. *Curr Opin Cell Biol.* Jun;15(3):304-10.

Bernstein M, Rosenbaum JL. (1994). Kinesin-like proteins in the flagella of Chlamydomonas. *Trends Cell Biol.* Jul;4(7):236-40.

Bitto A, Sell C, Crowe E, Lorenzini A, Malaguti M, Hrelia S, Torres C. (2010). Stress-induced senescence in human and rodent astrocytes. *Exp Cell Res.* Oct 15;316(17): 2961-8.

Blagosklonny MV. (2011). Cell cycle arrest is not senescence*. Aging (Albany NY).* Feb;3(2):94-101.

Bolzer A, Kreth G, Solovei I, Koehler D, Saracoglu K, Fauth C, Müller S, Eils R, Cremer C, Speicher MR, Cremer T. (2005). Three-Dimensional Maps of All Chromosomes in Human Male Fibroblast Nuclei and Prometaphase Rosettes. *PLoS Biol.* May 3;(5):e157.

Borsari B, Villegas-Mirón P, Pérez-Lluch S, Turpin I, Laayouni H, Segarra-Casas A, Bertranpetit J, Guigó R, Acosta S. (2021). Enhancers with tissue-specific activity are enriched in intronic regions. *Genome Res.* Aug;31(8):1325-1336.

Botchkarev VA, Gdula MR, Mardaryev AN, Sharov AA, Fessing MY. (2012). Epigenetic regulation of gene expression in keratinocytes. *J Invest Dermatol.* 132(11):2505-21.

Bowsher CG, Swain PS. (2014). Environmental sensing, information transfer, and cellular decision-making. *Curr Opin Biotechnol.* Aug;28:149-55.

Boyle S, Gilchrist S, Bridger JM, Mahy NL, Ellis JA, Bickmore WA. (2001). The spatial organization of human chromosomes within the nuclei of normal and emerin-mutant cells. *Hum Mol Genet.* Feb 1;10(3):211-9.

Bridger JM, Arican-Gotkas HD, Foster HA, Godwin LS, Harvey A, Kill IR, Knight M, Mehta IS, Ahmed MH. (2014). The non-random repositioning of whole chromosomes and individual gene loci in interphase nuclei and its relevance in disease, infection, aging, and cancer. *Adv Exp Med Biol.*773:263-79.

Bridger JM. (2011). Chromobility: the rapid movement of chromosomes in interphase nuclei. *Biochem Soc Trans.* Dec;39(6):1747-51.

Bridger JM, Boyle S, Kill IR, Bickmore WA. (2000). Re-modelling of nuclear architecture in quiescent and senescent human fibroblasts. *Curr Biol.* Feb 10;10(3):149-52.

Bridger JM, Herrmann H, Münkel C, Lichter P. (1998). Identification of an interchromosomal compartment by polymerization of nuclear-targeted vimentin. *J Cell Sci.* May;111 (Pt 9):1241-53.

Bridger JM, Kalla C, Wodrich H, Weitz S, King JA, Khazaie K, Kräusslich HG, Lichter P. (2005). Nuclear RNAs confined to a reticular compartment between chromosome territories. *Exp Cell Res.* Jan 15;302(2):180-93.

Bridger JM, Kill IR. (2004). Aging of Hutchinson-Gilford progeria syndrome fibroblasts is characterised by hyperproliferation and increased apoptosis. *Exp Gerontol.* May;39(5):717-24.

Bridger JM, Kill IR, Lichter P. (1998). Association of pKi-67 with satellite DNA of the human genome in early G1 cells. *Chromosome Res.* Jan;6(1):13-24.

Cai L, Tu BP. (2012). Driving the cell cycle through metabolism. *Annu Rev Cell Dev Biol.* 28:59-87.

Carmo-Fonseca M, Platani M, Swedlow JR. (2002). Macromolecular mobility inside the cell nucleus. *Trends Cell Biol.*12(11):491-5.

Carragher BO, Cheng N, Wang ZY, Korn ED, Reilein A, Belnap DM, Hammer JA 3rd, Steven AC. (1998). Structural invariance of constitutively active and inactive mutants of acanthamoeba myosin IC bound to F-actin in the rigor and ADP-bound states. *Proc Natl Acad Sci U S A.* Dec 22;95(26):15206-11.

Cameron RS, Liu C, Pihkala JP. (2013). Myosin 16 levels fluctuate during the cell cycle and are downregulated in response to DNA replication stress. *Cytoskeleton* (Hoboken). Jun;70(6):328-48.

Chang FT, McGhie JD, Chan FL, Tang MC, Anderson MA, Mann JR, Andy Choo KH, Wong LH. (2013). PML bodies provide an important platform for the maintenance of telomeric chromatin integrity in embryonic stem cells. *Nucleic Acids Res.* Apr;41(8):4447-58.

Chantler PD, Wylie SR, Wheeler-Jones CP, McGonnell IM. (2010). Conventional myosins - unconventional functions. *Biophys Rev.* May;2(2):67-82.

Ching RW, Dellaire G, Eskiw CH, Bazett-Jones DP. (2005). PML bodies: a meeting place for genomic loci? *J Cell Sci.* Mar 1;118(Pt 5):847-54.

Chuang CH, Carpenter AE, Fuchsova B, Johnson T, de Lanerolle P and Belmont AS. (2006). Long-range directional movement of an interphase chromosome site. *Curr Biol.* 16, 825–831.

Collado M, Serrano M. (2010). Senescence in tumours: evidence from mice and humans. *Nat Rev Cancer.* Jan;10(1):51-7.

Coller HA, Sang L, Roberts JM. (2006). A new description of cellular quiescence. *PLoS Biol.* Mar;4(3):e83.

Cook PR. (1999). The organization of replication and transcription.
Science. Jun 11;284(5421):1790-5.

Cook AW, Gough RE, Toseland CP. (2020). Nuclear myosins - roles for molecular transporters and anchors. *J Cell Sci*. Jun 4;133(11):jcs242420.

Cremer M, Küpper K, Wagler B, Wizelman L, von Hase J, Weiland Y, Kreja L, Diebold J, Speicher MR, Cremer T. (2003). Inheritance of gene density-related higher order chromatin arrangements in normal and tumor cell nuclei.
J Cell Biol. Sep 1;162(5):809-20.

Cremer T, Cremer C. (2001). Chromosome territories, nuclear architecture and gene regulation in mammalian cells. *Nat Rev Genet*. Apr;2(4):292-301.

Cremer T, Cremer M. (2010). Chromosome Territories.
Cold Spring Harb Perspect Biol. Mar;2(3):a003889.

Cremer T, Cremer M, Dietzel S, Müller S, Solovei I, Fakan S. (2006). Chromosome territories--a functional nuclear landscape. *Curr Opin Cell Biol*. Jun;18(3):307-16.

Cremer T, Cremer M, Hübner B, Silahtaroglu A, Hendzel M, Lanctôt C, Strickfaden H, Cremer C. (2020). The Interchromatin Compartment Participates in the Structural and Functional Organization of the Cell Nucleus. *Bioessays*. Feb;42(2):e1900132.

Croft JA, Bridger JM, Boyle S, Perry P, Teague P, Bickmore WA. (1999). Differences in the localization and morphology of chromosomes in the human nucleus.
J Cell Biol. Jun 14;145(6):1119-31.

Daelman B, Moons P. (2023). Ageing and age-related issues in congenital heart disease: a new niche in treatment, care, and research.
Eur J Cardiovasc Nurs. May 25;22(4):e29-e31.

David A, Dolan BP, Hickman HD, Knowlton JJ, Clavarino G, Pierre P, Bennink JR, Yewdell JW. (2012). Nuclear translation visualized by ribosome-bound nascent chain puromycylation. *J Cell Biol*. Apr 2;197(1):45-57.

Davidson EH, Levine MS. (2008). Properties of developmental gene regulatory networks. *Proc Natl Acad Sci U S A*. Dec 23;105(51):20063-6.

Dechat T, Pfleghaar K, Sengupta K, Shimi T, Shumaker DK, Solimando L, Goldman RD. (2008). Nuclear lamins: major factors in the structural organization and function of the nucleus and chromatin. *Genes Dev*. Apr 1;22(7):832-53.

de Lanerolle P. (2012). Nuclear actin and myosins at a glance.
J Cell Sci. Nov 1;125(Pt 21):4945-9.

de Lanerolle P, Johnson T, Hofmann WA. (2005). Actin and myosin I in the nucleus: what next? *Nat Struct Mol Biol*. Sep;12(9):742-6.

de Lanerolle P, Serebryannyy L. (2011). Nuclear actin and myosins: life without filaments. *Nat Cell Biol*. Nov 2;13(11):1282-8.

De Magistris P, Antonin W. (2018). The Dynamic Nature of the Nuclear Envelope. *Curr Biol.* Apr 23;28(8):R487-R497.

Di Micco R, Krizhanovsky V, Baker D, d'Adda di Fagagna F. (2021). Cellular senescence in ageing: from mechanisms to therapeutic opportunities. *Nat Rev Mol Cell Biol.* Feb;22(2):75-95.

Dingová H, Fukalová J, Maninová M, Philimonenko VV, Hozák P. (2009). Ultrastructural localization of actin and actin-binding proteins in the nucleus. *Histochem Cell Biol.* Mar;131(3):425-34.

Dion V, Shimada K, Gasser SM. (2010). Actin-related proteins in the nucleus: life beyond chromatin remodelers. *Curr Opin Cell Biol.* Jun;22(3):383-91.

Dixon JR, Gorkin DU, Ren B. (2016). Chromatin Domains: The Unit of Chromosome Organization. *Mol Cell.* Jun 2;62(5):668-80.

Dultz E, Wojtynek M, Medalia O, Onischenko E. (2022). The Nuclear Pore Complex: Birth, Life, and Death of a Cellular Behemoth. *Cells.* Apr 25;11(9):1456.

Dundr M, Misteli T. (2001). Functional architecture in the cell nucleus. *Biochem J.* June 1;356(Pt 2):297-310.

Dundr M, Ospina JK, Sung MH, John S, Upender M, Ried T, Hager GL, Matera AG. (2007). Actin-dependent intranuclear repositioning of an active gene locus in vivo. *J Cell Biol.* Dec 17;179(6):1095-103.

Dzijak R, Yildirim S, Kahle M, Novák P, Hnilicová J, Venit T, Hozák P. (2012). Specific nuclear localizing sequence directs two myosin isoforms to the cell nucleus in calmodulin-sensitive manner. *PLoS One.* 7(1):e30529.

Eskiw CH, Fraser P. (2001). Ultrastructural study of transcription factories in mouse erythroblasts. *J Cell Sci.* Nov 1;124(Pt 21):3676-83.

Eskiw CH, Rapp A, Carter DR, Cook PR. (2008). RNA polymerase II activity is located on the surface of protein-rich transcription factories. *J Cell Sci.* Jun 15;121(Pt 12):1999-2007.

Fakan S, van Driel R. (2007). The perichromatin region: a functional compartment in the nucleus that determines large-scale chromatin folding. *Semin Cell Dev Biol.* Oct;18(5):676-81.

Falahzadeh Kh, Banaei-Esfahani A, Shahhoseini M. (2015). The potential roles of actin in the nucleus. *Cell J.* Spring;17(1):7-14.

Falanga V. (2012). Stem cells in tissue repair and regeneration. *J Invest Dermatol.* Jun;132(6):1538-41.

Fili N, Toseland CP. (2019). Unconventional Myosins: How Regulation Meets Function. *Int J Mol Sci.* Dec 20;21(1):67.

Fortin JP, Hansen KD. (2015). Reconstructing A/B compartments as revealed by Hi-C using long-range correlations in epigenetic data. *Genome Biol.* Aug 28;16(1):180.

Foster HA, Abeydeera LR, Griffin DK, Bridger JM. (2005). Non-random chromosome positioning in mammalian sperm nuclei, with migration of the sex chromosomes during late spermatogenesis. *J Cell Sci.* May 1;118(Pt 9):1811-20.

Foster HA, Bridger JM. (2005). The genome and the nucleus: a marriage made by evolution. Genome organisation and nuclear architecture. *Chromosoma.* Sep;114(4):212-29.

Franceschi C. (1989). Cell proliferation, cell death and aging. *Aging (Milano).* Sep;1(1):3-15.

Fritz AJ, Barutcu AR, Martin-Buley L, van Wijnen AJ, Zaidi SK, Imbalzano AN, Lian JB, Stein JL, Stein GS. (2016). Chromosomes at Work: Organization of Chromosome Territories in the Interphase Nucleus. *J Cell Biochem.* Jan;117(1):9-19.

Fujimaki K, Li R, Chen H, Della Croce K, Zhang HH, Xing J, Bai F, Yao G. (2019). Graded regulation of cellular quiescence depth between proliferation and senescence by a lysosomal dimmer switch. *Proc Natl Acad Sci U S A.* Nov 5;116(45):22624-22634.

Fujiwara K, Hasegawa K, Oka M, Yoneda Y, Yoshikawa K. (2016). Terminal differentiation of cortical neurons rapidly remodels RanGAP-mediated nuclear transport system. *Genes Cells.* Nov;21(11):1176-1194.

Gauthier J, Vincent AT, Charette SJ, Derome N. (2019). A brief history of bioinformatics. *Brief Bioinform.* Nov 27;20(6):1981-1996.

Gerace L and Huber MD (2012). Nuclear lamina at the crossroads of the cytoplasm and nucleus. *J Struct Biol.* Jan;177(1): 24–31.

Gesson K, Vidak S, Foisner R. (2014). Lamina-associated polypeptide (LAP)2α and nucleoplasmic lamins in adult stem cell regulation and disease. *Semin Cell Dev Biol.* May;29(100):116-24.

Ghamari A, van de Corput MP, Thongjuea S, van Cappellen WA, van Ijcken W, van Haren J, Soler E, Eick D, Lenhard B, Grosveld FG. (2013). In vivo live imaging of RNA polymerase II transcription factories in primary cells. *Genes Dev.* Apr 1;27(7):767-77.

Ghosh K, Capell BC. (2016). The Senescence-Associated Secretory Phenotype: Critical Effector in Skin Cancer and Aging. *J Invest Dermatol.* Nov;136(11):2133-2139.

Gilbert SF, Bosch TC, Ledón-Rettig C. (2015). Eco-Evo-Devo: developmental symbiosis and developmental plasticity as evolutionary agents. *Nat Rev Genet.* Oct;16(10):611-22.

Gire V, Dulic V. (2015). Senescence from G2 arrest, revisited.
Cell Cycle. 14(3):297-304.

Goode BL, Drubin DG, Barnes G. (2000). Functional cooperation between the microtubule and actin cytoskeletons. *Curr Opin Cell Biol*. Feb;12(1):63-71.

Gos M, Miloszewska J, Swoboda P, Trembacz H, Skierski J, Janik P. (2005). Cellular quiescence induced by contact inhibition or serum withdrawal in C3H10T1/2 cells. *Cell Prolif*. Apr;38(2):107-16.

Hagen JB. (2000). The origins of bioinformatics. *Nat Rev Genet*. Dec;1(3):231-6.

Hall LL, Smith KP, Byron M, Lawrence JB. (2006). Molecular anatomy of a speckle. *Anat Rec A Discov Mol Cell Evol Biol*. Jul;288(7):664-75.

Hartman MA, Finan D, Sivaramakrishnan S, Spudich JA. (2011). Principles of unconventional myosin function and targeting. *Annu Rev Cell Dev Biol*. 27:133-55.

Hayflick L. (1965). The limited in vitro lifetime of human diploid cell strains.
Exp Cell Res. Mar;37:614-36.

Hayflick L, Moorhead PS. (1961). The serial cultivation of human diploid cell strains.
Exp Cell Res. Dec;25:585-621.

Hernandez OM, Jones M, Guzman G, Szczesna-Cordary D. (2007). Myosin essential light chain in health and disease.
Am J Physiol Heart Circ Physiol. Apr;292(4):H1643-54.

Hernandez-Segura A, de Jong TV, Melov S, Guryev V, Campisi J, Demaria M. (2017). Unmasking Transcriptional Heterogeneity in Senescent Cells.
Curr Biol. Sep 11;27(17):2652-2660.e4.

Hernandez-Verdun D, Roussel P, Thiry M, Sirri V, Lafontaine DL. (2010). The nucleolus: structure/function relationship in RNA metabolism.
Wiley Interdiscip Rev RNA. Nov-Dec;1(3):415-31.

Hnisz D, Weintraub AS, Day DS, Valton AL, Bak RO, Li CH, Goldmann J, Lajoie BR, Fan ZP, Sigova AA, Reddy J, Borges-Rivera D, Lee TI, Jaenisch R, Porteus MH, Dekker J, Young RA. (2016). Activation of proto-oncogenes by disruption of chromosome neighborhoods. *Science*. Mar 25;351(6280):1454-1458.

Hofmann WA, Johnson T, Klapczynski M, Fan JL, de Lanerolle P. (2006). From transcription to transport: emerging roles for nuclear myosin I. *Biochem Cell Biol*. Aug;84(4):418-26.

Hogeweg P. (2011). The roots of bioinformatics in theoretical biology.
PLoS Comput Biol. Mar;7(3):e1002021.

Hu Q, Kwon YS, Nunez E, Cardamone MD, Hutt KR, Ohgi KA, Garcia-Bassets I, Rose DW, Glass CK, Rosenfeld MG, Fu XD. (2008). Enhancing nuclear receptor-induced transcription requires nuclear motor and LSD1-dependent gene networking in interchromatin granules. *Proc Natl Acad Sci U S A*. Dec 9;105(49):19199-204.

Huang T, Rivera-Pérez JA. (2014). Senescence-associated β-galactosidase activity marks the visceral endoderm of mouse embryos but is not indicative of senescence. *Genesis*. Apr;52(4):300-8.

Huitorel P. (1988). From cilia and flagella to intracellular motility and back again: a review of a few aspects of microtubule-based motility. *Biol Cell*. 63(2):249-58.

Iborra FJ, Pombo A, McManus J, Jackson DA, Cook PR. (1996). The topology of transcription by immobilized polymerases. *Exp Cell Res*. Dec 15;229(2):167-73.

Jackson DA, Hassan AB, Errington RJ, Cook PR. (1993). Visualization of focal sites of transcription within human nuclei. *EMBO J*. Mar;12(3):1059-65.

Jackson DA. (1997). Chromatin domains and nuclear compartments: establishing sites of gene expression in eukaryotic nuclei. *Mol Biol Rep*. Aug;24(3):209-20.

Jackson DA. (2005). The amazing complexity of transcription factories. *Brief Funct Genomic Proteomic*. Jul;4(2):143-57.

Jansen RC. (2003). Studying complex biological systems using multifactorial perturbation. *Nat Rev Genet*. Feb;4(2):145-51.

Jez JM. (2017). Revisiting protein structure, function, and evolution in the genomic era. *J Invertebr Pathol*. Jan;142:11-15.

Johnson MS, Cook JG. (2023). Cell cycle exits and U-turns: Quiescence as multiple reversible forms of arrest. *Fac Rev*. Mar 8;12:5.

Kabachinski G, Schwartz TU. (2015). The nuclear pore complex--structure and function at a glance. *J Cell Sci*. Feb 1;128(3):423-9.

Kaas JH. (1989). The evolution of complex sensory systems in mammals. *J Exp Biol*. Sep;146:165-76.

Kaur G, Sundar IK, Rahman I. (2021). p16-3MR: A Novel Model to Study Cellular Senescence in Cigarette Smoke-Induced Lung Injuries. *Int J Mol Sci*. May 3;22(9):4834.

Kawano T, Araseki M, Araki Y, Kinjo M, Yamamoto T, Suzuki T. (2012). A small peptide sequence is sufficient for initiating kinesin-1 activation through part of TPR region of KLC1. *Traffic*. Jun;13(6):834-48.

Kiesslich A, von Mikecz A, Hemmerich P. (2002). Cell cycle-dependent association of PML bodies with sites of active transcription in nuclei of mammalian cells. *J Struct Biol*. Oct-Dec;140(1-3):167-79.

Klimova TA, Bell EL, Shroff EH, Weinberg FD, Snyder CM, Dimri GP, Schumacker PT, Budinger GR, Chandel NS. (2009). Hyperoxia-induced premature senescence requires p53 and pRb, but not mitochondrial matrix ROS. *FASEB J.* Mar;23(3):783-94.

Knight M, Ittiprasert W, Odoemelam EC, Adema CM, Miller A, Raghavan N and Bridger JM. (2011). Non-random organization of the *Biomphalaria glabrata* genome in interphase Bge cells and the spatial repositioning of activated genes in cells co-cultured with *Schistosoma mansoni. Int. J. Parasitol.* Jan;41(1):61–70.

Kollmar M. (2006). Thirteen is enough: the myosins of Dictyostelium discoideum and their light chains. *BMC Genomics.* Jul 20;7:183.

Kosinski J, Mosalaganti S, von Appen A, Teimer R, DiGuilio AL, Wan W, Bui KH, Hagen WJ, Briggs JA, Glavy JS, Hurt E, Beck M. (2016). Molecular architecture of the inner ring scaffold of the human nuclear pore complex. *Science.* Apr 15;352(6283):363-5.

Krasteva V, Buscarlet M, Diaz-Tellez A, Bernard MA, Crabtree GR, Lessard JA. (2012). The BAF53a subunit of SWI/SNF-like BAF complexes is essential for hemopoietic stem cell function. *Blood.* Dec 6;120(24):4720-32.

Krendel M, Mooseker MS. (2005). Myosins: tails (and heads) of functional diversity. *Physiology (Bethesda).* Aug;20:239-51.

Kuilman T, Michaloglou C, Mooi WJ, Peeper DS. (2010). The essence of senescence. *Genes Dev.* Nov 15;24(22):2463-79.

Kumari R, Jat P. (2021). Mechanisms of Cellular Senescence: Cell Cycle Arrest and Senescence Associated Secretory Phenotype. *Front Cell Dev Biol.* Mar 29;9:645593.

Kuroda M, Tanabe H, Yoshida K, Oikawa K, Saito A, Kiyuna T, Mizusawa H, Mukai K. (2004). Alteration of chromosome positioning during adipocyte differentiation*. J Cell Sci.* Nov 15;117(Pt 24):5897-903.

Kwon JS, Everetts NJ, Wang X, Wang W, Della Croce K, Xing J, Yao G. (2017). Controlling Depth of Cellular Quiescence by an Rb-E2F Network Switch. *Cell Rep.* Sep 26;20(13):3223-3235.

Lamond AI, Earnshaw WC. (1998). Structure and function in the nucleus. *Science.* 24;280(5363):547-53.

Lapierre LA, Kumar R, Hales CM, Navarre J, Bhartur SG, Burnette JO, Provance DW Jr, Mercer JA, Bähler M, Goldenring JR. (2001). Myosin vb is associated with plasma membrane recycling systems. *Mol Biol Cell.* Jun;12(6):1843-57.

Laurent JM, Vogel C, Kwon T, Craig SA, Boutz DR, Huse HK, Nozue K, Walia H, Whiteley M, Ronald PC, Marcotte EM. (2010). Protein abundances are more conserved than mRNA abundances across diverse taxa. *Proteomics.* Dec;10(23):4209-12.

Lee BY, Han JA, Im JS, Morrone A, Johung K, Goodwin EC, Kleijer WJ, DiMaio D, Hwang ES. (2006). Senescence-associated beta-galactosidase is lysosomal beta-galactosidase. *Aging Cell*. Apr;5(2):187-95.

Lelièvre SA, Bissell MJ, Pujuguet P. (2000). Cell nucleus in context. *Crit Rev Eukaryot Gene Expr*.10 (1):13-20.

Lemons JM, Feng XJ, Bennett BD, Legesse-Miller A, Johnson EL, Raitman I, Pollina EA, Rabitz HA, Rabinowitz JD, Coller HA. (2010). Quiescent fibroblasts exhibit high metabolic activity. *PLoS Biol*. Oct 19;8(10):e1000514.

Li Y, Fong KW, Tang M, Han X, Gong Z, Ma W, Hebert M, Songyang Z, Chen J. (2014). Fam118B, a newly identified component of Cajal bodies, is required for Cajal body formation, snRNP biogenesis and cell viability. *J Cell Sci*. May 1;127(Pt 9):2029-39.

Lin F, Blake DL, Callebaut I, Skerjanc IS, Holmer L, McBurney MW, Paulin-Levasseur M, Worman HJ. (2000). MAN1, an inner nuclear membrane protein that shares the LEM domain with lamina-associated polypeptide 2 and emerin. *J Biol Chem Feb* 18;275(7):4840-7.

Lindsay AJ, McCaffrey MW. (2009). Myosin Vb localises to nucleoli and associates with the RNA polymerase I transcription complex. *Cell Motil Cytoskeleton*. Dec;66(12):1057-72.

Liu J, Ali M, Zhou Q. (2020). Establishment and evolution of heterochromatin. *Ann N Y Acad Sci*. Sep;1476(1):59-77.

Logan MK, McLaurin DM, Hebert MD. (2020). Synergistic interactions between Cajal bodies and the miRNA processing machinery. *Mol Biol Cell*. Jul 15;31(15):1561-1569.

Lopes-Paciencia S, Saint-Germain E, Rowell MC, Ruiz AF, Kalegari P, Ferbeyre G. (2019). The senescence-associated secretory phenotype and its regulation. *Cytokine*. May;117:15-22.

Lu W, Gotzmann J, Sironi L, Jaeger VM, Schneider M, Lüke Y, Uhlén M, Szigyarto CA, Brachner A, Ellenberg J, Foisner R, Noegel AA, Karakesisoglou I. (2008). Sun1 forms immobile macromolecular assemblies at the nuclear envelope. *Biochim Biophys Acta*. Dec;1783(12):2415-26.

Lu W, Schneider M, Neumann S, Jaeger VM, Taranum S, Munck M, Cartwright S, Richardson C, Carthew J, Noh K, Goldberg M, Noegel AA, Karakesisoglou I. (2012). Nesprin interchain associations control nuclear size. *Cell Mol Life Sci*. Oct;69(20):3493-509.

Lupiáñez DG, Spielmann M, Mundlos S. (2016). Breaking TADs: How Alterations of Chromatin Domains Result in Disease. *Trends Genet*. Apr;32(4):225-237.

Macieira-Coelho A, Taboury F. (1982). A re-evaluation of the changes in proliferation in human fibroblasts during ageing in vitro. *Cell Tissue Kinet*. Mar;15(2):213-24.

Maeda M, Hayashi T, Mizuno N, Hattori Y, Kuzuya M. (2015). Intermittent high glucose implements stress-induced senescence in human vascular endothelial cells: role of superoxide production by NADPH oxidase.
PLoS One. Apr 16;10(4):e0123169.

Magwere T, West M, Riyahi K, Murphy MP, Smith RA, Partridge L. (2006). The effects of exogenous antioxidants on lifespan and oxidative stress resistance in Drosophila melanogaster. *Mech Ageing Dev.* Apr;127(4):356-70.

Maiser A, Dillinger S, Längst G, Schermelleh L, Leonhardt H, Németh A. (2020). Super-resolution in situ analysis of active ribosomal DNA chromatin organization in the nucleolus. *Sci Rep.* May 4;10(1):7462.

Mallik R, Gross SP. (2004). Molecular motors: strategies to get along.
Curr Biol. Nov 23;14(22):R971-82.

Maly IV, Hofmann WA. (2020). Myosins in the Nucleus.
*Adv Exp Med Biol.*1239:199-231.

Mao Z, Ke Z, Gorbunova V, Seluanov A. (2012). Replicatively senescent cells are arrested in G1 and G2 phases. *Aging (Albany NY).* Jun;4(6):431-5.

Marella NV, Seifert B, Nagarajan P, Sinha S, Berezney R. (2009). Chromosomal rearrangements during human epidermal keratinocyte differentiation.
J Cell Physiol. Oct;221(1):139-46.

Marescal O, Cheeseman IM. (2020). Cellular Mechanisms and Regulation of Quiescence. *Dev Cell.* Nov 9;55(3):259-271.

Marsden RL, Ranea JA, Sillero A, Redfern O, Yeats C, Maibaum M, Lee D, Addou S, Reeves GA, Dallman TJ, Orengo CA. (2006). Exploiting protein structure data to explore the evolution of protein function and biological complexity.
Philos Trans R Soc Lond B Biol Sci. Mar 29;361(1467):425-40.

Masiello I, Siciliani S, Biggiogera M. (2018). Perichromatin region: a moveable feast. *Histochem Cell Biol.* Sep;150(3):227-233.

Meaburn KJ, Newbold RF, Bridger JM. (2008). Positioning of human chromosomes in murine cell hybrids according to synteny*. Chromosoma.* Dec;117(6):579-91.

McGraw-Hill Concise Encyclopedia of Bioscience (2002). Cell Nucleus.
The McGraw-Hill Companies, Inc.

McIntosh BB, Ostap EM. (2016). Myosin-I molecular motors at a glance.
J Cell Sci. Jul 15;129(14):2689-95.

McLeod T, Abdullahi A, Li M, Brogna S. (2014). Recent studies implicate the nucleolus as the major site of nuclear translation.
Biochem Soc Trans. Aug;42(4):1224-8.

Mehta IS. (2009). Chromosome Territory Position and Active Relocation in Normal and Hutchinson-Gilford Progeria Fibroblasts. *PhD Thesis*.

Mehta IS, Amira M, Harvey AJ and Bridger JM (2010). Rapid chromosome territory relocation by nuclear motor activity in response to serum removal in primary human fibroblasts. *Genome Biol*. Jan 13;11(1):R5.

Mehta IS, Eskiw CH, Arican, HD, Kill IR and Bridger JM. (2011). Farnesyltransferase inhibitor treatment restores chromosome territory positions and active chromosome dynamics in Hutchinson–Gilford progeria syndrome cells.
Genome Biol. Aug 12;12(8):R74.

Mehta IS, Riyahi K, Pereira RT, Meaburn KJ, Figgitt M, Kill IR, Eskiw CH and Bridger JM. (2021). Interphase Chromosomes in Replicative Senescence: Chromosome Positioning as a Senescence Biomarker and the Lack of Nuclear Motor-Driven Chromosome Repositioning in Senescent Cells.
Front. Cell Dev. Biol. May 24;9:640200.

Melcák, I., Cermanová, S., Jirsová, K., Koberna, K., Malínský, J., & Raska, I. (2000). Nuclear pre-mRNA compartmentalization: trafficking of released transcripts to splicing factor reservoirs. *Mol Biol Cell*. Feb;11(2):497-510.

Melé M, Ferreira PG, Reverter F, DeLuca DS, Monlong J, Sammeth M, Young TR, Goldmann JM, Pervouchine DD, Sullivan TJ, Johnson R, Segrè AV, Djebali S, Niarchou A; GTEx Consortium; Wright FA, Lappalainen T, Calvo M, Getz G, Dermitzakis ET, Ardlie KG, Guigó R. Human genomics. (2015). The human transcriptome across tissues and individuals. *Science*. May 8;348(6235):660-5.

Melnik S, Deng B, Papantonis A, Baboo S, Carr IM, Cook PR. (2011). The proteomes of transcription factories containing RNA polymerases I, II or III.
Nat Methods. Sep 25;8(11):963-8.

Mercer, T. R., & Mattick, J. S. (2013). Understanding the regulatory and transcriptional complexity of the genome through structure.
Genome Res. Jul;23(7):1081-8.

Mische S, He Y, Ma L, Li M, Serr M, Hays TS. (2008). Dynein light intermediate chain: an essential subunit that contributes to spindle checkpoint inactivation.
Mol Biol Cell. Nov;19(11):4918-29.

Montgomery TH. (1898). Comparative cytological studies, with especial regard to the morphology of the nucleolus. *J Morphol*. 15:265–582.

Miwa S, Riyahi K, Partridge L, Brand MD. (2004). Lack of correlation between mitochondrial reactive oxygen species production and life span in Drosophila.
Ann N Y Acad Sci. Jun;1019:388-91.

Morris GE. (2008). The Cajal body. *Biochim Biophys Acta*. Nov;1783(11):2108-15.

Mullins RD, Pollard TD. (1999). Structure and function of the Arp2/3 complex.
Curr Opin Struct Biol. Apr;9(2):244-9.

Muñoz-Espín D, Cañamero M, Maraver A, Gómez-López G, Contreras J, Murillo-Cuesta S, Rodríguez-Baeza A, Varela-Nieto I, Ruberte J, Collado M, Serrano M. (2013). Programmed cell senescence during mammalian embryonic development. *Cell.* Nov 21;155(5):1104-18.

Mylonas A, O'Loghlen A. (2022). Cellular Senescence and Ageing: Mechanisms and Interventions. *Front Aging.* Mar 29;3:866718.

Newport JW, Forbes DJ. (1987). The nucleus: structure, function, and dynamics. *Annu Rev Biochem.* 56:535-65.

Nowak MA, Boerlijst MC, Cooke J, Smith JM. (1997). Evolution of genetic redundancy. *Nature.* Jul 10;388(6638):167-71.

Nowak G, Pestic-Dragovich L, Hozák P, Philimonenko A, Simerly C, Schatten G, de Lanerolle P. (1997). Evidence for the presence of myosin I in the nucleus. *J Biol Chem.* Jul 4;272(27):17176-81.

Odronitz F, Kollmar M. (2007). Drawing the tree of eukaryotic life based on the analysis of 2,269 manually annotated myosins from 328 species. *Genome Biol.* 8(9):R196.

Ogg SC, Lamond AI. (2002). Cajal bodies and coilin--moving towards function. *J Cell Biol.* Oct 14;159(1):17-21.

Oma Y, Harata M. (2011). Actin-related proteins localized in the nucleus: from discovery to novel roles in nuclear organization. *Nucleus.* Jan-Feb;2(1):38-46.

Osborne CS, Chakalova L, Brown KE, Carter D, Horton A, Debrand E, Goyenechea B, Mitchell JA, Lopes S, Reik W & Fraser P. (2004). Active genes dynamically colocalize to shared sites of ongoing transcription. *Nat Genet.* Oct;36(10):1065-71.

Oteiza P, Baldwin MW. (2021). Evolution of sensory systems. *Curr Opin Neurobiol.* Dec;71:52-59.

Paci G, Caria J, Lemke EA. (2021). Cargo transport through the nuclear pore complex at a glance. *J Cell Sci.* Jan 25;134(2):jcs247874.

Palibrk V, Lång E, Lång A, Schink KO, Rowe AD, Bøe SO. (2014). Promyelocytic leukemia bodies tether to early endosomes during mitosis*. Cell Cycle.* 13(11):1749-55.

Papantonis A, Larkin JD, Wada Y, Ohta Y, Ihara S, Kodama T, et al. (2010). Active RNA Polymerases: Mobile or Immobile Molecular Machines*? PLoS Biol.* July 13;8(7):e1000419.

Papantonis A, Cook PR. (2011). Fixing the model for transcription: the DNA moves, not the polymerase. *Transcription.* Jan-Feb;2(1):41-4.

Paramos-de-Carvalho D, Jacinto A, Saúde L. (2021). The right time for senescence. *Elife.* Nov 10;10:e72449.

Pederson T. (2011). The nucleolus. *Cold Spring Harb Perspect Biol.* Mar 1;3(3):a000638.

Peng G, Han JJ. (2018). Regulatory network characterization in development: challenges and opportunities. *F1000Res.* Sep 17;7:F1000 Faculty Rev-1477.

Pestic-Dragovich L, Stojiljkovic L, Philimonenko AA, Nowak G, Ke Y, Settlage RE, Shabanowitz J, Hunt DF, Hozak P, de Lanerolle P. (2000). A myosin I isoform in the nucleus. *Science.* Oct 13;290(5490):337-41.

Percipalle P, Vartiainen M. (2019). Cytoskeletal proteins in the cell nucleus: a special nuclear actin perspective. *Mol Biol Cell.* Jul 15;30(15):1781-1785.

Phillips R, Kondev J, Theriot J, Garcia H. (2012). Physical Biology of the Cell. 2nd Edition. *Garland Science.*

Pontes O, Pikaard CS. (2008). siRNA and miRNA processing: new functions for Cajal bodies. *Curr Opin Genet Dev.* Apr;18(2):197-203.

Porter JR, Meller A, Zimmerman MI, Greenberg MJ, Bowman GR. (2020). Conformational distributions of isolated myosin motor domains encode their mechanochemical properties. *Elife.* May 29;9:e55132.

Pranchevicius MC, Baqui MM, Ishikawa-Ankerhold HC, Lourenço EV, Leão RM, Banzi SR, dos Santos CT, Roque-Barreira MC, Espreafico EM, Larson RE. (2008). Myosin Va phosphorylated on Ser1650 is found in nuclear speckles and redistributes to nucleoli upon inhibition of transcription. *Cell Motil Cytoskeleton.* Jun;65(6):441-56.

Quinlan ME, Heuser JE, Kerkhoff E, Mullins RD. (2005). Drosophila Spire is an actin nucleation factor. *Nature.* Jan 27;433(7024):382-8.

Rajderkar S, Barozzi I, Zhu Y, Hu R, Zhang Y, Li B, Alcaina Caro A, Fukuda-Yuzawa Y, Kelman G, Akeza A, Blow MJ, Pham Q, Harrington AN, Godoy J, Meky EM, von Maydell K, Hunter RD, Akiyama JA, Novak CS, Plajzer-Frick I, Afzal V, Tran S, Lopez-Rios J, Talkowski ME, Lloyd KCK, Ren B, Dickel DE, Visel A, Pennacchio LA. (2023). Topologically associating domain boundaries are required for normal genome function. *Commun Biol.* Apr 20;6(1):435.

Rajgor D, Shanahan CM. (2013). Nesprins: from the nuclear envelope and beyond. *Expert Rev Mol Med.* Jul 5;15:e5.

Ranade D, Pradhan R, Jayakrishnan M, Hegde S, Sengupta K. (2019). Lamin A/C and Emerin depletion impacts chromatin organization and dynamics in the interphase nucleus. *BMC Mol Cell Biol.* May 22;20(1):11.

Rapali P, Szenes Á, Radnai L, Bakos A, Pál G, Nyitray L. (2011). DYNLL/LC8: a light chain subunit of the dynein motor complex and beyond. *FEBS J.* Sep;278(17):2980-96.

Razin SV, Gavrilov AA, Pichugin A, Lipinski M, Iarovaia OV, Vassetzky YS. (2011). Transcription factories in the context of the nuclear and genome organization. *Nucleic Acids Res.* Nov;39(21):9085-92.

Reid DW, Nicchitta CV.(2012). The enduring enigma of nuclear translation. *J Cell Biol.* Apr 2;197(1):7-9.

Rhinn M, Ritschka B, Keyes WM. (2019). Cellular senescence in development, regeneration and disease. *Development.* Oct 1;146(20):dev151837.

Richards TA, Cavalier-Smith T. (2005). Myosin domain evolution and the primary divergence of eukaryotes. *Nature.* Aug 25;436(7054):1113-8.

Rieder D, Trajanoski Z, McNally JG. (2012). Transcription factories. *Front Genet.* Oct 23;3:221.

Rippe K. (2007). Dynamic organization of the cell nucleus. *Curr Opin Genet Dev.* Oct;17(5):373-80.

Rizzuto D, Orsini N, Qiu C, Wang HX, Fratiglioni L. (2012). Lifestyle, social factors, and survival after age 75: population based study. *BMJ.* Aug 29;345:e5568.

Roger L, Tomas F, Gire V. (2021). Mechanisms and Regulation of Cellular Senescence. *Int J Mol Sci.* Dec 6;22(23):13173.

Roland JT, Bryant DM, Datta A, Itzen A, Mostov KE, Goldenring JR. (2011). Rab GTPase-Myo5B complexes control membrane recycling and epithelial polarization. *Proc Natl Acad Sci U S A.* Feb 15;108(7):2789-94.

Roncaglia P, van Dam TJP, Christie KR, Nacheva L, Toedt G, Huynen MA, Huntley RP, Gibson TJ, Lomax J. (2017). The Gene Ontology of eukaryotic cilia and flagella. *Cilia.* Nov 16;6:10.

Rouquette J, Genoud C, Vazquez-Nin GH, Kraus B, Cremer T, Fakan S. (2009). Revealing the high-resolution three-dimensional network of chromatin and interchromatin space: a novel electron-microscopic approach to reconstructing nuclear architecture. *Chromosome Res.*17(6):801-10.

Roux KJ, Crisp ML, Liu Q, Kim D, Kozlov S, Stewart CL, Burke B. (2009). Nesprin 4 is an outer nuclear membrane protein that can induce kinesin-mediated cell polarization. *Proc Natl Acad Sci U S A.* Feb 17;106(7):2194-9.

Salamon M, Millino C, Raffaello A, Mongillo M, Sandri C, Bean C, Negrisolo E, Pallavicini A, Valle G, Zaccolo M, Schiaffino S, Lanfranchi G. (2003). Human MYO18B, a novel unconventional myosin heavy chain expressed in striated muscles moves into the myonuclei upon differentiation. *J Mol Biol.* Feb 7;326(1):137-49.

Sato H, Das S, Singer RH, Vera M. (2020). Imaging of DNA and RNA in Living Eukaryotic Cells to Reveal Spatiotemporal Dynamics of Gene Expression. *Annu Rev Biochem.* Jun 20;89:159-187.

Schenk J, Wilsch-Bräuninger M, Calegari F, Huttner WB. (2009). Myosin II is required for interkinetic nuclear migration of neural progenitors. *Proc Natl Acad Sci U S A*. Sep 22;106(38):16487-92.

Schneider M, Noegel AA, Karakesisoglou I. (2008). KASH-domain proteins and the cytoskeletal landscapes of the nuclear envelope. *Biochem Soc Trans*. Dec;36(Pt 6):1368-72.

Schuller AP, Wojtynek M, Mankus D, Tatli M, Kronenberg-Tenga R, Regmi SG, Dip PV, Lytton-Jean AKR, Brignole EJ, Dasso M, Weis K, Medalia O, Schwartz TU. (2021). The cellular environment shapes the nuclear pore complex architecture. *Nature*. Oct;598(7882):667-671.

Sebé-Pedrós A, Grau-Bové X, Richards TA, Ruiz-Trillo I. (2014). Evolution and classification of myosins, a paneukaryotic whole-genome approach. *Genome Biol Evol*. Feb;6(2):290-305.

Shahid-Fuente IW, Toseland CP. (2023). Myosin in chromosome organisation and gene expression. *Biochem Soc Trans*. Jun 28;51(3):1023-1034.

Sharan R, Suthram S, Kelley RM, Kuhn T, McCuine S, Uetz P, Sittler T, Karp RM, Ideker T.(2005). Conserved patterns of protein interaction in multiple species. *Proc Natl Acad Sci U S A.* Feb 8;102(6):1974-9.

Sharpless NE, Sherr CJ. (2015). Forging a signature of in vivo senescence. *Nat Rev Cancer*. Jul;15(7):397-408.

Shea JR Jr, Leblond CP. (1966). Number of nucleoli in various cell types of the mouse. *J Morphol*. Aug;119(4):425-33.

Sherr EH, Joyce MP, Greene LA. (1993). Mammalian myosin I alpha, I beta, and I gamma: new widely expressed genes of the myosin I family. *J Cell Biol*. Mar;120(6):1405-16.

Shevelyov YY, Nurminsky DI. (2012). The nuclear lamina as a gene-silencing hub. *Curr Issues Mol Biol*. 14(1):27-38.

Shevelyov YY, Ulianov SV. (2019). The Nuclear Lamina as an Organizer of Chromosome Architecture. *Cells*. Feb 8;8(2):136.

Shields HJ, Traa A, Van Raamsdonk JM. (2021). Beneficial and Detrimental Effects of Reactive Oxygen Species on Lifespan: A Comprehensive Review of Comparative and Experimental Studies. *Front Cell Dev Biol*. Feb 11;9:628157.

Shiels C, Islam SA, Vatcheva R, Sasieni P, Sternberg MJ, Freemont PS, Sheer D. (2001). PML bodies associate specifically with the MHC gene cluster in interphase nuclei. *J Cell Sci*. Oct;114(Pt 20):3705-16.

Shimi T, Goldman RD. (2014). Nuclear lamins and oxidative stress in cell proliferation and longevity. *Adv Exp Med Biol*. 773:415-30.

Smits JPH, Dirks RAM, Qu J, Oortveld MAW, Brinkman AB, Zeeuwen PLJM, Schalkwijk J, Zhou H, Marks H, van den Bogaard EH. (2021). Terminal keratinocyte differentiation in vitro is associated with a stable DNA methylome. *Exp Dermatol.* Aug;30(8):1023-1032.

Snel B, Lehmann G, Bork P, Huynen MA. (2000). STRING: a web-server to retrieve and display the repeatedly occurring neighbourhood of a gene. *Nucleic Acids Res.* Sep 15;28(18):3442-4.

Sonawane AR, Platig J, Fagny M, Chen CY, Paulson JN, Lopes-Ramos CM, DeMeo DL, Quackenbush J, Glass K, Kuijjer ML. (2017). Understanding Tissue-Specific Gene Regulation. *Cell Rep.* Oct 24;21(4):1077-1088.

Spector DL and Lamond AI. (2011). Nuclear Speckles. *Cold Spring Harb Perspect Biol.* Feb 1;3(2):a000646.

Sperry AO (Editor). (2007). Molecular Motors: Methods and Protocols. *Humana Press.*

Spilianakis CG, Lalioti MD, Town T, Lee GR, Flavell RA. (2005). Interchromosomal associations between alternatively expressed loci. *Nature.* Jun 2;435(7042):637-45.

Stanek D, Neugebauer KM. (2006). The Cajal body: a meeting place for spliceosomal snRNPs in the nuclear maze. *Chromosoma.* Oct;115(5):343-54.

Suntharalingam M, Wente SR. (2003). Peering through the pore: nuclear pore complex structure, assembly, and function. *Dev Cell.* Jun;4(6):775-89.

Szczerbal I, Bridger JM. (2010). Association of adipogenic genes with SC-35 domains during porcine adipogenesis. *Chromosome Res.* Dec;18(8):887-95.

Szklarczyk D, Gable AL, Lyon D, Junge A, Wyder S, Huerta-Cepas J, Simonovic M, Doncheva NT, Morris JH, Bork P, Jensen LJ, Mering CV. (2019). STRING v11: protein-protein association networks with increased coverage, supporting functional discovery in genome-wide experimental datasets. *Nucleic Acids Res.* Jan 8;47(D1):D607-D613.

Szklarczyk D, Gable AL, Nastou KC, Lyon D, Kirsch R, Pyysalo S, Doncheva NT, Legeay M, Fang T, Bork P, Jensen LJ, von Mering C. (2021). The STRING database in 2021: customizable protein-protein networks, and functional characterization of user-uploaded gene/measurement sets. *Nucleic Acids Res.* Jan 8;49(D1):D605-D612.

Tai H, Wang Z, Gong H, Han X, Zhou J, Wang X, Wei X, Ding Y, Huang N, Qin J, Zhang J, Wang S, Gao F, Chrzanowska-Lightowlers ZM, Xiang R, Xiao H. (2017). Autophagy impairment with lysosomal and mitochondrial dysfunction is an important characteristic of oxidative stress-induced senescence. *Autophagy.* Jan 2;13(1):99-113.

Taranum S, Sur I, Müller R, Lu W, Rashmi RN, Munck M, Neumann S, Karakesisoglou I, Noegel AA. (2012). Cytoskeletal interactions at the nuclear envelope mediated by nesprins. *Int J Cell Biol*. 2012:736524.

Tavaria M, Gabriele T, Anderson RL, Mirault ME, Baker E, Sutherland G, Kola I. (1995). Localization of the gene encoding the human heat shock cognate protein, HSP73, to chromosome 11. *Genomics*. Sep 1;29(1):266-8.

Tavaria M, Gabriele T, Kola I, Anderson RL. (1996). A hitchhiker's guide to the human Hsp70 family. *Cell Stress Chaperones*. Apr;1(1):23-8.

Taylor KA. (2007). Regulation and recycling of myosin V. *Curr Opin Cell Biol*. Feb;19(1):67-74.

Telek E, Kengyel A, Bugyi B. (2020). Myosin XVI in the Nervous System. *Cells*. Aug 15;9(8):1903.

Telenius H, Pelmear AH, Tunnacliffe A, Carter NP, Behmel A, Ferguson-Smith MA, Nordenskjöld M, Pfragner R, Ponder BA. (1992). Cytogenetic analysis by chromosome painting using DOP-PCR amplified flow-sorted chromosomes. *Genes Chromosomes Cancer*. Apr;4(3):257-63.

Theodoridis PR, Bokros M, Marijan D, Balukoff NC, Wang D, Kirk CC, Budine TD, Goldsmith HD, Wang M, Audas TE, Lee S. (2021). Local translation in nuclear condensate amyloid bodies. *Proc Natl Acad Sci U S A*. Feb 16;118(7).

Thoeni CE, Vogel GF, Tancevski I, Geley S, Lechner S, Pfaller K, Hess MW, Müller T, Janecke AR, Avitzur Y, Muise A, Cutz E, Huber LA. (2014). Microvillus inclusion disease: loss of Myosin vb disrupts intracellular traffic and cell polarity. *Traffic*. Jan;15(1):22-42.

Szabo Q, Bantignies F, Cavalli G. (2019). Principles of genome folding into topologically associating domains. *Sci Adv*. Apr 10;5(4):eaaw1668.

Tsai RY, Pederson T. (2014). Connecting the nucleolus to the cell cycle and human disease. *FASEB J*. Aug;28(8):3290-6.

Vale RD. (2003). The molecular motor toolbox for intracellular transport. *Cell*. Feb 21;112(4):467-80.

van Deursen JM. (2014). The role of senescent cells in ageing. *Nature*. May 22;509(7501):439-46.

van Driel R, Humbel B, de Jong L. (1991). The nucleus: a black box being opened. *J Cell Biochem*. Dec;47(4):311-6.

van Steensel B, Belmont AS. (2017). Lamina-Associated Domains: Links with Chromosome Architecture, Heterochromatin, and Gene Repression. *Cell*. May 18;169(5):780-791.

van Velthoven CTJ, Rando TA. (2019). Stem Cell Quiescence: Dynamism, Restraint, and Cellular Idling. *Cell Stem Cell*. Feb 7;24(2):213-225.

Vijg J, Suh Y. (2023). Functional genomics of ageing.
Mech Ageing Dev. Jan;124(1):3-8.

Volpi EV, Chevret E, Jones T, Vatcheva R, Williamson J, Beck S, Campbell RD, Goldsworthy M, Powis SH, Ragoussis J, Trowsdale J, Sheer D. (2000). Large-scale chromatin organization of the major histocompatibility complex and other regions of human chromosome 6 and its response to interferon in interphase nuclei.
J Cell Sci. May;113 (Pt 9):1565-76.

von Mering C, Jensen LJ, Snel B, Hooper SD, Krupp M, Foglierini M, Jouffre N, Huynen MA, Bork P. (2005). STRING: known and predicted protein-protein associations, integrated and transferred across organisms.
Nucleic Acids Res. Jan 1;33(Database issue):D433-7.

Vreugde S, Ferrai C, Miluzio A, Hauben E, Marchisio PC, Crippa MP, Bussi M, Biffo S. (2006). Nuclear myosin VI enhances RNA polymerase II-dependent transcription.
Mol Cell. Sep 1;23(5):749-55.

Wanner E, Thoppil H, Riabowol K. (2021). Senescence and Apoptosis: Architects of Mammalian Development. *Front Cell Dev Biol*. Jan 18;8:620089.

Wansink DG, Schul W, van der Kraan I, van Steensel B, van Driel R, de Jong L. (1993). Fluorescent labeling of nascent RNA reveals transcription by RNA polymerase II in domains scattered throughout the nucleus.
J Cell Biol. Jul;122(2):283-93.

Wente SR, Rout MP. (2010). The nuclear pore complex and nuclear transport.
Cold Spring Harb Perspect Biol. Oct;2(10):a000562.

Williams RR, Broad S, Sheer D, Ragoussis J. (2002). Subchromosomal positioning of the epidermal differentiation complex (EDC) in keratinocyte and lymphoblast interphase nuclei. *Exp Cell Res*. Jan 15;272(2):163-75.

Wing CE, Fung HYJ, Chook YM. (2022). Karyopherin-mediated nucleocytoplasmic transport. *Nat Rev Mol Cell Biol*. May;23(5):307-328.

Woolley D. (2000). The molecular motors of cilia and eukaryotic flagella.
Essays Biochem. 35:103-15.

Woolner S, Bement WM. (2009). Unconventional myosins acting unconventionally.
Trends *Cell Biol*. Jun;19(6):245-52.

Yang Z, Rannala B. (2012). Molecular phylogenetics: principles and practice.
Nat Rev Genet. Mar 28;13(5):303-14.

Ye G, Yang Q, Lei X, Zhu X, Li F, He J, Chen H, Ling R, Zhang H, Lin T, Liang Z, Liang Y, Huang H, Guo W, Deng H, Liu H, Hu Y, Yu J, Li G. (2020). Nuclear MYH9-induced CTNNB1 transcription, targeted by staurosporin, promotes gastric cancer cell anoikis resistance and metastasis. *Theranostics.* Jun 12;10(17):7545-7560.

Young PJ, Le TT, thi Man N, Burghes AH, Morris GE. (2000). The relationship between SMN, the spinal muscular atrophy protein, and nuclear coiled bodies in differentiated tissues and cultured cells. *Exp Cell Res.* May 1;256(2):365-74.

Yuan P, Wang Z, Lv W, Pan H, Yang Y, Yuan X, Hu J. (2014). Telomerase Cajal body protein 1 depletion inhibits telomerase trafficking to telomeres and induces G_1 cell cycle arrest in A549 cells. *Oncol Lett.* Sep;8(3):1009-1016.

Zhang Q, Kota KP, Alam SG, Nickerson JA, Dickinson RB, Lele TP. (2016). Coordinated Dynamics of RNA Splicing Speckles in the Nucleus. *J Cell Physiol.* Jun;231(6):1269-75.

Zidovska A. (2020). The rich inner life of the cell nucleus: dynamic organization, active flows, and emergent rheology. *Biophys Rev.* Oct;12(5):1093-1106.

Zirbel RM, Mathieu UR, Kurz A, Cremer T, Lichter P. (1993). Evidence for a nuclear compartment of transcription and splicing located at chromosome domain boundaries. *Chromosome Res.* Jul;1(2):93-106.

Zuleger N, Robson MI, Schirmer EC. (2011). The nuclear envelope as a chromatin organizer. *Nucleus.* Sep-Oct;2(5):339-49.